MICROCIRCULATION GUIDED/ TARGETED RESUSCITATION

EDITED BY: Inge Bauer and Mihály Boros

PUBLISHED IN: Frontiers in Medicine

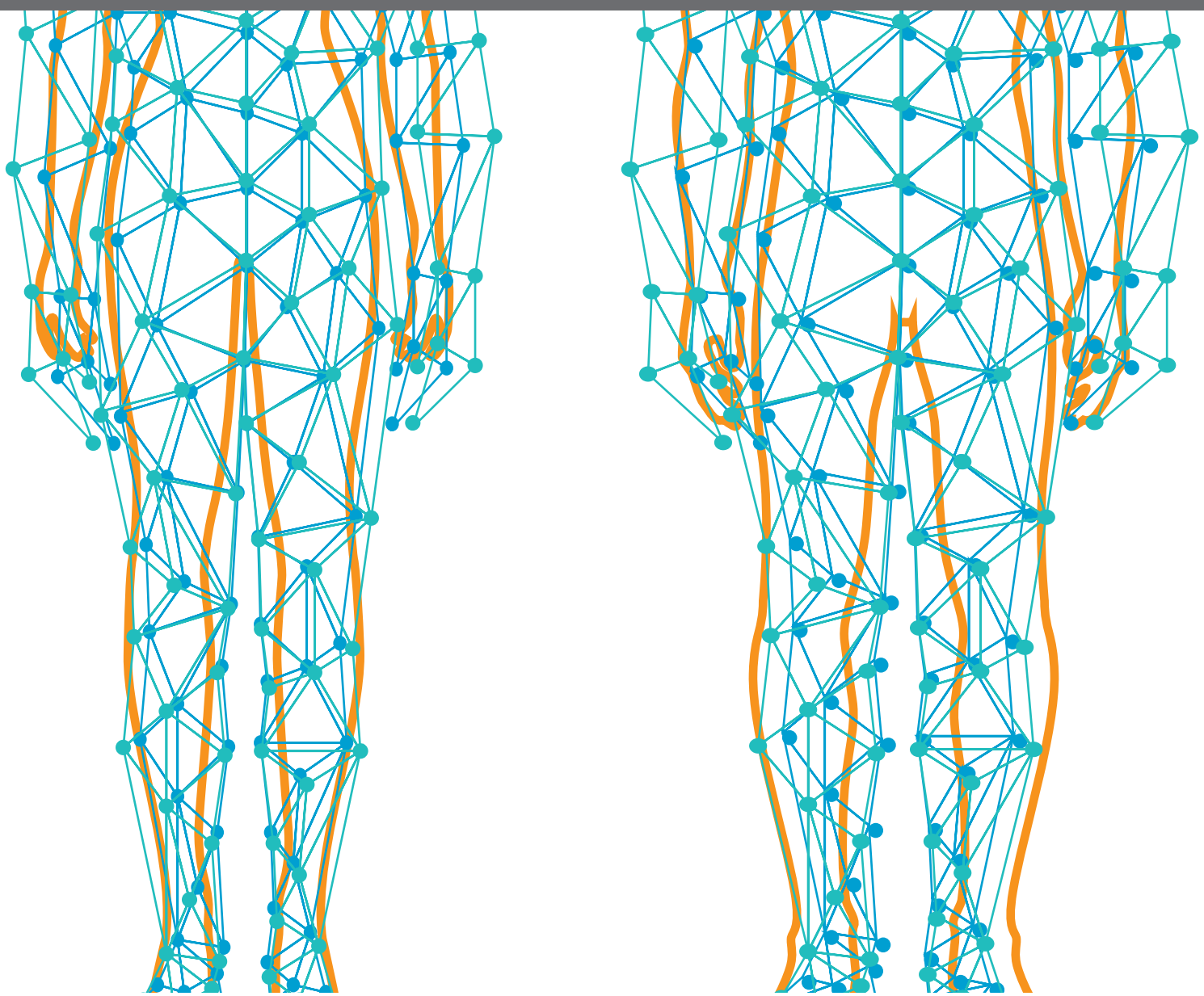

frontiers Research Topics

frontiers

ISSN 1664-8714
ISBN 978-2-88966-710-9
DOI 10.3389/978-2-88966-710-9

About Frontiers

Frontiers is more than just an open-access publisher of scholarly articles: it is a pioneering approach to the world of academia, radically improving the way scholarly research is managed. The grand vision of Frontiers is a world where all people have an equal opportunity to seek, share and generate knowledge. Frontiers provides immediate and permanent online open access to all its publications, but this alone is not enough to realize our grand goals.

Frontiers Journal Series

The Frontiers Journal Series is a multi-tier and interdisciplinary set of open-access, online journals, promising a paradigm shift from the current review, selection and dissemination processes in academic publishing. All Frontiers journals are driven by researchers for researchers; therefore, they constitute a service to the scholarly community. At the same time, the Frontiers Journal Series operates on a revolutionary invention, the tiered publishing system, initially addressing specific communities of scholars, and gradually climbing up to broader public understanding, thus serving the interests of the lay society, too.

Dedication to Quality

Each Frontiers article is a landmark of the highest quality, thanks to genuinely collaborative interactions between authors and review editors, who include some of the world's best academicians. Research must be certified by peers before entering a stream of knowledge that may eventually reach the public - and shape society; therefore, Frontiers only applies the most rigorous and unbiased reviews.
Frontiers revolutionizes research publishing by freely delivering the most outstanding research, evaluated with no bias from both the academic and social point of view. By applying the most advanced information technologies, Frontiers is catapulting scholarly publishing into a new generation.

What are Frontiers Research Topics?

Frontiers Research Topics are very popular trademarks of the Frontiers Journals Series: they are collections of at least ten articles, all centered on a particular subject. With their unique mix of varied contributions from Original Research to Review Articles, Frontiers Research Topics unify the most influential researchers, the latest key findings and historical advances in a hot research area! Find out more on how to host your own Frontiers Research Topic or contribute to one as an author by contacting the Frontiers Editorial Office: frontiersin.org/about/contact

MICROCIRCULATION GUIDED/ TARGETED RESUSCITATION

Topic Editors:
Inge Bauer, University Hospital of Düsseldorf, Germany
Mihály Boros, University of Szeged, Hungary

Citation: Bauer, I., Boros, M., eds. (2021). Microcirculation Guided/Targeted Resuscitation. Lausanne: Frontiers Media SA. doi: 10.3389/978-2-88966-710-9

Table of Contents

frontiers in Medicine

EDITORIAL
published: 08 March 2021
doi: 10.3389/fmed.2021.649828

Editorial: Microcirculation Guided/Targeted Resuscitation

Mihály Boros[1]* *and Inge Bauer*[2]

[1] *Faculty of Medicine, University of Szeged, Szeged, Hungary,* [2] *Department of Anaesthesiology, University Hospital of Düsseldorf, Düsseldorf, Germany*

Keywords: shock, microcirculation, mitochondria, resuscitation strategy, oxygen dynamics, hemodynamic coherence

Editorial on the Research Topic

Microcirculation Guided/Targeted Resuscitation

In 1740, Henri-François Le Dran, a French surgeon, observed and described a peculiar state of "*saissisement*," which commonly follows gunshot wounds. When his treatise was published in London in 1743, this French term was translated as "shock and agitation," the first noted description of a syndrome "*which suspends the laws of economy for a few moments*" (1). The 280 years since then have seen numerous advances in the mechanism and treatment of this condition through meticulous experimental and clinical research, and our current knowledge on shock categories is deeply rooted in the classical work of George Crile, William Bayliss, Walter Cannon, and Alfred Blalock, to name just a few of the exceptional scientists in the field. Today, their well-established tradition defines shock as circulatory failure, which results in inadequate cellular oxygen utilization and shock conditions, which are characterized by generalized hypoxia/dysoxia or by circulatory dysfunction leading to systemic hypoxia. Nevertheless, shock classifications once thought appropriate and shock mechanisms based on clinical etiologies have been revised numerous times, and today it is perhaps timely to point in new directions again, which would conceivably improve our understanding of this still deadly syndrome.

Of these directions, the importance of microcirculatory investigations should be highlighted first. Like the long evolutionary history of shock research itself, attempts to measure and characterize the performance of human microcirculation have spanned a number of decades, from the first reports on the use of capillary microscopy in 1916 (2) to the first handheld video microscope that provided real-time, dynamic observations at the bedside (3). With these incremental technical advances, it is now recognized that shock-induced peripheral microcirculatory responses are not always connected to macrocirculatory changes, and, likewise, macrohaemodynamic variables cannot always be relied upon to monitor the outcome of shock conditions. Therefore, according to our current understanding, the circulatory consequences of shock can be broadly categorized into those where the macrohaemodynamics are deranged and those where the microcirculation is malfunctioning.

Another related area to be explored in more detail is mitochondrial energetics. The human body employs a wide range of defense mechanisms which react to all types and levels of severity of external or internal insults that disrupt the physiological homeostasis, and, after various durations of compensation, the common denominator of shock states is the failure of energy production essential to maintaining a low-entropy intracellular state. Several reliable techniques are now available to measure the respiratory properties of mitochondria in cells, tissue fractions or whole tissue samples. Protocols for high-resolution respirometry

OPEN ACCESS

Edited by:
Borna Relja,
Otto von Guericke University, Germany

Reviewed by:
Niklas Franz,
Goethe University Frankfurt, Germany

***Correspondence:**
Mihály Boros
boros.mihaly@med.u-szeged.hu

Specialty section:
This article was submitted to Intensive Care Medicine and Anesthesiology, a section of the journal Frontiers in Medicine

Received: *05 January 2021*
Accepted: *17 February 2021*
Published: *08 March 2021*

Citation:
Boros M and Bauer I (2021) Editorial: Microcirculation Guided/Targeted Resuscitation. Front. Med. 8:649828. doi: 10.3389/fmed.2021.649828

offer sensitive analyses of oxidative phosphorylation and diagnostics for the pathophysiology of a wide array of mitochondrial dysfunctions and with a novel technique (introduced by Baumbach et al. in this issue) non-invasive *in vivo* mitoPO$_2$ measurement is also possible.

Substrates and carrier capacity are necessary for the mitochondrion to produce energy. According to this logic, the origins of irreversible, shock-related functional/structural defects should be located at the business end of the cardiovascular system, at the arteriolo-capillary and/or intracellular-mitochondrial junctions. Not surprisingly, the mechanisms of microcirculatory-mitochondrial failures are in the focus of renewed scientific interest. According to this unifying reasoning, whatever the etiology, microcirculatory failure is involved in the syndrome which we call "shock," and, whatever the mechanism, the mitochondria do not receive sufficient fuel to maintain the energy production necessary for a non-equilibrated cellular metabolic system. This approach may seem to be simplified, but at this stage we can introduce a newly coined term to describe the main components of shock-induced generalized derangements within the circulatory system. According to thought-provoking suggestions by Can Ince, the haemodynamic coherence between the macro- and microcirculation can be defined as "the condition in which resuscitation procedures aimed at the correction of systemic haemodynamic variables are effective in correcting regional and microcirculatory perfusion and oxygen delivery to the parenchymal cells such that the cells are able to perform their functional activities in support of organ function" (4). Most importantly, this interpretation can be expanded to cover the totality of shock pathophysiology, toward the central, macro-, micro-, and subcellular pieces of the patchwork. **Figure 1** shows a conceptual framework with connection points where the coherence between the main performers can be lost—and can also be rebuilt, starting from the central pumping station down to the subcellular oxygen dynamics and vice-versa. This might be true in the given coordinates, and, if we accept this holistic view, the final task of a researcher could be to determine the weight of each component in a given timeframe and in a given shock scenario so as to influence the completeness of the "uncoupled" process.

We felt especially privileged to write this editorial for a Research Topic that offered high-caliber articles, highlighting many advances in the field. Of the 11 publications, three can be considered to address mechanistic pathways, two to refine existing diagnostic methodologies, and six to improve our understanding of treatment options. In the next part, a brief background outlines the rationale for and novel findings of each study.

MECHANISM

The first article in this series is a thought-provoking paper by Merz et al., where the authors provide a very thorough discussion of a philosophical question (i.e., what to choose for resuscitation in shock conditions, the microcirculation or the mitochondria?) In this line, the review synthesizes our current knowledge of the technical background on how to measure microcirculation and mitochondrial function and the possibilities of microcirculation- or mitochondrion-directed therapies and the advantages and disadvantages of tailoring resuscitation protocols to one or another direction, while the authors remind us that none of the promising microvasculature- or mitochondrial-targeted pre-clinical therapeutic approaches have yet found their way into clinical practice. Readers will find this article of great interest as it presents an excellent review of a critical question and provides many clues, hints, and guidelines for the design of future therapies.

The next two articles are basic science papers that evaluate and further elucidate important mechanistic pathways. Luís et al. provide new insights into the involvement of circulating microRNAs (miRNAs) in endoplasmic reticulum (ER) stress and unfolded protein response (UPR). The authors identified 40 differently upregulated miRNAs in a rodent model of trauma-haemorrhagic shock, of which the vast majority was in close correlation with liver injury markers. Since extracellular vesicles carrying miRNAs have been identified as regulators of intercellular communication, data from these elegant studies indicate that miRNA profiles can provide a rationale for the development of novel therapeutic strategies.

A paper by Warenits et al. reports on the results of a long-term observation study of the pathomechanism of cerebral neurodegeneration caused by cardiac arrest and resuscitation. The authors analyzed several markers of gliosis and parameters of activation of inflammatory and cell-death pathways in the hippocampus and motor cortex in a clinically relevant animal model. Their data revealed decreased haem oxygenase (HO) activity in these brain regions 2 weeks after global ischemia, suggesting causality for HO or HO products in the delayed neurodegenerative processes in these vulnerable brain regions.

Diagnostics

Methane in the human body can originate in the gastrointestinal tract, and the reduction of mesenteric perfusion is among the first homeostatic responses during internal bleeding. This is the background for a basic science article by Bársony et al. which explored the diagnostic value of continuous, real-time detection of exhaled methane levels as compared to intravital sublingual microscopy, a clinical method already in use; the final goal was to recognize internal hemorrhage in a large animal model. The methane-based detection indicated the presence of bleeding at an early stage and closely followed changes in mesenteric perfusion during hemorrhage and resuscitation as well, with a diagnostic value comparable to the sublingual microcirculatory monitoring. The study therefore presents an interesting consideration for the development of future clinical trials.

A clinical article by Baumbach et al. reports on a novel non-invasive diagnostic device for an *in vivo* assessment of mitochondrial oxygen tension (mitoPO$_2$) in humans. The mitochondrial performance parameters were measured in the skin with the protoporphyrin IX-triplet state lifetime technique (PpIX-TSLT), with mitochondrial oxygen consumption changes closely related to gas exchange variables and blood gas parameters during cardiopulmonary exercise testing. As this device allows

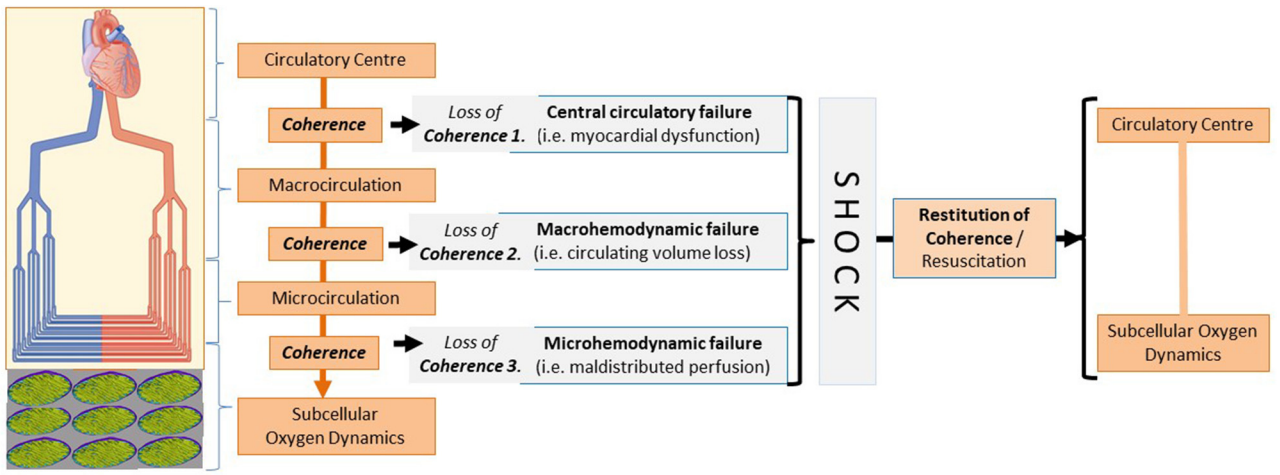

FIGURE 1 | Loss of coherence between the components of hemodynamics - leading to circulatory shock.

the direct measurement of oxygen metabolism on the cellular level, it could be a promising tool not only in high-performance sports, but in a clinical setting as well.

THERAPIES

Despite fairly extensive studies, the exact mechanistic details behind the side-effects of non-steroid anti-inflammatory drugs (NSAIDs) are not completely understood as yet. To address this, Herminghaus et al. investigated the concentration- and tissue-dependent effects of indomethacin on mitochondrial respiration in different organs, and the data revealed that indomethacin increases the efficacy of oxygen utilization of colonic mitochondria but uncouples hepatic mitochondria, predominantly through complex I. Taken together, the organ-specific, dose-dependent, and complex-specific effects of indomethacin warrant further confirmation with *in vivo* studies.

The next preclinical study focuses on a special subtype of shock. Rewarming victims of hypothermia is often accompanied by reduced cardiac output (CO) and decreased mean arterial blood pressure, which is termed "rewarming shock." Håheim et al. used a rat model instrumented for measurements of haemodynamic function and organ blood flow (OBF) during stable hypothermia and rewarming to document the effects of two pharmacologic strategies employing vasodilator or inodilator compounds. In terms of blood flow to the brain, both approaches were effective, while CO was elevated to different levels. Mechanistically, the findings indicated that increased vascular resistance is a central element in the complex pathophysiology of rewarming from hypothermia.

The tryptophan-L-kynurenine pathway has been implicated in many inflammatory disorders in the central nervous system, and elevated plasma levels of the glutamate receptor antagonist kynurenic acid (KYNA) have been reported in septic shock patients as well. The next basic science paper by Juhász et al. used a rodent model of intraabdominal sepsis to investigate whether the microcirculation and mitochondrial function is affected by exogenously administered KYNA or a synthetic analog. Both treatment protocols attenuated the deleterious consequences of oxidative/nitrosative stress and resulted in lower inflammatory mediator release. The synthetic KYNA analog SZR-72 markedly improved the key indices of mitochondrial function in liver homogenate after sepsis induction, but only KYNA ameliorated sepsis-related microcirculatory perfusion deficit (a reduction in capillary perfusion and an increase in perfusion heterogeneity), suggesting again a dissociation between the efficacy of mitochondrial and/or microcirculatory treatment strategies in sepsis.

Haemorrhagic shock is the leading cause of preventable death after severe traumas, and melatonin administration during resuscitation improved survival in animal models of haemorrhagic shock and polytrauma. In the next basic science study, Truse et al. tested whether the topical application of melatonin to the gastric mucosa may influence gastric microcirculation in the context of haemorrhagic shock. Melatonin application had no influence on macrohaemodynamic variables, but, besides anti-inflammatory and anti-oxidative actions, the authors demonstrated the significant modulation of the gastric microcirculatory oxygenation as a novel aspect of the tissue-protective effects of melatonin.

The anti-inflammatory potential of ethyl pyruvate (EtP) is associated with reduced systemic inflammation. In relation to trauma, using a clinically-relevant double-hit model of hemorrhage and blunt chest trauma, Dieteren et al. demonstrated a mechanism through which the organ-protective effects of EtP may be linked to the decreased systemic activation of circulating leukocytes. This important line of investigation supports the need for additional studies to further discern the specific dose- and time-dependent influence of EtP on post-traumatic inflammatory response and outcomes.

Traumas and surgeries often present significant challenges to providing accurate resuscitation when blood products or whole blood are not available. To address this anticipated medical need, many possibilities are explored employing solutions that carry oxygen as alternatives. Munoz et al. provided an excellent review of the microvascular pathophysiology of clinical and experimental haemorrhagic shock. The authors innovatively—and convincingly—suggest that the present focus on restoring blood volume and oxygen-carrying capacity should be redirected toward artificial blood substitutes which are designed to restore blood viscosity.

In summary, the studies presented here have provided a significantly greater understanding of the components of shock syndrome that affect critically ill and injured patients. We thank the authors for their original and thought-provoking contributions.

AUTHOR CONTRIBUTIONS

All authors listed have made a substantial, direct and intellectual contribution to the work, and approved it for publication.

REFERENCES

1. LeDran HF. *A Treatise or Reflections Driven from Practice on Gun-Shot Wounds*. London: J. Clarke (1743).
2. Weiss E. Beobachtung und mikrophotographische Darstellung der Hautkapillaren am lebenden Menschen. *Deutsch. Arch. f. klin. Med.* (1916) 119:1.
3. Groner W, Winkelman JW, Harris AG, Ince C, Bouma GJ, Messmer K, et al. Orthogonal polarization spectral imaging: a new method for study of the microcirculation. *Nat Med*. (1999) 5:1209–12.
4. Ince C. Hemodynamic coherence and the rationale for monitoring the microcirculation. *Crit Care.* (2015) 19(Suppl.3):S8. doi: 10.1186/cc14726

Conflict of Interest: The authors declare that the research was conducted in the absence of any commercial or financial relationships that could be construed as a potential conflict of interest.

frontiers in Medicine

PERSPECTIVE
published: 05 August 2020
doi: 10.3389/fmed.2020.00416

Microcirculation vs. Mitochondria—What to Target?

Tamara Merz[1], Nicole Denoix[2], Markus Huber-Lang[3], Mervyn Singer[4], Peter Radermacher[1] and Oscar McCook[1]*

[1] Institute for Anesthesiological Pathophysiology and Process Engineering, Ulm University Medical Center, Ulm, Germany, [2] Clinic for Psychosomatic Medicine and Psychotherapy, Ulm University Medical Center, Ulm, Germany, [3] Institute for Clinical and Experimental Trauma-Immunology, University Hospital of Ulm, Ulm, Germany, [4] Bloomsbury Institute for Intensive Care Medicine, University College London, London, United Kingdom

Circulatory shock is associated with marked disturbances of the macro- and microcirculation and flow heterogeneities. Furthermore, a lack of tissue adenosine trisphosphate (ATP) and mitochondrial dysfunction are directly associated with organ failure and poor patient outcome. While it remains unclear if microcirculation-targeted resuscitation strategies can even abolish shock-induced flow heterogeneity, mitochondrial dysfunction and subsequently diminished ATP production could still lead to organ dysfunction and failure even if microcirculatory function is restored or maintained. Preserved mitochondrial function is clearly associated with better patient outcome. This review elucidates the role of the microcirculation and mitochondria during circulatory shock and patient management and will give a viewpoint on the advantages and disadvantages of tailoring resuscitation to microvascular or mitochondrial targets.

Keywords: circulatory shock, oxidative stress, hypoxia, organ failure, inflammation

OPEN ACCESS

Edited by:
Mihaly Boros,
University of Szeged, Hungary

Reviewed by:
Eizo Watanabe,
Chiba University, Japan
Andrea Szabó,
University of Szeged, Hungary

****Correspondence:***
Tamara Merz
tamara.merz@uni-ulm.de

Specialty section:
This article was submitted to Intensive Care Medicine and Anesthesiology, a section of the journal Frontiers in Medicine

Received: *19 May 2020*
Accepted: *29 June 2020*
Published: *05 August 2020*

Citation:
Merz T, Denoix N, Huber-Lang M, Singer M, Radermacher P and McCook O (2020) Microcirculation vs. Mitochondria—What to Target? Front. Med. 7:416. doi: 10.3389/fmed.2020.00416

INTRODUCTION

Shock can be defined as the "*imbalance between oxygen supply and requirements*" (1). This imbalance can be due to "*inadequate O_2 transport*" resulting from "*hypovolemia,*" "*cardiogenic factors*" (e.g., myocardial infarction), "*obstruction*" (e.g., pulmonary embolism), and/or "*distributive shock*" (e.g., septic shock), which is characterized by "*decreased systemic vascular resistance and altered oxygen extraction*" (1). Hence, cellular hypoxia is central to shock pathophysiology. Current resuscitation strategies mainly address macrocirculatory targets to restore appropriate tissue perfusion, but achieving these targets does not necessarily result in improved microcirculatory perfusion, since there may be a marked dissociation between the former and the latter (2–4).

It is beyond any doubt that circulatory shock, no matter whether it is septic (5) or traumatic-hemorrhagic (i.e., hypovolemic) (6), is associated with marked disturbances of the microcirculation. Moreover, it is well-established that survivors present with improved markers of microcirculatory perfusion (7, 8). Nevertheless, it remains a matter of debate as to whether this is an epiphenomenon or a causal relationship, in other words, whether "*recruiting the microcirculation*" (9) or "*microvascular resuscitation*" (10) is the "*magic bullet*" that will improve survival after circulatory shock. This question still raises fairly equivocal viewpoints (9, 11, 12). Trezciak et al. (13) failed to demonstrate any relationship between changes in microcirculatory markers and the severity of organ failure. Furthermore, in resuscitated patients with septic shock, a direct relationship was noted between eventual outcome and skeletal muscle adenosine trisphosphate (ATP) (14), suggesting a perhaps more important role for cellular metabolic capacity compared

to microcirculatory O_2 supply, at least in sepsis. This review covers the respective roles of the microcirculation and mitochondria in circulatory shock (summarized in **Figure 1**), with a particular focus on traumatic-hemorrhagic vs. septic shock. It addresses the question as to whether altered mitochondrial respiration and subsequently diminished ATP production could still lead to organ dysfunction and failure, despite adequate tissue oxygenation, even if microcirculatory function is restored or maintained (15, 16).

EVIDENCE FOR IMPAIRED MICROCIRCULATORY PERFUSION DURING SHOCK

There is numerous experimental and clinical evidence for impaired microcirculatory perfusion during shock, no matter whether the origin is sepsis or trauma-hemorrhage (i.e., hypovolemic). In experimental animal models, impaired microcirculatory perfusion has been demonstrated using various techniques in the heart, kidney, liver, gut, and brain, even after resuscitation had restored the macrocirculatory hemodynamics (17–22).

The disturbance of the microcirculation is characterized by a markedly enhanced heterogeneity of blood flow comprising obstructed vessels, vessels with stagnant or intermittently on/off flow related to vasoconstriction, and vessels with an increased blood flow velocity (2). All these effects, together with an increased O_2 diffusion distance (e.g., due to tissue edema) and/or reduced systemic O_2 transport capacity (e.g., due to hemodilution) will result in impaired tissue O_2 availability (4). In fact, in the intestinal mucosa, increased O_2 extraction was directly related to the degree of these microcirculatory disturbances (23). Finally, the increased heterogeneity of the intestinal mucosal microcirculation, characterized by a substantial proportion of non-perfused capillaries, coincided with increased regional venous lactate/pyruvate ratios, a well-established marker for cellular dysoxia, and tissue acidosis (17).

This experimental evidence is supported by clinical observations. In a seminal study in stabilized septic patients, De Backer et al. (5) demonstrated the presence of marked microcirculatory disturbances characterized by a decreased density of perfused small vessels, and a large number of either non-perfused or only intermittently perfused vessels. While the proportion of perfused capillaries was not related to systemic macro-hemodynamics, it was significantly lower in non-survivors. This group (7, 24) and others have subsequently confirmed these findings in patients with sepsis (8, 25, 26) and following trauma-hemorrhage (6).

DOES "MICROVASCULAR RESUSCITATION" HELP?

Given the importance of an impaired microcirculation, "*microvascular resuscitation*" (10) or "*recruiting the microcirculation*" (9) has been advocated. Strikingly, few clinical studies have been published to date that integrate a microcirculation-targeted resuscitation into the study protocol. One, by Boerma et al. (27), found no outcome benefit from targeting the sublingual microcirculation with nitroglycerin. Whether such an approach may provide a "*magic bullet*" to improve survival after circulatory shock has generated conflicting views (9, 11, 12). This is in part due to the ongoing lack of readily accessible data from bedside techniques that assess the microcirculation, notwithstanding the conclusions of a recent consensus conference (28). Moreover, despite the undoubtedly existing impairment of microcirculatory perfusion in shock, the subsequent conclusion that tissue O_2 availability is reduced to a meaningful degree has been questioned, at least in resuscitated septic shock: in one study, not only was skeletal tissue PO_2 not reduced in such patients, but—in sharp contrast to patients with cardiac pump failure—was even higher than a healthy control group (29).

Any recruitment maneuver targeting the microcirculation will comprise two aspects, i.e., the "*(re-)opening*" of the capillary network (e.g., using fluid resuscitation, ino-dilation and restriction of vasoconstriction) and the subsequent attenuation of flow heterogeneity (summarized in **Figure 2A**) (2). Based on this rationale, fluid resuscitation (30–34), dobutamine (35), levosimendan (36), milrinone (37), nitric oxide (NO) donors (38–40), and prostacyclin (PGI_2) (40–42) have all been tested. In experimental settings, this approach was often successful but the majority of animal studies were only of short duration and/or did not include standard intensive care measures, which may limit transferability into clinical practice (43). Given the potential NO- or NO-derivatives induced uncoupling of mitochondrial respiration and inhibition of complex I and complex IV (14, 44–46), caution must be taken with NO-donors as a therapeutic strategy to avoid detrimental effects on the mitochondria. In longer-term, fluid-resuscitated large animal models, therapeutic interventions that attenuated shock-related cellular dysoxia (e.g., selective inhibition of the inducible NO synthase (iNOS), antioxidant infusion, therapeutic hyperoxia) revealed that any beneficial effect on the microcirculation coincided with improved parameters of inflammation, oxidative and nitrosative stress, and/or cellular metabolism (21, 47, 48). It thus remains unclear whether the beneficial effect on the microcirculation is the cause or the result of these responses. Indeed, neither selective iNOS inhibition nor infusion of the PGI_2 analog iloprost had any effect on the measured parameters of microcirculation at all, but still resulted in improved markers of cellular dysoxia (49, 50).

To date, the results of clinical interventional studies that have integrated monitoring of microcirculatory perfusion and oxygenation have failed to show a direct relationship between the effects of the respective intervention on the measured markers of microcirculation and either mortality and/or morbidity. For example, Ospina-Tascon et al. (51) found that fluid resuscitation (infusion of at least 1,000 ml Ringer's lactate or 400 ml 4% albumin solution) within the first 24 h of diagnosis of sepsis increased the fraction of perfused small vessels, and this effect was directly related to a decrease in lactate concentration. Beyond 48 h of diagnosis, no effect was observed (51).

Dobutamine can recruit the microcirculation in septic patients but, again, its effects were directly related to a decrease

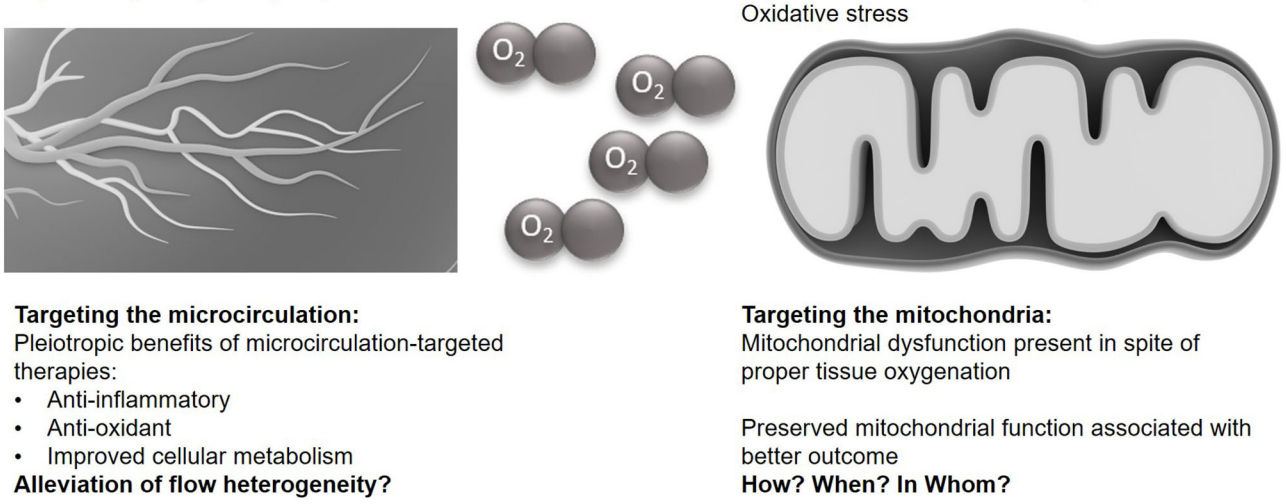

FIGURE 1 | The microvasculature and mitochondria in circulatory shock. Illustrations of the microcirculation and the mitochondrium are taken from the Library of Science and Medical Illustrations (somersault18:24, https://creativecommons.org/licenses/by-nc-sa/4.0/).

in lactate levels, rather than the individual macrocirculatory response (52). More recently, Hernandez et al. (53) failed to demonstrate any beneficial effect of dobutamine neither on the sublingual microcirculation nor on metabolic, hepatosplanchnic or peripheral perfusion parameters. Based on a theoretical benefit of vasodilating drugs (54–56) the use of NO releasing compounds has been investigated. Administration of nitroglycerin increased the perfusion of sublingual microvessels (57), but, as mentioned previously, continuous infusion over 24 h trended to a worse outcome in a study including 70 patients ($p = 0.08$) (27). Inhaling 40 ppm of NO over 6 h after initial resuscitation neither improved microcirculatory flow, lactate clearance, nor organ dysfunction, and no association was found between parameters of microcirculatory perfusion and organ dysfunction after initial resuscitation (13). Based on promising results with infusion of PGI_2 (or its analogs) (58, 59), a multicenter randomized controlled trial is currently under way in patients with septic shock and "persistent microperfusion defects" (I-MICRO, NCT03788837). However, it must be underscored that PGI_2 and its analogs have effects beyond those on the microcirculation (60), in particular with respect to cellular energy metabolism (61–65). Whether or not vasoconstrictors have deleterious effects on the microcirculation has also been recently questioned. In healthy volunteers, neither norepinephrine, phenylephrine nor vasopressin affected microcirculatory parameters prior to or after bolus injection of endotoxin, despite an immediate rise in blood pressure (66). Overall, a recent meta-analysis on the impact of vasoactive drugs on microcirculatory blood flow concluded that there is "*no robust evidence that any agent can lead to improved microvascular flow*" and that "*no study demonstrated outcome benefit*" (67).

EVIDENCE FOR CELLULAR ENERGETIC FAILURE RESULTING FROM REDUCED MITOCHONDRIAL RESPIRATORY ACTIVITY

Some two decades ago, the late Mitchell Fink created the term "*cytopathic hypoxia*" (68, 69). The above-detailed disturbances of the microcirculation could result in inadequate cellular O_2 supply as a reason for decreased ATP production and subsequent hyperlactatemia. Clearly, aggravation of microvascular heterogeneity with mismatch of the local O_2-transport/uptake relationship could explain at least in part, why the threshold of O_2 supply, below which hyperlactatemia occurs, is much higher during sepsis than under normal conditions (70, 71). In this context, the concept of cytopathic hypoxia (or, perhaps, more accurately, cytopathic dysoxia) attempts to reconcile the phenomenon that organ failure coincides with hardly any cell death, availability of oxygen at the cellular level, relatively minor inflammatory cell migration, and capacity of these failed organs to recover (72, 73). Cytopathic dysoxia refers to impaired ATP formation despite normal [or even supra-normal (20)] tissue PO_2 levels. It can result from several factors, for instance, diminished delivery of key substrates (e.g., pyruvate) into the tricarboxylic acid (TCA) cycle, inhibition of various TCA cycle or (in particular) electron transport chain enzymes such as Complexes I and IV (74, 75), and

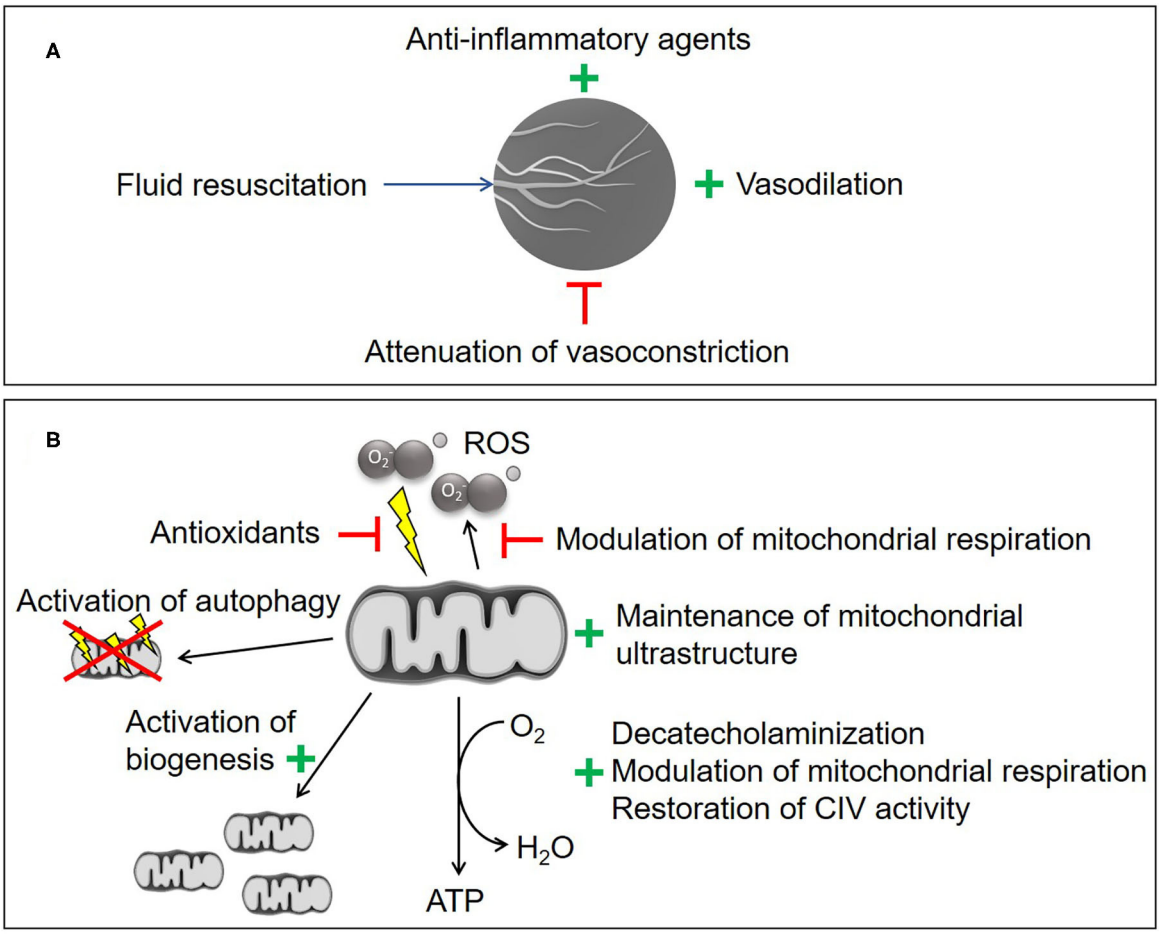

FIGURE 2 | Experimental therapeutic strategies. **(A)** Microvascular recruitment. **(B)** Mitochondrial protection and stimulation. CIV, cytochrome c oxidase; ROS, reactive oxygen species. Illustrations of the microcirculation and the mitochondrium are taken from the Library of Science and Medical Illustrations (somersault18:24, https://creativecommons.org/licenses/by-nc-sa/4.0/) .

uncoupling ["slipping" (76)] of the electron transport chain with a decrease in the proton gradient across the inner mitochondrial membrane resulting in production of heat rather than generation of ATP.

To date, the assessment of mitochondrial function is mostly limited to *ex vivo* methods, which might misrepresent the *in vivo* situation. A detailed discussion of available methods for *ex vivo* and *in vivo* mitochondrial measurements are beyond the scope of this paper, but have been recently compared by Bettink et al. (77), with a particular focus on the protoporphyrin IX-triplet state lifetime technique, which is applicable *in vivo* (78). However, in the light of the absolute values reported for the latter *in vivo* measurement technique, which range between 30 and 110 mmHg (77, 79), the results obtained with this method have to be interpreted with care. In contrast to these "mitochondrial" PO_2 levels, reports of tissue PO_2 measured with the Pd-phosphorescence quenching method typically range between 20 and 25 mmHg, with maximally 52 mmHg and even levels as low as 5 mmHg detected, which is the threshold for tissue to be considered anoxic (80). A steep O_2 pressure gradient is needed to facilitate O_2 diffusion from capillaries through the interstitium to cells/mitochondria. Thus, it is not surprising to see reports of intracellular PO_2 of no more than 1–10 mmHg (81). Mitochondrial ATP supply is stable over a wide range of intracellular PO_2, measured *ex vivo* by oxygraphy, and will only suffer if the mitochondrial PO_2 is lower than 0.1–0.5 mmHg (81). Thus, the values reported for mitoPO_2 of 30–110 mmHg may represent a mixture of PO_2 values from different compartments rather than solely mitoPO_2.

Despite these limitations in determining mitochondrial function, there is ample experimental evidence that reduced (disturbed) mitochondrial respiratory activity assumes crucial importance for shock-related organ dysfunction or failure, similar to the potential role of impaired microcirculatory perfusion and oxygenation. Several rodent studies that included resuscitation demonstrated hyperlactatemia despite unchanged or even increased tissue PO_2, and this coincided with both reduced function and structural damage to mitochondria (74,

82–85). Resuscitated models investigating higher species (cats, swine, baboons) and characterized by a normotensive and a normo- or even hyperdynamic circulation, confirmed these findings (20, 86–89). In this context, studies simultaneously recording parameters of both microcirculation and cellular O_2 utilization assume particular importance: LPS-challenged, fluid-resuscitated swine showed a reduced efficiency of hepatic mitochondrial respiration despite maintained liver surface laser Doppler blood flow (20). The same group however reported in a longer-term model, unchanged liver tissue mitochondrial resuscitation with a tendency toward enhanced microcirculatory blood flow (88). They undertook a meta-analysis reviewing both experimental models and clinical studies and reported variable results on mitochondrial function depending on the species, organ, and time point investigated (90). However, the available experimental literature mainly originates from young and otherwise healthy animals, which does not represent the more frequent clinical scenario of elderly patients with comorbidities, a common pitfall of experimental studies in shock research in general (43). Nevertheless, there is elegant clinical evidence that despite adequate resuscitation, reduced mitochondrial respiration is (i) present in patients after the initial management of circulatory shock, and (ii) associated with worse outcomes. In a landmark study in patients with septic shock, complex I activity was lower in non-survivors than in survivors; and corresponding tissue ATP content values mirrored this result (14). Moreover, complex I activity was inversely related to the mitochondrial antioxidant, glutathione, and directly related to nitrate/nitrite concentrations, suggesting a crucial role of oxidative and nitrosative stress in shock-related mitochondrial (dys)function. The same group subsequently demonstrated that impaired mitochondrial function coincided with a decrease in mitochondrial respiratory protein content in non-survivors. In contrast, survivors showed an early activation of mitochondrial biogenesis (91). A *post-hoc* analysis of the HYPER2S trial (92) in patients with sepsis-induced hypotension found that hyperoxia during the first 24 h of treatment increased mortality rate at day 28 ($p = 0.054$) in hyperlactatemic patients, whereas in those with lactate levels $\leq$ 2 mmol/L there was no effect on mortality or morbidity. Since hyperoxia increases tissue O_2 partial pressure, even under conditions of profound reduction of O_2 supply (93), this finding implicitly suggests that outcome of septic shock is associated with impaired cellular O_2 utilization rather than microcirculatory O_2 availability, possibly due to aggravated oxidative and nitrosative stress (94).

DOES "MITOCHONDRIAL RESUSCITATION" HELP?

Multiple mitochondria-targeted therapeutic strategies have been proposed (summarized in **Figure 2B**) (95–98). Despite several promising experimental therapies, there are currently no clinically-approved strategies for mitochondrial protection. Metformin has been shown to be beneficial for the attenuation of mitochondrial transition pore opening (99), stimulation of mitochondrial biogenesis and reduction of mitochondrial ROS production, but has to be used with caution in shock patients due to its potentially severe side effects, i.e., renal impairment, and lactic acidosis (100).

In contrast, the glucose-lowering compound Imeglimine, though to date only tested experimentally, has none of the side effects as metformin, but inhibited mitochondrial permeability transition, improved mitochondrial function, and was associated with less acidosis (100, 101). The inhibition of the mitochondrial permeability transition pore with cyclosporine A showed promise in a pre-clinical sepsis model and a large-animal model of traumatic brain injury (102, 103). In humans, cyclosporine A did not show a benefit in cardiac arrest and acute myocardial infarct (104, 105), and it was never clinically approved for the treatment of any type of circulatory shock.

Given the above-mentioned role of oxidative and nitrosative stress, mitochondria-targeted antioxidant strategies and manipulation of shock-related excess formation of nitric oxide (NO) and/or peroxynitrite ($ONOO^-$) have been suggested but so far, despite promising results even in clinically relevant, resuscitated large animal models (47, 48, 106–110), none have made their way into clinical practice. Other strategies have targeted restoration of cytochrome-c-oxidase (Complex IV) activity (111, 112), maintenance of mitochondrial inner membrane integrity (113), activation of autophagy to clear damaged mitochondria to promote biogenesis (114), direct activation of mitochondrial biogenesis (95), and modulation of mitochondrial respiration using gaseous mediators (115, 116). To date, only experimental evidence is available for all of the latter strategies. In contrast, tight blood glucose control preserved both mitochondrial function and ultrastructure, and, thereby, attenuated organ dysfunction independently of organ perfusion in a rabbit model of prolonged critical illness (85). The protective effect of this strategy was associated with better maintenance of mitochondrial activity and morphological integrity in patients (117).

In the context of mitochondrial dysfunction-induced organ failure, the "*decatecholaminization*" paradigm (118, 119) may assume particular importance. It is well-established that catecholamines, beyond their effects of hemodynamics, have profound immune- and metabolism-modulating properties (120, 121), ultimately resulting in "*metabolic stress*" (122), the degree of which is directly related to their β-adrenergic activity (123). Catecholamines inhibit cellular respiration *in vitro* in a dose-dependent manner (124, 125). In clinically relevant, resuscitated, large animal models, the degree of impaired mitochondrial respiration and, ultimately, organ dysfunction was directly related to the norepinephrine infusion rates required to achieve hemodynamic targets (55, 89). It is tempting to speculate that this finding is related to the well-known norepinephrine-related aggravation of oxidative (126, 127) and nitrosative stress: in patients, nitrite/nitrate concentrations were inversely related to both tissue complex I activity and glutathione concentrations, but directly related to

norepinephrine requirements which, in turn, coincided with low complex I activities (14).

CONCLUSION

Both microvascular and mitochondrial alterations are consequences of circulatory shock and associated with worse outcomes. However, none of the promising microvasculature- or mitochondrial-targeted pre-clinical therapeutic approaches have yet translated to clinical practice. The challenges of assessing microvascular and/or mitochondrial function in patients limit the current understanding in this field. Simultaneous measurements of both parameters, such as recently performed by Rutai et al. (128) in a pre-clinical study, might help to alleviate this issue. To date, it remains unclear whether any of the microcirculation therapies currently under investigation will be successful in abolishing shock-induced flow heterogeneity, rather than having beneficial effects through their anti-inflammatory and/or anti-oxidant properties. Similarly, mitochondrial dysfunction may result in organ failure despite adequate tissue perfusion and oxygenation. Therefore, a crucial question to address in the future is: how, when and in whom should we protect/support the mitochondria?

DATA AVAILABILITY STATEMENT

The original contributions presented in the study are included in the article/supplementary material, further inquiries can be directed to the corresponding author/s.

AUTHOR CONTRIBUTIONS

PR envisioned, drafted, and corrected the final version of the manuscript. TM drafted, created the figures, and edited the final version of the manuscript. MS contributed to the draft and edited the final version of the manuscript. ND, OM, and MH-L edited the manuscript. All authors read and approved the final version.

FUNDING

TM, PR, and MH-L received funding of the Deutsche Forschungsgemeinschaft (DFG, German Research Foundation)—Project-ID 251293561—Collaborative Research Center (CRC) 1149. PR received funding of the Deutsche Forschungsgemeinschaft (DFG, German Research Foundation) and GRK 2203 (PulmoSens).

REFERENCES

1. Vincent JL, De Backer D. Circulatory shock. *N Engl J Med.* (2013) 369:1726–34. doi: 10.1056/NEJMra1208943
2. Elbers PW, Ince C. Mechanisms of critical illness–classifying microcirculatory flow abnormalities in distributive shock. *Crit Care.* (2006) 10:221. doi: 10.1186/cc4969
3. De Backer D, Ortiz JA, Salgado D. Coupling microcirculation to systemic hemodynamics. *Curr Opin Crit Care.* (2010) 16:250–4. doi: 10.1097/MCC.0b013e3283383621
4. Ince C, Guerci P. Why and when the microcirculation becomes disassociated from the macrocirculation. *Intensive Care Med.* (2016) 42:1645–6. doi: 10.1007/s00134-016-4494-1
5. De Backer D, Creteur J, Preiser JC, Dubois MJ, Vincent JL. Microvascular blood flow is altered in patients with sepsis. *Am J Respir Crit Care Med.* (2002) 166:98–104. doi: 10.1164/rccm.200109-016OC
6. Hutchings SD, Naumann DN, Hopkins P, Mellis C, Riozzi P, Sartini S, et al. Microcirculatory impairment is associated with multiple organ dysfunction following traumatic hemorrhagic shock: The MICROSHOCK Study. *Crit Care Med.* (2018) 46:e889–96. doi: 10.1097/CCM.0000000000003275
7. De Backer D, Donadello K, Sakr Y, Ospina-Tascon G, Salgado D, Scolletta S, et al. Microcirculatory alterations in patients with severe sepsis: impact of time of assessment and relationship with outcome. *Crit Care Med.* (2013) 41:791–9. doi: 10.1097/CCM.0b013e3182742e8b
8. Massey MJ, Hou PC, Filbin M, Wang H, Ngo L, Huang DT, et al. Microcirculatory perfusion disturbances in septic shock: results from the ProCESS trial. *Crit Care.* (2018). 22:308. doi: 10.1186/s13054-018-2240-5
9. Legrand M, Ait-Oufella H, Ince C. Could resuscitation be based on microcirculation data? Yes. *Intensive Care Med.* (2018) 44:944–6. doi: 10.1007/s00134-018-5121-0
10. Bateman RM, Walley KR. Microvascular resuscitation as a therapeutic goal in severe sepsis. *Crit Care.* (2005) 9(Suppl. 4):S27–32. doi: 10.1186/cc3756
11. Monnet X, Saugel B. Could resuscitation be based on microcirculation data? We are not sure. *Intensive Care Med.* (2018) 44:950–3. doi: 10.1007/s00134-018-5180-2
12. Naumann DN, Lima A. Could resuscitation be based on microcirculation data? No. *Intensive Care Med.* (2018) 44:947–9. doi: 10.1007/s00134-018-5095-y
13. Trzeciak S, Glaspey LJ, Dellinger RP, Durflinger P, Anderson K, Dezfulian C, et al. Randomized controlled trial of inhaled nitric oxide for the treatment of microcirculatory dysfunction in patients with sepsis. *Crit Care Med.* (2014) 42:2482–92. doi: 10.1097/CCM.0000000000000549
14. Brealey D, Brand M, Hargreaves I, Heales S, Land J, Smolenski R, et al. Association between mitochondrial dysfunction and severity and outcome of septic shock. *Lancet.* (2002) 360:219–23. doi: 10.1016/S0140-6736(02)09459-X
15. Bar-Or D, Carrick MM, Mains CW, Rael LT, Slone D, Brody EN. Sepsis, oxidative stress, and hypoxia: are there clues to better treatment? *Redox Rep.* (2015) 20:193–7. doi: 10.1179/1351000215Y.0000000005
16. Østergaard L, Granfeldt A, Secher N, Tietze A, Iversen NK, Jensen MS, et al. Microcirculatory dysfunction and tissue oxygenation in critical illness. *Acta Anaesthesiol Scand.* (2015) 59:1246–59. doi: 10.1111/aas.12581
17. Tugtekin IF, Radermacher P, Theisen M, Matejovic M, Stehr A, Ploner F, et al. Increased ileal-mucosal-arterial PCO2 gap is associated with impaired villus microcirculation in endotoxic pigs. *Intensive Care Med.* (2001) 27:757–66. doi: 10.1007/s001340100871
18. Benes J, Chvojka J, Sykora R, Radej J, Krouzecky A, Novak I, et al. Searching for mechanisms that matter in early septic acute kidney injury: an experimental study. *Crit Care.* (2011) 15:R256. doi: 10.1186/cc10517
19. Chvojka J, Sykora R, Krouzecky A, Radej J, Varnerova V, Karvunidis T, et al. Renal haemodynamic, microcirculatory, metabolic and histopathological responses to peritonitis-induced septic shock in pigs. *Crit Care.* (2008) 12:R164. doi: 10.1186/cc7164
20. Porta F, Takala J, Weikert C, Bracht H, Kolarova A, Lauterburg BH, et al. Effects of prolonged endotoxemia on liver, skeletal muscle and kidney mitochondrial function. *Crit Care.* (2006) 10:R118. doi: 10.1186/cc5013
21. He X, Su F, Xie K, Taccone FS, Donadello K, Vincent JL. Should hyperoxia be avoided during sepsis? An experimental study in ovine peritonitis. *Crit Care Med.* (2017) 45:e1060–7. doi: 10.1097/CCM.0000000000002524
22. Taccone FS, Su F, De Deyne C, Abdellhai A, Pierrakos C, He X, et al. Sepsis is associated with altered cerebral microcirculation and tissue

hypoxia in experimental peritonitis. *Crit Care Med.* (2014) 42:e114–22. doi: 10.1097/CCM.0b013e3182a641b8
23. Ellis CG, Bateman RM, Sharpe MD, Sibbald WJ, Gill R. Effect of a maldistribution of microvascular blood flow on capillary O(2) extraction in sepsis. *Am J Physiol Heart Circ Physiol.* (2002) 282:H156–64. doi: 10.1152/ajpheart.2002.282.1.H156
24. Sakr Y, Dubois MJ, De Backer D, Creteur J, Vincent JL. Persistent microcirculatory alterations are associated with organ failure and death in patients with septic shock. *Crit Care Med.* (2004) 32:1825–31. doi: 10.1097/01.CCM.0000138558.16257.3F
25. Trzeciak S, Dellinger RP, Parrillo JE, Guglielmi M, Bajaj J, Abate NL, et al. Microcirculatory alterations in resuscitation and shock investigators. early microcirculatory perfusion derangements in patients with severe sepsis and septic shock: relationship to hemodynamics, oxygen transport, and survival. *Ann Emerg Med.* (2007). 49:88–98, 98.e1–2. doi: 10.1016/j.annemergmed.2006.08.021
26. Trzeciak S, McCoy JV, Phillip Dellinger R, Arnold RC, Rizzuto M, Abate NL, et al. Microcirculatory alterations in resuscitation and Shock (MARS) investigators. Early increases in microcirculatory perfusion during protocol-directed resuscitation are associated with reduced multi-organ failure at 24 h in patients with sepsis. *Intensive Care Med.* (2008) 34:2210–7. doi: 10.1007/s00134-008-1193-6
27. Boerma EC, Koopmans M, Konijn A, Kaiferova K, Bakker AJ, van Roon EN, et al. Effects of nitroglycerin on sublingual microcirculatory blood flow in patients with severe sepsis/septic shock after a strict resuscitation protocol: a double-blind randomized placebo controlled trial. *Crit Care Med.* (2010) 38:93–100. doi: 10.1097/CCM.0b013e3181b02fc1
28. Ince C, Boerma EC, Cecconi M, De Backer D, Shapiro NI, Duranteau J, et al. Second consensus on the assessment of sublingual microcirculation in critically ill patients: results from a task force of the european society of intensive care medicine. *Intensive Care Med.* (2018) 44:281–99. doi: 10.1007/s00134-018-5070-7
29. Boekstegers P1, Weidenhöfer S, Kapsner T, Werdan K. Skeletal muscle partial pressure of oxygen in patients with sepsis. *Crit Care Med.* (1994) 22:640–50. doi: 10.1097/00003246-199404000-00021
30. Obonyo NG, Fanning JP, Ng AS, Pimenta LP, Shekar K, Platts DG, et al. Effects of volume resuscitation on the microcirculation in animal models of lipopolysaccharide sepsis: a systematic review. *Intensive Care Med Exp.* (2016) 4:38. doi: 10.1186/s40635-016-0112-3
31. Hutchings S, Naumann DN, Harris T, Wendon J, Midwinter MJ. Observational study of the effects of traumatic injury, haemorrhagic shock and resuscitation on the microcirculation: a protocol for the MICROSHOCK study. *BMJ Open.* (2016) 6:e010893. doi: 10.1136/bmjopen-2015-010893
32. Orbegozo D, Su F, Santacruz C, He X, Hosokawa K, Creteur J, et al. Effects of different crystalloid solutions on hemodynamics, peripheral perfusion, and the microcirculation in experimental abdominal sepsis. *Anesthesiology.* (2016) 125:744–54. doi: 10.1097/ALN.0000000000001273
33. Ferrara G, Kanoore Edul VS, Caminos Eguillor JF, Buscetti MG, Canales HS, Lattanzio B, et al. Effects of fluid and norepinephrine resuscitation in a sheep model of endotoxin shock and acute kidney injury. *J Appl Physiol.* (2019). 127:788–97. doi: 10.1152/japplphysiol.00172.2019
34. Arnemann PH, Hessler M, Kampmeier T, Seidel L, Malek Y, Van Aken H, et al. Resuscitation with hydroxyethyl starch maintains hemodynamic coherence in ovine hemorrhagic shock. *Anesthesiology.* (2020) 132:131–9. doi: 10.1097/ALN.0000000000002998
35. Ospina-Tascón GA, García Marin AF, Echeverri GJ, Bermudez WF, Madriñán-Navia H, Valencia JD, et al. Effects of dobutamine on intestinal microvascular blood flow heterogeneity and O2 extraction during septic shock. *J Appl Physiol.* (2017). 122:1406–17. doi: 10.1152/japplphysiol.00886.2016
36. Fries M, Ince C, Rossaint R, Bleilevens C, Bickenbach J, Rex S, et al. Levosimendan but not norepinephrine improves microvascular oxygenation during experimental septic shock. *Crit Care Med.* (2008) 36:1886–91. doi: 10.1097/CCM.0b013e31817cede9
37. de Miranda ML, Pereira SJ, Santos AO, Villela NR, Kraemer-Aguiar LG, Bouskela E. Milrinone attenuates arteriolar vasoconstriction and capillary perfusion deficits on endotoxemic hamsters. *PLoS ONE.* (2015) 10:e0117004. doi: 10.1371/journal.pone.0117004
38. Johannes T, Mik EG, Klingel K, Goedhart PT, Zanke C, Nohé B, et al. Effects of 1400W and/or nitroglycerin on renal oxygenation and kidney function during endotoxaemia in anaesthetized rats. *Clin Exp Pharmacol Physiol.* (2009) 36:870–9. doi: 10.1111/j.1440-1681.2009.05204.x
39. Siegemund M, Van Bommel J, Sinaasappel M, Schwarte LA, Studer W, Girard T, et al. The NO donor SIN-1 improves intestinal-arterial P(CO(2)) gap in experimental endotoxemia: an animal study. *Acta Anaesthesiol Scand.* (2007) 51:693–700. doi: 10.1111/j.1399-6576.2007.01334.x
40. Johannes T, Ince C, Klingel K, Unertl KE, Mik EG. Iloprost preserves renal oxygenation and restores kidney function in endotoxemia-related acute renal failure in the rat. *Crit Care Med.* (2009) 37:1423–32. doi: 10.1097/CCM.0b013e31819b5f4e
41. Truse R, Hinterberg J, Schulz J, Herminghaus A, Weber A, Mettler-Altmann T, et al. Effect of topical iloprost and nitroglycerin on gastric microcirculation and barrier function during hemorrhagic shock in dogs. *J Vasc Res.* (2017) 54:109–121. doi: 10.1159/000464262
42. Lehmann C, König JP, Dettmann J, Birnbaum J, Kox WJ. Effects of iloprost, a stable prostacyclin analog, on intestinal leukocyte adherence and microvascular blood flow in rat experimental endotoxemia. *Crit Care Med.* (2001) 29:1412–6. doi: 10.1097/00003246-200107000-00019
43. Guillon A, Preau S, Aboab J, Azabou E, Jung B, Silva S, et al. Preclinical septic shock research: why we need an animal ICU. *Ann Intensive Care.* (2019). 9:66. doi: 10.1186/s13613-019-0543-6
44. Brown GC. Regulation of mitochondrial respiration by nitric oxide inhibition of cytochrome c oxidase. *Biochim Biophys Acta.* (2001) 1504:46–57. doi: 10.1016/S0005-2728(00)00238-3
45. Sarti P, Forte E, Mastronicola D, Giuffrè A, Arese M. Cytochrome C oxidase and nitric oxide in action: molecular mechanisms and pathophysiological implications. *Biochim Biophys Acta.* (2012) 1817:610–9. doi: 10.1016/j.bbabio.2011.09.002
46. Poderoso JJ, Helfenberger K, Poderoso C. The effect of nitric oxide on mitochondrial respiration. *Nitric Oxide.* (2019) 88:61–72. doi: 10.1016/j.niox.2019.04.005
47. Matejovic M, Krouzecky A, Martinkova V, Rokyta R Jr, Kralova H, Treska V, et al. Selective inducible nitric oxide synthase inhibition during long-term hyperdynamic porcine bacteremia. *Shock.* (2004) 21:458–65. doi: 10.1097/00024382-200405000-00010
48. Matejovic M, Krouzecky A, Martinkova V, Rokyta R Jr, Radej J, Kralova H, et al. Effects of tempol, a free radical scavenger, on long-term hyperdynamic porcine bacteremia. *Crit Care Med.* (2005) 33:1057–63. doi: 10.1097/01.CCM.0000162927.94753.63
49. Pittner A, Nalos M, Asfar P, Yang Y, Ince C, Georgieff M, et al. Mechanisms of inducible nitric oxide synthase (iNOS) inhibition-related improvement of gut mucosal acidosis during hyperdynamic porcine endotoxemia. *Intensive Care Med.* (2003) 29:312–6. doi: 10.1007/s00134-002-1577-y
50. Träger K, Matejovic M, Zülke C, Vlatten A, Vogt J, Wachter U, et al. Hepatic O2 exchange and liver energy metabolism in hyperdynamic porcine endotoxemia: effects of iloprost. *Intensive Care Med.* (2000) 26:1531–9. doi: 10.1007/s001340000645
51. Ospina-Tascon G, Neves AP, Occhipinti G, Donadello K, Büchele G, Simion D, et al. Effects of fluids on microvascular perfusion in patients with severe sepsis. *Intensive Care Med.* (2010) 36:949–55. doi: 10.1007/s00134-010-1843-3
52. De Backer D, Creteur J, Dubois MJ, Sakr Y, Koch M, Verdant C, et al. The effects of dobutamine on microcirculatory alterations in patients with septic shock are independent of its systemic effects. *Crit Care Med.* (2006) 34:403–8. doi: 10.1097/01.CCM.0000198107.61493.5A
53. Hernandez G, Bruhn A, Luengo C, Regueira T, Kattan E, Fuentealba A, et al. Effects of dobutamine on systemic, regional and microcirculatory perfusion parameters in septic shock: a randomized, placebo-controlled, double-blind, crossover study. *Intensive Care Med.* (2013) 39:1435–43. doi: 10.1007/s00134-013-2982-0
54. Buwalda M, Ince C. Opening the microcirculation: can vasodilators be useful in sepsis? *Intensive Care Med.* (2002) 28:1208–17. doi: 10.1007/s00134-002-1407-2
55. Corrêa TD, Pereira AJ, Brandt S, Vuda M, Djafarzadeh S, Takala J, et al. Time course of blood lactate levels, inflammation, and

mitochondrial function in experimental sepsis. *Crit Care.* (2017) 21:105. doi: 10.1186/s13054-017-1691-4
56. Legrand M, De Backer D, Dépret F, Ait-Oufella H. Recruiting the microcirculation in septic shock. *Ann Intensive Care.* (2019) 9:102. doi: 10.1186/s13613-019-0581-0
57. Spronk PE, Ince C, Gardien MJ, Mathura KR, Oudemans-van Straaten HM, Zandstra DF. Nitroglycerin in septic shock after intravascular volume resuscitation. *Lancet.* (2002) 360:1395–6. doi: 10.1016/S0140-6736(02)11393-6
58. Pittet JF, Lacroix JS, Gunning K, Laverriere MC, Morel DR, Suter PM. Prostacyclin but not phentolamine increases oxygen consumption and skin microvascular blood flow in patients with sepsis and respiratory failure. *Chest.* (1990) 98:1467–72. doi: 10.1378/chest.98.6.1467
59. Dépret F1, Sitbon A, Soussi S, De Tymowski C, Blet A, Fratani A, et al. Intravenous iloprost to recruit the microcirculation in septic shock patients? *Intensive Care Med.* (2018) 44:121–2. doi: 10.1007/s00134-017-4935-5
60. De Backer D. Is there a place for prostacyclin in the treatment of septic shock? *Intensive Care Med.* (2001) 27:1110–2. doi: 10.1007/s001340100988
61. Bihari DJ. Indomethacin and arterial oxygenation in critically ill patients with severe bacterial pneumonia. *Lancet.* (1987) 1:755. doi: 10.1016/S0140-6736(87)90405-3
62. Scheeren T, Susanto F, Reinauer H, Tarnow J, Radermacher P. Prostacyclin improves glucose utilization in patients with sepsis. *J Crit Care.* (1994) 9:175–84. doi: 10.1016/0883-9441(94)90014-0
63. Radermacher P, Buhl R, Santak B, Klein M, Kniemeyer HW, Becker H, et al. The effects of prostacyclin on gastric intramucosal pH in patients with septic shock. *Intensive Care Med.* (1995) 21:414–21. doi: 10.1007/BF01707410
64. Eichelbrönner O, Reinelt H, Wiedeck H, Mezödy M, Rossaint R, Georgieff M, et al. Aerosolized prostacyclin and inhaled nitric oxide in septic shock–different effects on splanchnic oxygenation? *Intensive Care Med.* (1996) 22:880–7. doi: 10.1007/BF02044111
65. Kiefer P, Tugtekin I, Wiedeck H, Bracht H, Vogt J, Wachter U, et al. Hepato-splanchnic metabolic effects of the stable prostacyclin analogue iloprost in patients with septic shock. *Intensive Care Med.* (2001) 27:1179–86. doi: 10.1007/s001340100954
66. van Loon LM, Stolk RF, van der Hoeven JG, Veltink PH, Pickkers P, Lemson J, et al. Effect of vasopressors on the macro- and microcirculation during systemic inflammation in humans *in vivo*. *Shock.* (2020) 53:171–4. doi: 10.1097/SHK.0000000000001357
67. Potter EK, Hodgson L, Creagh-Brown B, Forni LG. Manipulating the microcirculation in sepsis - the impact of vasoactive medications on microcirculatory blood flow: a systematic review. *Shock.* (2019) 52:5–12. doi: 10.1097/SHK.0000000000001239
68. Fink M. Cytopathic hypoxia in sepsis. *Acta Anaesthesiol Scand Suppl.* (1997) 110:87–95. doi: 10.1111/j.1399-6576.1997.tb05514.x
69. Fink MP. Bench-to-bedside review: cytopathic hypoxia. *Crit Care.* (2002) 6:491–9. doi: 10.1186/cc1824
70. Curtis SE, Cain SM. Regional and systemic oxygen delivery/uptake relations and lactate flux in hyperdynamic, endotoxin-treated dogs. *Am Rev Respir Dis.* (1992) 145:348–54. doi: 10.1164/ajrccm/145.2_Pt_1.348
71. Suetrong B, Walley KR. Lactic acidosis in sepsis: it's not all anaerobic: implications for diagnosis and management. *Chest.* (2016) 149:252–61. doi: 10.1378/chest.15-1703
72. Hotchkiss RS, Swanson PE, Freeman BD, Tinsley KW, Cobb JP, Matuschak GM, et al. Apoptotic cell death in patients with sepsis, shock, and multiple organ dysfunction. *Crit Care Med.* (1999) 27:1230–51. doi: 10.1097/00003246-199907000-00002
73. Takasu O, Gaut JP, Watanabe E, To K, Fagley RE, Sato B, et al. Mechanisms of cardiac and renal dysfunction in patients dying of sepsis. *Am J Respir Crit Care Med.* (2013) 187:509–17. doi: 10.1164/rccm.201211-1983OC
74. Brealey D, Karyampudi S, Jacques TS, Novelli M, Stidwill R, Taylor V, et al. Mitochondrial dysfunction in a long-term rodent model of sepsis and organ failure. *Am J Physiol Regul Integr Comp Physiol.* (2004) 286:R491–7. doi: 10.1152/ajpregu.00432.2003
75. Levy RJ, Deutschman CS. Cytochrome c oxidase dysfunction in sepsis. *Crit Care Med.* (2007) 35(Suppl. 9):S468–75. doi: 10.1097/01.CCM.0000278604.93569.27
76. Leverve XM. Mitochondrial function and substrate availability. *Crit Care Med.* (2007) 35(Suppl. 9):S454–60. doi: 10.1097/01.CCM.0000278044.19217.73
77. Wefers Bettink MA, Harms FA, Dollee N, Specht PAC, Raat NJH, Schoonderwoerd GC, et al. Non-invasive versus *ex vivo* measurement of mitochondrial function in an endotoxemia model in rat: toward monitoring of mitochondrial therapy. *Mitochondrion.* (2020) 50:149–57. doi: 10.1016/j.mito.2019.11.003
78. Mik EG. Special article: measuring mitochondrial oxygen tension: from basic principles to application in humans. *Anesth Analg.* (2013) 117:834–46. doi: 10.1213/ANE.0b013e31828f29da
79. Neu C, Baumbach P, Plooij AK, Skitek K, Götze J, von Loeffelholz C, et al. Non-invasive assessment of mitochondrial oxygen metabolism in the critically ill patient using the protoporphyrin IX-triplet state lifetime technique-a feasibility study. *Front Immunol.* (2020) 11:757. doi: 10.3389/fimmu.2020.00757
80. Tsai AG, Johnson PC, Intaglietta M. Is the distribution of tissue pO(2) homogeneous? *Antioxid Redox Signal.* (2007) 9:979–84. doi: 10.1089/ars.2007.1633
81. Connett RJ, Honig CR, Gayeski TE, Brooks GA. Defining hypoxia: a systems view of VO2, glycolysis, energetics, and intracellular PO2. *J Appl Physiol (1985).* (1990) 68:833–42. doi: 10.1152/jappl.1990.68.3.833
82. Merz T, Vogt JA, Wachter U, Calzia E, Szabo C, Wang R, et al. Impact of hyperglycemia on cystathionine-γ-lyase expression during resuscitated murine septic shock. *Intensive Care Med Exp.* (2017) 5:30. doi: 10.1186/s40635-017-0140-7
83. Arulkumaran N, Pollen S, Greco E, Courtneidge H, Hall AM, Duchen MR, et al. Renal tubular cell mitochondrial dysfunction occurs despite preserved renal oxygen delivery in experimental septic acute kidney injury. *Crit Care Med.* (2018) 46:e318–25. doi: 10.1097/CCM.0000000000002937
84. Rosser BG, Gores GJ. Liver cell necrosis: cellular mechanisms and clinical implications. *Gastroenterology.* (1995) 108:252–75. doi: 10.1016/0016-5085(95)90032-2
85. Vanhorebeek I, Gunst J, Ellger B, Boussemaere M, Lerut E, Debaveye Y, et al. Hyperglycemic kidney damage in an animal model of prolonged critical illness. *Kidney Int.* (2009) 76:512–20. doi: 10.1038/ki.2009.217
86. Gellerich FN, Trumbeckaite S, Hertel K, Zierz S, Müller-Werdan U, Werdan K, et al. Impaired energy metabolism in hearts of septic baboons: diminished activities of complex i and complex II of the mitochondrial respiratory chain. *Shock.* (1999) 11:336–41. doi: 10.1097/00024382-199905000-00006
87. Crouser ED, Julian MW, Blaho DV, Pfeiffer DR. Endotoxin-induced mitochondrial damage correlates with impaired respiratory activity. *Crit Care Med.* (2002) 30:276–84. doi: 10.1097/00003246-200202000-00002
88. Regueira T, Djafarzadeh S, Brandt S, Gorrasi J, Borotto E, Porta F, et al. Oxygen transport and mitochondrial function in porcine septic shock, cardiogenic shock, and hypoxaemia. *Acta Anaesthesiol Scand.* (2012) 56:846–59. doi: 10.1111/j.1399-6576.2012.02706.x
89. Merz T, Wepler M, Nußbaum B, Vogt J, Calzia E, Wang R, et al. Cystathionine-γ-lyase expression is associated with mitochondrial respiration during sepsis-induced acute kidney injury in swine with atherosclerosis. *Intensive Care Med Exp.* (2018) 6:43. doi: 10.1186/s40635-018-0208-z
90. Jeger V, Djafarzadeh S, Jakob SM, Takala J. Mitochondrial function in sepsis. *Eur J Clin Invest.* (2013) 43:532–42. doi: 10.1111/eci.12069
91. Carré JE, Orban JC, Re L, Felsmann K, Iffert W, Bauer M, et al. Survival in critical illness is associated with early activation of mitochondrial biogenesis. *Am J Respir Crit Care Med.* (2010) 182:745–51. doi: 10.1164/rccm.201003-0326OC
92. Asfar P, Schortgen F, Boisramé-Helms J, Charpentier J, Guérot E, Megarbane B, et al. REVA research network. Hyperoxia and hypertonic saline in patients with septic shock (HYPERS2S): a two-by-two factorial, multicentre, randomised, clinical trial. *Lancet Respir Med.* (2017) 5:180–90. doi: 10.1016/S2213-2600(17)30046-2
93. Dyson A, Simon F, Seifritz A, Zimmerling O, Matallo J, Calzia E, et al. Bladder tissue oxygen tension monitoring in pigs subjected to a range of cardiorespiratory and pharmacological challenges. *Intensive Care Med.* (2012) 38:1868–76. doi: 10.1007/s00134-012-2712-z

94. Demiselle J, Wepler M, Hartmann C, Radermacher P, Schortgen F, Meziani F, et al. Hyperoxia toxicity in septic shock patients according to the Sepsis-3 criteria: a *post hoc* analysis of the HYPER2S trial. *Ann Intensive Care*. (2018). 8:90. doi: 10.1186/s13613-018-0435-1
95. Supinski GS, Schroder EA, Callahan LA. Mitochondria and critical illness. *Chest*. (2020) 157:310–22. doi: 10.1016/j.chest.2019.08.2182
96. Arulkumaran N, Deutschman CS, Pinsky MR, Zuckerbraun B, Schumacker PT, Gomez H, et al. ADQI XIV workgroup. mitochondrial function in sepsis. *Shock*. (2016) 45:271–81. doi: 10.1097/SHK.0000000000000463
97. Mantzarlis K, Tsolaki V, Zakynthinos E. Role of oxidative stress and mitochondrial dysfunction in sepsis and potential therapies. *Oxid Med Cell Longev*. (2017) 2017:5985209. doi: 10.1155/2017/5985209
98. Protti A, Singer M. Bench-to-bedside review: potential strategies to protect or reverse mitochondrial dysfunction in sepsis-induced organ failure. *Crit Care*. (2006) 10:228. doi: 10.1186/cc5014
99. Detaille D, Guigas B, Chauvin C, Batandier C, Fontaine E, Wiernsperger N, et al. Metformin prevents high-glucose-induced endothelial cell death through a mitochondrial permeability transition-dependent process. *Diabetes*. (2005) 54:2179–87. doi: 10.2337/diabetes.54.7.2179
100. Vogt JA, Wachter U, Wagner K, Calzia E, Gröger M, Weber S, et al. Effects of glycemic control on glucose utilization and mitochondrial respiration during resuscitated murine septic shock. *Intensive Care Med Exp*. (2014) 2:19. doi: 10.1186/2197-425X-2-19
101. Detaille D, Vial G, Borel AL, Cottet-Rouselle C, Hallakou-Bozec S, Bolze S, et al. Imeglimin prevents human endothelial cell death by inhibiting mitochondrial permeability transition without inhibiting mitochondrial respiration. *Cell Death Discov*. (2016) 2:15072. doi: 10.1038/cddiscovery.2015.72
102. Larche J, Lancel S, Hassoun SM, Favory R, Decoster B, Marchetti P, et al. Inhibition of mitochondrial permeability transition prevents sepsis-induced myocardial dysfunction and mortality. *J Am Coll Cardiol*. (2006) 48:377–85. doi: 10.1016/j.jacc.2006.02.069
103. Karlsson M, Pukenas B, Chawla S, Ehinger JK, Plyler R, Stolow M, et al. Neuroprotective effects of cyclosporine in a porcine pre-clinical trial of focal traumatic brain injury. *J Neurotrauma*. (2018) 36:14–24. doi: 10.1089/neu.2018.5706
104. Argaud L, Cour M, Dubien PY, Giraud F, Jossan C, Riche B, et al. Effect of cyclosporine in nonshockable out-of-hospital cardiac arrest: the CYRUS randomized clinical trial. *JAMA Cardiol*. (2016). 1:557–65. doi: 10.1001/jamacardio.2016.1701
105. Cung TT, Morel O, Cayla G, Rioufol G, Garcia-Dorado D, Angoulvant D, et al. Cyclosporine before PCI in patients with acute myocardial infarction. *N Engl J Med*. (2015) 373:1021–31. doi: 10.1056/NEJMoa1505489
106. Matejovic M, Krouzecky A, Rokyta R Jr, Radej J, Kralova H, Treska V, et al. Effects of combining inducible nitric oxide synthase inhibitor and radical scavenger during porcine bacteremia. *Shock*. (2007) 27:61–8. doi: 10.1097/01.shk.0000235088.53421.6f
107. Soejima K, McGuire R, Snyder N IV, Uchida T, Szabó C, Salzman A, et al. The effect of inducible nitric oxide synthase (iNOS) inhibition on smoke inhalation injury in sheep. *Shock*. (2000) 13:261–6. doi: 10.1097/00024382-200004000-00002
108. Yamamoto Y, Sousse LE, Enkhbaatar P, Kraft ER, Deyo DJ, Wright CL, et al. γ-tocopherol nebulization decreases oxidative stress, arginase activity, and collagen deposition after burn and smoke inhalation in the ovine model. *Shock*. (2012). 38:671–6. doi: 10.1097/SHK.0b013e3182758759
109. Enkhbaatar P, Murakami K, Shimoda K, Mizutani A, Traber L, Phillips GB, et al. The inducible nitric oxide synthase inhibitor BBS-2 prevents acute lung injury in sheep after burn and smoke inhalation injury. *Am J Respir Crit Care Med*. (2003) 167:1021–6. doi: 10.1164/rccm.200209-1031PP
110. Su F, Huang H, Akieda K, Occhipinti G, Donadello K, Piagnerelli M, et al. Effects of a selective iNOS inhibitor versus norepinephrine in the treatment of septic shock. *Shock*. (2010) 34:243–9. doi: 10.1097/SHK.0b013e3181d75967
111. Piel DA, Gruber PJ, Weinheimer CJ, Courtois MR, Robertson CM, Coopersmith CM, et al. Mitochondrial resuscitation with exogenous cytochrome c in the septic heart. *Crit Care Med*. (2007) 35:2120–7. doi: 10.1097/01.CCM.0000278914.85340.FE
112. Verma R, Huang Z, Deutschman CS, Levy RJ. Caffeine restores myocardial cytochrome oxidase activity and improves cardiac function during sepsis. *Crit Care Med*. (2009) 37:1397–402. doi: 10.1097/CCM.0b013e31819cecd6
113. Crouser ED. Respiratory failure during critical illness: are mitochondria to blame? *Am J Respir Crit Care Med*. (2005) 172:793–4. doi: 10.1164/rccm.2507005
114. Sun Y, Yao X, Zhang QJ, Zhu M, Liu ZP, Ci B, et al. Beclin-1-Dependent autophagy protects the heart during sepsis. *Circulation*. (2018) 138:2247–62. doi: 10.1161/CIRCULATIONAHA.117.032821
115. Hartmann C, Nussbaum B, Calzia E, Radermacher P, Wepler M. Gaseous mediators and mitochondrial function: the future of pharmacologically induced suspended animation? *Front Physiol*. (2017) 8:691. doi: 10.3389/fphys.2017.00691
116. Dyson A, Dal-Pizzol F, Sabbatini G, Lach AB, Galfo F, Dos Santos Cardoso J, et al. Ammonium tetrathiomolybdate following ischemia/reperfusion injury: chemistry, pharmacology, and impact of a new class of sulfide donor in preclinical injury models. *PLoS Med*. (2017) 14:e1002310. doi: 10.1371/journal.pmed.1002310
117. Vanhorebeek I, De Vos R, Mesotten D, Wouters PJ, De Wolf-Peeters C, Van den Berghe G. Protection of hepatocyte mitochondrial ultrastructure and function by strict blood glucose control with insulin in critically ill patients. *Lancet*. (2005) 365:53–9. doi: 10.1016/S0140-6736(04)17665-4
118. Singer M, Matthay MA. Clinical review: thinking outside the box–an iconoclastic view of current practice. *Crit Care*. (2011) 15:225. doi: 10.1186/cc10245
119. Rudiger A, Singer M. Decatecholaminisation during sepsis. *Crit Care*. (2016) 20:309. doi: 10.1186/s13054-016-1488-x
120. Andreis DT, Singer M3. Catecholamines for inflammatory shock: a Jekyll-and-Hyde conundrum. *Intensive Care Med*. (2016) 42:1387–97. doi: 10.1007/s00134-016-4249-z
121. Hartmann C, Radermacher P, Wepler M, Nußbaum B. Non-Hemodynamic effects of catecholamines. *Shock*. (2017) 48:390–400. doi: 10.1097/SHK.0000000000000879
122. Mizock BA. Alterations in carbohydrate metabolism during stress: a review of the literature. *Am J Med*. (1995) 98:75–84. doi: 10.1016/S0002-9343(99)80083-7
123. De Backer D, Creteur J, Silva E, Vincent JL. Effects of dopamine, norepinephrine, and epinephrine on the splanchnic circulation in septic shock: which is best? *Crit Care Med*. (2003) 31:1659–67. doi: 10.1097/01.CCM.0000063045.77339.B6
124. Lünemann JD, Buttgereit F, Tripmacher R, Baerwald CG, Burmester GR, Krause A. Effects of norepinephrine on oxygen consumption of quiescent and activated human peripheral blood mononuclear cells. *Ann N Y Acad Sci*. (2002) 966:365–8. doi: 10.1111/j.1749-6632.2002.tb04236.x
125. Porta F, Bracht H, Weikert C, Beck M, Takala J, Brandt S, et al. Effects of endotoxin and catecholamines on hepatic mitochondrial respiration. *Inflammation*. (2009) 32:315–21. doi: 10.1007/s10753-009-9138-y
126. Rump AF, Klaus W. Evidence for norepinephrine cardiotoxicity mediated by superoxide anion radicals in isolated rabbit hearts. *Naunyn Schmiedebergs Arch Pharmacol*. (1994) 349:295–300. doi: 10.1007/BF00169296
127. Neri M, Cerretani D, Fiaschi AI, Laghi PF, Lazzerini PE, Maffione AB, et al. Correlation between cardiac oxidative stress and myocardial pathology due to acute and chronic norepinephrine administration in rats. *J Cell Mol Med*. (2007) 11:156–70. doi: 10.1111/j.1582-4934.2007.00009.x
128. Rutai A, Fejes R, Juhász L, Tallósy SP, Poles MZ, Földesi I, et al. Endothelin a and b receptors: potential targets for microcirculatory-mitochondrial therapy in experimental sepsis. *Shock*. (2020) 54:87–95. doi: 10.1097/SHK.0000000000001414

Conflict of Interest: The authors declare that the research was conducted in the absence of any commercial or financial relationships that could be construed as a potential conflict of interest.

frontiers in Medicine

ORIGINAL RESEARCH
published: 21 August 2020
doi: 10.3389/fmed.2020.00463

Indomethacin Increases the Efficacy of Oxygen Utilization of Colonic Mitochondria and Uncouples Hepatic Mitochondria in Tissue Homogenates From Healthy Rats

Anna Herminghaus[1], Albert J. Buitenhuis[1†], Jan Schulz[1], Richard Truse[1], Christian Vollmer[1], Borna Relja[2], Inge Bauer[1] and Olaf Picker[1]*

[1] Department of Anaesthesiology, University Hospital Duesseldorf, Duesseldorf, Germany, [2] Experimental Radiology, Department of Radiology and Nuclear Medicine, Otto von Guericke University, Magdeburg, Germany

OPEN ACCESS

Edited by:
Enrico Calzia, University of Ulm, Germany

Reviewed by:
Danina M. Muntean, Victor Babes University of Medicine and Pharmacy, Romania
Johanna Catharina Duvigneau, University of Veterinary Medicine, Austria

****Correspondence:***
Anna Herminghaus
anna.herminghaus@med.uni-duesseoldorf.de

[†]In partial fulfillment of the requirements for a doctoral thesis

Specialty section:
This article was submitted to Intensive Care Medicine and Anesthesiology, a section of the journal Frontiers in Medicine

Received: *27 April 2020*
Accepted: *10 July 2020*
Published: *21 August 2020*

Citation:
Herminghaus A, Buitenhuis AJ, Schulz J, Truse R, Vollmer C, Relja B, Bauer I and Picker O (2020) Indomethacin Increases the Efficacy of Oxygen Utilization of Colonic Mitochondria and Uncouples Hepatic Mitochondria in Tissue Homogenates From Healthy Rats. Front. Med. 7:463. doi: 10.3389/fmed.2020.00463

Background: Studies suggest that indomethacin (Indo) exhibits detrimental changes in the small intestine (microvascular disorder, villus shortening, and epithelial disruption), mainly due to mitochondrial uncoupling. The effects of Indo on colon and liver tissue are unclear. The aim of this study was to determine the effects of Indo on mitochondrial respiration in colonic and hepatic tissue.

Methods: Mitochondrial oxygen consumption was assessed in colon and liver homogenates from healthy rats. Homogenates were incubated without drug (control) or Indo (colon: 0.36, 1, 30, 179, 300, 1,000, 3,000 μM; liver: 0.36, 1, 3, 10, 30, 100, 179 μM; $n = 6$). State 2 (substrate-dependent) and state 3 (ADP-dependent respiration) were evaluated with respirometry. The respiratory control index (RCI) was derived and the ADP/O ratio was calculated.

Statistics: Data presented as % of control, min/median/max, Kruskal–Wallis+Dunn's correction, $*p < 0.05$ vs. control.

Results: Indo had no effect on RCI of colonic mitochondria. ADP/O ratio increased in complex I at concentrations of 1,000 and 3,000 μM (Indo 1,000 μM: 113.9/158.9/166.9%*; Indo 3,000 μM: 151.5/183.0/361.5%*) and in complex II at concentrations of 179 and 3,000 μM vs. control (179 μM: 111.3/73.1/74.9%*; 3,000 μM: 132.4/175.0/339.4%*). In hepatic mitochondria RCI decreased at 179 μM for both complexes vs. control (complex I: 25.6/40.7/62.9%*, complex II: 57.0/73.1/74.9%*). The ADP/O ratio was only altered in complex I at a concentration of 179 μM Indo vs. control (Indo 179 μM: 589.9/993.7/1195.0 %*).

Conclusion: Indo affected parameters of mitochondrial function in an organ-specific and concentration-dependent manner. In colonic tissue, RCI remained unaltered whereas the ADP/O ratio increased. Indo at the highest concentration decreased the RCI for both complexes in hepatic mitochondria. The large increase in ADP/O ratio in complex I at the highest concentration likely reflects terminal uncoupling.

Keywords: indomethacin, mitochondrial function, colon, liver, adverse event

INTRODUCTION

Non-steroidal anti-inflammatory drugs (NSAIDs) are widely used for various indications. They are generally considered as safe medication, but are also known to cause different adverse events, which potentially limit their use. The main complication of the therapy with NSAIDs is gastrointestinal (GI) damage. Although the most frequent disturbances are upper GI-bleeding, adverse events affecting lower GI still account for 40% of all NSAID-related serious GI complications (1). It is generally accepted that the inhibition of cyclooxygenase (COX), followed by multiple pathogenic events like increased intestinal permeability, infiltration of neutrophils and microcirculatory dysregulation play a critical role in the development of inflammation and ulcers (2, 3). Further studies suggest that mucosal concentration of prostaglandins could be decreased without mucosal damage and that inhibition of COX 1 and 2 causes gastrointestinal lesions, but less severe than those caused by NSAIDs (4, 5). Thus, inhibition of COX does not seem to be the single mechanism of NSAID-induced gastrointestinal damage. Evidence suggests that affecting mitochondrial function with a consecutive decrease in cellular ATP-production may be the underlying biochemical mechanism of the toxicity of NSAIDs (3). However, data available on effects of NSAIDs on mitochondrial function are inconsistent showing impaired (6) or unchanged (7) mitochondrial function in rat jejunum. Similar to upper gastrointestinal complications, the pathogenesis and prevention of NSAID-associated lower GI complications remain unclear (8). A number of studies suggest that NSAIDs can cause damage of the large intestine by a negative impact on the mucosal permeability (9). Data concerning mitochondrial function in the colon under NSAIDs-therapy are lacking completely.

NSAIDs are also associated with hepatotoxicity ranging from asymptomatic elevations in serum aminotransferase levels to severe liver failure (10, 11). Although clinically apparent liver injury from NSAIDs is rare (∼1–10 cases per 100,000 prescriptions) the massive consumption of NSAIDs worldwide makes them an important cause of drug-induced liver injury (12). The molecular mechanisms underlying this toxicity have not yet been fully clarified. However, experimental data suggests that they include increased drug concentration in the hepatobiliary compartment, formation of reactive metabolites that cause oxidative stress, and mitochondrial dysfunction (13). In this context, the mitochondrial dysfunction is mainly described as an uncoupling and reduction of ATP production (6, 14, 15). Lipophilic and weakly acidic drugs like NSAIDs can easily pass through the outer mitochondrial membrane and shuttle protons from the intermembraneous space back into the matrix. This proton cycling scatters the proton gradient which is continuously maintained by the electron transport chain. This weakens the activity of the ATP synthetase, which is normally driven by this proton gradient (13). There is also ambiguity concerning toxic concentrations of NSAIDs affecting mitochondrial function. While an uncoupling effect of indomethacin on hepatic mitochondria could be shown with concentrations lower than 200 μM (14) another study rather suggests a stimulating effect of indomethacin on mitochondrial respiration at lower concentrations (0.02–2.7 μM) (16). The comparison of NSAID-induced cytotoxicity *in vitro* showed a large difference between compounds which was not related to their chemical structures (15). Indomethacin seems to be among the most cytotoxic NSAIDs and serves a gold standard to study NSAID toxicity (3, 17, 18).

Taken together, the effects of NSAIDs on mitochondrial function in different organs have been insufficiently examined. Data concerning hepatic mitochondria are inconsistent and are lacking completely for other organs like the colon. The aim of this study was therefore to investigate the concentration dependent effect of indomethacin on mitochondrial respiration in hepatic and colonic tissue homogenates from healthy rats.

MATERIALS AND METHODS

Animals

The study was approved by the Animal Ethics Committee of the University of Duesseldorf, Germany (project identification code: O27/12) and conducted in accordance with the Guide for the Care and Use of Laboratory Animals of the National Institutes of Health (19).

Male Wistar rats (∼3 months old) were kept at an artificial 12-h light/dark cycle at controlled room temperature with free access to standard chow and water. 48 rats were sacrificed by decapitation under deep sedation with sodium pentobarbital (90 mg/kg) and liver and colon tissues were harvested.

Preparation of Liver and Colon Homogenates

Liver and colon homogenates were prepared as described previously (20–22). Briefly, liver tissue was placed in 4°C-cold isolation buffer (130 mM KCl, 5 mM K_2HPO_4, 20 mM MOPS, 2.5 mM EGTA, 1 μM $Na_4P_2O_7$, 0.1% bovine serum albumin (BSA) pH 7.15), minced into 2–3-mm^3 pieces, rinsed twice in isolation buffer to remove traces of blood, and homogenized (Potter-Elvehjem, 5 strokes, 2,000 rpm). Freshly harvested colon tissue was placed in 4°C-cold isolation buffer (as for the liver but containing 2% BSA), opened longitudinally, and cleaned softly with a cotton compress. After treatment with 0.05% trypsin for 5 min on ice, the tissue was placed in 4°C-cold isolation buffer containing 2% BSA and protease inhibitors (cOmplete™ Protease Inhibitor Cocktail, Roche Life Science, Mannheim, Germany), minced into 2–3-mm^3 pieces, and homogenized (Potter-Elvehjem, 5 strokes, 2,000 rpm). Protein concentration in the tissue homogenates with supplemented BSA was determined using Lowry method (23) with bovine serum albumin as a standard. We used a higher BSA concentration for the preparation of colon homogenates than for liver homogenates to prevent an uncoupling effect of fatty acids, which are present in the submucosa of the colon (24).

Measurement of Mitochondrial Respiratory Rates

The assessment of mitochondrial respiration was performed after addition of carrier substance (DMSO, Sigma Aldrich Chemie GmbH, Steinheim, Germany)—control, or different

concentrations of indomethacin (Sigma Aldrich Chemie GmbH, Steinheim, Germany) (0.36, 1, 30, 179, 300, 1,000, and 3,000 for the colon and 0.36, 1, 3, 10, 30, 100, and 179 μM for the liver). The incubation took place at room temperature (kept at 21°C) for 3 min. Six biological and 2–3 technical (2–3 separate measurements from a single homogenate) replicates were performed.

Mitochondrial oxygen consumption was measured as described previously (21, 22). Briefly, the measurement was performed at 30°C using a Clark-type electrode (model 782, Strathkelvin instruments, Glasgow, Scotland). Tissue homogenates were suspended in respiration medium (130 mM KCl, 5 mM K_2HPO_4, 20 mM MOPS, 2.5 mM EGTA, 1 μM $Na_4P_2O_7$, 0.1% BSA for liver, and 2% BSA for colon, pH 7.15) to yield a protein concentration of 4 or 6 mg/ml for liver and colon, respectively.

Mitochondrial state two respiration was measured in the presence of either substrates for complex I–glutamate and malate (both 2.5 mM, G-M) or for complex II–succinate (10 mM for liver, 5 mM for colon, S) combined with 0.5 μM rotenone–the inhibitor of complex I activity.

The maximal mitochondrial respiration (state 3) was recorded after the addition of ADP (250 μM for liver, 50 μM for colon). The concentrations of ADP were empirically adapted to the different tissue homogenates (hepatic and colonic tissue) in pilot experiments and as published previously (21, 22, 25). We used different concentrations of ADP for liver and colon since we identified these concentrations as non-saturated for the used amount of protein (4 mg/ml for the liver and 6 mg/ml for the colon). The respiratory control index (RCI) was calculated (state 3/state 2) to define the coupling between the electron transport system (ETS) and oxidative phosphorylation (OXPHOS). To reflect the efficacy of OXPHOS, the ADP/O ratio was calculated from the amount of ADP added and oxygen consumed in state 3. The average oxygen consumption was calculated as the mean from two or three technical replicates.

Respiration rates were expressed as nanomoles O_2 per minute per milligram protein. Mitochondria were checked for damage by the addition of 2.5 μM cytochrome c and 0.05 μg/ml oligomycin. Lack of increase in flux after the addition of cytochrome c indicated integrity of the mitochondrial outer membrane. After inhibition of the ATP synthesis by oligomycin, the mitochondria were transferred to state 2, which reflects the respiration rate compensating the proton leak. The lack of difference in O_2 consumption after adding oligomycin compared to state 2 indicates that the inner membrane was intact, and mitochondria were not damaged through the preparation procedure.

Statistical Analysis

Statistical analysis was conducted using GraphPad Prism 8.0 (GraphPad Software, Inc, La Jolla, USA). After testing for normality (Kolmogorov-Smirnov) the non-parametric data were analyzed using the Kruskal-Wallis test of variance followed by *post-hoc* Dunn's correction. Data are presented as percentage of control values, $p < 0.05$ was considered significant.

RESULTS

Effect of Indomethacin on Mitochondrial Respiration in Colon Homogenate

State 3 was reduced at concentrations of 1,000 and 3,000 μM for complex I (control 100%, 1,000 μM: 60.63/66.66/88.9%; 3,000 μM: 29.56/51.23/61.75%) (**Figure 1A**) and at 179 μM and 3,000 μM for complex II (control 100%, 179 μM: 63.53/75.15/86.93%; 3,000 μM: 35.87/63.97/72.61%) (**Figure 1D**). The RCI remained unchanged for both complexes under the influence of indomethacin (**Figures 1B,E**). An increase in ADP/O ratio was seen at 1,000 and 3,000 μM for complex I (control 100%, 1,000 μM: 113.9/158.9/166.9%; 3,000 μM: 151.5/183.0/361.5%) (**Figure 1C**) and at 179 and 3,000 μM for complex II (control 100%, 179 μM: 111.3/142.2/156.7%; 3,000 μM: 132.4/175.0/339.4%) (**Figure 1F**). Original data on State 2, 3, and 4 are presented in **Supplementary Material**.

Effect of Indomethacin on Hepatic Mitochondrial Function

State 3 was decreased only for complex I at 100 and 179 μM (control 100%, 100 μM: 53.08/64.63/66.19%; 179 μM: 28.14/40.65/49:00%) (**Figure 2A**). The RCI was decreased for both complexes but only at the highest concentration of 179 μM (control 100%, complex I: 28.14/40.65/49.00%, complex II: 57.01/73.11/74.88%) (**Figures 2B,E**). The ADP/O ratio was increased only for complex I at 179 μM (control 100%, 179 μM: 589.9/993.7/1195.00%) (**Figure 2C**). State 3 and the ADP/O ratio for complex II stayed unchanged (**Figures 2D,F**). Original data on State 2, 3 and 4 are presented in **Supplementary Material**.

DISCUSSION

The main results from this study are that indomethacin increases the efficacy of oxygen utilization of colonic mitochondria but uncouples hepatic mitochondria, predominantly through complex I.

The experimental setting is well-established and based on our previous publications (21, 22). The chosen concentrations of indomethacin are based on data from similar *in vitro* studies with isolated hepatic mitochondria and cell culture (14, 17, 26). The used concentrations of the drug differ between the tissues. We adjusted the drug concentrations since the maximal uncoupling of the respiratory chain from the ATP-synthase in hepatic mitochondria was observed after stimulation through complex I at a concentration of 179 μM. Since in contrast, in colonic mitochondria indomethacin hardly showed any effect up to 179 μM, we additionally applied higher drug concentrations.

The applied drug concentrations include the clinically relevant range as well as higher concentrations. After oral administration of an average dose of 75–200 mg/day the plasma concentrations in humans (27) reach 0.3–3 μM and after i.v., application of 0.2 mg/kg in sheep (28) reach 14 μM, however with a high inter-individual variability–up to 20 fold (29). In rats, the plasma concentration after an oral dose of 10 mg/kg reached 140 μM (30). Generally, indomethacin is dosed higher (10–40 mg/kg) for rats (6, 7, 30) than for humans (1 mg/kg) (27). Thus, our

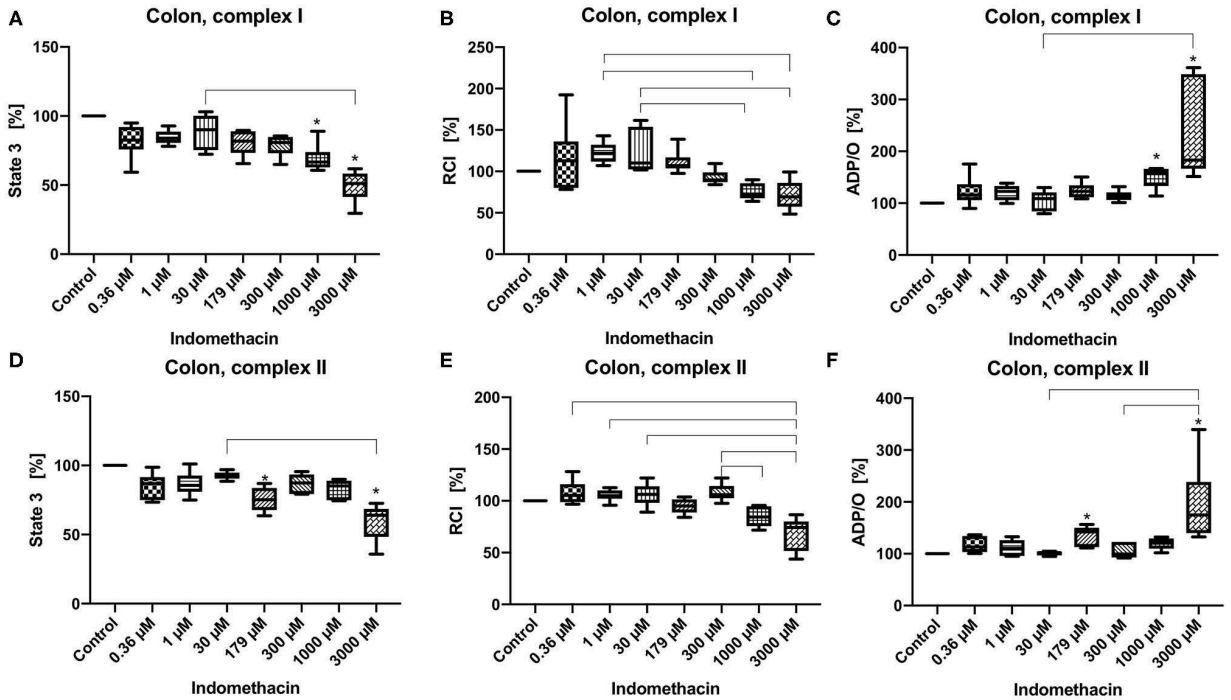

FIGURE 1 | Effect of indomethacin (0.36, 1, 30, 179, 300, 1,000, and 3,000 µM) on colonic mitochondrial function: State 3 for complex I **(A)** and II **(D)**, respiratory control index (RCI) for complex I **(B)** und II **(E)** and ADP/O ratio for complex I **(C)** and II **(F)**. Data are shown as percentage of the control value (median/min/max), $n = 6$, $^*p < 0.05$ vs. control, ⌐¬ $p < 0.05$ between groups.

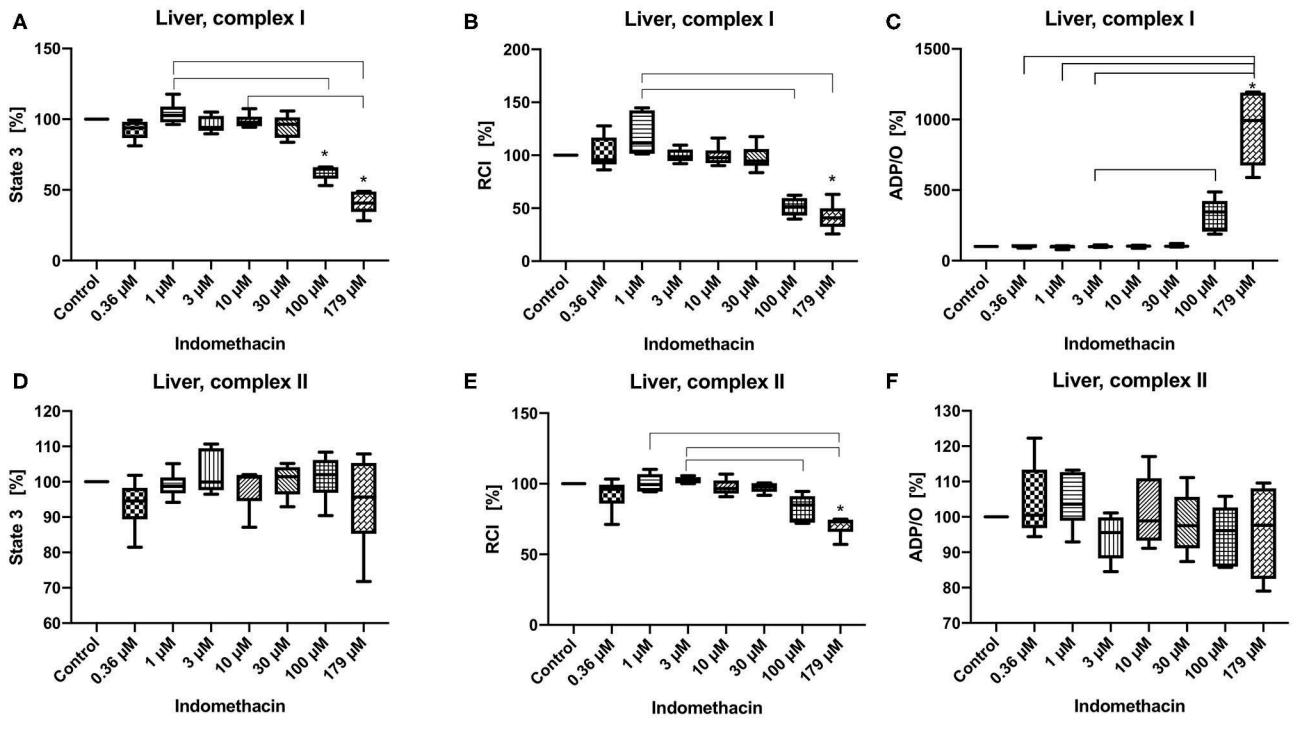

FIGURE 2 | Effect of indomethacin (0.36, 1, 3, 10, 30, 100, and 179 µM) on hepatic mitochondrial function: State 3 for complex I **(A)** and II **(D)**, respiratory control index (RCI) for complex I **(B)** und II **(E)** and ADP/O ratio for complex I **(C)** and II **(F)**. Data are presented as percentage of the control value (median/min/max), $n = 6$, $^*p < 0.05$ vs. control, ⌐¬ $p < 0.05$ between groups.

results may be relevant for the *in vivo* situation since adverse events already occur with recommended dosages and aggravate after accidental or intentional overdosing of the drug (31). Moreover, many patients suffer from multimorbidity. Preexisting or NSAIDs-induced renal and/or liver insufficiency can also result in supraclinical or even toxic drug plasma concentrations (31, 32).

In colonic mitochondria indomethacin at higher concentrations (1,000 and 3,000 μM for complex I and 179 and 3,000 μM for complex II) reduced state 3 without affecting the RCI and increased ADP/O ratio. As the RCI reflects the coupling between the respiratory chain and the ATP-synthase and the ADP/O-ratio reflects the efficacy of the oxidative phosphorylation, indomethacin seems to have rather positive effects on colonic cell metabolism resulting in a more effective ATP-production. Based on our data, we cannot explain the lack of effect of indomethacin at 300 and 1,000 μM on colonic mitochondria after stimulation of the respiratory chain through complex II. To address this question more deeply, further investigations, like assessment of the activities of the single complexes are necessary. To the best of our knowledge, we are the first to examine the effect of indomethacin on colonic mitochondrial function. Jacob et al. investigated the impact of this drug on jejunal mitochondria. In their study, no alterations were observed in the mitochondrial oxygen uptake, neither *ex vivo,* nor *in vitro* (7). The difference between their and our results could be explained by the different tissues investigated (jejunum vs. colon) and different experimental settings (whole tissue vs. tissue homogenate). However, the drug concentrations used in the study by Jacob et al. were similar to the concentrations, which caused an alteration of oxygen uptake in our experiments (2.5 vs. 1–3 mM). Basivireddy et al. examined the influence of indomethacin on mitochondrial function in enterocytes isolated from rat small intestine and obtained different results compared to those of Jacob et al. and to ours (6). In their experiments rats were dosed with 40 mg/kg indomethacin by gavage. They showed a decreased RCI, swelling of the mitochondria and a decreased influx of calcium into the mitochondria. These changes could be interpreted as rather harmful to the cell. Also, in this case the differences could be explained by the different tissues, divergent application forms (oral application in *in vivo* experiments vs. *in vitro* incubation) and possibly varying drug concentrations. Since the plasma concentrations of indomethacin after oral application are well-examined, our knowledge about tissue concentrations of the drug is very limited. There are only few data about calculated hepatic concentration of indomethacin (33) and data about intestinal concentrations are lacking completely.

The effect of indomethacin on hepatic mitochondria was different than on colonic mitochondria. We observed a dose-dependent and complex-specific effect. The impact of indomethacin on complex II was mild—only the high concentration (179 μM) decreased RCI without affecting state 3 and ADP/O ratio. When the respiratory chain was stimulated through complex I, indomethacin at higher concentrations (100 and 179 μM) decreased state 3 and consecutively the RCI (but only at a concentration of 179 μM). The dramatically reduced oxygen consumption during state 3 led to an increase of ADP/O ratio (ADP added/oxygen consumed), which might be interpreted as toxic discoupling rather than an increase of the efficacy of the oxidative phosphorylation. A selective or stronger effect of a drug on one particular complex of the respiratory chain is a well-known phenomenon. For instance, metformin is known to inhibit complex I selectively (34). Furthermore, antipsychotic drugs like haloperidol, and to a lesser degree chlorpromazine and risperidone have been found to inhibit only complex I. Antidepressant drugs are able to interact with complexes I, II, and IV, but the inhibition of complex I is most pronounced (35). It is not fully elucidated, why some drugs have stronger affinity to certain complexes. It is suggested that the lipophilic domain of the antidepressant drugs can compete with the substrate for binding to complex I. Concerning indomethacin, Boushel et al. suggested in their study on human muscle mitochondria that the underlying mechanisms of stronger inhibition of complex I include leakage of electrons, iron release and superoxide and hydroxyl radical production (36). Moreover, the drug effect can be organ specific, like by serotonin reuptake inhibitors, which block complex I and IV in the brain, but complex I and V in the liver (35).

Our results concerning hepatic mitochondria are not in line with the results of other researchers. Somasundaram et al. could show a dose dependent effect of indomethacin on hepatic mitochondrial function for complex II. In their experiments, stimulation of respiration (state 3) occurred at concentrations up to 0.5 mM, followed by a progressive decrease in oxygen consumption with further increases in drug concentrations up to 2 mM, which is indicative of inhibition of the electron transport chain (26). The effect of indomethacin on the mitochondrial function after stimulation of the respiratory chain through complex I was not examined. Mahmud et al. also tested the influence of indomethacin on hepatic mitochondria but again only for complex II. They achieved similar results as Somasundaram et al. however, at substantially lower concentrations of the drug. They observed a stimulating effect on state 3 respiration up to 0.5 μM and inhibitory effect at higher concentrations (up to 3 μM) (16).

The effect of indomethacin on hepatic mitochondria is similar to the effects of other NSAIDs. Most NSAIDs are lipid soluble weak acids, which is a common feature of all uncouplers of oxidative phosphorylation (37). Acetylsalicylic acid, naproxen, and piroxicam show a similar uncoupling effect on hepatic mitochondria to that of indomethacin (14, 26). Moreover, some of the NSAIDs like diclofenac or fenoprofen reduce the ATP concentration in isolated hepatocytes (15). Data about NSAIDs and colon are lacking in the literature.

Our results showing opposite effects of the drug on mitochondrial function in different tissues confirming the well-accepted theory that the impact of various stimuli on mitochondria is organ specific (38).

CONCLUSIONS

Taken together, indomethacin has organ-specific, dose-dependent, and complex-specific effects on mitochondrial

respiration. While it shows rather positive effects on colonic mitochondrial function, the impact on oxidative phosphorylation in the liver is rather deleterious.

This could possibly be one of the mechanisms contributing to indomethacin-related hepatotoxicity. However, this hypothesis must be considered very carefully. The transfer of results performed *in vitro* using tissues from young and healthy animals into human medicine can only be performed with reservation. Moreover, adverse effects are complex processes including many factors like pre-existing organ damage and co-medication.

The positive effect of indomethacin on colonic mitochondrial respiration cannot explain the lower GI-complications described under NSAID therapy. To better understand the pathomechanisms of these adverse events, further research on this field is needed. Our data extend our knowledge about a possible mode of action of NSAIDs and offer a new insight into conceivable mechanisms of their side effects.

DATA AVAILABILITY STATEMENT

All datasets generated for this study are included in the article/**Supplementary Material**.

ETHICS STATEMENT

The animal study was reviewed and approved by University of Duesseldorf, Universitaetstrasse 1, 40225 Duesseldorf, Germany.

AUTHOR CONTRIBUTIONS

AH, IB, and OP: conceptualization, supervision, and project administration. AH and AB: methodology, software, investigation, and data curation. AH, AB, JS, BR, and RT: validation. AH, AB, IB, and OP: formal analysis. IB and OP: resources. AH: writing—original draft preparation and visualization. AH, AB, JS, RT, BR, CV, IB, and OP: writing—review and editing. All authors contributed to the article and approved the submitted version.

SUPPLEMENTARY MATERIAL

The Supplementary Material for this article can be found online at: https://www.frontiersin.org/articles/10.3389/fmed.2020.00463/full#supplementary-material

REFERENCES

1. Laine L, Curtis SP, Langman M, Jensen DM, Cryer B, Kaur A, et al. Lower gastrointestinal events in a double-blind trial of the cyclo-oxygenase-2 selective inhibitor etoricoxib and the traditional nonsteroidal anti-inflammatory drug diclofenac. *Gastroenterology*. (2008) 135:1517–25. doi: 10.1053/j.gastro.2008.07.067
2. Somasundaram S, Hayllar H, Rafi S, Wrigglesworth JM, Macpherson AJ, Bjarnason I. The biochemical basis of non-steroidal anti-inflammatory drug-induced damage to the gastrointestinal tract: a review and a hypothesis. *Scand J Gastroenterol*. (1995) 30:289–99. doi: 10.3109/00365529509093280
3. Bjarnason I, Scarpignato C, Holmgren E, Olszewski M, Rainsford KD, Lanas A. Mechanisms of damage to the gastrointestinal tract from nonsteroidal anti-inflammatory drugs. *Gastroenterology*. (2018) 154:500–14. doi: 10.1053/j.gastro.2017.10.049
4. Langenbach R, Morham SG, Tiano HF, Loftin CD, Ghanayem BI, Chulada PC, et al. Prostaglandin synthase 1 gene disruption in mice reduces arachidonic acid-induced inflammation and indomethacin-induced gastric ulceration. *Cell*. (1995) 83:483–92. doi: 10.1016/0092-8674(95)90126-4
5. Sigthorsson G, Simpson RJ, Walley M, Anthony A, Foster R, Hotz-Behoftsitz C, et al. COX-1 and 2, intestinal integrity, and pathogenesis of nonsteroidal anti-inflammatory drug enteropathy in mice. *Gastroenterology*. (2002) 122:1913–23. doi: 10.1053/gast.2002.33647
6. Basivireddy J, Vasudevan A, Jacob M, Balasubramanian KA. Indomethacin-induced mitochondrial dysfunction and oxidative stress in villus enterocytes. *Biochem Pharmacol*. (2002) 64:339–49. doi: 10.1016/S0006-2952(02)01067-5
7. Jacob M, Bjarnason I, Simpson RJ. Effects of indomethacin on energy metabolism in rat jejunal tissue *in vivo*. *Clin Sci*. (2002) 102:541–6. doi: 10.1042/cs1020541
8. Guo CG, Leung WK. Potential strategies in the prevention of nonsteroidal anti-inflammatory drugs-associated adverse effects in the lower gastrointestinal tract. *Gut Liver*. (2020) 14:179–89. doi: 10.5009/gnl19201
9. Laine L, Smith R, Min K, Chen C, Dubois RW. Systematic review: the lower gastrointestinal adverse effects of non-steroidal anti-inflammatory drugs. *Aliment Pharmacol Ther*. (2006) 24:751–67. doi: 10.1111/j.1365-2036.2006.03043.x
10. Conaghan PG. A turbulent decade for NSAIDs: update on current concepts of classification, epidemiology, comparative efficacy, and toxicity. *Rheumatol Int*. (2012) 32:1491–502. doi: 10.1007/s00296-011-2263-6
11. Teoh NC, Farrell GC. Hepatotoxicity associated with non-steroidal anti-inflammatory drugs. *Clin Liver Dis*. (2003) 7:401–13. doi: 10.1016/S1089-3261(03)00022-9
12. Sriuttha P, Sirichanchuen B, Permsuwan U. Hepatotoxicity of nonsteroidal anti-inflammatory drugs: a systematic review of randomized controlled trials. *Int J Hepatol*. (2018) 2018:5253623. doi: 10.1155/2018/5253623
13. Boelsterli UA. Mechanisms of NSAID-induced hepatotoxicity. *Drug Saf*. (2002) 25:633–48. doi: 10.2165/00002018-200225090-00003
14. Somasundaram S, Rafi S, Hayllar J, Sigthorsson G, Jacob M, Price AB, et al. Mitochondrial damage: a possible mechanism of the "topical" phase of NSAID induced injury to the rat intestine. *Gut*. (1997) 41:344–53. doi: 10.1136/gut.41.3.344
15. Masubuchi Y, Saito H, Horie T. Structural requirements for the hepatotoxicity of nonsteroidal anti-inflammatory drugs in isolated rat hepatocytes. *J Pharmacol Exp Ther*. (1998) 287:208–13.
16. Mahmud T, Rafi SS, Scott DL, Wrigglesworth JM, Bjarnason I. Nonsteroidal antiinflammatory drugs and uncoupling of mitochondrial oxidative phosphorylation. *Arthritis Rheum*. (1996) 39:1998–2003. doi: 10.1002/art.1780391208
17. Omatsu T, Naito Y, Handa O, Hayashi N, Mizushima K, Qin Y, et al. Involvement of reactive oxygen species in indomethacin-induced apoptosis of small intestinal epithelial cells. *J Gastroenterol*. (2009) 44 (Suppl. 19):30–4. doi: 10.1007/s00535-008-2293-3
18. Thakre-Nighot M, Blikslager AT. Indomethacin induces increase in gastric epithelial tight junction permeability via redistribution of occludin and activation of p38 MAPK in MKN-28 Cells. *Tissue Barriers*. (2016) 4:e1187325. doi: 10.1080/21688370.2016.1187325
19. National Research Council (US) Committee for the Update of the Guide for the Care and Use of Laboratory Animals. *Guide for the Care and Use of Laboratory Animals. 8th ed.* Washington, DC: National Academies Press (2011). Available at: http://www.ncbi.nlm.nih.gov/books/NBK54050/ (accessed April 9, 2020).
20. Herminghaus A, Eberhardt R, Truse R, Schulz J, Bauer I, Picker O, et al. Nitroglycerin and iloprost improve mitochondrial function in colon homogenate without altering the barrier integrity of caco-2 mzonolayers. *Front Med*. (2018) 5:291. doi: 10.3389/fmed.2018.00291

21. Herminghaus A, Buitenhuis AJ, Schulz J, Vollmer C, Scheeren TWL, Bauer I, et al. Propofol improves colonic but impairs hepatic mitochondrial function in tissue homogenates from healthy rats. *Eur J Pharmacol*. (2019) 853:364–70. doi: 10.1016/j.ejphar.2019.04.031
22. Herminghaus A, Laser E, Schulz J, Truse R, Vollmer C, Bauer I, et al. Pravastatin and gemfibrozil modulate differently hepatic and colonic mitochondrial respiration in tissue homogenates from healthy rats. *Cells*. (2019) 8:983. doi: 10.3390/cells8090983
23. Lowry OH, Rosebrough NJ, Farr AL, Randall RJ. Protein measurement with the folin phenol reagent. *J Biol Chem*. (1951) 193:265–75.
24. Tretter L, Mayer-Takacs D, Adam-Vizi V. The effect of bovine serum albumin on the membrane potential and reactive oxygen species generation in succinate-supported isolated brain mitochondria. *Neurochem Int*. (2007) 50:139–47. doi: 10.1016/j.neuint.2006.07.010
25. Herminghaus A, Papenbrock H, Eberhardt R, Vollmer C, Truse R, Schulz J, et al. Time-related changes in hepatic and colonic mitochondrial oxygen consumption after abdominal infection in rats. *Intensive Care Med Exp*. (2019) 7:4. doi: 10.1186/s40635-018-0219-9
26. Somasundaram S, Sigthorsson G, Simpson RJ, Watts J, Jacob M, Tavares IA, et al. Uncoupling of intestinal mitochondrial oxidative phosphorylation and inhibition of cyclooxygenase are required for the development of NSAID-enteropathy in the rat. *Aliment Pharmacol Ther*. (2000) 14:639–50. doi: 10.1046/j.1365-2036.2000.00723.x
27. Huntjens DRH, Danhof M, Della Pasqua OE. Pharmacokinetic-pharmacodynamic correlations and biomarkers in the development of COX-2 inhibitors. *Rheumatol Oxf Engl*. (2005) 44:846–59. doi: 10.1093/rheumatology/keh627
28. Upton RN, Rasmussen M, Grant C, Martinez AM, Cold GE, Ludbrook GL. Pharmacokinetics and pharmacodynamics of indomethacin: effects on cerebral blood flow in anaesthetized sheep. *Clin Exp Pharmacol Physiol*. (2008) 35:317–23. doi: 10.1111/j.1440-1681.2007.04818.x
29. Brash AR, Hickey DE, Graham TP, Stahlman MT, Oates JA, Cotton RB. Pharmacokinetics of indomethacin in the neonate. Relation of plasma indomethacin levels to response of the ductus arteriosus. *N Engl J Med*. (1981) 305:67–72. doi: 10.1056/NEJM198107093050203
30. Wright MR, Davies NM, Jamali F. Toxicokinetics of indomethacin-induced intestinal permeability in the rat. *Pharmacol Res*. (1997) 35:499–504. doi: 10.1006/phrs.1997.0194
31. Hunter LJ, Wood DM, Dargan PI. The patterns of toxicity and management of acute nonsteroidal anti-inflammatory drug (NSAID) overdose. *Open Access Emerg Med*. (2011) 3:39–48. doi: 10.2147/OAEM.S22795
32. Khan S, Yusufi FNK, Yusufi ANK. Comparative effect of indomethacin (IndoM) on the enzymes of carbohydrate metabolism, brush border membrane and oxidative stress in the kidney, small intestine and liver of rats. *Toxicol Rep*. (2019) 6:389–94. doi: 10.1016/j.toxrep.2019.04.010
33. Alqahtani S, Kaddoumi A. Development of physiologically based pharmacokinetic/pharmacodynamic model for indomethacin disposition in pregnancy. *PLOS ONE*. (2015) 10:e0139762. doi: 10.1371/journal.pone.0139762
34. Bridges HR, Jones AJY, Pollak MN, Hirst J. Effects of metformin and other biguanides on oxidative phosphorylation in mitochondria. *Biochem J*. (2014) 462:475–87. doi: 10.1042/BJ20140620
35. Hargreaves IP, Al Shahrani M, Wainwright L, Heales SJR. Drug-induced mitochondrial toxicity. *Drug Saf*. (2016) 39:661–74. doi: 10.1007/s40264-016-0417-x
36. Boushel R, Fuentes T, Hellsten Y, Saltin B. Opposing effects of nitric oxide and prostaglandin inhibition on muscle mitochondrial Vo(2) during exercise. *Am J Physiol Regul Integr Comp Physiol*. (2012) 303:R94–100. doi: 10.1152/ajpregu.00044.2012
37. Tyler DD. Chapter 4 the mitochondrion. In: Bittar EE, Bittar N, editors. *Principles of Medical Biology Cellular Organelles and the Extracellular Matrix* (Madison, WI: Elsevier). p. 59–132.
38. Jeger V, Djafarzadeh S, Jakob SM, Takala J. Mitochondrial function in sepsis. *Eur J Clin Invest*. (2013) 43:532–42. doi: 10.1111/eci.12069

Conflict of Interest: The authors declare that the research was conducted in the absence of any commercial or financial relationships that could be construed as a potential conflict of interest.

frontiers in Medicine

ORIGINAL RESEARCH
published: 28 August 2020
doi: 10.3389/fmed.2020.00510

Topical Melatonin Improves Gastric Microcirculatory Oxygenation During Hemorrhagic Shock in Dogs but Does Not Alter Barrier Integrity of Caco-2 Monolayers

Richard Truse†, Inga Nolten†, Jan Schulz, Anna Herminghaus, Tobias Holtmanns‡, Lukas Gördes‡, Annika Raupach, Inge Bauer, Olaf Picker and Christian Vollmer*

Department of Anesthesiology, Düsseldorf University Hospital, Düsseldorf, Germany

OPEN ACCESS

Edited by:
Samir G. Sakka, Witten/Herdecke University, Germany

Reviewed by:
Wolfgang Weihs, Medical University of Vienna, Austria
Johanna Catharina Duvigneau, University of Veterinary Medicine Vienna, Austria

***Correspondence:**
Richard Truse
richard.truse@med.uni-duesseldorf.de

†*These authors have contributed equally to this work*

‡*In partial fulfillment of the requirements of the MD thesis of T. Holtmanns and L. Gördes*

Specialty section:
This article was submitted to Intensive Care Medicine and Anesthesiology, a section of the journal Frontiers in Medicine

Received: *07 May 2020*
Accepted: *23 July 2020*
Published: *28 August 2020*

Citation:
Truse R, Nolten I, Schulz J, Herminghaus A, Holtmanns T, Gördes L, Raupach A, Bauer I, Picker O and Vollmer C (2020) Topical Melatonin Improves Gastric Microcirculatory Oxygenation During Hemorrhagic Shock in Dogs but Does Not Alter Barrier Integrity of Caco-2 Monolayers. Front. Med. 7:510. doi: 10.3389/fmed.2020.00510

Systemic administration of melatonin exerts tissue protective effects in the context of hemorrhagic shock. Intravenous application of melatonin prior to hemorrhage improves gastric microcirculatory perfusion and maintains intestinal barrier function in dogs. The aim of the present study was to analyze the effects of a topical mucosal melatonin application on gastric microcirculation during hemorrhagic shock *in vivo* and on mucosal barrier function *in vitro*. In a randomized cross-over study, six anesthetized female foxhounds received 3.3 mg melatonin or the vehicle as a bolus to the gastric and oral mucosa during physiological and hemorrhagic (−20% blood volume) conditions. Microcirculation was analyzed with reflectance spectrometry and laser doppler flowmetry. Systemic hemodynamic variables were measured with transpulmonary thermodilution. For analysis of intestinal mucosal barrier function *in vitro* Caco-2 monolayers were used. The transepithelial electrical resistance (TEER) and the passage of Lucifer Yellow (LY) from the apical to the basolateral compartment of Transwell chambers were measured. Potential barrier protective effects of melatonin against oxidative stress were investigated in the presence of the oxidant H_2O_2. During physiologic conditions topical application of melatonin had no effect on gastric and oral microcirculation *in vivo*. During hemorrhagic shock, gastric microcirculatory oxygenation (μHbO_2) was decreased from 81 ± 8% to 50 ± 15%. Topical treatment with melatonin led to a significant increase in μHbO_2 to 60 ± 13%. Topical melatonin treatment had no effect on gastric microcirculatory perfusion, oral microcirculation or systemic hemodynamics. Incubation of H_2O_2 stressed Caco-2 monolayers with melatonin did neither influence transepithelial electrical resistance nor LY translocation. Topical treatment of the gastric mucosa with melatonin attenuates the shock induced decrease in microcirculatory oxygenation. As no effects on local microcirculatory and systemic perfusion were recorded, the improved μHbO_2 is most likely caused by a modulation of local oxygen consumption. *In vitro* melatonin treatment did not improve intestinal barrier integrity in the context of oxidative stress. These results extend the current knowledge on melatonin's protective effects during hemorrhage *in vivo*.

Topical application of melatonin exerts differential effects on local microcirculation compared to systemic pretreatment and might be suitable as an adjunct for resuscitation of hemorrhagic shock.

Keywords: gastric microcirculation, μHbO_2, melatonin, hemorrhagic shock, Caco-2 monolayer, mucosal barrier integrity

INTRODUCTION

Profound hemorrhage and associated hypovolemic shock are leading causes of potentially preventable deaths in the in-hospital and pre-hospital setting, resulting in annual deaths of more than five million people worldwide (1). During hemorrhagic shock, blood flow is redistributed early in favor of more vital organs (i.e., heart and brain) and splanchnic perfusion is usually impaired (2). Mesenteric hypoperfusion induces tissue hypoxia, ultimately causing organ failure. The local attenuation of microcirculatory oxygen supply reduces mucosal barrier function and has been shown to enable translocation of bacteria and endotoxins into portal venous blood and mesenteric lymph circulation, thereby mediating systemic inflammation (3). Maintaining adequate splanchnic perfusion, especially during circulatory shock is considered crucial for prevention and therapy of critical illness (4, 5). In this context melatonin is known to improve microcirculation and has been found in many tissues of the gastrointestinal tract. Melatonin is mainly released by the pineal gland at night, acting as the signal of darkness. However, exogenous administration of melatonin improves hepatic microcirculation and liver function and reduces stress-induced gastric lesions (6). In a previous investigation we were able to show that intravenous administration of melatonin prior to subsequent hemorrhage improves regional gastric microcirculatory perfusion during mild hemorrhagic shock in dogs and blunted the shock-induced damage to the intestinal barrier (7). However, whether melatonin exerts its protective impact via direct effects on the gastric mucosa, or via systemic effects remains unknown. Therefore, the objective of this study was to test whether the topical application of melatonin to the gastric mucosa may influence gastric microcirculation similar to systemic melatonin application in the context of hemorrhagic shock in dogs. As a pretreatment regime prior to a subsequent hemorrhagic shock in many cases does not reflect the clinical reality, in this setting the mucosal melatonin application was performed after onset of experimental hemorrhage. To further elucidate the protective properties of melatonin on gastrointestinal mucosal barrier function independent of microcirculatory changes, we analyzed its effects on the integrity of a Caco-2 cell monolayer during stress conditions.

MATERIALS AND METHODS

Animals

The data were derived from repetitive experiments on six dogs (female foxhounds, 28–36 kg) treated in accordance with NIH guidelines for animal care and the ARRIVE guidelines. Experiments were performed with approval of the local animal care and use committee (North Rhine-Westphalia State Agency for Nature, Environment and Consumer Protection, Recklinghausen, Germany; reference number 84-02.04.2011.A288).

To exclude effects of the oestrus cycle, all dogs were castrated before inclusion into the study. Prior to the experiments, food was withheld overnight with water *ad libitum* to ensure complete gastric depletion and to avoid changes in perfusion and oxygenation due to digestive activity. Each dog underwent each experimental protocol in a randomized order and served as its own control (**Supplementary Table 1**). Experiments were performed at least 3 weeks apart to prevent carryover effects. The experiments were performed under general anesthesia (induction of anesthesia with $4\,mg \cdot kg^{-1}$ propofol, maintenance with sevoflurane, end-tidal concentration 3.0%, 1.5 MAC in dogs). The animals were mechanically ventilated after endotracheal intubation [$F_iO_2 = 0.3$, $VT = 12.5\,ml \cdot kg^{-1}$, a normal tidal volume for dogs (8)] with the respiratory frequency adjusted to achieve normocapnia (end-expiratory carbon dioxide $etCO_2 = 35$ mmHg). During baseline conditions, the dogs were placed on their right side and covered with warming blankets to maintain body temperature at 37.5°C. Throughout the experiments, no additional fluid replacement was administered to avoid volume effects that could influence tissue perfusion and oxygenation. However, after withdrawal of each blood sample for blood gas analysis and measurement of melatonin plasma concentration, normal saline was infused three times the sampling volume to maintain blood volume.

Measurements

Systemic Hemodynamic and Oxygenation Variables

The aorta was catheterized via the left carotid artery for continuous measurement of mean arterial pressure (MAP, Gould-Statham pressure transducers P23ID, Elk Grove, IL) and intermittent arterial blood gas samples adjusted for temperature (Rapidlab 865, Siemens, Eschborn, Germany) from appropriate syringes (PICO50, Radiometer Medical, Brønshøj, Denmark). Cardiac output (CO) was determined via transpulmonary thermodilution (PiCCO 4.2 non US, PULSION Medical Systems, Munich, Germany) at the end of each intervention, at least every 30 min. Heart rate (HR) was continuously measured by electrocardiography (Powerlab, ADInstruments, Castle Hill, Australia). All hemodynamic and respiratory variables were recorded on a personal computer after analog to digital conversion (Powerlab, ADInstruments, Castle Hill, Australia) for later analysis.

Mucosal Oxygenation and Perfusion

Microvascular hemoglobin oxygenation (μHbO_2) and perfusion (μflow) of the gastric and oral mucosa were continuously assessed by tissue reflectance spectrophotometry and laser Doppler flowmetry (O2C, LEA Medizintechnik, Gießen, Germany), as detailed previously (9). Briefly, white light (450–1,000 nm) and laser light (820 nm, 30 mW) is transmitted to the tissue of interest via a micro-lightguide and the reflected light is analyzed. The wavelength-dependent absorption and overall absorption of the applied white light can be used to calculate the percentage of oxygenated hemoglobin (μHbO_2). Due to the Doppler effect, magnitude and frequency distribution of changes in wavelength are proportional to the number of blood cells multiplied by the measured mean velocity (μVel) of these cells. This product is proportional to flow and expressed in arbitrary perfusion units (aU). Hence, this method allows assessment and comparison of oxygenation and perfusion of the same region at the same time.

Since light is totally absorbed in vessels with a diameter >100 μm only microvascular oxygenation of nutritive vessels of the mucosa is measured. The biggest fraction of the blood volume is stored in venous vessels, therefore, mainly postcapillary oxygenation is measured which represents the critical partial pressure of oxygen (pO_2) for ischemia (10).

One flexible light-guide probe is placed in the mouth facing the buccal side of the oral mucosa and a second probe is introduced into the stomach via an orogastric silicone tube and positioned facing the greater curvature. Both sites of measurement represent the microcirculation of different gastrointestinal mucosa regions (11). Online evaluation of the signal quality throughout the experiments allows verification of the correct position of the probe tip. The μHbO_2 and μflow values reported are the means of the last 5 min (150 spectra, 2 s each) of the respective intervention under steady state conditions. The non-traumatic instrumentation and in particular non-traumatic access to the gastric mucosa allows the determination of mucosal microcirculation in the absence of surgical stress. This is particularly desirable with respect to the marked alterations that surgical stress exerts on splanchnic circulation (12). In this situation reflectance spectrophotometry reliably detects even clinically asymptomatic reductions in μHbO_2 (13) and highly correlates with the morphologic severity and extent of gastric mucosal tissue injury (14).

Melatonin Plasma Levels

Plasma melatonin levels during baseline conditions were compared to plasma levels 30 min after topical melatonin administration. Plasma was collected in EDTA-Tubes (Vacutainer K2E EDTA 18.0 mg, Plymouth, UK) and stored at −80°C for later analysis. Plasma melatonin levels were assessed by means of enzyme-linked immunosorbent assay (ELISA) using commercially available kits (IBL International, Hamburg, Germany). Data were collected and analyzed according to the manufacturer's instructions and standards.

Induction of Hemorrhagic Shock

Hemorrhagic shock was induced by removing 20% of the estimated total blood volume via a large bore intravenous catheter in a peripheral vein and the arterial catheter (i.e., 16 ml · kg^{-1} of whole blood over 5 min). According to Advanced Trauma Life Support this model represents a class II shock (15). This reversible and non-lethal shock model allows the investigation of either protective or harmful effects of various interventions, i.e., melatonin. Heparinized shed blood was stored and later retransfused using an infusion set with a 200 μm filter.

Experimental Protocol

Under steady state conditions baseline values were recorded before the animals were randomized to the respective protocol (**Figure 1**). Steady state conditions were defined as stability of hemodynamic variables (heart rate and mean arterial pressure) as well as ventilation parameters (endtidal CO_2, endtidal sevoflurane concentration and inspiratory oxygen fraction). Content of the syringes (melatonin or vehicle) was blinded to the investigator during the experiments and data acquisition. Four different groups were analyzed:

Melatonin (Group M)

To study the effects of melatonin, in total 3.3 mg melatonin [Melatonin powder, Sigma-Aldrich, St. Louis, MO, USA; 0.3 mg melatonin diluted in NaCl 0.9% to a total volume of 3 ml, 5 min later followed by 3 mg melatonin diluted in 3 ml NaCl 0.9% containing 5% ethanol (Carl Roth, Karlsruhe, Germany)] was applied to the oral and gastric mucosa, and all variables were recorded for 2.5 h. Melatonin was applied next to the site of the microcirculation measurement. The gastric bolus reached the stomach via a gastric tube fixed to the O2C probe, whereas the bolus to the oral mucosa was applied around the measuring point via a perforated silicon tube. As melatonin is poorly soluble in water, we choose the solvent ethanol. Melatonin mediated effects on local microcirculation may be superseded by direct effects of ethanol. Therefore, melatonin was applied in two subsequent dosages with the lower concentration dissolved in NaCl 0.9% and the higher dissolved in ethanol. To assess early effects of melatonin on local microcirculation, microcirculatory oxygenation and perfusion were analyzed 5 min after each melatonin application.

Control Experiment (Group C)

As time control experiment, only the solvent (NaCl 0.9% followed by 5% ethanol solution, 3 ml) was applied topically to the oral and gastric mucosa, and all variables were recorded for 2.5 h.

Melatonin + Hemorrhagic Shock (Group MH)

To study the effect of melatonin on hemorrhage and retransfusion, after baseline measurements hemorrhagic shock was induced as described above and values were recorded for 30 min. Then melatonin was topically applied as described above and hemorrhagic shock was continued for further 30 min, followed by retransfusion of the shed blood with an additional observation period of 60 min.

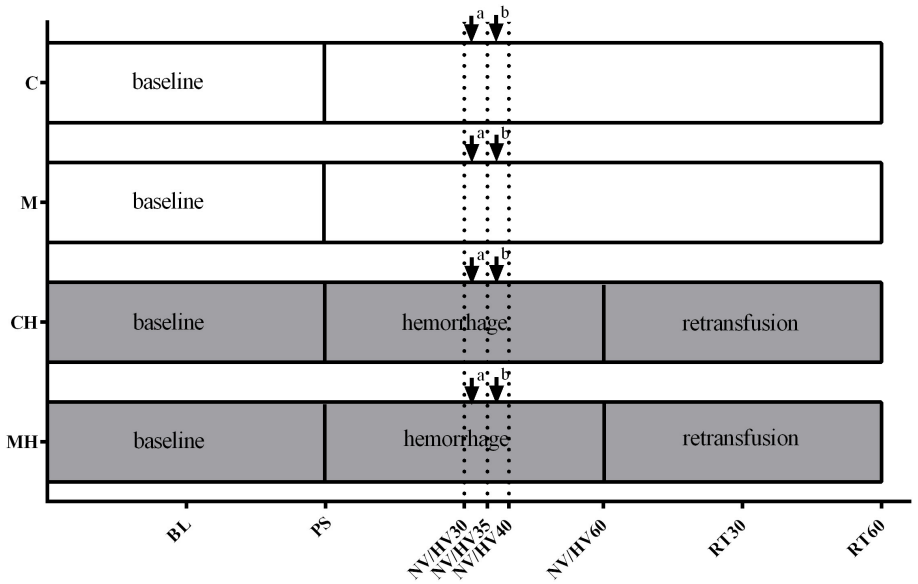

FIGURE 1 | Experimental protocol. Experimental protocol: Application of the vehicle (C) or melatonin (M) during physiological conditions or 30 min after induction of hemorrhagic shock (CH, MH), ↓ bolus application to the oral and gastric mucosa, $\downarrow^{a}$ melatonin 0.3 mg (M, MH)/NaCl 0.9% (C, CH); $\downarrow^{b}$ melatonin 3 mg (M, MH)/ethanol 5% (C, CH). BL, baseline; PS, preshock; HV30/35/40/60 = 30/35/40/60 min after shock induction, NV30/35/40/60 = respective normvolemic control, RT30/60 = retransfusion.

Control Experiment, Hemorrhagic Shock (Group CH)

To study the effects of hemorrhage alone, only the solvent was applied during hemorrhage, followed by retransfusion as described above.

Every 30 min blood samples were obtained for blood gas analysis.

Effects of Melatonin on Caco-2 Monolayer Integrity

Various confounders, like altered macro- and microcirculation, influence the intestinal barrier function *in vivo*. To separate potential direct effects of melatonin on barrier function from those mediated by improvement of microcirculation, we performed the analysis of the intestinal barrier function *in vitro*. We used Caco-2 cells grown on porous membranes as a model system of intact intestinal epithelium (16). These cells exert functional and anatomic similarities to absorptive intestinal enterocytes and hence this a well-established model to study intestinal permeability (17).

Reagents

Minimal essential medium eagle (MEME) was purchased from Sigma-Aldrich (Munich, Germany). Other cell culture reagents were obtained from Biochrom (Berlin, Germany) or life Technologies (Darmstadt, Germany).

Cell Culture

The human colon adenocarcinoma cell line Caco-2 (European Collection of Cell Cultures No. 86010202) was kindly provided by Dr. H. Steinbrenner (Institute for Biochemistry and Molecular Biology I, Heinrich-Heine-University Duesseldorf, Germany). Cells were cultured as described before (18) in MEME, containing 20% fetal calf serum, 1% non-essential amino acids, 1% L-alanyl-L glutamine-dipeptide (Glutamax) and 1% penicillin/streptomycin in a humidified atmosphere (5% CO_2, 95% air, 37°C). The cells were grown under standard conditions until 60–70% confluency. Medium was changed three times a week.

Porous Membrane Supports

Porous membrane supports (Transwell-Clear, 12 mm diameter, 0.4 μm pore size, Corning Incorporated, NY, USA) were coated with 10 $\mu g/cm^2$ collagen (Sigma-Aldrich, Munich, Germany). Then Caco-2 cells were harvested, seeded on the porous membrane inserts at a density of 2×10^5 cells/cm^2 and placed in a Transwell chamber. Cells were grown for 21–28 days to allow differentiation to build an intact, confluent layer, before experiments were performed.

Permeability Measurement

For permeability measurement of the Caco-2 monolayer the trans-epithelial electrical resistance (TEER) and the paracellular passage of Lucifer Yellow (LY, 444 Da, Thermo Fisher Scientific) from the apical to the basolateral compartment of the Transwell chamber were detected. All experiments were performed with $n = 3$ biological replicates, each assayed in duplicates.

Baseline TEER (Ωcm^2) was measured using the EVOM2 Voltmeter (World Precision Instruments, Sarasota, FL, USA) with the Endohm2 chamber (World Precision Instruments, Sarasota, FL, USA) according to manufacturer's instructions. The unit "area resistance" is obtained by multiplying the meter readings by the effective surface area of the filter membrane.

The dimension is Ωcm^2. Values higher than 500 Ωcm^2 were considered as sufficient confluence (19). After detection of baseline TEER, the medium was removed, and the inserts were incubated with 500 µl of the test component in the apical compartment and 1,000 µl of medium in the basal compartment for the determined period of time. Thereafter TEER (Ωcm^2) measurement was repeated. Then medium was replaced with freshly prepared Hank's balanced salt solution adjusted to pH 7.4 for 15 min in non-CO_2 atmospheric conditions. LY (200 µg/ml) was administered to the apical compartment. After 2 h LY concentration was measured in both compartments using a fluorescence spectrophotometer (excitation wavelength: 485 nm, emission wavelength: 535 nm). LY translocation was determined by calculating the ratio of basolateral to apical LY concentration as marker of barrier function.

Effect of Melatonin on Barrier Function

To test the effect of melatonin on TEER and LY translocation, damage was induced by the oxidant H_2O_2 [10 and 30 mM, incubation for 4 h, based on pilot experiments (**Supplementary Figure 1**)]. In a first set of experiments melatonin (0.1 mg/ml) was administered into the apical and basolateral compartment of the Transwell chamber diluted in the Caco-2 cell culture medium (see above) simultaneously with the administration of H_2O_2 and incubated for 4 h. In another set of experiments melatonin was added to the chamber 30 min prior to H_2O_2 followed by incubation for further 4 h.

Statistical Analysis

Primary endpoints were defined as gastric/oral microcirculation *in vivo* and changes in LY translocation and TEER *in vitro*. Secondary endpoints were defined as systemic hemodynamic and oxygenation variables and plasma melatonin levels. All data are presented as mean ± standard deviation (mean ± SD). Statistical differences were analyzed with GraphPad Prism version 6.03 for Windows, GraphPad Software, La Jolla California USA. In the *in vivo* experiments a repeated measures two-way ANOVA followed by Dunnett's multiple comparisons test (*in vivo* experiments, vs. HV30) or Sidak *post hoc* test (*in vivo* experiments, vs. respective control group) were used. An *a priori* power analysis (G*Power Version 3.1.9.2) revealed a power of 0.85 for detection of differences between the different groups with $n = 6$ in four groups, repeated measurements, $\alpha < 0.05$ and η^2 of 0.5 (calculated from previous experiments). In the *in vitro* experiments the Kruskal-Wallis test followed by Dunn's multiple comparison test (non-parametric data) was performed. $p < 0.05$ was considered significant.

RESULTS

Effects of Melatonin Under Physiological Conditions (Groups C and M)

Under physiological conditions, melatonin had no effect on gastric and oral µHbO_2 and µflow (**Table 1**). During baseline conditions, gastric µflow was lower in group M compared to the control group. This effect was no longer evident in the further course of the experiment. Systemic hemodynamic variables remained stable throughout the experiment without differences to the control group. Microcirculatory and systemic variables are presented in **Tables 2**, **3**, respectively.

Effects of Melatonin During Hemorrhage and Retransfusion (Groups CH and MH)

Gastric Microcirculation

Hemorrhagic shock reduced gastric µHbO_2 from 80 ± 8 to 51 ± 14% (group CH) and from 81 ± 8 to 50 ± 15% (group MH) (**Table 1**). In the control group µHbO_2 remained depressed after 60 min of shock. In contrast, melatonin application led to a significant increase in µHbO_2 (HV35: 60 ± 13%; HV40: 60 ± 16%) compared to HV30 immediately before the local treatment. This increase sustained throughout the remaining state of shock (**Figure 2**). No significant differences to the control group were observed. After retransfusion of the shed blood µHbO_2 was restored in both groups to 79 ± 9% (group CH) and 83 ± 6% (group MH) without differences between the groups. Gastric µflow was reduced during hemorrhage from 98 ± 21 to 69 ± 7 aU (group CH) and from 118 ± 33 to 83 ± 36 aU (group MH) (**Table 1**). The velocity of gastric microcirculatory perfusion (µvel) was higher in group MH compared to the control group during baseline conditions. After retransfusion µvel was higher in group MH compared to CH, similar to the significantly higher starting level (**Table 1**). Topical application of melatonin did not modulate local gastric perfusion.

Oral Microcirculation

During hemorrhagic shock, oral µHbO_2 decreased from 85 ± 5 to 48 ± 2% (group CH) and from 84 ± 6 to 47 ± 3% (group MH) (**Table 1**). Oral µHbO_2 showed an early recovery in the control group (HV35: 54 ± 5%) and melatonin group (HV40: 54 ± 10%). During the subsequent shock period oral µHbO_2 recovered to 57 ± 7% in both groups (group CH and MH). In contrast to gastric microcirculation, extent of the recovery in microcirculatory oxygenation were not modulated by melatonin. During hemorrhage, oral µflow and µvelo were depressed in both groups. In parallel to the findings at the gastric mucosa, topical application of melatonin had no effect on oral microcirculatory blood flow and velocity **(Table 1)**.

Systemic Hemodynamic Variables

DO_2 decreased during hemorrhage equally in both groups from 12 ± 3 min^{-1} to 7 ± 1 ml kg^{-1} min^{-1} (group CH) and from 12 ± 3 to 7 ± 2 ml kg^{-1} min^{-1} and was restored after retransfusion to 12 ± 3 ml kg^{-1} min^{-1} in both groups (**Figure 3**). The decrease of DO_2 is based on a similar decrease of cardiac output and an increase in SVR. Application of melatonin did not alter systemic hemodynamic variables during the subsequent 30 min of shock and following retransfusion period (**Table 2**). A metabolic acidosis evolved during hemorrhage, without differences between the melatonin treated group and the control group. Further metabolic variables are displayed in **Table 3**.

Melatonin Plasma Levels

Plasma melatonin levels remained within the physiological range during baseline conditions in all groups. During the course of

TABLE 1 | Microcirculatory variables.

Parameter	Group	BL		PS		NV/HV30		NV/HV35		NV/HV40		NV/HV60		RT30		RT60	
gastric μHbO_2 [%]	C	77 ± 3		80 ± 2		79 ± 7		79 ± 6		75 ± 3		77 ± 4		74 ± 6		74 ± 7	
	CH	79 ± 8	*	81 ± 8	*	51 ± 14		56 ± 14		58 ± 13		56 ± 12		78 ± 14	*	79 ± 9	*
	M	77 ± 6		77 ± 7		76 ± 7		77 ± 6		76 ± 8		76 ± 7		75 ± 8		76 ± 8	
	MH	81 ± 8	*	84 ± 6	*	50 ± 15		60 ± 13	*	60 ± 16	*	59 ± 13	*	81 ± 6	*	83 ± 6	*
gastric µflow [aU]	C	120 ± 39		117 ± 26		122 ± 14		117 ± 14		112 ± 11		100 ± 37		102 ± 28		104 33	
	CH	98 ± 21	*	93 ± 15		69 ± 7		76 ± 11		72 ± 9		77 ± 9		105 ± 11	*	102 37	*
	M	86 ± 42	#	112 ± 30		106 ± 41		119 ± 31		118 ± 35		108 ± 44		115 ± 40		111 37	
	MH	118 ± 33	*	130 ± 28	#*	83 ± 36		91 ± 31		91 ± 40		96 ± 35		118 ± 28	*	123 33	*
gastric µvel [aU]	C	17 ± 2		16 ± 2		16 ± 1		16 ± 1		15 ± 0		16 ± 2		16 ± 2		16 2	
	CH	16 ± 2		15 ± 2		14 ± 2		14 ± 1		14 ± 1		14 ± 1		16 ± 1		16 4	*
	M	15 ± 4		17 ± 3		16 ± 3		17 ± 2		17 ± 2		16 ± 3		17 ± 3		17 3	
	MH	18 ± 4	#*	19 ± 4	#*	15 ± 3		15 ± 2		15 ± 3		16 ± 3		16 ± 1		18 4	#*
oral μHbO_2 [%]	C	83 ± 6		81 ± 6		81 ± 5		83 ± 4		83 ± 4		84 ± 4		85 ± 5		85 ± 4	
	CH	85 ± 5	*	83 ± 2	*	48 ± 6		54 ± 5	*	57 ± 5	*	57 ± 7	*	90 ± 6	*	95 ± 2	*
	M	83 ± 7		81 ± 6		81 ± 5		83 ± 4		84 ± 4		84 ± 4		84 ± 5		85 ± 5	
	MH	84 ± 6	*	82 ± 4	*	47 ± 6		51 ± 7		54 ± 10	*	57 ± 7	*	90 ± 6	*	92 ± 6	*
oral µflow [aU]	C	169 ± 49		158 ± 53		157 ± 55		161 ± 57		164 ± 48		173 ± 60		175 ± 62		175 ± 51	
	CH	159 ± 45	*	142 ± 42	*	54 ± 30		59 ± 31		64 ± 25		70 ± 35		202 ± 64	*	241 ± 52	*
	M	172 ± 56		168 ± 48		168 ± 48		173 ± 48		179 ± 48		183 ± 53		177 ± 61		175 ± 66	
	MH	186 ± 84	*	182 ± 87	*	67 ± 57		73 ± 61		76 ± 64		87 ± 72		224 ± 67	*	256 ± 62	*
oral µvel [aU]	C	29 ± 5		28 ± 6		28 ± 7		28 ± 7		28 ± 7		29 ± 7		29 ± 8		29 ± 7	
	CH	26 ± 5	*	25 ± 5	*	17 ± 5		17 ± 5		18 ± 4		18 ± 5		31 ± 7	*	35 ± 6	*
	M	31 ± 12		31 ± 13		31 ± 12		31 ± 11		31 ± 9		31 ± 9		30 ± 9		30 ± 9	
	MH	29 ± 12	*	30 ± 11	*	19 ± 9		20 ± 9		20 ± 9		21 ± 10		34 ± 10	*	38 ± 10	*

*Microcirculatory variables of the experimental groups—gastric and oral mucosal hemoglobin oxygenation (μHbO_2); gastric and oral mucosal microcirculatory perfusion (µflow) and perfusion velocity (µvel). Data are presented as absolute values, mean ± SD, n = 6, *p < 0.05 vs. NV/HV30, 2-way ANOVA for repeated measurements followed by Dunnett's post hoc test; #p < 0.05 vs. respective control group (vs. C for M, vs. CH for MH). 2-way ANOVA for repeated measurements followed by Sidak post hoc test. BL, baseline; PS, preshock; NV/HV30/35/40/60 = 30/35/40/60 min after shock induction or the respective time control, RT30/60 = retransfusion.*

TABLE 2 | Systemic hemodynamic.

Parameter	Group	BL			PS			NV/HV30			NV/HV35			NV/HV40			NV/HV60			RT30			RT60		
MAP [mmHg]	C	60 ± 4	*		63 ± 5			64 ± 5			63 ± 5			63 ± 4			63 ± 4			64 ± 6			64 ± 7		
	CH	58 ± 2	*		61 ± 5	*		49 ± 3			51 ± 4			53 ± 4			56 ± 5	*		71 ± 6	*		64 ± 5	*	
	M	61 ± 4			62 ± 3			62 ± 3			62 ± 3			62 ± 3			62 ± 3			63 ± 4			62 ± 5		
	MH	63 ± 6	#*		63 ± 3	*		48 ± 2			50 ± 6			51 ± 5			56 ± 3	*		71 ± 5	*		67 ± 5	*	
HR [min^{-1}]	C	116 ± 9			117 ± 11			115 ± 11			114 ± 11			114 ± 11			114 ± 11			112 ± 11			109 ± 12		
	CH	117 ± 8			115 ± 6			117 ± 13			140 ± 60			141 ± 61			120 ± 13			107 ± 6			107 ± 6		
	M	115 ± 12			113 ± 9			113 ± 9			112 ± 10			112 ± 10			112 ± 10			112 ± 9			109 ± 10		
	MH	116 ± 7			114 ± 5			115 ± 12			137 ± 60			138 ± 60			119 ± 11			105 ± 5			107 ± 5		
CO [$ml \cdot kg^{-1} \cdot min^{-1}$]	C	80 ± 12			79 ± 11			77 ± 8									75 ± 7			76 ± 8			77 ± 9		
	CH	82 ± 10	*		85 ± 17	*		46 ± 2									53 ± 3			81 ± 10	*		84 ± 10	*	
	M	79 ± 13			78 ± 12			77 ± 9									76 ± 9			76 ± 9			77 ± 10		
	MH	78 ± 9	*		77 ± 8	*		45 ± 7									52 ± 5	*		79 ± 9	*		82 ± 10	*	
DO_2 [$ml \cdot kg^{-1} \cdot min^{-1}$]	C	12 ± 3			12 ± 3			11 ± 2									11 ± 2			11 ± 2			11 ± 2		
	CH	12 ± 3	*		13 ± 3	*		7 ± 1									8 ± 1			12 ± 2	*		12 ± 3	*	
	M	12 ± 3			11 ± 3			11 ± 2									11 ± 2			11 ± 2			11 ± 2		
	MH	12 ± 3	*		12 ± 3	*		7 ± 2									8 ± 1			12 ± 3	*		12 ± 3	*	
SVR [$mmHg \cdot l^{-1} \cdot min$]	C	25 ± 5			27 ± 6			28 ± 5									28 ± 5			28 ± 6			27 ± 5		
	CH	24 ± 4	*		24 ± 6	*		35 ± 5									35 ± 5			29 ± 4	*		25 ± 4	*	
	M	22 ± 6			22 ± 6			21 ± 5									21 ± 5			21 ± 5			22 ± 6		
	MH	26 ± 5	*		27 ± 5	*		35 ± 6									35 ± 5			30 ± 5	*		27 ± 4	*	
SV [ml]	C	22 ± 5			21 ± 5			21 ± 5									21 ± 4			21 ± 4			22 ± 4		
	CH	22 ± 4	*		23 ± 6	*		12 ± 2									14 ± 3			23 ± 3	*		24 ± 4	*	
	M	22 ± 6			22 ± 6			21 ± 5									21 ± 5			21 ± 5			22 ± 6		
	MH	21 ± 4	*		21 ± 4	*		12 ± 2									14 ± 2			24 ± 4	*		24 ± 5	*	

*Systemic hemodynamic variables of the experimental groups—mean arterial pressure (MAP), heart rate (HR), cardiac output (CO), systemic oxygen delivery (DO_2), systemic vascular resistance (SVR) and stroke volume (SV). Data are presented as absolute values, mean ± SD, n = 6, *p < 0.05 vs. NV/HV30, 2-way ANOVA for repeated measurements followed by Dunnett's post hoc test; #p < 0.05 vs. respective control group (vs. C for M, vs. CH for MH). 2-way ANOVA for repeated measurements followed by Sidak post hoc test. Due to occasionally missing values of heart rate, no statistical analysis was performed. BL, baseline; PS, preshock; NV/HV30/35/40/60 = 30/35/40/60 min after shock induction or the respective time control, RT30/60 = retransfusion.*

TABLE 3 | Blood gas analysis and metabolic variables.

Parameter	Group	BL				PS				NV/HV30				NV/HV60				RT30				RT60			
SAT [%]	C	98.8	±	1.0		98.8	±	0.9		98.9	±	0.9		98.8	±	0.9		98.8	±	0.9		98.9	±	0.9	
	CH	98.3	±	1.1	*	98.5	±	0.9	*	97.6	±	1.4		98.0	±	1.2	*	98.6	±	0.8	*	98.6	±	0.8	*
	M	99.0	±	0.8	#	99.0	±	0.8	#	99.0	±	0.7	#	99.0	±	0.8	#	99.0	±	0.7	#	99.0	±	0.7	#
	MH	98.8	±	1.0	#*	98.8	±	1.0	*	98.2	±	1.6	#	98.4	±	1.4	#	98.9	±	0.9	*	98.8	±	0.9	*
pCO_2 [mmHg]	C	37.4	±	2.5		37.1	±	2.7		37.4	±	2.3		37.9	±	2.2		37.9	±	1.8		38.8	±	3.4	*
	CH	36.7	±	2.6	*	36.6	±	2.1	*	41.5	±	3.1		40.2	±	2.5	*	36.8	±	1.9	*	36.8	±	1.9	*
	M	36.6	±	2.6		36.7	±	3.0		37.0	±	2.7		37.3	±	2.5		37.3	±	2.1		37.8	±	3.2	
	MH	36.6	±	2.4	*	36.3	±	2.4	*	41.1	±	3.9		40.0	±	4.1		36.7	±	2.4	*	37.3	±	2.2	*
pO_2 [mmHg]	C	139.8	±	11.0	*	143.2	±	11.1		146.0	±	10.7		145.2	±	9.2		146.3	±	11.3		144.9	±	8.3	
	CH	139.0	±	14.2	*	142.5	±	10.6	*	128.0	±	10.5		136.5	±	9.9	*	148.8	±	10.9	*	149.2	±	10.5	*
	M	141.7	±	8.3		144.2	±	6.9		145.2	±	7.6		145.7	±	5.5		147.0	±	6.2		147.8	±	9.6	
	MH	143.2	±	11.2	*	144.0	±	9.0	*	131.5	±	10.3		137.5	±	10.4	*	152.5	±	8.9	*	148.2	±	7.8	*
pH	C	7.38	±	0.03		7.38	±	0.03		7.38	±	0.02		7.38	±	0.02		7.38	±	0.03		7.37	±	0.03	
	CH	7.38	±	0.03	*	7.38	±	0.03	*	7.31	±	0.03		7.32	±	0.03	*	7.37	±	0.02	*	7.37	±	0.02	*
	M	7.38	±	0.02		7.38	±	0.03		7.38	±	0.02		7.38	±	0.02		7.38	±	0.02		7.37	±	0.03	
	MH	7.38	±	0.03	*	7.38	±	0.02	*	7.32	±	0.04		7.33	±	0.04	*	7.37	±	0.03	*	7.37	±	0.03	*
HCO_3 [mmol·l^{-1}]	C	21.3	±	0.7		21.3	±	0.7		21.3	±	0.7		21.5	±	0.6		21.4	±	0.6		21.7	±	0.8	*
	CH	21.0	±	0.6	*	20.9	±	0.5	*	20.2	±	0.6		20.1	±	0.5		20.4	±	0.6		20.4	±	0.5	
	M	21.1	±	0.8		21.0	±	0.9		21.0	±	0.6		21.1	±	0.5		21.1	±	0.4		21.1	±	0.5	#
	MH	21.1	±	0.7	*	20.9	±	0.7	*	20.4	±	0.7		20.3	±	0.7		20.5	±	0.8		20.7	±	0.8	
Hb [g·100 ml^{-1}]	C	11.1	±	1.1		11.0	±	1.1		10.9	±	1.0		10.8	±	1.1		10.9	±	1.2		10.8	±	1.3	
	CH	10.9	±	1.3		10.8	±	1.4		10.8	±	1.3		10.5	±	1.2	*	10.4	±	1.2	*	10.4	±	1.4	*
	M	10.7	±	1.2	#	10.5	±	1.3	#	10.5	±	1.3	#	10.4	±	1.3	#	10.5	±	1.3	#	10.4	±	1.3	#
	MH	10.9	±	1.4		10.8	±	1.5		11.0	±	1.4	#	10.8	±	1.2	#	10.6	±	1.3	#*	10.6	±	1.4	#*
lactate [mmol·l^{-1}]	C	0.9	±	0.4		1.0	±	0.4		1.1	±	0.4		0.9	±	0.3		0.9	±	0.3		0.9	±	0.3	
	CH	0.9	±	0.3		1.1	±	0.4		1.4	±	0.3		1.2	±	0.3		1.0	±	0.3		1.0	±	0.3	
	M	1.0	±	0.4		1.1	±	0.4		1.2	±	0.4		1.1	±	0.3		1.1	±	0.3		1.1	±	0.3	
	MH	0.8	±	0.2		0.9	±	0.3		1.2	±	0.3		1.0	±	0.3		0.8	±	0.2		0.8	±	0.2	
BE [mmol·l^{-1}]	C	−3.0	±	1.2		−2.9	±	0.8		−3.0	±	0.9		−2.8	±	0.9		−2.9	±	1.0		−2.7	±	0.7	
	CH	−3.0	±	0.8	*	−3.2	±	0.7	*	−4.9	±	0.7		−4.8	±	0.8		−3.8	±	0.8	*	−3.8	±	0.6	*
	M	−2.9	±	0.8		−3.1	±	0.8		−3.1	±	0.6		−3.1	±	0.5		−3.0	±	0.5		−3.1	±	0.5	
	MH	−2.9	±	0.9	*	−3.1	±	0.8	*	−4.6	±	0.8		−4.5	±	0.9		−3.7	±	1.0	*	−3.5	±	1.0	*

Metabolic variables of the experimental groups—arterial oxygen saturation (SAT), arterial carbon dioxide partial pressure ($PaCO_2$), arterial oxygen partial pressure (P_aO_2), pH, bicarbonate (HCO_3), hemoglobin concentration (Hb), lactate plasma concentration, and base excess (BE). Data are presented as absolute values, mean ± SD, n = 6, $^*p < 0.05$ vs. NV/HV30, 2-way ANOVA for repeated measurements followed by Dunnett's post hoc test; #$p < 0.05$ vs. respective control group (vs. C for M, vs. CH for MH). 2-way ANOVA for repeated measurements followed by Sidak post hoc test. Due to occasionally missing values of lactate plasma concentration, no statistical analysis was performed. BL, baseline; PS, preshock; NV/HV30/60 = 30/60 min after shock induction or the respective time control, RT30/60 = retransfusion.

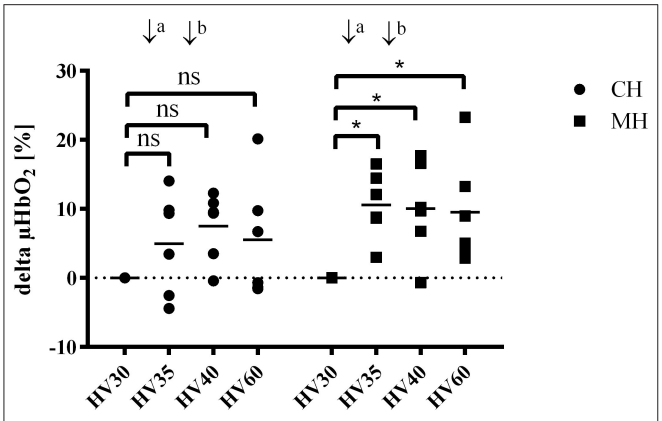

FIGURE 2 | Δ gastric μHbO_2 during hemorrhagic shock (hemorrhagic groups). Changes in gastric microcirculatory oxygenation (delta μHbO_2) compared to the pretreament value (HV30) in anesthetized dogs during hemorrhagic shock with topical application (↓) of vehicle (CH, $\downarrow^a$ NaCl 0.9%; $\downarrow^b$ ethanol 5%) or melatonin (MH; $\downarrow^a$ 0.3 mg; $\downarrow^b$ 3 mg). Data are presented as individual values and mean for $n = 6$ dogs; $^*p < 0.05$ vs. HV30, 2-way ANOVA for repeated measurements followed by Dunnett's *post hoc* test. HV30/35/40/60 = 30/35/40/60 min after shock induction.

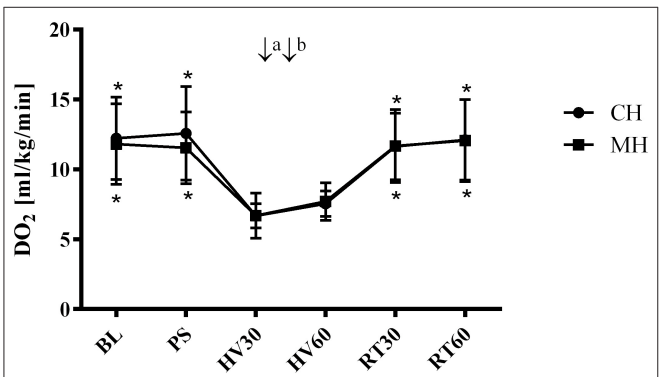

FIGURE 3 | Systemic oxygen delivery (hemorrhagic groups). Systemic arterial oxygen delivery (DO_2) in anesthetized dogs during hemorrhagic shock with topical application (↓) of vehicle (CH, $\downarrow^a$ NaCl 0.9%; $\downarrow^b$ ethanol 5%) or melatonin (MH; $\downarrow^a$ 0.3 mg; $\downarrow^b$ 3 mg). Data are presented as mean ± SD for $n = 6$ dogs; $^*p < 0.05$ vs. HV30, 2-way ANOVA for repeated measurements followed by Dunnett's *post hoc* test. BL, baseline; PS, preshock; HV30/60 = 30/60 min after shock induction, RT30/60 = retransfusion.

the experiment no significant fluctuation in melatonin plasma concentration was seen in the control groups. Melatonin plasma concentration increased significantly to supraphysiological levels in melatonin treated animals (**Figure 4**).

Effect of Melatonin on Caco-2 Cell Layer Integrity

Melatonin showed no effect on Caco-2 cell layer integrity under physiologic conditions. Oxidative stress by incubation of the monolayer with 10 mM H_2O_2 let to a pronounced decline in cellular integrity as indicated by increased paracellular passage of LY and diminished TEER (**Figure 5**). The decrease

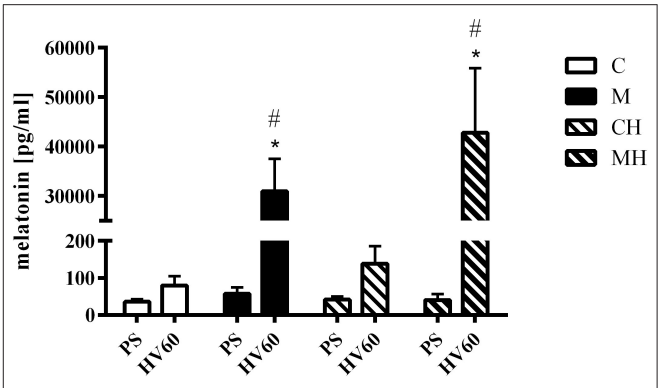

FIGURE 4 | Melatonin plasma concentration. Melatonin plasma concentrations during baseline conditions and 30 min after topical application of the vehicle (C, CH) or melatonin (M, MH). Data are presented as mean ± SD for n = 6 dogs; $^*p < 0.05$ vs. basic value (PS), $\#p < 0.05$ vs. respective control group (vs. C for M, vs. CH for MH), 2-way ANOVA for repeated measurements followed by Sidak *post hoc* test. PS, preshock; HV60 = 60 min after shock induction.

in TEER was obvious but due to large standard deviation not significant. Melatonin had no direct effect on Caco-2 cell layer integrity, neither with pre-incubation prior to oxidative stress (**Supplementary Figure 2**) nor when co-incubated with H_2O_2 (**Figure 5**).

DISCUSSION

The main aim of the present study was to analyze the effects of topically applied melatonin on gastric and oral mucosal microcirculation during a mild hemorrhagic shock *in vivo* and the direct impact of melatonin on mucosal barrier integrity *in vitro*. Here, we could show that application of melatonin during a hemorrhagic shock may improve gastric microcirculatory oxygenation in dogs. Incubation of a CaCo-2 monolayer with melatonin did not directly influence mucosal barrier integrity.

In the *in vivo* part of this study we investigated the impact of melatonin on mucosal microcirculation using 0.3 mg melatonin solved NaCl 0.9% followed 5 min later by 3 mg melatonin solved in 5% ethanol. The chosen concentration is based on our previous *in vivo* study in dogs (7) and corresponds to ∼100 µg kg^{-1} which has been shown to be protective in various settings in different species (20). The observed effects on gastric μHbO_2 are independent of the solvent and 3 mg melatonin did not further increase gastric μHbO_2. However, the study was not designed to compare different drug concentrations.

During physiological conditions in normovolemic anesthetized dogs, melatonin had no effect on micro- and macrohemodynamic variables. In contrast, melatonin was able to improve gastric microcirculatory oxygenation when applied topically to the gastric mucosa during hemorrhagic shock. The observed effect on gastric μHbO_2 is rather small. Whereas, in the control group gastric μHbO_2 remained depressed during the shock period, melatonin application enhanced gastric μHbO_2 recovery during hemorrhage compared to the state

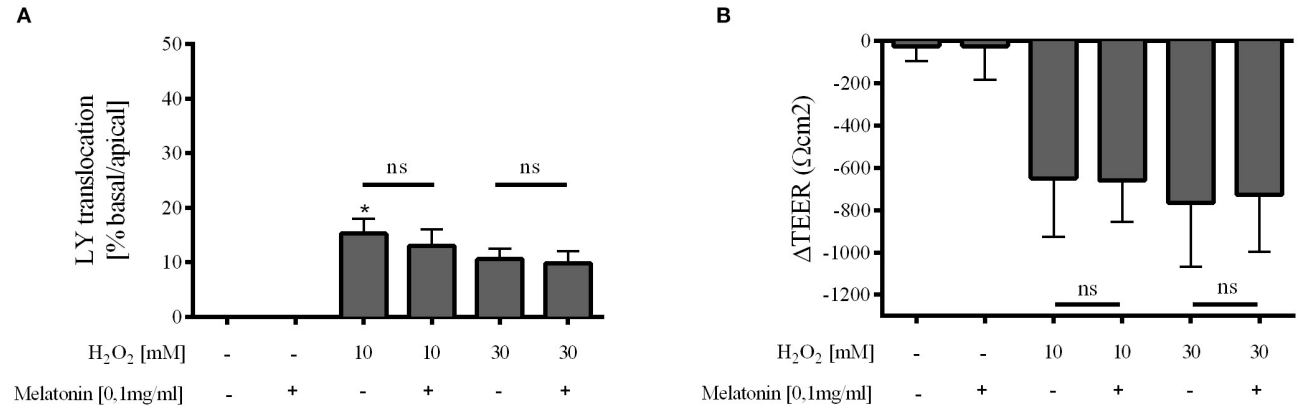

FIGURE 5 | Caco-2 monolayer integrity. Relative translocation of LY **(A)** and transepithelial electrical resistance (TEER) **(B)** over the epithelial barrier from the apical to the basolateral compartment after co-incubation with melatonin 0.1 mg/ml and H_2O_2 10 and 30 mM compared to the control group. Data shown as mean ± SD. *$p <$ 0.05 vs. control, ns, not significant, $n = 3$, Kruskal-Wallis test with Dunn's multiple comparison test.

of shock immediately before local treatment. These results are quite interesting and of potential clinical importance. Improving microcirculatory perfusion might fall short in improving local tissue function, as enhanced perfusion does not necessarily ensure sufficient oxygenation. Concerning gut integrity especially microcirculatory oxygenation is a major determinant for anastomotic healing (21). In a previous study we could demonstrate that an improved gastric μHbO_2 by pretreatment with nitroglycerin prior to a hemorrhagic shock was associated with an ameliorated, shock induced damage to the gastric mucosal barrier (22). In this study, regional mucosal oxygenation was improved but regional perfusion remained unchanged. This observation contrasts with other reports on melatonin's effect on microcirculatory perfusion. Pretreatment or therapy with melatonin was able to improve hepatic and gastric perfusion in the context of a hemorrhagic shock in rats (23, 24) and dogs (7). However, in the present study we choose a regime with topical application of melatonin as a treatment during hemorrhagic shock. The regional gastrointestinal perfusion is mainly regulated at the level of the mesenteric arterioles (25). A pronounced vasoconstriction in these arterioles upstream the mucosal microcirculation, as part of the sympathetic mediated counter regulation to acute blood loss, may attenuate a potential melatonin mediated vasodilation in the capillary bed. As the systemic oxygen delivery and local gastric perfusion are not improved by melatonin, our results indicate, that the increased microcirculatory oxygenation did not result from improved local oxygen supply. Hence, μHbO_2 increases due to a reduced oxygen demand or a cellular inability to extract oxygen. An oxygen extraction deficit seems to be unlikely, as melatonin is known to exert tissue protective effects even during conditions where oxygen delivery is impaired. More to the contrary, melatonin treatment has been shown to evoke a rightward shift of the oxygen dissociation curve of hemoglobin, thereby promoting tissue oxygenation. This was demonstrated in a rat model exposed to hypothermia (26). Whether similar effects may provide protective effects in the context of hemorrhage has to be studied in further detail. On the other hand, melatonin may improve mitochondrial respiration during pathologic conditions like hemorrhagic shock by inhibition of oxidative stress-induced mitochondrial damage (27). Furthermore, melatonin increased the activity of the mitochondrial complexes I and IV in brain and liver mitochondria, the only two tissues studied (28). Therefore, modulation of mitochondrial function may account for the increased postcapillary μHbO_2 observed in the present study. While melatonin plasma concentrations during baseline and control conditions were similar to those described in different studies in various species (7, 29–31), local melatonin application led to a pronounced increase in plasma levels. We can only speculate, whether the observed effects on gastric μHbO_2 are mediated via local mucosal or systemic effects of melatonin. The melatonin plasma levels measured 25 min after mucosal application corresponds to ∼30–50% of the plasma concentrations after systemic melatonin application (7). However, as the topical melatonin application led to a modulation of gastric μHbO_2 within minutes, a direct effect on local mucosal microcirculation is plausible.

Melatonin's microcirculatory protective effects are restricted to the gastric mucosa. A similar treatment of the oral mucosa showed inconclusive results, as oral μHbO_2 improved after the second melatonin dose, but increased early in the control group, too. These observations are well in line with our previous results, indicating that the oral mucosa reacts differently compared to the gastric mucosa when treated with various vasoactive drugs (22, 32). At both locations, the verum was applied in direct proximity to the measuring site of the O2C device. During sevoflurane anesthesia the gastric motility is decreased, and gastric emptying is markedly prolonged (33). Therefore, dog's stomach is considered to be a relatively closed system with a minor clearance of gastric content toward the small intestine. Compared to this, after bolus application to the oral mucosa a relevant distribution of the active ingredient is likely, causing a

consecutive reduction in effective concentration. Furthermore, the different histologic structure of the oral and gastric mucosa with diverse composition of the local microcirculation may account to the varying effects of mucosal application of vasoactive drugs. Once more our results underline, that a focus on the readily accessible oral microcirculation may not be suitable for the interpretation of further aboral parts of the gastrointestinal mucosal microcirculation by all means.

In the *in vivo* part of this study a cross-over design was chosen to reduce the number of animals needed to reach a sufficient power. However, the experimental group was not perfectly homogenous, indicated by occasional significant differences in micro-and macrocirculatory variables at baseline and pre-shock conditions. Although the exact reason is unclear, numerous factors, i.e., age of the animals or differences in stress hormone levels, could be causative. Carry-over effects of the preceding treatment are improbable, as melatonin has a half-life time of 20 min (34) and in humans elevated plasma levels after intake of 1–5 mg melatonin normalized within 8 h (35). After a single application of melatonin, a long-lasting (i.e., over 3 weeks) modulation of protein expression seems to be unlikely.

In the *in vitro* part of our experiments we analyzed the direct effects of melatonin on mucosal barrier integrity using the well-established Caco-2 cell culture model. To roughly simulate the conditions of oxidative stress induced by shock and reperfusion, the cells were exposed to exogenous administration of H_2O_2. Powers and colleagues demonstrated a similar reaction pattern of alveolar macrophages to oxidative stress generated by shock and reperfusion *in vivo* and by H_2O_2 *in vitro* (36). In the present study melatonin had no effect on mucosal barrier function. Neither LY translocation nor transepithelial electrical resistance was modulated after exogenous melatonin application. This is rather astonishing taken into account the known tissue protective properties of melatonin. In isolated fish hepatocytes exposed to 50 μM H_2O_2, addition of 0.1 mg/ml melatonin was sufficient to prevent the accumulation of free radicals and reactive oxygen species and to ameliorate the antioxidant status through modulation of transcription factors, e.g., NF-κB, ERK/Akt (37). Large datasets exist concerning melatonin's hepatoprotective properties [see (20) for further information], usually with a melatonin pretreatment regime for a couple of days or sometimes even weeks in advance to the harmful stimulus. Studies concerning the protective effect on the gut are sparse. Long-term administration of oral melatonin was demonstrated to maintain duodenal mucosal permeability during ethanol-induced stress (38) and to reduce colitis induced elevated gut permeability (39), thus improving intestinal barrier function in chronic disease. In contrast to these long-term pretreatment protocols, the present study focused on short term effects. While melatonin's antioxidative characteristics might be effective in the presence of H_2O_2, its anti-inflammatory properties will be secondary in the cell culture model. Furthermore, it remains unclear whether melatonin's tissue protective effects are mainly attributed to anti-oxidative radical scavenging properties or to systemic receptor-mediated effects, e.g., on regional microcirculation. In our previous study an increase in μflow after i.v. melatonin application was associated with a preserved intestinal barrier function during hemorrhagic shock (7). The missing protective effect of melatonin in the *in vitro* model indicates that melatonin's protective effect on intestinal barrier function is possibly not mediated via direct effects on the intestinal mucosa, but perhaps via an improvement of local microcirculation. However, the experimental setup does not mimic a therapeutically approach with initiation of the treatment after onset of oxidative stress. Therefore, the pre- and co-incubation regime limits the transferability of our results to the clinical setting. In the present model, application of H_2O_2 led to a pronounced increase in LY translocation and reduction in TEER. No dose dependence could be observed in cells treated with 10 mM and 30 mM H_2O_2. As even 10 mM H_2O_2 could result in an irreversible damage of the barrier function (40), an extensive cell breakdown could counteract any melatonin mediated potentially protective effects. These limitations could possibly explain the observed lack of influence of melatonin on Caco-2 monolayer integrity.

Clinical Impact

Application of melatonin during resuscitation improved survival in a rat and porcine model of polytrauma and hemorrhagic shock (41, 42). No microcirculatory variables were assessed in these studies. However, a subsequent investigation revealed an increased urinary output in the first hours of resuscitation in melatonin treated pigs after trauma/hemorrhage (43). This could be related to an improved renal function. One might speculate, that an improved renal microcirculation during resuscitation enhanced renal recovery. Similar to our results, melatonin application had no effect on macrohemodynamic variables. However, melatonin application in these studies resulted in plasma concentrations of 8–10 mM, which are several orders of magnitude higher than the plasma levels observed in our present study (∼17 nM). Therefore, application of higher melatonin concentrations may result in more pronounced microcirculatory effects. This has to be investigated in the future. Together with the results of our previous study (7) our present results confirm, that exogenous melatonin ameliorates gastric microcirculatory derangements during hemorrhagic shock. Beside the well-known anti-inflammatory and anti-oxidative properties, modulation of the microcirculation could be a new aspect of melatonin's known tissue protective effects. Several tissues including the intestine have been shown to express melatonin receptors (44) and the antioxidative effects of melatonin are potentially receptor mediated (20). Whether the melatonin-mediated attenuation of the microcirculation during hemorrhage and the modulation of mitochondrial function are receptor dependent has to be addressed in further studies.

DATA AVAILABILITY STATEMENT

All datasets presented in this study are included in the article/**Supplementary Material**.

ETHICS STATEMENT

The animal study was reviewed and approved by North Rhine-Westphalia State Agency for Nature, Environment and Consumer Protection, Recklinghausen, Germany.

AUTHOR CONTRIBUTIONS

RT and IN: conception and design, acquisition of data, analysis and interpretation of data, and drafting the article. JS: analysis and interpretation of data and revising the article. AH: conception, analysis and interpretation of data, and revising the article. TH and LG: acquisition of data, analysis and interpretation of data, and revising the article. AR: conception and design, acquisition of data, analysis and interpretation of data, and revising the article. IB, OP, and CV: conception and design, analysis and interpretation of data, and revising the article. All authors read and approved the final manuscript.

FUNDING

This work was supported by departmental funds and by a grant of the Strategic Research Fund, Heinrich-Heine-University (No. 1229) to CV.

SUPPLEMENTARY MATERIAL

The Supplementary Material for this article can be found online at: https://www.frontiersin.org/articles/10.3389/fmed.2020.00510/full#supplementary-material

REFERENCES

1. Murray CJ, Lopez AD. Alternative projections of mortality and disability by cause 1990-2020: Global Burden of Disease Study. *Lancet Lond Engl.* (1997) 349:1498–504. doi: 10.1016/S0140-6736(96)07492-2
2. Jakob SM, Takala J. Gut perfusion in the critically ill. *Intensive Care Med.* (2000) 26:813–5. doi: 10.1007/s001340051253
3. Deitch EA, Xu D, Kaise VL. Role of the gut in the development of injury- and shock induced SIRS and MODS: the gut-lymph hypothesis, a review. *Front Biosci J Virtual Libr.* (2006) 11:520–8. doi: 10.2741/1816
4. Trzeciak S, Dellinger RP, Parrillo JE, Guglielmi M, Bajaj J, Abate NL, et al. Early microcirculatory perfusion derangements in patients with severe sepsis and septic shock: relationship to hemodynamics, oxygen transport, and survival. *Ann Emerg Med.* (2007) 49:88–98:98.e1–2. doi: 10.1016/j.annemergmed.2006.08.021
5. Chierego M, Verdant C, De Backer D. Microcirculatory alterations in critically ill patients. *Minerva Anestesiol.* (2006) 72:199–205.
6. Brzozowski T, Konturek PC, Zwirska-Korczala K, Konturek SJ, Brzozowska I, Drozdowicz D, et al. Importance of the pineal gland, endogenous prostaglandins and sensory nerves in the gastroprotective actions of central and peripheral melatonin against stress-induced damage. *J Pineal Res.* (2005) 39:375–85. doi: 10.1111/j.1600-079X.2005.00264.x
7. Vollmer C, Weber APM, Wallenfang M, Hoffmann T, Mettler-Altmann T, Truse R, et al. Melatonin pretreatment improves gastric mucosal blood flow and maintains intestinal barrier function during hemorrhagic shock in dogs. *Microcirc N Y N.* (1994) 24:e12345. doi: 10.1111/micc.12345
8. Dyson DH. Positive pressure ventilation during anesthesia in dogs: assessment of surface area derived tidal volume. *Can Vet J Rev Vét Can.* (2012) 53:63–6.
9. Krug A. CME: Mikrozirkulation und Sauerstoffversorgung des Gewebes - Methode des so genannten O2C (oxygen to see). *Phlebologie.* (2006) 35:300–12. doi: 10.1055/s-0037-1622158
10. Siegemund M, van Bommel J, Ince C. Assessment of regional tissue oxygenation. *Intensive Care Med.* (1999) 25:1044–60. doi: 10.1007/s001340051011
11. Temmesfeld-Wollbrück B, Szalay A, Mayer K, Olschewski H, Seeger W, Grimminger F. Abnormalities of gastric mucosal oxygenation in septic shock: partial responsiveness to dopexamine. *Am J Respir Crit Care Med.* (1998) 157(5 Pt 1):1586–92. doi: 10.1164/ajrccm.157.5.9710017
12. Mythen MG, Purdy G, Mackie IJ, McNally T, Webb AR, Machin SJ. Postoperative multiple organ dysfunction syndrome associated with gut mucosal hypoperfusion, increased neutrophil degranulation and C1-esterase inhibitor depletion. *Br J Anaesth.* (1993) 71:858–63. doi: 10.1093/bja/71.6.858
13. Fournell A, Schwarte LA, Kindgen-Milles D, Müller E, Scheeren TWL. Assessment of microvascular oxygen saturation in gastric mucosa in volunteers breathing continuous positive airway pressure. *Crit Care Med.* (2003) 31:1705–10. doi: 10.1097/01.CCM.0000063281.47070.53
14. Sato N, Kawano S, Kamada T, Takeda M. Hemodynamics of the gastric mucosa and gastric ulceration in rats and in patients with gastric ulcer. *Dig Dis Sci.* (1986) 31 (2 Suppl.):35S−41S. doi: 10.1007/BF01309321
15. Kortbeek JB, Al Turki SA, Ali J, Antoine JA, Bouillon B, Brasel K, et al. Advanced trauma life support, 8th edition, the evidence for change. *J Trauma.* (2008) 64:1638–50. doi: 10.1097/ta.0b013e3181744b03
16. Herminghaus A, Eberhardt R, Truse R, Schulz J, Bauer I, Picker O, et al. Nitroglycerin and iloprost improve mitochondrial function in colon homogenate without altering the barrier integrity of caco-2 monolayers. *Front Med.* (2018) 5:291. doi: 10.3389/fmed.2018.00291
17. Hidalgo IJ, Raub TJ, Borchardt RT. Characterization of the human colon carcinoma cell line (Caco-2) as a model system for intestinal epithelial permeability. *Gastroenterology.* (1989) 96:736–49. doi: 10.1016/S0016-5085(89)80072-1
18. Speckmann B, Pinto A, Winter M, Förster I, Sies H, Steinbrenner H. Proinflammatory cytokines down-regulate intestinal selenoprotein P biosynthesis via NOS2 induction. *Free Radic Biol Med.* (2010) 49:777–85. doi: 10.1016/j.freeradbiomed.2010.05.035
19. Feighery LM, Cochrane SW, Quinn T, Baird AW, O'Toole D, Owens S-E, et al. Myosin light chain kinase inhibition: correction of increased intestinal epithelial permeability in vitro. *Pharm Res.* (2008) 25:1377–86. doi: 10.1007/s11095-007-9527-6
20. Mathes AM. Hepatoprotective actions of melatonin: possible mediation by melatonin receptors. *World J Gastroenterol.* (2010) 16:6087–97. doi: 10.3748/wjg.v16.i48.6087
21. Sheridan WG, Lowndes RH, Young HL. Tissue oxygen tension as a predictor of colonic anastomotic healing. *Dis Colon Rectum.* (1987) 30:867–71. doi: 10.1007/BF02555426
22. Truse R, Hinterberg J, Schulz J, Herminghaus A, Weber A, Mettler-Altmann T, et al. Effect of topical iloprost and nitroglycerin on gastric microcirculation and barrier function during hemorrhagic shock in dogs. *J Vasc Res.* (2017) 54:109–21. doi: 10.1159/000464262
23. Mathes AM, Kubulus D, Pradarutti S, Bentley A, Weiler J, Wolf B, et al. Melatonin pretreatment improves liver function and hepatic perfusion after hemorrhagic shock. *Shock Augusta Ga.* (2008) 29:112–8. doi: 10.1097/shk.0b013e3180644ca3
24. Mathes AM, Kubulus D, Weiler J, Bentley A, Waibel L, Wolf B, et al. Melatonin receptors mediate improvements of liver function but not of hepatic perfusion and integrity after hemorrhagic shock in rats. *Crit Care Med.* (2008) 36:24–9. doi: 10.1097/01.CCM.0000292088.33318.F0
25. Shah V, Lyford G, Gores G, Farrugia G. Nitric oxide in gastrointestinal health and disease. *Gastroenterology.* (2004) 126:903–13. doi: 10.1053/j.gastro.2003.11.046
26. Hlutkin S, Zinchuk V. Effect of melatonin on the blood oxygen transport during hypothermia and rewarming in rats. *Adv Med Sci.* (2008) 53:234–9. doi: 10.2478/v10039-008-0035-7

27. Reiter RJ, Tan DX, Manchester LC, El-Sawi MR. Melatonin reduces oxidant damage and promotes mitochondrial respiration: implications for aging. *Ann N Y Acad Sci.* (2002) 959:238–50. doi: 10.1111/j.1749-6632.2002.tb02096.x
28. Martín M, Macías M, Escames G, León J, Acuña-Castroviejo D. Melatonin but not vitamins C and E maintains glutathione homeostasis in t-butyl hydroperoxide-induced mitochondrial oxidative stress. *FASEB J Off Publ Fed Am Soc Exp Biol.* (2000) 14:1677–9. doi: 10.1096/fj.99-0865fje
29. Wehr TA, Aeschbach D, Duncan WC. Evidence for a biological dawn and dusk in the human circadian timing system. *J Physiol.* (2001) 535 (Pt 3):937–51. doi: 10.1111/j.1469-7793.2001.t01-1-00937.x
30. Chuffa LGA, Seiva FRF, Fávaro WJ, Teixeira GR, Amorim JPA, Mendes LO, et al. Melatonin reduces LH, 17 beta-estradiol and induces differential regulation of sex steroid receptors in reproductive tissues during rat ovulation. *Reprod Biol Endocrinol RBE.* (2011) 9:108. doi: 10.1186/1477-7827-9-108
31. Lazado CC, Kumaratunga HPS, Nagasawa K, Babiak I, Giannetto A, Fernandes JMO. Daily rhythmicity of clock gene transcripts in atlantic cod fast skeletal muscle. *PLoS ONE.* (2014) 9:e99172. doi: 10.1371/journal.pone.0099172
32. Truse R, Voß F, Herminghaus A, Schulz J, Weber A, Mettler-Altmann T, et al. Local gastric RAAS-inhibition improves gastric microvascular perfusion in dogs. *J Endocrinol.* (2019) 241:235–47. doi: 10.1530/JOE-19-0030
33. Boscan P, Cochran S, Monnet E, Webb C, Twedt D. Effect of prolonged general anesthesia with sevoflurane and laparoscopic surgery on gastric and small bowel propulsive motility and pH in dogs. *Vet Anaesth Analg.* (2014) 41:73–81. doi: 10.1111/vaa.12093
34. Claustrat B, Brun J, Chazot G. The basic physiology and pathophysiology of melatonin. *Sleep Med Rev.* (2005) 9:11–24. doi: 10.1016/j.smrv.2004.08.001
35. Tordjman S, Chokron S, Delorme R, Charrier A, Bellissant E, Jaafari N, et al. Melatonin: pharmacology, functions and therapeutic benefits. *Curr Neuropharmacol.* (2017) 15:434–43. doi: 10.2174/1570159X14666161228122115
36. Powers KA, Szászi K, Khadaroo RG, Tawadros PS, Marshall JC, Kapus A, et al. Oxidative stress generated by hemorrhagic shock recruits Toll-like receptor 4 to the plasma membrane in macrophages. *J Exp Med.* (2006) 203:1951–61. doi: 10.1084/jem.20060943
37. Moniruzzaman M, Ghosal I, Das D, Chakraborty SB. Melatonin ameliorates H2O2-induced oxidative stress through modulation of Erk/Akt/NFkB pathway. *Biol Res.* (2018) 51:17. doi: 10.1186/s40659-018-0168-5
38. Sommansson A, Yamskova O, Schiöth HB, Nylander O, Sjöblom M. Long-term oral melatonin administration reduces ethanol-induced increases in duodenal mucosal permeability and motility in rats. *Acta Physiol Oxf Engl.* (2014) 212:152–65. doi: 10.1111/apha.12339
39. Trivedi PP, Jena GB. Melatonin reduces ulcerative colitis-associated local and systemic damage in mice: investigation on possible mechanisms. *Dig Dis Sci.* (2013) 58:3460–74. doi: 10.1007/s10620-013-2831-6
40. Catalioto R-M, Festa C, Triolo A, Altamura M, Maggi CA, Giuliani S. Differential effect of ethanol and hydrogen peroxide on barrier function and prostaglandin E2 release in differentiated Caco-2 cells: selective prevention by growth factors. *J Pharm Sci.* (2009) 98:713–27. doi: 10.1002/jps.21439
41. Klein AH, Wendroth SM, Drewes LR, Andrews MT. Small-volume d-β-hydroxybutyrate solution infusion increases survivability of lethal hemorrhagic shock in rats. *Shock Augusta Ga.* (2010) 34:565–72. doi: 10.1097/SHK.0b013e3181e15063
42. Mulier KE, Lexcen DR, Luzcek E, Greenberg JJ, Beilman GJ. Treatment with beta-hydroxybutyrate and melatonin is associated with improved survival in a porcine model of hemorrhagic shock. *Resuscitation.* (2012) 83:253–8. doi: 10.1016/j.resuscitation.2011.08.003
43. Wolf A, Mulier KE, Iyegha UP, Asghar JI, Beilman GJ. Safety of D-ß-hydroxybutyrate and melatonin for the treatment of hemorrhagic shock with polytrauma. *Shock Augusta Ga.* (2015) 44 (Suppl. 1):79–89. doi: 10.1097/SHK.0000000000000315
44. Sallinen P, Saarela S, Ilves M, Vakkuri O, Leppäluoto J. The expression of MT1 and MT2 melatonin receptor mRNA in several rat tissues. *Life Sci.* (2005) 76:1123–34. doi: 10.1016/j.lfs.2004.08.016

Conflict of Interest: The authors declare that the research was conducted in the absence of any commercial or financial relationships that could be construed as a potential conflict of interest.

frontiers in Medicine

ORIGINAL RESEARCH
published: 10 September 2020
doi: 10.3389/fmed.2020.00513

Motor Cortex and Hippocampus Display Decreased Heme Oxygenase Activity 2 Weeks After Ventricular Fibrillation Cardiac Arrest in Rats

Alexandra-Maria Warenits[1], Jasmin Hatami[2], Andrea Müllebner[2,3], Florian Ettl[1], Ursula Teubenbacher[1,4], Ingrid Anna Maria Magnet[1], Barbara Bauder[4], Andreas Janata[1], Ingrid Miller[2], Rudolf Moldzio[2], Anne-Margarethe Kramer[5], Fritz Sterz[1], Michael Holzer[1], Sandra Högler[6], Wolfgang Weihs[1†] and Johanna Catharina Duvigneau[2†]*

[1] Department of Emergency Medicine, Medical University of Vienna, Vienna, Austria, [2] Institute for Medical Biochemistry, University of Veterinary Medicine Vienna, Vienna, Austria, [3] Ludwig Boltzmann Institute for Experimental and Clinical Traumatology, Vienna, Austria, [4] Institute of Pathology, University of Veterinary Medicine Vienna, Vienna, Austria, [5] Center for Biomedical Research, Medical University of Vienna, Vienna, Austria, [6] Unit of Laboratory Animal Pathology, University of Veterinary Medicine Vienna, Vienna, Austria

OPEN ACCESS

Edited by:
Mihaly Boros,
University of Szeged, Hungary

Reviewed by:
Tunde Tokes,
ELI-ALPS Research Institute, Hungary
Michael Fries,
St. Vincenz-Krankenhaus Limburg, Germany

***Correspondence:**
Johanna Catharina Duvigneau
catharina.duvigneau@vetmeduni.ac.at

† These authors have contributed equally to this work

Specialty section:
This article was submitted to Intensive Care Medicine and Anesthesiology, a section of the journal Frontiers in Medicine

Received: *28 May 2020*
Accepted: *24 July 2020*
Published: *10 September 2020*

Citation:
Warenits A-M, Hatami J, Müllebner A, Ettl F, Teubenbacher U, Magnet IAM, Bauder B, Janata A, Miller I, Moldzio R, Kramer A-M, Sterz F, Holzer M, Högler S, Weihs W and Duvigneau JC (2020) Motor Cortex and Hippocampus Display Decreased Heme Oxygenase Activity 2 Weeks After Ventricular Fibrillation Cardiac Arrest in Rats. Front. Med. 7:513. doi: 10.3389/fmed.2020.00513

Heme oxygenase (HO) and biliverdin reductase (BVR) activities are important for neuronal function and redox homeostasis. Resuscitation from cardiac arrest (CA) frequently results in neuronal injury and delayed neurodegeneration that typically affect vulnerable brain regions, primarily hippocampus (Hc) and motor cortex (mC), but occasionally also striatum and cerebellum. We questioned whether these delayed effects are associated with changes of the HO/BVR system. We therefore analyzed the activities of HO and BVR in the brain regions Hc, mC, striatum and cerebellum of rats subjected to ventricular fibrillation CA (6 min or 8 min) after 2 weeks following resuscitation, or sham operation. From all investigated regions, only Hc and mC showed significantly decreased HO activities, while BVR activity was not affected. In order to find an explanation for the changed HO activity, we analyzed protein abundance and mRNA expression levels of HO-1, the inducible, and HO-2, the constitutively expressed isoform, in the affected regions. In both regions we found a tendency for a decreased immunoreactivity of HO-2 using immunoblots and immunohistochemistry. Additionally, we investigated the histological appearance and the expression of markers indicative for activation of microglia [*tumor necrosis factor receptor type I* (TNFR1) mRNA and immunoreactivity for ionized calcium-binding adapter molecule 1 (Iba1])], and activation of astrocytes [immunoreactivity for glial fibrillary acidic protein (GFAP)] in Hc and mC. Morphological changes were detected only in Hc displaying loss of neurons in the cornu ammonis 1 (*CA1*) region, which was most pronounced in the 8 min CA group. In this region also markers indicating inflammation and activation of pro-death pathways (expression of HO-1 and TNFR1 mRNA, as well as Iba1 and GFAP immunoreactivity) were upregulated. Since HO products are relevant for maintaining neuronal function, our data suggest that neurodegenerative processes following CA may be associated with a decreased capacity to convert heme into HO products in particularly vulnerable brain regions.

Keywords: cardiac arrest, global cerebral ischemia, reperfusion injury, heme degradation pathway, brain regions, neurodegeneration, biliverdin reductase, enzyme activity

INTRODUCTION

Neurologic outcome in patients resuscitated from cardiac arrest (CA) remains poor, despite improvements in advanced life support and post-resuscitation care. Brain injury starts during the initial CA (no-flow time), continues during resuscitation (low-flow time) and culminates after re-oxygenation with the return of spontaneous circulation (ROSC). These pathophysiological events prepare the base of the post-cardiac arrest syndrome (1, 2) and lead to neurologic and motor deficits (3), which were shown to persist for a long time (4, 5). Using animal models, like others we have previously shown that CA induced global ischemia causes delayed neurodegeneration and neuronal dysfunction, which is associated with decreased cognitive capabilities (6–9). An experimental study using rats revealed that cognitive deficits in response to global ischemia continue to develop and were most severe after 6 months when rats are in their middle age (10). The same group also showed that cognitive deficits produced by ischemia are severe in middle aged rats, suggesting that repair mechanisms decline with age (11).

Multiple mechanisms are initiated immediately after ROSC involving an imbalanced redox homeostasis (12), increased cell stress, initiation of inflammation and cell death signaling (13–15) followed by death of vulnerable neurons. The most frequent structural changes occur in the hippocampus (Hc), consisting of loss of pyramidal neurons in the cornu ammonis 1 (*CA1*) region (16), which are associated with behavioral alterations (17).

The heme oxygenase (HO) system supports neuronal function and contributes to the oxidative defense (18, 19). HO degrades heme via oxidation yielding carbon monoxide (CO), free iron, and biliverdin (BV), which is afterwards converted to bilirubin (BR) (19). There are two catalytically active isoforms of HO in mammals, HO-1 and HO-2. In neuronal tissue nearly all of the HO-activity is ascribable to the constitutive HO isoform HO-2, and contribution of HO-1 is almost absent in physiological conditions (20). Functional HO is required for modulation of the synaptic activity, for memory consolidation, and maintenance of microperfusion, which operates predominantly via the heme degradation product CO (21–23).

Apart from the exclusive role of HO-2 for maintaining homeostasis and function in neuronal tissues, upregulation of the inducible isoform of HO-1, synonym with heat shock protein 32 is observed in response to acute cell stress, such as hypoxia and ischemia (24). Within several hours cerebral ischemia leads to the induction of HO-1, initially in astrocytes, which is subsequently extended on neuronal cells (25–27). Additionally to the HO-1 induction, also up-regulation of HO-2 protein has occasionally been described in response to cerebral ischemia (28). Experimental models inhibiting HO or overexpressing HO prior to an ischemic insult documented the neuroprotective effects of HO, particularly that of HO-2 (29). HO mediated cytoprotection can be mimicked by application of the HO reaction products CO (30) or BV/BR (31, 32).

Given the particular role of HO in preserving neuronal morphology and function, we questioned whether delayed neurodegeneration caused by resuscitated cardiac arrest is associated with changes of HO activity. Most studies delimitate their investigation to the expression of mRNA or protein level of either HO-1 or HO-2, or both HO isoforms in a few cases. Several studies show an acutely increased mRNA and/or protein expression of the HO-1 isoform in response to global ischemia (28, 29). However, HO activity of brain regions following CA has not been investigated yet. Instead, HO activity is extrapolated from the observed expression levels of HO-1 and/or HO-2 mRNA or protein, although it is known that both enzymes, HO-1 and HO-2, may be subjected to posttranslational modifications, influencing their catalytic activity (33, 34). Therefore, the capacity to degrade heme may be different from what mRNA or protein levels suggest.

Thus, our study aimed at understanding whether HO activity and expression do indeed correlate in vulnerable brain regions, as is generally assumed. To test our hypothesis we applied an experimental ventricular fibrillation model of 6 or 8 min CA, followed by cardiopulmonary resuscitation (CPR) using rats (7). After 2 weeks, we analyzed in Hc, motor cortex (mC), striatum and cerebellum the activity and expression levels of enzymes of the heme degradation pathway. To understand whether changes of the HO system are associated with neurodegenerative processes, we further analyzed the affected regions for relevant markers indicating gliosis and activation of inflammatory cell death pathway processes.

MATERIALS AND METHODS

Animals and Experimental Protocol

The experimental protocol was approved by the Institutional Animal Care and Use Committee of the Medical University of Vienna and the Austrian Ministry of Science, Research and Economy (GZ.: 66.009/0064-II/3b/2011). The experiments were conducted in compliance with EU regulations for animal experimentation (Directive 2010/63/EU of the European Parliament and of the Council) and followed the ARRIVE guidelines (35).

A total of 32 adult male Sprague-Dawley rats, 389 ± 56 g body weight (BW), 10 weeks of age (Himberg, Austria) were randomly allocated into the two resuscitation groups of 6 and 8 min CA (6 min CA, $n = 10$; 8 min CA, $n = 12$) and a sham operated group (sham, $n = 10$). In the 8 min CA group, more animals were allocated, because we expected a higher loss of animals due to longer CA times. In the sham group the same surgical procedures were performed, without the induction of ventricular fibrillation and consequent CA.

The experimental resuscitation model was described in detail earlier (7). Briefly, sedation of the animals was induced via the administration of sevoflurane 6% in FiO_2 1.0 for 4 min in a box. The rats were endotracheally intubated with an adapted venous cannula (14GA Venflon BD Luer-Lok, Helsingborg, Sweden) and mechanically ventilated, volume-controlled with 65/min, 7 mL/kg BW and 0.3 FiO_2 (Havard Inspira advanced safety ventilator, volume controlled, MA1 55-7058, Holliston, MA, USA). Buprenorphine (50 μg/kg BW) was given subcutaneously (s.c.) after intubation and sevoflurane 3.5% was further administered via the ventilator for continuous

anesthesia during surgery. Rectal and esophageal temperature was kept stable at 37 ± 0.2°C with a heated operating table. The animals were catheterized via surgical cut-down into the left femoral artery and vein (Argyle Polyurethane Umbilical Vessel Catheter; 2.5 Fr, Convidien, Mansfield, MA, USA) for arterial blood sampling, measurement of mean arterial pressure (MAP) and venous drug administration. A human neonatal pacing catheter (Vygon GmbH & Co Bi-Pacing-ball 3 Fr, Aachen, Germany) was inserted in the cranially ligated right jugular vein, with the tip ending in the inferior vena cava for inducing ventricular fibrillation cardiac arrest.

After successful surgery, a baseline arterial blood gas analysis was performed, and sevoflurane sedation was stopped 1.5 min before the induction of ventricular fibrillation and the end of mechanical ventilation. After untreated CA (6 min CA, or 8 min CA), bicarbonate (1 mmol/kg BW), unfractionated heparin (100 I.U.), and epinephrine were given (20 μg/kg BW) intravenously (i.v.) 60 s before the initiation of resuscitation. Resuscitation was started with mechanical chest compressions (200/min) delivered with a pneumatic chest compression device (Streubel Automation, Grampersdorf, Germany) and mechanical ventilation (20/min, 7 mL/kg BW, 1.0 FiO_2). The animals were defibrillated (2 times each with 5 Joule, biphasic; repeated every 2 min if ventricular fibrillation was present) and received epinephrine (10 μg/kg BW) i.v. 60 s after start of CPR and repeated every 2 min to achieve ROSC.

After ROSC, the ventilation settings were adapted (65/min, 7 mL/kg BW and 0.5 FiO_2) and an arterial blood gas sample was taken 5 min after ROSC. The catheters were removed, vessels ligated, and skin incisions sutured using aseptic techniques. After successful weaning from mechanical ventilation, the unconscious rats were extubated, received oxygen via a nose cone mask and buprenorphine (24 μg/kg BW) s.c. as long as pain or distress was present. Further information regarding clinical data (mean arterial pressure, blood gas analyses prior and after CA and ROSC) is given as **Table S1**.

The rats were evaluated daily and neurologic status was assessed on day 1 and day 14 after ROSC by an investigator blinded to the study group, using neurological deficit score (NDS; NDS 0% = normal, NDS = 100% dead) (36) and overall performance category score (OPC; OPC 1 = normal, 2 = moderate disability, 3 = severe disability, 4 = comatose, 5 = dead (37). The neurological scoring system of NDS and OPC is described in the **Tables S2, S3**. A schematic overview of the experimental setup (a) and the study timeline (b) is shown in **Figure 1**.

Sampling

At day 14 rats were euthanized with a sevoflurane and buprenorphine overdose and perfused with saline (0.9% NaCl). After perfusion, brains were removed from the skull and cut into hemispheres. One half was fixed in 7.5% neutral buffered formaldehyde solution for histological examination, and regions of the other hemisphere (mC, Hc, striatum, and cerebellum) were sampled for gene expression analysis and enzyme assays. For this purpose, coronary sections at Bregma 1.7, −1.4, and −5.2 (38) were cut. The mC was taken from the rostral section, striatum from the next section and Hc from the third section. Cerebellar peduncles were cut to remove the cerebellum from the brain stem. The entire sampling process was done on a chilled marble plate and lasted not longer than 30 min. Brain regions were snap frozen in liquid nitrogen and stored at −80°C until use. The entire procedure with analyses performed is shown in **Figure 2**.

Preparation of Tissue Homogenates for Enzyme Assays and Expression Analysis

Homogenates of entire brain regions were prepared (**Figure 2**) instead of using only parts/pieces, in order to avoid biases due to potential tissue inhomogeneity. These homogenates were used for the determination of the HO and BVR activity and for the protein and gene expression analyses. Frozen tissue was homogenized in 1:20 (w/v) Tris-buffer containing 300 mM sucrose, 20 mM Tris, and 2 mM EDTA at pH 7.4 using a Potter-Elvehjem with PTFE pestle on ice. The homogenates were distributed in 30 μL portions directly into liquid nitrogen. The formed frozen droplets were stored at −80°C until being used.

Determination of the Activity of HO Enzyme by an Optimized Photometric Enzyme-Coupled Assay

The determination of enzyme activities (HO and BVR) was performed as previously described (39) with the following modifications. Two droplets (corresponding to approximately 1 mg of protein) were added to a reaction mixture containing 500 nmol NADPH (Sigma) in a total volume of 150 μL assay buffer (100 mM potassium phosphate buffer; 1 mM EDTA; pH 7.4), supplemented with 20 nmol of hemin (for determination of HO activity), or with 200 nmol BV (for determination of BVR) and 250 nmol of NADPH. The residual homogenate was used to determine the protein concentration using a Coomassie Brilliant Blue binding assay (Bradford), as described elsewhere (40). The mixture was incubated under constant agitation in darkness for 30 min at 37°C. The reaction was stopped by transferring the samples onto ice. BR was extracted into benzene as described previously (41). BR concentration was determined using a double beam spectrophotometer (U-3000, Hitachi) and a standard calibration curve, which was generated by adding known amounts of bilirubin to assay buffer followed by subsequent extraction. The detection limit of BR using this method was determined as 5 pmol BR. In all tissues the BVR activity (the capacity to convert BV into BR) was much higher (i.e., 10 times) than that of HO (the capacity to convert heme to BR). This indicates that BVR activity is not limited and that all BV formed by the HO enzyme is completely reduced to BR by the underlying BVR. Enzyme activities were expressed as pmol BR formed per mg protein in 30 min.

Analysis of HO Protein Levels by Immunoblots

Proteins from droplets were separated under reducing conditions by sodium dodecyl sulfate polyacrylamide gel electrophoresis (SDS-PAGE) on 10–15% PAGE gradient gels and blotted onto nitrocellulose as described earlier (40). Immunoprobing with two

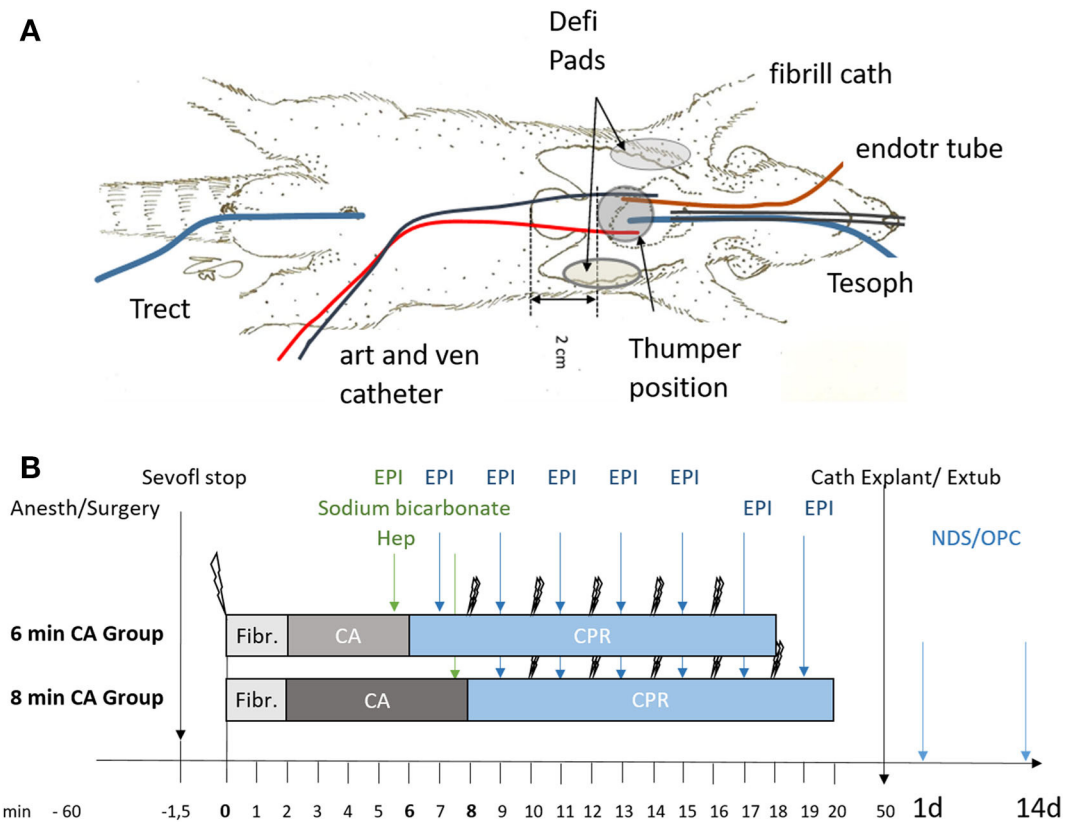

FIGURE 1 | Schematic representation of setup and timeline of the experiments. **(A)** Instrumentation of animals using an endotracheal tube (endotr tube), an arterial and venous catheter in the femoral artery and vein (art and ven catheter), an esophageal temperature probe (Tesoph), and a rectal temperature probe (Trect). Fibrillation catheter for inducing ventricular fibrillation (fibrill cath). For resuscitation defibrillation pads (Defi Pads) were placed as indicated and a thumper was positioned 2 cm cranial of the xiphoid process. **(B)** Animals were randomly allocated to sham (not shown) or the 6 or 8 min cardiac arrest (CA) group following anesthesia and surgery (Anesth/Surgery). Sevoflurane was stopped (Sevofl stop) and CA was induced by ventricular fibrillation (single lightning symbol; Fibr.). Heparin (Hep), epinephrine (EPI) and sodium bicarbonate were added prior to cardiopulmonary resuscitation (CPR) attempted by 2 consecutive defibrillation steps (double lightning bolts), repeated every 2 min of CPR and followed immediately by epinephrine (EPI) supplementation every 2 min of CPR. After successful resuscitation with maximal 5 defibrillation attempts catheters were explanted (Cath Explant) and animals extubated (Extub). Overall performance category score (OPC) and neurological deficit score (NDS) were determined in all surviving animals at day 1 and day 14 prior to sacrifice.

specific antibodies was performed: against HO-1 (Alexis Corp., Lausen, Switzerland) and HO-2 (Santa Cruz Biotechnology, Santa Cruz, CA, USA), followed by cross-absorbed anti-rabbit IgG-HRPO (Novex, Life Technologies Corporation, Grand Island, NY, USA) and enhanced chemiluminescent detection (ECL-detection). Fluorescence staining of the overall protein pattern (prior to immunostaining) was used as a loading control and for normalization (Overall protein stains are shown in **Figure S1**). HO-1 proved to be below detection limit in brain. Testing of Hc and mC specimens for HO-2 was performed on individual animal basis.

Analysis of Gene Expression

Gene expression analysis was performed using qPCR as described elsewhere (42). Briefly, RNA was isolated from 2 frozen droplets using 1 mL of TriReagent™. Extraction of RNA was performed in accordance to manufacturer's protocol. The amount of extracted RNA was determined spectrophotometrically at 260 nm and purity was assessed by the 260/280 nm ratio on an Eppendorf BioPhotometer plusUV/VIS (Eppendorf, Hamburg, Germany). Copy DNA was prepared as previously described (43). Equal aliquots from each cDNA were pooled to generate an internal standard (IS) which was used as reference for the quantification. Primer pairs used for the expression analysis of HO-1 and TNFR1, and for the internal reference genes *hypoxanthine ribosyltransferase* (HPRT), and *cyclophilin A* (Cyc) were previously published (42). Primer pairs for the analysis of HO-2 and BVR *isoform A* (BVRA) gene expression were newly established for this study. Results of validation experiments performed to verify the suitability of these qPCR assays in accordance to the MIQE guidelines (44) are available as **Tables S4, S5** and **Figure S2**. The qPCR was carried out on a CFX96™ (Bio-Rad, Hercules, CA, USA). Data were analyzed using the inbuilt software CFX manager (Version 2.0, Bio-Rad) in the linear regression mode. Expression of target genes was calculated against IS using a modified ΔΔCq method and normalized for the relative expression values obtained for internal reference genes HPRT & Cyc as

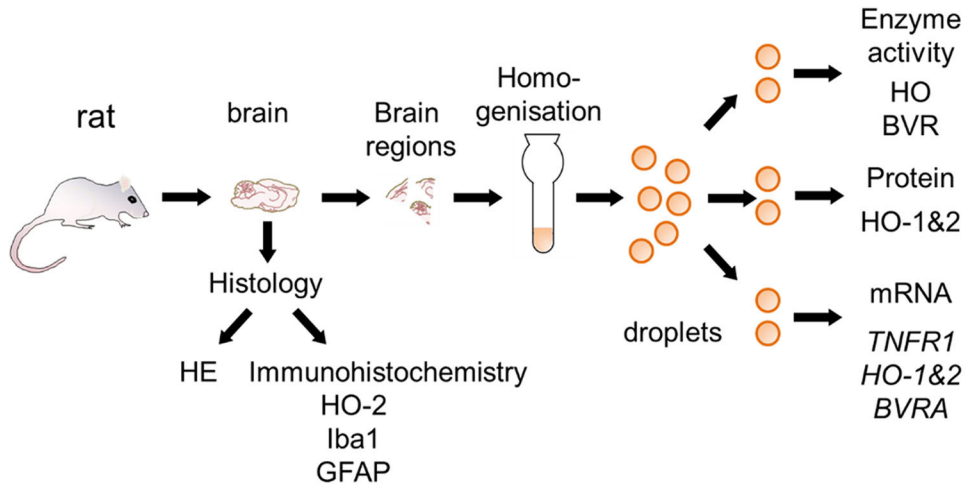

FIGURE 2 | Schematic overview for the preparation of brain sections used for the different analysis. Brain samples were taken from rats surviving 2 weeks following CA and processed as described in the Materials and Methods section. Half of the brain was fixed and used for histological examination [hematoxylin and eosin staining (HE), immunohistochemistry for heme oxygenase (HO)-2, ionized calcium-binding adapter molecule 1 (Iba-1), and glial fibrillary acidic protein (GFAP)]. Different regions were cut from the other half and immediately snap-frozen. In order to prevent biases frozen tissue pieces were homogenized and distributed into droplets prior to analysis of activity of HO and BVR, protein expression of HO-1 and HO-2, and gene expression [*Tumor necrosis factor receptor 1* (TNFR1), HO-1, HO-2, and *biliverdin reductase A* (BVRA)]. Analyses were performed in accordance to the procedures described in Materials and Methods section.

previously described (45). Values obtained from duplicates were averaged and expressed as $2^{-\Delta\Delta Cq}$ in fold changes relative to the IS.

Histological Analysis

Fixed brain hemispheres were cut into coronary sections, which were embedded in paraffin wax and cut into 5 µm thick sections. Sections containing Hc, mC, striatum and cerebellum were stained with hematoxylin and eosin (HE) and examined by a pathologist blinded to the study groups. The presence of neuronal necrosis was determined in a descriptive manner in HE stained sections of these brain regions.

Immunohistochemistry was used to determine activation of microglia (primary antibody against ionized calcium-binding adapter molecule 1 (Iba-1), FUJIFILM Wako Chemicals, Neuss, Germany, dilution 1:80,000) and astrocytes (primary antibody against glial fibrillary acidic protein (GFAP), Agilent Dako, Waldbronn, Germany, dilution 1:5,000) in the Hc in a semiquantitative manner. Furthermore, immunohistochemical investigations using a primary antibody against HO-2 (Santa Cruz Biotechnology, Santa Cruz, CA, USA, dilution 1:100) were performed to evaluate expression of HO-2 in Hc and mC. All immunohistochemical stainings were done automatically on an autostainer (Lab Vision AS 360, Thermo Fisher Scientific, Waltham, MA, USA). Briefly, sections were cut and antigen retrieval was performed in the Lab Vision PT Module (Thermo Fisher Scientific, Waltham, MA, USA) with citrate puffer (pH6, Iba1, and HO-2) and pronase digestion (GFAP), respectively. Endogenous peroxidase activity was blocked by incubation in H_2O_2. Ultra Vision Protein Blocking reagent (Labvision/Thermo Fisher Scientific, Fremont, CA, USA) was used to avoid non-specific binding of antibody. After application of the primary antibody a polymer detection system (Ultra Vision LP Large Detection System HRP, Labvision/Thermo Fisher Scientific, Fremont, CA, USA) consisting of a secondary antibody formulation conjugated to an enzyme-labeled polymer was used. The polymer complex was visualized with diaminobenzidine (Labvision/Thermo Fisher Scientific, Fremont, CA, USA). Subsequently, sections were counterstained with hematoxylin, dehydrated and mounted with Neo-Mount (Merck, Darmstadt, Germany).

For the semiquantitative analysis of gliosis and expression of HO-2, the region of interest was evaluated in the respective immunohistochemical staining. An increase or decrease of staining intensity and extent was assessed on a five-point scale. Normal expression of Iba1 (microglia) and GFAP (astrocytes) was assessed as "0," while an increase was assigned to the following categories: scattered (1), mild (2), moderate (3), or high (4) expression. For HO-2 expression, the normal expression pattern was rated as "4." The staining intensity was compared to the adjacent cortex tissue and a decrease was rated in four categories: mild (3), moderate (2), severe (1) reduction or no signal at all (0). Adobe Photoshop CC 2019 was used for white balance and to assemble representative histological pictures.

Statistics and Data Analysis

Data from quantitative analysis were calculated as medians as is recommended for qPCR data (46). Correlation between data sets was analyzed using the Spearman ranked sign test. Groups were compared by one-way non-parametric ANOVA (Kruskal Wallis) followed by Bonferroni-correction using IBM SPSS statistics (version 24). Values with $p < 0.05$ were considered significantly

TABLE 1 | Overview of animals enrolled in the study ($n = 32$).

State of the animal	Sham	6 min cardiac arrest	8 min cardiac arrest
Enrolled	10	10	12
Excluded from final examination	1	3	5
No return of spontaneous circulation (ROSC)	–	1	2
ROSC with overall performance category score = 5	–	2[a]	3[a]
ROSC with overall performance category score < 5	–	7	7
14-day survival	9	7	7[b]

[a] *Rats died before the end of the experiment and were excluded from final examination.*
[b] *From one animal only histological examinations and no biochemical analysis were performed (see above).*

TABLE 2 | Results of repetitive neurological scoring of experimental animals.

Neurological state	Day 1			Day 14		
	Sham	6 min CA[a]	8 min CA	Sham	6 min CA	8 min CA
OPC[b] 1	9	5	–	9	7	7
OPC 2	–	2	7	–	–	–
OPC 3	–	–	–	–	–	–
OPC 4	–	–	–	–	–	–
OPC 5 (dead)	–	2	3	–	–	–
NDS[c] (OPC 1–4)	0 ± 0	5 ± 2	13 ± 4	0 ± 0	0 ± 0	1 ± 2

[a] *CA, cardiac arrest.*
[b] *OPC, overall performance category score (OPC 1 = normal; 2 = moderate disability. 3 = severe disability; 4 = comatose; 5 = dead; for details of calculating OPC see* ***Table S2****).*
[c] *NDS, neurological deficit score (NDS 0% = normal; NDS 100% = dead; mean ± SD; for details of calculating NDS see* ***Table S3****).*

different. For visualization of data GraphPad PRIMS version 5.00 (GraphPad Software Inc.) was used, indicating the values of the single animals, and medians with 1st and 3rd quartiles per group. The numbers of independent samples (n) are indicated in the respective figure legends.

RESULTS

Of 32 enrolled rats, 9 rats had to be excluded from the study (**Table 1**). One of the 10 sham operated animals woke up during the surgery, anesthesia was deepened immediately and the rat survived (day 1 and 14: OPC 1; NDS 0%). This animal was excluded from final examinations. Three rats of the 6 min CA group and 5 of the 8 min CA group either had no ROSC or survived only few hours (6 min CA group: no ROSC, $n = 1$; OPC 5, $n = 2$; 8 min CA group: no ROSC, $n = 2$; OPC 5, $n = 3$). These animals were excluded from final examinations as well. A total of 23 animals (sham group, $n = 9$; 6 min CA group, $n = 7$; 8 min CA group, $n = 7$) remained for final examinations on day 14. From one rat of the 8 min CA group brain sample volume harvested was not sufficient for the biochemical analysis, only histological examinations and neurological scoring were performed. Mean arterial pressure and blood gas analysis at baseline (after surgery) and 5 min after ROSC are presented in **Table S5**. All surviving animals were scored for their neurological performance (OPC and NDS) at day 1 and at day 14 prior to sacrifice. We used repeated scoring as a suitable approach to rate the neurologic recovery, as was described earlier (7, 9). The results of the neurological scoring of CA animals with ROSC, including those with OPC 5 (= dead) at day 1, and the results obtained for animals surviving until day 14 are presented below (**Table 2**).

CA Leads to Decreased Activities of HO in Motor Cortex and Hippocampus, While BVR Activities Are Not Affected

From all investigated tissues we found HO activity to be lower in samples from mC and Hc, while striatum and cerebellum did not show changes (**Figure 3**), when compared to the sham control group. For the mC, the median of the 6 min CA group was decreased by 47% ($p = 0.009$) and of the 8 min CA group by 42% ($p = 0.043$). In the Hc, the activities were decreased to a lesser extent [6 min CA, 26% ($p = 0.136$); 8 min CA, 39% ($p = 0.029$)]. BVR activity was not affected in any brain region (**Figure 3**).

Decreased HO-2 Protein Levels in Response to CA Occur in mC (Immunoblot) and Hc (Immunohistochemistry)

Since we have found lower HO activity in mC and Hc homogenates, we questioned whether decreased levels of HO-2 protein caused this effect. Although both isoforms HO-1 and HO-2 contribute to the overall HO activity, the amount of HO-1 protein is generally very low in neuronal tissues (20). In line with these findings, we also could not determine HO-1 at protein level in immunoblots of tissue homogenates. Though, in homogenates of mC from CA animals we determined lower levels of HO-2 protein ($p = 0.01$ for 8 min CA; **Figures 4A,C**). Additionally, homogenates of Hc from 6 min CA animals displayed slightly lower HO-2 protein levels in comparison to the respective sham animals, but this difference was not significant ($p = 0.233$; **Figures 4B,D**). It is possible that the differences between groups in Hc did not result in statistical significances, because of the low sample numbers available for some of the groups. We also tested the immunohistochemical appearance of HO-2 specific staining in sections of both brain regions (mC and Hc).

In sham animals, immunohistochemical staining for HO-2 showed a consistent signal in all layers of the Hc *CA1*-region (**Figure 5A**). The signal intensity was nearly similar to the signal intensity in the cerebral cortex in the same section (**Figure 5A**). In contrast, in all CA animals, regardless of CA duration, the HO-2 signal was significantly reduced in all hippocampal layers compared to the corresponding cerebral cortex (**Figures 5B,C** and **Table 3**). The neuronal expression of HO-2 was present predominantly in surviving pyramidal neurons in CA animals (**Figures 5B,C** inserts). In all animals, a consistent signal was present in the neuropil of the mC, and in some neurons increased staining intensities were detectable (**Figures 5D–F**). In contrast

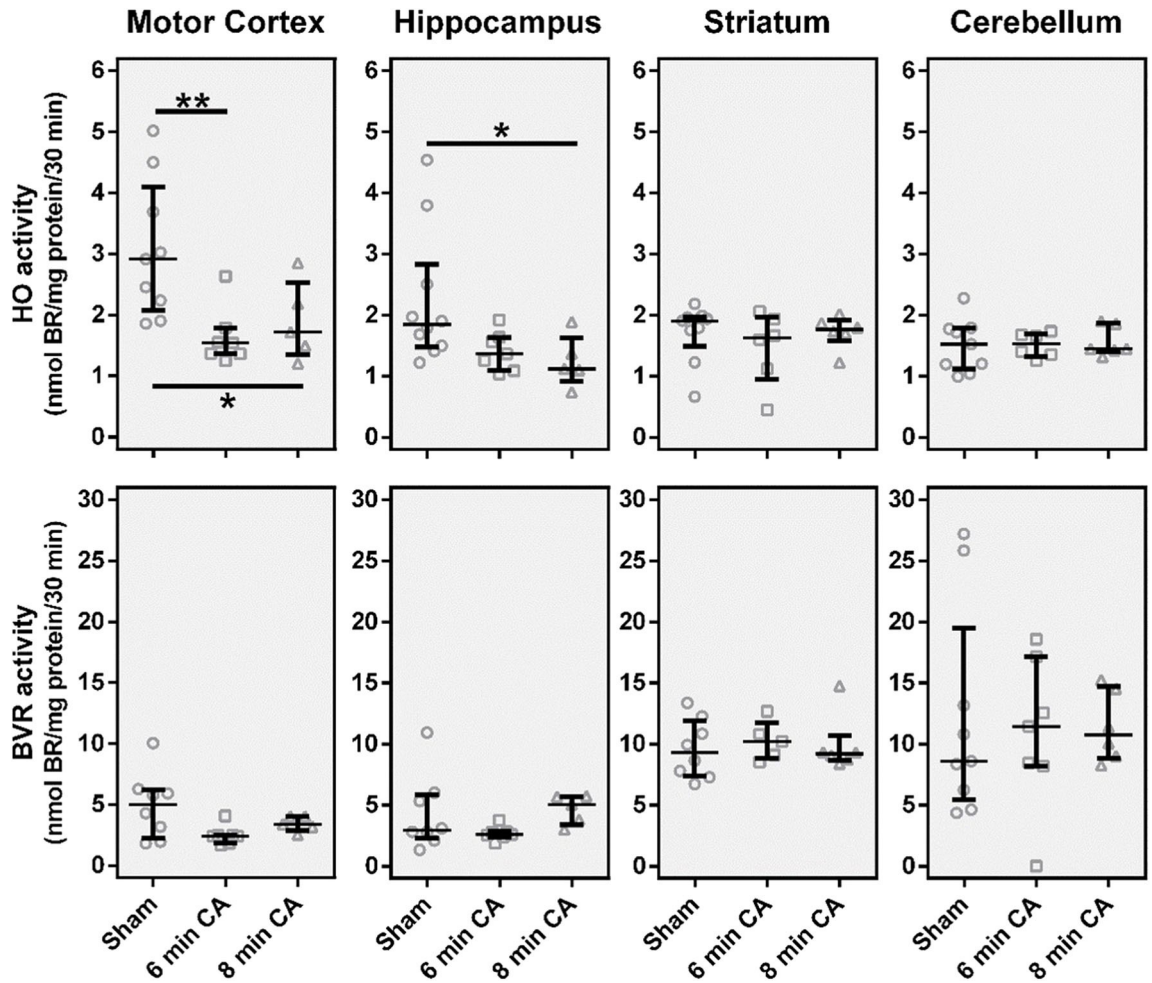

FIGURE 3 | Catalytic activities of the heme degradation pathway enzymes, HO and BVR, in brain regions 2 weeks after cardiac arrest (CA) (6 or 8 min) and resuscitation. Animals were subjected to CA for 6 min (CA 6 min) or 8 min (CA 8 min) or sham operated, as outlined in Materials and Method section. Brain regions were analyzed for enzyme activity by measuring the capacity of homogenized tissue to convert heme (HO activity) or biliverdin (BVR activity) into bilirubin within 30 min. The obtained amount of BR was corrected for the underlying protein concentration and enzyme activity is given in nmol BR formed per mg protein in 30 min (nmol BR/mg protein/30 min). Data are shown for single animals (gray open symbols) in each group: sham (instrumented animals, open circles, $n = 9$), rats subjected to CA for 6 min (CA 6 min, open squares, $n = 7$) or 8 min (CA 8 min, open triangles, $n = 6$), indicating additionally group medians (thin black line) and 1st and 3rd quartiles (bold black lines). Differences between groups are indicated (one-way non-parametric ANOVA (Kruskal Wallis) Bonferroni-corrected; $^{*}p < 0.05$; $^{**}p < 0.01$).

to Hc, in mC, the HO-2 specific staining was heterogeneous and cell type-specific, making quantitative considerations with this technique difficult. Nevertheless, the overall protein, determined by immunoblots, revealed that CA decreased HO-2 levels in mC as well. Therefore, our data suggest that the decreased HO activity may be caused by lower levels of HO-2 protein in mC and Hc.

Gene Expression Level of Enzymes of the Heme Degradation Pathway and Activation of Inflammatory Pathways (TNFR1)

In order to find out whether the decrease in HO-2 protein was caused by a decreased mRNA transcription, we determined gene expression levels. Additionally to HO-2 mRNA, we also analyzed HO-1 and BVRA mRNA levels to cover gene transcription of all enzymes of the heme degradation pathway. Contrary to our expectation, we did not find gene expression levels of either HO isoform decreased. In contrast, the expression levels of HO-1 were increased in Hc of rats subjected to 8 min CA (**Figure 6**). The HO-1 expression levels showed an association with the duration of CA, since highest levels were found in the 8 min CA group. The median of the 6 min CA group showed an increase of 91%, while the median of the group of animals with 8 min CA showed an increase of 132%. Neither HO-2, nor BVRA mRNA showed any changes (**Figure 6**).

It is known that HO-1 (synonym HSP32) is indicative for the activation of a stress response. Activation of astroglia is frequently associated with an increased HO-1 expression, along with other inflammation associated markers, such as TNFR1. Indeed, we could also show upregulation of TNFR1 mRNA in Hc of rats

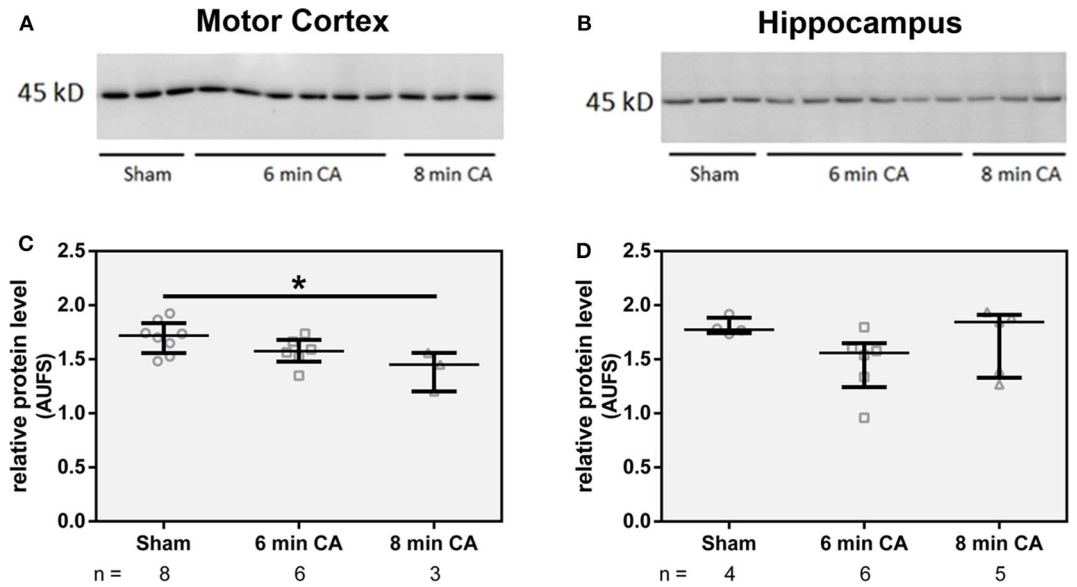

FIGURE 4 | Abundance of HO-2 in homogenates of mC **(A)** and Hc **(B)**. Homogenates from brain regions of single animals were analyzed by SDS-PAGE and immunostained for HO-2 as described in Materials and Methods section. For quantification, band intensities of HO-2 specific staining were normalized to total protein staining of the respective gel lanes, in **(C)** for mC and in **(D)** for Hc. Values are given as AUFS (arbitrary units) as single data (gray open symbols) for each group: sham animals (open circles), rats subjected to cardiac arrest (CA) for 6 min (CA 6 min, open squares) or 8 min (CA 8 min, open triangles), indicating additionally group medians (thin black line) and 1st and 3rd quartiles (bold black lines). The numbers of analyzed animals per group are indicated below the graphs; a selection is displayed here. Total protein patterns of the respective gels are shown in **Figure S1**. Differences between groups are indicated (one-way non-parametric ANOVA (Kruskal Wallis) Bonferroni-corrected; $^*p < 0.01$).

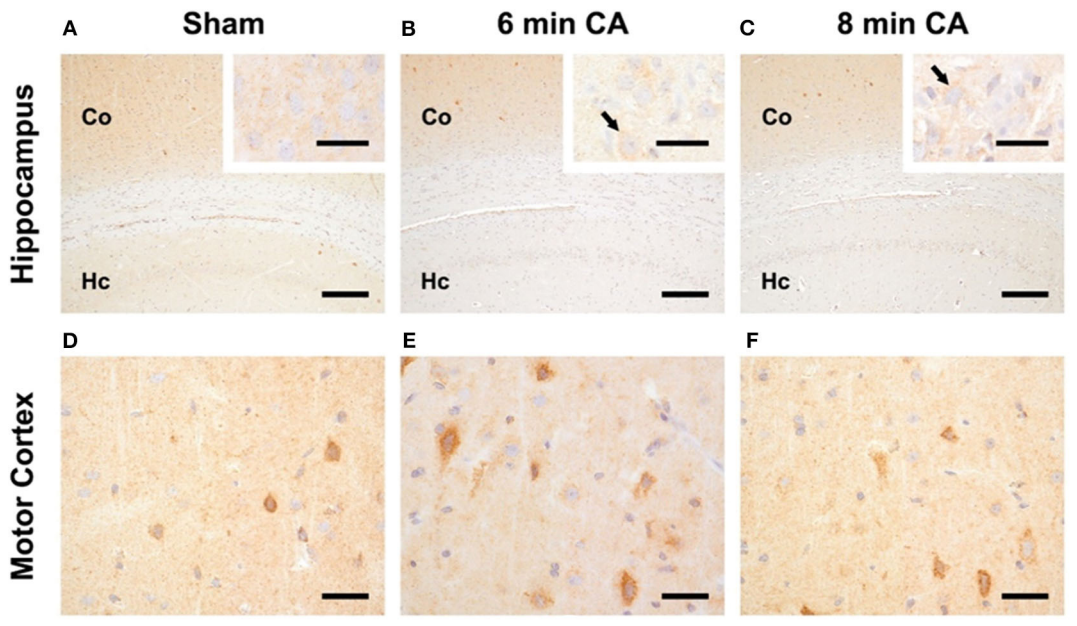

FIGURE 5 | Representative pictures of HO-2 expression in hippocampus and motor cortex. **(A–C)** Expression of HO-2 in the Hc, bar = 30 μm, bar in inserts = 150 μm. **(A)** The signal intensity in the hippocampus (Hc) of sham animals is nearly similar to the expression in the respective overlying cerebral cortex (Co). **(B,C)** Reduced expression of HO-2 in the Hc of 6 and 8 min CA animals compared to the respective cerebral cortex and compared to sham animals. Inserts: HO-2 expression is detectable in all pyramidal neurons of sham animals **(A)**, but only in viable pyramidal neurons [arrows in **(B,C)**] in CA animals. **(D–F)** Expression of HO-2 in the mC, bar = 30 μm; consistent expression of HO-2 in sham **(D)** as well as 6 **(E)** and 8 min **(F)** CA animals with increased staining intensity in some neurons.

subjected to 6 and 8 min of CA (**Figure 6**). The expression levels of TNFR1 mRNA showed a significant correlation with HO-1 mRNA (Spearman Rho, $R = 0.649$; $p = 0.001$, data not shown).

TABLE 3 | Semiquantitative evaluation of HO-2 and markers indicative for activation of astrocytes and microglia in hippocampal sections of rats after 2 weeks following cardiac arrest.

Marker	Sham	6 min CA[a]	8 min CA
HO-2	4 (4,4)	2 (1,2)***	1 (12)***
Iba1[b]	0 (0, 0)	3 (3,3)***	3.5 (3,4)***
GFAP[c]	0 (0, 0)	3 (2,4)***	4 (3,4)***

[a] *CA, cardiac arrest.*

[b] *Iba1, ionized calcium-binding adapter molecule 1 (microglia activation marker), activation of.*

[c] *Glial fibrillary acidic protein; data are given as mean ± SD. Details of the scoring system yielding median and interquartile ranges are described in the respective Materials and Methods section. Significant differences were detected between sham animals and animals subjected to CA for all markers (***p < 0.005 vs. sham), but not between 6 and 8 min CA animals.*

The median of the 6 min CA group showed an increase of 33%, while the median of the 8 min CA group showed a more than two-fold increase. Compared to the sham animals this increase was significant for the animals subjected to 8 min of CA ($p = 0.003$), but only by trend for the animals subjected to 6 min of CA ($p = 0.055$). None of the other regions displayed increased levels of TNFR1.

Histopathological Changes Only in Hc 2 Weeks After CA

The results of mRNA expression analyses suggested an ongoing stress response and additionally the number of HO-2 expressing neurons was diminished in Hc. In order to determine the morphological appearance of lesions in response to CA and reperfusion we evaluated HE-stained sections of all investigated regions.

Consistent lesions were detectable only in the Hc of animals with CA. Sham animals did not show any lesions in the *CA1* region (**Figure 7A**). Hypereosinophilic pyramidal neurons with shrunken nuclei (necrotic neurons) were present in animals

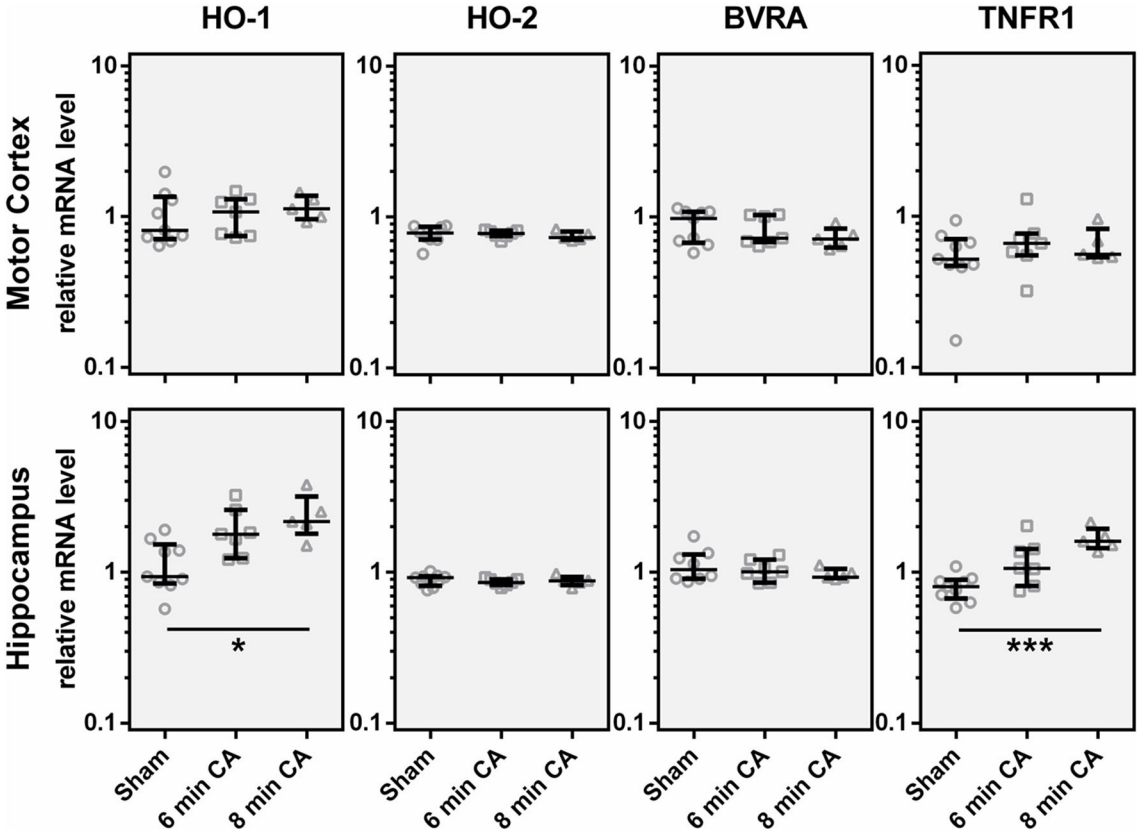

FIGURE 6 | Expression of, HO-1, HO-2, BVRA and TNFR1 mRNA in motor cortex and hippocampus 2 weeks following cardiac arrest (CA). Gene expression was quantified by qPCR. Data were normalized against the internal reference genes HPRT and *Cyclophilin A* and expressed relative to the IS (relative mRNA level). Gene expression levels are shown for single animals (gray open symbols) in each group: sham animals (open circles, $n = 9$), rats subjected to CA for 6 min (CA 6 min, open squares, $n = 7$) or 8 min (CA 8 min, open triangles, $n = 6$), indicating additionally group medians (thin black line) and 1st and 3rd quartiles (bold black lines). Significant differences between groups were calculated by one-way non-parametric ANOVA (Kruskal Wallis followed by Bonferroni-correction) and are indicated (*$p < 0.05$; ***$p < 0.005$).

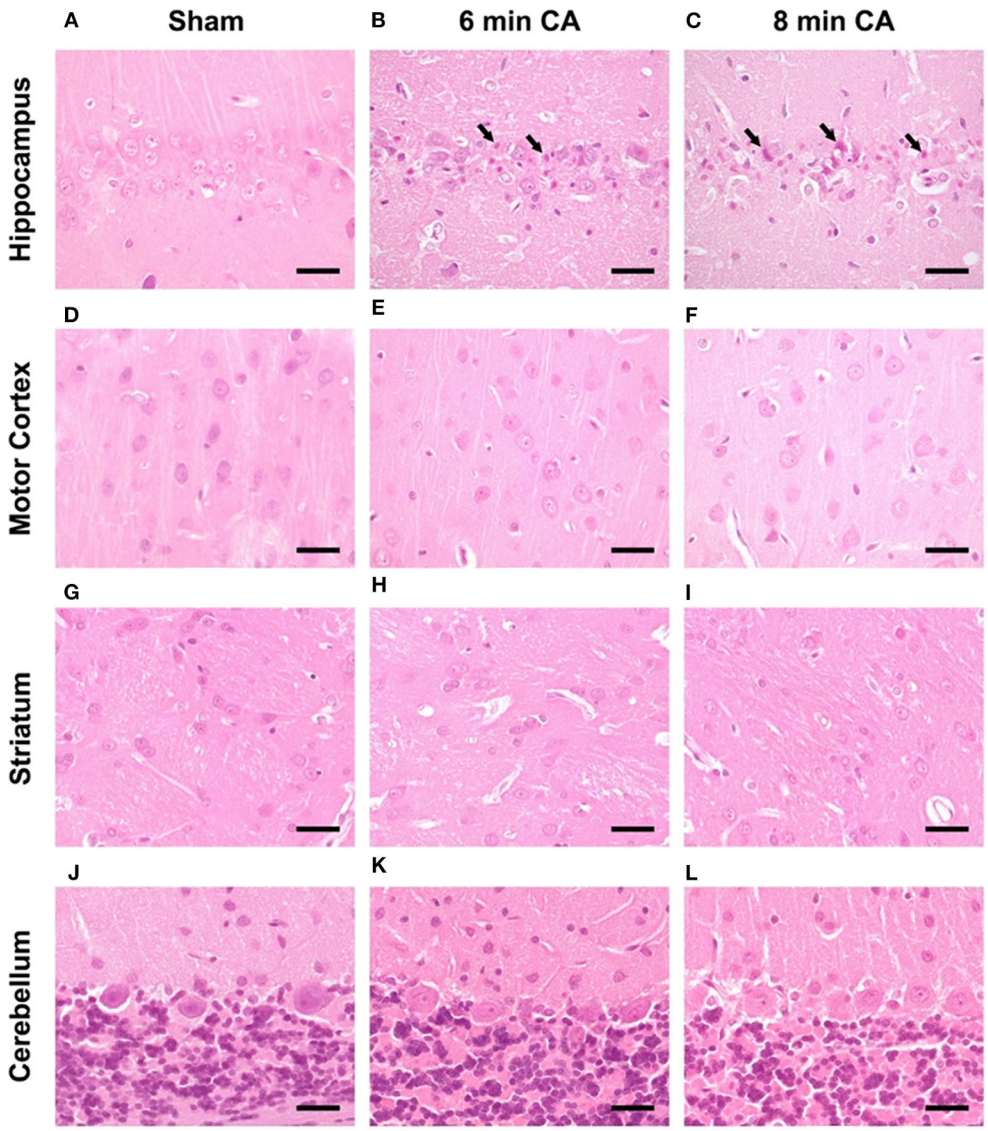

FIGURE 7 | Representative pictures of hippocampus, motor cortex, striatum and cerebellum at 14 days after CA, HE-staining, bar = 30 μm. **(A–C)** Hippocampus, **(A)** sham animal with viable pyramidal neurons, no lesions present. **(B)** 6 min CA animal with many necrotic neurons (arrows) and few viable pyramidal neurons; **(C)** 8 min CA animal with many necrotic neurons (arrows) and only scattered viable pyramidal neurons. **(D–F)** Motor cortex, viable neurons in sham **(D)** as well as 6 **(E)** and 8 min CA **(F)** animals, no lesions present. **(G–I)** Striatum, viable neurons in sham **(G)** as well as 6 **(H)** and 8 min CA **(I)** animals, no lesions present. **(J–L)** Cerebellum, viable neurons in sham **(J)** as well as 6 **(K)** and 8 min CA **(L)** animals, no lesions present. CA, cardiac arrest.

with 6 and 8 min CA (**Figures 7B,C**). Animals with 8 min CA showed a tendency toward more severe lesions, but no significant differences were found compared to 6 min CA animals. Lesions were not detected in mC (**Figures 7D–F**). Also striatum (**Figures 7G–I**) and cerebellum (**Figures 7J–L**) showed no lesions, regardless of CA duration and consistent with earlier findings (7).

CA Leads to Activation of Microglia and Astrocytes in Hc

Hc showed loss of pyramidal neurons in association with increased mRNA expression levels of inflammatory markers in animals subjected to CA surviving 14 days. We therefore aimed at confirming ongoing gliosis by additionally analyzing typical markers. Using immunohistochemistry we determined an increased staining of Iba1 and GFAP regarding extent and intensity in microglia (**Figures 8A–C**) and astrocytes (**Figures 8D–F**) in CA-animals. Microglia showed rod-shaped nuclei and soma with short thick processes consistent with activation. Cytoplasm and nuclei of astrocytes were swollen with large thick processes showing gemistocytic appearance. By semiquantitative evaluation of glial activation statistically significant differences were detected between sham and CA animals in Iba1 and GFAP immunohistochemistry ($p < 0.005$).

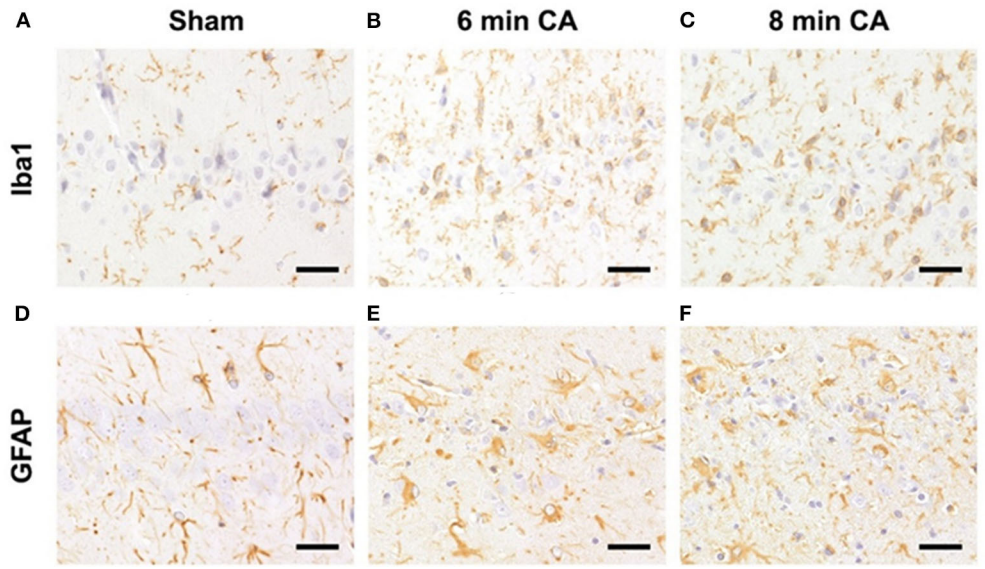

FIGURE 8 | Representative pictures of microglia and astrocyte activation after CA in the hippocampus, bar = 30 μm. **(A–C)** Detection of microglia (antibody against Iba1) in the Hc. **(A)** Normal appearance and numbers of microglial cells in sham animal. **(B,C)** Increased numbers of activated microglia in CA animals. **(D–F)** Detection of astrocytes (antibody against GFAP) in the Hc. **(D)** Normal appearance and numbers of astrocytes in sham animal. **(E,F)** Increased numbers of gemistocytes in CA animals. CA, cardiac arrest.

However, no differences were present between 6 and 8 min CA groups (**Table 3**).

DISCUSSION

We could show that 2 weeks after CA hippocampal and motor cortex tissues display decreased HO activity, which is a reduced capacity to convert heme. Although several reports have brought evidence for the relevance of HO in protecting susceptible neuronal structures against the consequences of ischemia, a complete assessment of region specific changes of the cerebral HO system in response to CA is not available yet.

Ischemia as a result from CA and resuscitation result in the well-described phenomenon of ischemia/reperfusion injury (47). Neuronal cells display a particular vulnerability, which depends primarily on the duration of the ischemic insult, but also on the brain region itself (48, 49) and *CA1* pyramidal neurons of the Hc appear consistently affected.

We found that 2 weeks after CA pyramidal neurons in the *CA1* region were lost and staining intensity of Iba1 and GFAP were increased, showing activation of microglia and astrocytes. In Hc, we found higher mRNA levels of HO-1, which correlated with TNFR1 mRNA, both markers of inflammatory cell stress. The degree of neurodegeneration seen in Hc showed a tendency to increase with the duration of CA, since animals subjected to 8 min of CA displayed changes that were more pronounced. Our findings confirm that cerebral ischemia affects nearly always the Hc region (15), in which neuroinflammation and neurodegeneration is persisting over long periods (17, 50).

Loss of pyramidal neurons in *CA1* is known to lead to learning and memory deficits, and the reappearance of neurons in *CA1* to improved learning and memory performance (51). Meanwhile it is well-accepted that HO plays an important role for survival of neurons, including *CA1* neurons of Hc in response to cell stress, such as ischemia. A model of asphyxia induced cardiac arrest showed that neuronal injury and neuronal loss in the *CA1* region were lower after 2 weeks when animals were pre-treated with heme, while neuronal loss was higher upon pre-treatment with a HO inhibitor (52). However, neither expression levels, nor activities of the enzymes of the heme degradation pathway were analyzed in the cited study. Nevertheless, a recent study suggested a close association of cognitive capabilities and the actual HO activity in Hc. Reversal of age-related cognitive deficits and neuronal loss in *CA1* was associated with an increase in heme degrading capacity of Hc and frontal cortex (53).

Functional HO enzyme maintains cellular homeostasis and protection of neurons by different means (54). HO reaction products play an important role in stress defense and tissue regeneration (30–32) and transiently increased HO activity therefore supports neuronal repair and regeneration following an insult (55). Decreased HO activity, in contrast, impairs neuronal function and aggravates neuronal injury. Deletion of HO-2 in neuronal cells of Hc and cortex resulted in oxidative stress mediated injury, which was absent in cells with functional HO-2. The neuroprotection was attributed to BR (56), which may protect cells against a 10,000-fold excess of H_2O_2 (57). Further, neuronal function requires CO (58), particularly that of neurons in Hc (59). Thus, inhibition of HO within the Hc by pharmacological means resulted in retrograde amnesia (60), showing that active HO is required for memory consolidation. Memory consolidation involves cGMP (21), a second messenger formed by soluble guanylate cyclase, of which CO, a product of the HO reaction, is a known activator.

The decrease in HO activity, which we have determined in mC and Hc tissue, is supposed to operate simultaneously in two adverse directions: on one hand, it will result in (i) heme accumulation and on the other hand in (ii) a decreased generation of HO reaction products (see below). Excess free heme is highly toxic, especially for neuronal cells, due to its ability to promote oxidative stress (61). Based on its lipophilic nature, heme may induce lipid peroxidation and subsequent membrane injury, which finally results in apoptosis. Indeed, scavenging of heme by intracerebroventricularly applied hemopexin reduced the infarct volumes, improved neurological function and cognitive function after focal ischemia (62, 63). We therefore think that the decreased HO activity, which is caused by CA, results in neuronal deficits.

Up to now, it is not possible to determine the contribution of the single HO isoforms to the overall heme degrading capacity in tissue homogenates, because isoform specific inhibitors are not available. However, it is known that in neuronal tissue nearly all of the HO-activity is ascribable to the constitutive HO isoform HO-2 (64), and the contribution of HO-1 is almost absent in physiological conditions (20). Accordingly, studies using HO-2 knockout mice showed that although traumatic brain injury dramatically upregulated HO-1, and HO activity was slightly increased shortly thereafter, the HO activity determined in injured mice remained far below the values found in wild type control mice (65). Only few studies, focusing on the events occurring shortly after the insult, investigated HO activity in neuronal tissues following ischemia. Spinal cord injury resulted in an increased HO activity few days later (66). In another model of focal cerebral ischemia injured areas displayed an increased HO-1 protein abundance 3 days later, which correlated with a locally increased capacity to produce BR (67). Thus, even though stressful conditions increase the concentration of HO-1 the contribution of this isoform to the overall HO activity appears limited and may be timely restricted in neuronal tissues. This interpretation is supported by the fact, that HO-1 protein was not detectable in mC and even in Hc, despite the increased mRNA expression. Therefore, we can assume that HO-1 protein did not contribute noteworthy to the measured HO activity.

In contrast, our findings suggest that the decreased HO activity in rats subjected to CA, results at least partially from lower HO-2 protein concentrations in mC and Hc tissue. The *in-situ* protein expression of HO-2 in both regions using immunohistochemistry showed that HO-2 expression varies among cell types. Neuronal cells displayed stronger staining intensities, and highest HO-2 levels were found in selected neurons in mC. Due to this heterogeneity, HO-2 quantification by immunohistochemistry is difficult. However, the overall quantification using western blots showed a decrease in HO-2 protein in mC, which was significant, when CA lasted 8 min. Although we could not find morphological signs for neuronal loss in mC a loss of a few of these HO-2 highly positive cells is supposed to contribute measurably to a decrease in the overall protein and enzyme activity. Compared to mC, in Hc HO-2 staining was more homogenous, enabling a semiquantitative approach using immunohistochemistry. In rats subjected to CA, HO-2 representation was lower in all layers of Hc. This difference became obvious, when comparing the staining intensity with the adjacent cortex tissue. Further, HO-2 staining was predominantly present in viable pyramidal neurons of *CA1*. Since these neurons are a significant source of HO protein, it is highly probable that a loss of these cells caused the decrease in HO activity. Unfortunately, our data obtained from HO-2 immunoblots of Hc tissue homogenates did not reveal significant differences among groups, possibly because not all animals were included into this analysis, due to the limited amount of tissue material. Nevertheless, using different approaches, our data suggest that the decreased HO activity in mC and Hc of rats subjected to CA may result from lower levels of HO-2 protein present in these regions.

We assume that this decrease in HO-2 was not caused by gene regulation, since HO-2 mRNA expression was unchanged in both regions, and in Hc, HO-1 mRNA was even increased in response to CA. We can rule out that the partially opposing results, which we have obtained, are caused by area specific effects associated with heterogeneous cellular composition and architecture of neuronal tissue. Our methodological approach of using homogenates of the entire regions of interest, allowed to directly compare the obtained data for all quantitative parameter. Probably, CA induced a loss of HO-2 positive cells.

Additionally, it is possible that posttranslational modifications that may affect the enzymatic activity (33, 68) are involved. Oxygen and nitrogen radicals induce HO-1 mRNA, but simultaneously, they may induce posttranslational protein modifications, which down-modulate HO-activity (68). Hippocampal tissue of aged subjects with cognitive impairment or Alzheimer disease display increased levels of HO-1 protein showing oxidative posttranslational modifications (33, 69). Further, amyloid precursor proteins may associate with HO (70), inhibit HO activity and thereby increase oxidative stress levels, attributed to a decreased production of BR (34). Interestingly, amyloid-β peptide is an integral part of the cGMP-induced memory induction (71) that requires functional HO enzyme. These findings suggest the existence of a vicious cycle consisting of oxidative stress induced HO-1 expression and a lower HO activity due to chronically enhanced oxidative stress levels.

Further studies are needed to clarify the cause for the decrease in HO activity; however, our findings suggest compromised neuronal function in both regions, Hc and mC. Additionally, the decreased HO activity in Hc may compromise the repair mechanisms and prevent reduction of oxidative stress levels. We think that the increased HO-1 mRNA levels in Hc seen at this late time point after CA stands for the attempt to compensate for the decreased HO activity in order to restore tissue homeostasis. Not necessarily, an increased HO activity must result thereof. In contrast, many studies show that changes in mRNA or protein levels also for other enzymes relevant for the antioxidant defense do not fully account for the changes in enzyme activity determined under certain stress conditions (72, 73). Thus, contrary to the general assumption, HO mRNA (and protein) expression levels are not suitable to predict the resulting HO activity in neuronal tissues.

Except for Hc, our model revealed absence of histological signs for neurodegeneration or gliosis at this late time point

(7, 9, 74). It has been shown, that the duration and the depth of the ischemic insult affect the chronology of the manifestation of neuronal damage in the different brain regions (75). Although we found decreased HO activity in mC, this region did not show morphological signs for neurodegeneration. However, mC might functionally respond to CA and the decreased HO activity may indicate a slowly progressing neuronal dysfunction, which is not leading to such an impressive loss of neurons, as is the case for Hc. However, further studies are required to elucidate the mechanism underlying the decrease in HO activity, which may contribute to the delayed neurodegeneration in Hc and mC after CA.

CONCLUSION

Our data revealed decreased HO activity in two brain regions, namely Hc and mC in a clinically relevant model for human ventricular fibrillation cardiac arrest and resuscitation 2 weeks after global ischemia. Our data suggest that reduced protein levels of HO-2 may contribute to the decreased tissue capacity to produce HO reaction products. In the *CA1* region of Hc, a region typically affected in cerebral ischemia, the decrease in HO activity went in parallel with neuronal loss in *CA1* and an increase in levels of markers indicating ongoing gliosis. Although the decreased HO activity in mC was not associated with visible lesions, HO-2 positive cells may have been lost in response to CA. Considering the importance of HO for neuronal protection and function, it is conceivable that decreased HO activity is causally involved in the delayed neurodegenerative processes, which contribute to neuronal dysfunction frequently occurring in CA patients. Our findings further suggest that protein or RNA expression data do not allow inferring HO activities in neuronal tissues.

DATA AVAILABILITY STATEMENT

All datasets presented in this study are included in the article/**Supplementary Material**.

ETHICS STATEMENT

The animal study was reviewed and approved by Committee of the Medical University of Vienna and the Austrian Ministry of Science, Research and Economy (GZ: 66.009/0064-II/3b/2011).

AUTHOR CONTRIBUTIONS

A-MW performed animal experiments and wrote the first draft of the manuscript. JH prepared and analyzed samples and performed the gene expression analysis with AM, FE, UT, IAM, BB, and A-MK and contributed with acquisition of data. AJ implemented the setup and procedures of the animal experiments and collected samples. IM and RM performed biochemical analysis and visualization of results. SH undertook the histological analysis and interpretation of results. JD performed the statistical analysis and prepared the final figures and tables. MH, FS, WW, and JD planned and designed the study. WW and JD wrote the final version of the manuscript. All authors approved the final version of the manuscript.

FUNDING

This research was partially funded by the Austrian Science Fund (FWF) [P 24824-824]. The funders had no role in the design of the study; in the collection, analysis, or interpretation of data; in the writing of the manuscript, or in the decision to publish the results. JH and Martina Kames were supported by Internships for female students from the Austrian Research Promotion Agency (FFG). AM was supported by the Austrian Research Promotion Agency with a Ph.D. grant: Industrienahe Dissertation (849090).

ACKNOWLEDGMENTS

The authors acknowledge Martina Kames and Katrin Virgolini for the skilled assistance in the sample preparation and all our students and the team (veterinarians, laboratory technicians, healthcare professionals, and animal keepers) of the Core Unit of Biomedical Research, Medical University of Vienna.

SUPPLEMENTARY MATERIAL

The Supplementary Material for this article can be found online at: https://www.frontiersin.org/articles/10.3389/fmed.2020.00513/full#supplementary-material

REFERENCES

1. Lemiale V, Dumas F, Mongardon N, Giovanetti O, Charpentier J, Chiche JD, et al. Intensive care unit mortality after cardiac arrest: the relative contribution of shock and brain injury in a large cohort. *Intensive Care Med.* (2013) 39:1972–80. doi: 10.1007/s00134-013-3043-4
2. Nolan JP, Neumar RW, Adrie C, Aibiki M, Berg RA, Boettiger BW, et al. Post-cardiac arrest syndrome: epidemiology, pathophysiology, treatment, and prognostication. A Scientific Statement from the International Liaison Committee on Resuscitation; the American Heart Association Emergency Cardiovascular Care Committee; the Council on Cardiovascular Surgery and Anesthesia; the Council on Cardiopulmonary, Perioperative, and Critical Care; the Council on Clinical Cardiology; the Council on Stroke. *Resuscitation.* (2008) 79:350–79. doi: 10.1016/j.resuscitation.2008.09.017
3. Frisch S, Thiel F, Schroeter ML, Jentzsch RT. Apathy and cognitive deficits in patients with transient global ischemia after cardiac arrest. *Cogn Behav Neurol.* (2017) 30:172–5. doi: 10.1097/WNN.0000000000000139
4. Nunes B, Pais J, Garcia R, Magalhaes Z, Granja C, Silva MC. Cardiac arrest: long-term cognitive and imaging analysis. *Resuscitation.* (2003) 57:287–97. doi: 10.1016/S0300-9572(03)00033-9
5. Stamenova V, Nicola R, Aharon-Peretz J, Goldsher D, Kapeliovich M, Gilboa A. Long-term effects of brief hypoxia due to cardiac arrest: hippocampal reductions and memory deficits. *Resuscitation.* (2018) 126:65–71. doi: 10.1016/j.resuscitation.2018.02.016

6. Abella BS, Zhao D, Alvarado J, Hamann K, Vanden Hoek TL, Becker LB. Intra-arrest cooling improves outcomes in a murine cardiac arrest model. *Circulation.* (2004) 109:2786–91. doi: 10.1161/01.CIR.0000131940.19833.85
7. Ettl F, Magnet IAM, Weihs W, Warenits AM, Grassmann D, Wagner M, et al. Establishing a rodent model of ventricular fibrillation cardiac arrest with graded histologic and neurologic damage with different cardiac arrest durations. *Shock.* (2018) 50:219–25. doi: 10.1097/SHK.0000000000001004
8. Janata A, Drabek T, Magnet IA, Stezoski JP, Janesko-Feldman K, Popp E, et al. Extracorporeal versus conventional cardiopulmonary resuscitation after ventricular fibrillation cardiac arrest in rats: a feasibility trial. *Crit Care Med.* (2013) 41:e211–22. doi: 10.1097/CCM.0b013e318287f51e
9. Weihs W, Warenits AM, Ettl F, Magnet IA, Teubenbacher U, Hilpold A, et al. Reduced long-term memory in a rat model of 8Â minutes ventricular fibrillation cardiac arrest: a pilot trial. *BMC Vet Res.* (2016) 12:103. doi: 10.1186/s12917-016-0740-6
10. Kiryk A, Pluta R, Figiel I, Mikosz M, Ulamek M, Niewiadomska G, et al. Transient brain ischemia due to cardiac arrest causes irreversible long-lasting cognitive injury. *Behav Brain Res.* (2011) 219:1–7. doi: 10.1016/j.bbr.2010.12.004
11. Cohan CH, Neumann JT, Dave KR, Alekseyenko A, Binkert M, Stransky K, et al. Effect of cardiac arrest on cognitive impairment and hippocampal plasticity in middle-aged rats. *PLoS ONE.* (2015) 10:e0124918. doi: 10.1371/journal.pone.0124918
12. Rohnert P, Schroder UH, Ziabreva I, Tager M, Reymann KG, Striggow F. Insufficient endogenous redox buffer capacity may underlie neuronal vulnerability to cerebral ischemia and reperfusion. *J Neurosci Res.* (2012) 90:193–202. doi: 10.1002/jnr.22754
13. Sairanen TR, Lindsberg PJ, Brenner M, Carpen O, Siren A. Differential cellular expression of tumor necrosis factor-alpha and Type I tumor necrosis factor receptor after transient global forebrain ischemia. *J Neurol Sci.* (2001) 186:87–99. doi: 10.1016/S0022-510X(01)00508-1
14. Yakubov E, Gottlieb M, Gil S, Dinerman P, Fuchs P, Yavin E. Overexpression of genes in the CA1 hippocampus region of adult rat following episodes of global ischemia. *Brain Res Mol Brain Res.* (2004) 127:10–26. doi: 10.1016/j.molbrainres.2004.05.010
15. Yin L, Ohtaki H, Nakamachi T, Kudo Y, Makino R, Shioda S. Delayed expressed TNFR1 co-localize with ICAM-1 in astrocyte in mice brain after transient focal ischemia. *Neurosci Lett.* (2004) 370:30–5. doi: 10.1016/j.neulet.2004.07.083
16. Hartman RE, Lee JM, Zipfel GJ, Wozniak DF. Characterizing learning deficits and hippocampal neuron loss following transient global cerebral ischemia in rats. *Brain Res.* (2005) 1043:48–56. doi: 10.1016/j.brainres.2005.02.030
17. Langdon KD, Granter-Button S, Corbett D. Persistent behavioral impairments and neuroinflammation following global ischemia in the rat. *Eur J Neurosci.* (2008) 28:2310–8. doi: 10.1111/j.1460-9568.2008.06513.x
18. Dennery PA. Signaling function of heme oxygenase proteins. *Antioxid Redox Signal.* (2014) 20:1743–53. doi: 10.1089/ars.2013.5674
19. Maines MD, Mark JA, Ewing JF. Heme oxygenase, a likely regulator of cGMP production in the brain: induction in vivo of HO-1 compensates for depression in NO synthase activity. *Mol Cell Neurosci.* (1993) 4:396–405. doi: 10.1006/mcne.1993.1050
20. Trakshel GM, Kutty RK, Maines MD. Resolution of the rat brain heme oxygenase activity: absence of a detectable amount of the inducible form (HO-1). *Arch Biochem Biophys.* (1988) 260:732–9. doi: 10.1016/0003-9861(88)90503-6
21. Bernabeu R, Schmitz P, Faillace MP, Izquierdo I, Medina JH. Hippocampal cGMP and cAMP are differentially involved in memory processing of inhibitory avoidance learning. *Neuroreport.* (1996) 7:585–8. doi: 10.1097/00001756-199601310-00050
22. Boehning D, Snyder SH. Novel neural modulators. *Annu Rev Neurosci.* (2003) 26:105–31. doi: 10.1146/annurev.neuro.26.041002.131047
23. Parfenova H, Leffler CW. Cerebroprotective functions of HO-2. *Curr Pharm Des.* (2008) 14:443–53. doi: 10.2174/138161208783597380
24. Imuta N, Hori O, Kitao Y, Tabata Y, Yoshimoto T, Matsuyama T, et al. Hypoxia-mediated induction of heme oxygenase type I and carbon monoxide release from astrocytes protects nearby cerebral neurons from hypoxia-mediated apoptosis. *Antioxid Redox Signal.* (2007) 9:543–52. doi: 10.1089/ars.2006.1519
25. Garnier P, Demougeot C, Bertrand N, Prigent-Tessier A, Marie C, Beley A. Stress response to hypoxia in gerbil brain: HO-1 and Mn SOD expression and glial activation. *Brain Res.* (2001) 893:301–9. doi: 10.1016/S0006-8993(01)02009-1
26. Geddes JW, Pettigrew LC, Holtz ML, Craddock SD, Maines MD. Permanent focal and transient global cerebral ischemia increase glial and neuronal expression of heme oxygenase-1, but not heme oxygenase-2, protein in rat brain. *Neurosci Lett.* (1996) 210:205–8. doi: 10.1016/0304-3940(96)12703-8
27. Wang R, Wang ST, Wang YD, Wu G, Du Y, Qian MQ, et al. Stress-responsive heme oxygenase-1 isoenzyme participates in Toll-like receptor 4-induced inflammation during brain ischemia. *Neuroreport.* (2016) 27:445–54. doi: 10.1097/WNR.0000000000000561
28. Sutherland BA, Rahman RM, Clarkson AN, Shaw OM, Nair SM, Appleton I. Cerebral heme oxygenase 1 and 2 spatial distribution is modulated following injury from hypoxia-ischemia and middle cerebral artery occlusion in rats. *Neurosci Res.* (2009) 65:326–34. doi: 10.1016/j.neures.2009.08.007
29. Dorè S, Sampei K, Goto S, Alkayed NJ, Guastella D, Blackshaw S, et al. Heme oxygenase-2 is neuroprotective in cerebral ischemia. *Mol Med.* (1999) 5:656–63. doi: 10.1007/BF03401984
30. Basuroy S, Tcheranova D, Bhattacharya S, Leffler CW, Parfenova H. Nox4 NADPH oxidase-derived reactive oxygen species, via endogenous carbon monoxide, promote survival of brain endothelial cells during TNF-α-induced apoptosis. *Am J Physiol Cell Physiol.* (2011) 300:C256–65. doi: 10.1152/ajpcell.00272.2010
31. Chen J, Regan RF. Increasing expression of heme oxygenase-1 by proteasome inhibition protects astrocytes from heme-mediated oxidative injury. *Curr Neurovasc Res.* (2005) 2:189–96. doi: 10.2174/1567202054368344
32. Dorè S, Takahashi M, Ferris CD, Zakhary R, Hester LD, Guastella D, et al. Bilirubin, formed by activation of heme oxygenase-2, protects neurons against oxidative stress injury. *Proc Natl Acad Sci USA.* (1999) 96:2445–50. doi: 10.1073/pnas.96.5.2445
33. Barone E, Di DF, Sultana R, Coccia R, Mancuso C, Perluigi M, et al. Heme oxygenase-1 posttranslational modifications in the brain of subjects with Alzheimer disease and mild cognitive impairment. *Free Radic Biol Med.* (2012) 52:2292–301. doi: 10.1016/j.freeradbiomed.2012.03.020
34. Takahashi M, Dorè S, Ferris CD, Tomita T, Sawa A, Wolosker H, et al. Amyloid precursor proteins inhibit heme oxygenase activity and augment neurotoxicity in Alzheimer's disease. *Neuron.* (2000) 28:461–73. doi: 10.1016/S0896-6273(00)00125-2
35. Kilkenny C, Browne WJ, Cuthill IC, Emerson M, Altman DG. Improving bioscience research reporting: the ARRIVE guidelines for reporting animal research. *PLoS Biol.* (2010) 8:e1000412. doi: 10.1371/journal.pbio.1000412
36. Katz L, Ebmeyer U, Safar P, Radovsky A, Neumar R. Outcome model of asphyxial cardiac arrest in rats. *J Cereb Blood Flow Metab.* (1995) 15:1032–9. doi: 10.1038/jcbfm.1995.129
37. Xiao F, Safar P, Radovsky A. Mild protective and resuscitative hypothermia for asphyxial cardiac arrest in rats. *Am J Emerg Med.* (1998) 16:17–25. doi: 10.1016/S0735-6757(98)90059-6
38. George Paxinos AO, Watson C. *The Rat Brain in Stereotaxic Coordinates*. 7th ed. San Diego, CA: Academic Press (2013).
39. Muellebner A, Dorighello GG, Kozlov AV, Duvigneau JC. Interaction between mitochondrial reactive oxygen species, heme oxygenase, and nitric oxide synthase stimulates phagocytosis in macrophages. *Front Med.* (2017) 4:252. doi: 10.3389/fmed.2017.00252
40. Postl A, Zifko C, Hartl RT, Ebel T, Miller I, Moldzio R, et al. Transient increase of free iron in rat livers following hemorrhagic-traumatic shock and reperfusion is independent of heme oxygenase 1 upregulation. *Shock.* (2011) 36:501–9. doi: 10.1097/SHK.0b013e318231822d
41. Jais A, Einwallner E, Sharif O, Gossens K, Lu TT, Soyal SM, et al. Heme oxygenase-1 drives metaflammation and insulin resistance in mouse and man. *Cell.* (2014) 158:25–40. doi: 10.1016/j.cell.2014.04.043
42. Kozlov AV, Duvigneau JC, Miller I, Nuernberger S, Gesslbauer B, Kungl A, et al. Endotoxin causes functional endoplasmic reticulum failure, possibly mediated by mitochondria. *Biochim Biophys Acta.* (2009) 1792:521–30. doi: 10.1016/j.bbadis.2009.03.004
43. Mkrtchyan GV, Uecal M, Muellebner A, Dumitrescu S, Kames M, Moldzio R, et al. Thiamine preserves mitochondrial function in a rat model of traumatic brain injury, preventing inactivation of the 2-oxoglutarate

dehydrogenase complex. *Biochim Biophys Acta Bioenerg.* (2018) 1859:925–31. doi: 10.1016/j.bbabio.2018.05.005
44. Bustin SA, Benes V, Garson JA, Hellemans J, Huggett J, Kubista M, et al. The MIQE guidelines: minimum information for publication of quantitative real-time PCR experiments. *Clin Chem.* (2009) 55:611–22. doi: 10.1373/clinchem.2008.112797
45. Soler L, Gutierrez A, Muellebner A, Ceron JJ, Duvigneau JC. Towards a better understanding of salivary and meat juice acute phase proteins determination in pigs: an expression study. *Vet Immunol Immunopathol.* (2013) 156:91–8. doi: 10.1016/j.vetimm.2013.09.018
46. Pabinger S, Rodiger S, Kriegner A, VierlingerK, Weinhausel A. A survey of tools for the analysis of quantitative PCR (qPCR) data. *Biomol Detect Quantif.* (2014) 1:23–33. doi: 10.1016/j.bdq.2014.08.002
47. Boettiger BW, Schmitz B, Wiessner C, Vogel P, Hossmann KA. Neuronal stress response and neuronal cell damage after cardiocirculatory arrest in rats. *J Cereb Blood Flow Metab.* (1998) 18:1077–87. doi: 10.1097/00004647-199810000-00004
48. Pulsinelli WA, Brierley JB, Plum F. Temporal profile of neuronal damage in a model of transient forebrain ischemia. *Ann Neurol.* (1982) 11:491–8. doi: 10.1002/ana.410110509
49. Hoegler S, Sterz F, Sipos W, Schratter A, Weihs W, Holzer M, et al. Distribution of neuropathological lesions in pig brains after different durations of cardiac arrest. *Resuscitation.* (2010) 81:1577–83. doi: 10.1016/j.resuscitation.2010.07.005
50. Yasuda Y, Shimoda T, Uno K, Tateishi N, Furuya S, Tsuchihashi Y, et al. Temporal and sequential changes of glial cells and cytokine expression during neuronal degeneration after transient global ischemia in rats. *J Neuroinflammation.* (2011) 8:70. doi: 10.1186/1742-2094-8-70
51. Bueters T, von Euler M, Bendel O, von Euler G. Degeneration of newly formed CA1 neurons following global ischemia in the rat. *Exp Neurol.* (2008) 209:114–24. doi: 10.1016/j.expneurol.2007.09.005
52. Zhang B, Wei X, Cui X, Kobayashi T, Li W. Effects of heme oxygenase 1 on brain edema and neurologic outcome after cardiopulmonary resuscitation in rats. *Anesthesiology.* (2008) 109:260–8. doi: 10.1097/ALN.0b013e31817f5c2e
53. Kurucz A, Bombicz M, Kiss R, Priksz D, Varga B, Hortobágyi T, et al. Heme oxygenase-1 activity as a correlate to exercise-mediated amelioration of cognitive decline and neuropathological alterations in an aging rat model of dementia. *Biomed Res Int.* (2018) 2018:7212861. doi: 10.1155/2018/7212861
54. Schipper HM. Glial HO-1 expression, iron deposition and oxidative stress in neurodegenerative diseases. *Neurotox Res.* (1999) 1:57–70. doi: 10.1007/BF03033339
55. Shefa U, Yeo SG, Kim MS, Song IO, Jung J, Jeong NY, et al. Role of gasotransmitters in oxidative stresses, neuroinflammation, and neuronal repair. *Biomed Res Int.* (2017) 2017:1689341. doi: 10.1155/2017/1689341
56. Dorè S. Decreased activity of the antioxidant heme oxygenase enzyme: implications in ischemia and in Alzheimer's disease. *Free Radic Biol Med.* (2002) 32:1276–82. doi: 10.1016/S0891-5849(02)00805-5
57. Baranano DE, Rao M, Ferris CD, Snyder SH. Biliverdin reductase: a major physiologic cytoprotectant. *Proc Natl Acad Sci USA.* (2002) 99:16093–8. doi: 10.1073/pnas.252626999
58. Verma A, Hirsch DJ, Glatt CE, Ronnett GV, Snyder SH. Carbon monoxide: a putative neural messenger. *Science.* (1993) 259:381–4. doi: 10.1126/science.7678352
59. Bernabeu R, Princ F, de Stein ML, Fin C, Juknat AA, Batile A, et al. Evidence for the involvement of hippocampal CO production in the acquisition and consolidation of inhibitory avoidance learning. *Neuroreport.* (1995) 6:516–8. doi: 10.1097/00001756-199502000-00027
60. Fin C, Schmitz PK, Da Silva RC, Bernabeu R, Medina JH, Izquierdo I. Intrahippocampal, but not intra-amygdala, infusion of an inhibitor of heme oxygenase causes retrograde amnesia in the rat. *Eur J Pharmacol.* (1994) 271:227–9. doi: 10.1016/0014-2999(94)90284-4
61. Goldstein L, Teng ZP, Zeserson E, Patel M, Regan RF. Hemin induces an iron-dependent, oxidative injury to human neuron-like cells. *J Neurosci Res.* (2003) 73:113–21. doi: 10.1002/jnr.10633
62. Dong B, Cai M, Fang Z, Wei H, Zhu F, Li G, Dong H, et al. Hemopexin induces neuroprotection in the rat subjected to focal cerebral ischemia. *BMC Neurosci.* (2013) 14:58. doi: 10.1186/1471-2202-14-58
63. Dong B, Yang Y, Zhang Z, Xie K, Su L, Yu Y. Hemopexin alleviates cognitive dysfunction after focal cerebral ischemia-reperfusion injury in rats. *BMC Anesthesiol.* (2019) 19:13. doi: 10.1186/s12871-019-0681-2
64. Ewing JF, Maines MD. *In situ* hybridization and immunohistochemical localization of heme oxygenase-2 mRNA and protein in normal rat brain: differential distribution of isozyme 1 and 2. *Mol Cell Neurosci.* (1992) 3:559–70. doi: 10.1016/1044-7431(92)90068-D
65. Chang EF, Wong RJ, Vreman HJ, Igarashi T, Galo E, Sharp FR, et al. Heme oxygenase-2 protects against lipid peroxidation-mediated cell loss and impaired motor recovery after traumatic brain injury. *J Neurosci.* (2003) 23:3689–96. doi: 10.1523/JNEUROSCI.23-09-03689.2003
66. Diaz-Ruiz A, Maldonado PD, Mendez-Armenta M, Jimenez-Garcia K, Salgado-Ceballos H, Santander I, et al. Activation of heme oxygenase recovers motor function after spinal cord injury in rats. *Neurosci Lett.* (2013) 556:26–31. doi: 10.1016/j.neulet.2013.08.067
67. Koistinaho J, Miettinen S, Keinaenen R, Vartiainen N, Roivainen R, Laitinen JT. Long-term induction of haem oxygenase-1 (HSP-32) in astrocytes and microglia following transient focal brain ischaemia in the rat. *Eur J Neurosci.* (1996) 8:2265–72. doi: 10.1111/j.1460-9568.1996.tb01190.x
68. Kinobe R, Ji Y, Nakatsu K. Peroxynitrite-mediated inactivation of heme oxygenases. *BMC Pharmacol.* (2004) 4:26. doi: 10.1186/1471-2210-4-26
69. Barone E, Di DF, Cenini G, Sultana R, Coccia R, Preziosi P, et al. Oxidative and nitrosative modifications of biliverdin reductase-A in the brain of subjects with Alzheimer's disease and amnestic mild cognitive impairment. *J Alzheimers Dis.* (2011) 25:623–33. doi: 10.3233/JAD-2011-110092
70. Takahashi M, Snyder SH. Interaction of amyloid precursor proteins and heme oxygenase. *Alzheimer Dis Assoc Disord.* (2000) 14(Suppl. 1):S67–71. doi: 10.1097/00002093-200000001-00011
71. Palmeri A, Ricciarelli R, Gulisano W, Rivera D, Rebosio C, Calcagno E, et al. Amyloid-β peptide is needed for cGMP-induced long-term potentiation and memory. *J Neurosci.* (2017) 37:6926–37. doi: 10.1523/JNEUROSCI.3607-16.2017
72. Hochscheid R, Heinrichs S, Kranz S, Garn H, Mueller B. Differences in mRNA expression, protein content, and enzyme activity of superoxide dismutases in type II pneumocytes of acute and chronic lung injury. *Free Radic Res.* (2002) 36:759–67. doi: 10.1080/10715760290032601
73. Xu CL, Wang YZ, Guo J, Liu JX, Feng J. Comparison of age-related differences in expression of antioxidant enzyme mRNA and activity in various tissues of pigs. *Comp Biochem Physiol B Biochem Mol Biol.* (2007) 147:445–51. doi: 10.1016/j.cbpb.2007.02.007
74. Schober A, Warenits AM, Testori C, Weihs W, Hosmann A, Hoegler S, et al. Microdialysis assessment of cerebral perfusion during cardiac arrest, extracorporeal life support and cardiopulmonary resuscitation in rats—a pilot trial. *PLoS ONE.* (2016) 11:e0155303. doi: 10.1371/journal.pone.0155303
75. Nakano S, Kogure K, Fujikura H. Ischemia-induced slowly progressive neuronal damage in the rat brain. *Neuroscience.* (1990) 38:115–24. doi: 10.1016/0306-4522(90)90378-H

Conflict of Interest: The authors declare that the research was conducted in the absence of any commercial or financial relationships that could be construed as a potential conflict of interest.

frontiers in Medicine

ORIGINAL RESEARCH
published: 24 September 2020
doi: 10.3389/fmed.2020.568096

Circulating miRNAs Associated With ER Stress and Organ Damage in a Preclinical Model of Trauma Hemorrhagic Shock

*Andreia Luís[1], Matthias Hackl[2,3], Mohammad Jafarmadar[1], Claudia Keibl[1], Julia M. Jilge[1], Johannes Grillari[1,3,4], Soheyl Bahrami[1] and Andrey V. Kozlov[1,5]**

[1] Ludwig Boltzmann Institute for Experimental and Clinical Traumatology, Vienna, Austria, [2] TAmiRNA GmbH, Vienna, Austria, [3] Austrian Cluster for Tissue Regeneration, Medical University of Vienna, Vienna, Austria, [4] Christian Doppler Laboratory for Biotechnology of Skin Aging, Department of Biotechnology, Institute of Molecular Biotechnology, BOKU-University of Natural Resources and Life Sciences, Vienna, Austria, [5] Laboratory of Navigational Redox Lipidomics and Department of Human Pathology, IM Sechenov Moscow State Medical University, Moscow, Russia

OPEN ACCESS

Edited by:
Mihály Boros,
University of Szeged, Hungary

Reviewed by:
Petra Hartmann,
University of Szeged, Hungary
Wolfgang Weihs,
Medical University of Vienna, Austria
Andrea Szabó,
University of Szeged, Hungary

***Correspondence:**
Andrey V. Kozlov
andrey.kozlov@trauma.lbg.ac.at

Specialty section:
This article was submitted to Intensive Care Medicine and Anesthesiology, a section of the journal Frontiers in Medicine

Received: *31 May 2020*
Accepted: *18 August 2020*
Published: *24 September 2020*

Citation:
Luís A, Hackl M, Jafarmadar M, Keibl C, Jilge JM, Grillari J, Bahrami S and Kozlov AV (2020) Circulating miRNAs Associated With ER Stress and Organ Damage in a Preclinical Model of Trauma Hemorrhagic Shock. Front. Med. 7:568096. doi: 10.3389/fmed.2020.568096

Circulating microRNAs (miRNA) alterations have been reported in severe trauma patients but the pathophysiological relevance of these changes is still unclear. miRNAs are critical biologic regulators of pathological events such as hypoxia and inflammation, which are known to induce endoplasmic reticulum (ER) stress. ER stress is emerging as an important process contributing to the development of single and/or multiple organ dysfunction after trauma hemorrhagic shock (THS) accompanied by impaired tissue microcirculation and inflammation. Here, we aim to bring new insights into the involvement of miRNAs associated with ER stress in THS. THS was induced in rats by a median laparotomy and blood withdrawal until mean arterial pressure (MAP) dropped to 30-35 mmHg followed by a restrictive (40 min) and full reperfusion (60 min) with Ringer's solution. Tunicamycin was used to induce ER stress. Blood samples were collected 24 h after THS for the determination of pathological changes in the blood (PCB) and circulating miRNAs. Plasma levels of circulating miRNAs were compared between THS, tunicamycin, and sham groups and correlated to biomarkers of PCB. MiRNA profile of THS animals showed that 40 out of 91 (44%) miRNAs were significantly upregulated compared to sham ($p < 0.01$). The data showed a very strong correlation between liver injury and miR−122-5p ($r = 0.91$, $p < 0.00001$). MiR-638, miR−135a-5p, miR−135b-5p, miR-668-3p, miR-204-5p, miR−146a-5p, miR−200a-3p, miR−17-5p, miR−30a-5p, and miR−214-3p were found positively correlated with lactate ($r > 0.7$, $p < 0.05$), and negatively with base excess ($r \leq 0.8$, $p < 0.05$) and bicarbonate ($r \leq 0.8$, $p < 0.05$), which are clinical parameters that reflected the shock severity. Tunicamycin significantly modified the microRNA profile of the animals, 33 out of 91 miRNAs were found differentially expressed. In addition, principal component analysis revealed that THS and tunicamycin induced similar changes in plasma miRNA patterns. Strikingly, the data showed that 15 (25.9%) miRNAs were regulated by both THS and tunicamycin ($p < 0.01$). This included miR−122-5p, a liver-specific microRNA, but also miR−17-5p and miR-125b-5p which are miRNAs remarkably involved in unfolded protein response

(UPR)-mediating pro-survival signaling (IRE1α). Since miRNAs associated with ER stress are clearly correlated with THS, our data strongly suggest that interaction between miRNAs and ER stress is an important pathologic event occurring during THS. Overall, we consider that the miRNA profile developed in this study can provide a rationale for the development of bench-to-bedside strategies that target miRNAs in critical care diseases or be used as biomarkers in the prognosis of trauma patients.

Keywords: circulating miRNAs, trauma hemorrhagic shock, ER stress, organ damage, multiple organ dysfunction

INTRODUCTION

Trauma hemorrhagic shock (THS) is a leading cause of death worldwide (1). THS is a form of hypovolemic shock in which blood loss leads to impaired oxygen delivery and later on to inflammation and/or impaired immune response (1–4). The most dramatic consequence of THS is the so-called multiple organ dysfunction syndrome (MODS) (5–7). Cellular, tissue, and vascular alterations play a central role in the pathophysiology of organ failure but yet the death of patients upon MODS has no clear rational explanation. Biological consequences resulting from THS as hypoxia and inflammation are consistent factors required to trigger endoplasmic reticulum (ER) stress (8, 9). Activation of ER stress upon trauma hemorrhage was previously reported in preclinical models (10–12). We showed that the first signs of ER stress are detectable 40 min after reperfusion and persisted for up to 18 h after THS (11). Similarly, THS with sustained hypotension (without fluid resuscitation) simultaneously impacted mitochondrial function and ER stress response (12).

ER stress is known to trigger the unfolded protein response (UPR), an evolutionary conserved adaptive response that aims to resolve ER stress (adaptation, autophagy) or induce cell death if ER stress cannot be solved (8, 13). THS is based on a primary induction of shock by bleeding upon which an induction of acute inflammation occurs as a secondary aseptic inflammation which is mainly induced by damage-associated molecular patterns (DAMPs) (14), but also by gut-derived bacterial translocation (15). Recently, it was anticipated that ER stress is linked to sterile inflammation due to the release of misfolded (unfolded) proteins which may activate immune responses through the release of DAMPs into the circulation (16). And, in fact, it was previously shown that severe ER stress causes the release of extracellular vesicles carrying proinflammatory DAMPs molecules (17). Exactly how ER stress would lead to the release of DAMPs is still not clear, but it is assumed that autophagic vesicles create amphisomes that fuse to the plasma membrane to free the excess of misfolded proteins in an effort to support proteostasis recovery (16). Experimentally (*in vitro* and *in vivo*) ER stress is broadly induce by tunicamycin, thapsigargin, and brefeldin A (18). Although those chemicals target distinct ER machinery, all lead to ER protein misfolding. In this study, activation of ER stress by tunicamycin treatment was chosen since it is the most prototypical agent used to induce pharmacologic ER stress and UPR. Tunicamycin is an inhibitor of protein N-linked glycosylation impairing newly synthesized proteins (19), leading to the disruption of their folding and to the accumulation of unfolded proteins in the ER.

Recently, extracellular vesicles and particles carrying microRNAs (miRNAs) have been identified as new important regulators of intercellular communication and signaling. miRNAs are fine-tune regulators of multiple processes such as gene and protein expression (20, 21), but also of cellular stress responses such as ER stress (22–24). While we have a substantial understanding of mechanisms that control gene expression and protein translation, the involvement of miRNAs in UPR has only been investigated in the past few years (25). MiRNAs circulating in the bloodstream have also been reported to serve as an important diagnostic tool since they are accessible, stable, biologically relevant, and can, therefore, function as clinical biomarkers (26–29). In this scenario, miRNAs released into the blood offer an advantage over miRNAs expressed in tissues since in human studies fresh biopsy material with yielding high-quality RNA is not always possible to obtain (30). In 2014, the group of Stephen L. Barnes identified circulating miRNAs differentially expressed in hemorrhagic shock patients (31). Thereby, direct and indirect correlations within the differentially expressed miRNAs and genes involved in the toll-like receptors (TLRs) signaling pathways were described (31). TLR4 is known to be a prerequisite for activation of a systemic inflammatory response associated with hepatocellular injury after hemorrhagic shock and resuscitation (32). In general, attenuation of inflammatory response ameliorates organ damage (33). Hemorrhagic shock-activated neutrophils augment TLR4 signaling in lung injury (34). Induction of IL-6, a cytokine activated by TLR4, has been reported to ameliorate liver injury in THS (35), and TNF-α release is suppressed immediately after hemorrhage and resuscitation (15). MiRNAs are also recognized as important regulators of the inflammatory response (36–38) but the relationship between miRNAs, inflammation, and tissue damage is unclear and profiling of miRNA patterns upon THS is very scarce. Knowledge on such miRNA patterns, however, might provide valuable information for better diagnosis and a

Abbreviations: ABEc, base excess; ALT, alanine aminotransferase; AST, aspartate aminotransferase; CK,creatine kinase; CREA, creatinine; cTnI, cardiac troponin I; DAMPs, damage-associated molecular patterns; ER, endoplasmic reticulum; HCO_3^-,bicarbonate; IRE1α, inositol-requiring enzyme 1 α; Lac, lactate; LDH, lactate dehydrogenase; LYM, lymphocyte; MAP, mean arterial pressure; miRNA, microRNA; MODS, multiple organ dysfunction syndrome; MONO, monocytes; NEU, neutrophils; NLR, neutrophil to lymphocyte ratio; PCB, pathological changes in the blood; qPCR, quantitative polymerase chain reaction; RNA, ribonucleic acid; THS, trauma hemorrhagic shock; TUN, tunicamycin; UPR, unfolded protein response; WBC, white blood cells.

rationale for the development of bench-to-bedside strategies by e.g. targeting miRNAs. We here assumed that miRNAs are key regulators of cellular processes such as ER stress that occurs after THS. Consequently, the aim of this study was to bring new insights into the involvement of circulating miRNAs associated with organ damage and ER stress in THS and its relevance in the development of multiple organ dysfunction. Indeed, we here identified circulating miRNAs in a preclinical model of THS and correlated them with pathological changes in the blood (PCB). In addition, we compared the miRNA profile obtained upon THS with miRNAs induced by tunicamycin in order to clarify whether or not ER stress mediates the release of similar miRNAs as THS does.

MATERIALS AND METHODS

Ethics

The animal protocol was reviewed by the board of the city government of Vienna, Austria and approved for all experimental procedures (GZ: 593334/2016/13). All experiments were conducted in a manner that discomfort, pain, distress and suffering was avoided or minimized and in accordance with the Guide for the Care and Use of Laboratory Animals as defined by the National Institutes of Health. 3Rs concept: All experiments were planned carefully to ensure a sufficient number of animals to enable statistical analysis but not more than that. Experiments were combined to reduce the number of animals. All animal experiments were performed under deep anesthesia (during surgical intervention) and pain killers in pre and post-operative stage (refinement).

Animals

In total, 17 male Sprague-Dawley rats (400-450g, Janvier Labs, France) were kept under standard conditions, with free access to standard laboratory chow diet and water. All animal experiments were randomized.

Traumatic Hemorrhagic Shock Model

The traumatic hemorrhagic shock model used in this study is a well-established and clinically relevant model that has been used and reported in previous studies (11, 12). The animals were fasted for 12 h before the experiment with free access to water and received 0.05 mg/kg buprenorphine (Bupaq, Richter Pharma AG, Vienna) subcutaneous at least 1 h before experiment started. Under isoflurane inhalation (Forane, AbbVie, Austria) anesthesia a catheter was placed in the jugular vein. Once the catheterization was completed, the isoflurane anesthesia was terminated and preserved with intravenous continuous drip application of S-ketamine (60 mg/kg/h, Ketanest-S, Pfizer, Austria) followed by an intramuscular application of xylazine (2.5 mg/kg, Rompun, Bayer, Austria). The intravenous application of the S-ketamine permits a well-controlled deep anesthesia (39). Animals were placed on a temperature-controlled surgical board (36–37°C) during operation. A scheme of the experimental procedure is deciped in **Supplementary Figure 1A**. A catheter for MAP, heart rate, volume therapy, and blood sampling was placed intraoperative in the femoral artery. After cannulation of the jugularis vein and femoral artery, hemodynamic parameters were allowed to stabilize for at least 10 min (baseline—**Supplementary Figure 1A**). MAP and heart rate were monitored using a PowerLab software system (ADInstruments Ltd., Oxford, UK)—data is displayed in **Supplementary Figures 1B,C**, respectively. Subsequently, a median laparotomy was performed to mimic tissue trauma (40). The incision remained protected with saline-soaked gauze and sutured after 20 min. The shock phase was initiated by blood withdrawal via the femoral artery catheter. The first 6 mL of blood were manually drained using syringes (baseline sampling). Then 10 mL of blood were withdrawn with a pump (1 ml/min) to reduce the blood pressure (30–35 mmHg) and maintained until reversible decompensation (end of shock—**Supplementary Figure 1A**). By definition, cardiovascular decompensation is the failure of the cardiovascular system to regulate blood pressure in the face of extreme intravascular volume loss (hypotension), which at this phase can only be prevented by constant fluid infusion. In our experiments, beginning of reversible decompensation was characterized by a rapid drop in MAP from 35 mmHg to around 30 mmHg despite immediate intra-arterial application of small amounts of Ringer's lactate. MAP, heart rate, and blood gas parameters were used to determine the beginning of decompensation, which was quantitatively confirmed by pH about 7.25–7.15, base excess between−11 and−14 and lactate >50 mg/dL. The volume of shed blood (including sampling volumes) withdrawn from THS animals was ∼45% of the total blood volume, which represents 7% of the rat body weight. A restrictive reperfusion (MAP at 40–50 mmHg) of 40 min was performed to simulate the transport from the local accident to the hospital and it was followed by a full reperfusion phase for 60 min. The infused volume of Ringer's lactate solution during reperfusion was 5 times the shed volume. Blood samples were withdrawn before shock (baseline), at the end of shock, and 24 h after THS for different analysis. Catheters were removed at the end of reperfusion (**Supplementary Figure 1A**) and wounds were closed. Subsequently, the animals under analgesia were transferred to their cages and observed until 24 h post-THS. The animals were euthanized under deep anesthesia by decapitation with a guillotine to avoid secondary effects since the animal's main organs were saved for future studies. Here, 14 male Sprague-Dawley rats were randomly distributed into two groups: the sham group ($n = 4$) and THS group ($n = 8$). Two animals (one from the sham group and other from THS group) died before the endpoint (24 h) and were therefore excluded from the analysis. One animal died during preparation (sham group) and the other died after THS. The sham group represents the group of animals subjected only to placebo surgery without the trauma procedure and hemorrhage. Only THS group received phosphate buffered saline with 0.67% of DMSO (3 ml).

ER Stress Induction

Tunicamycin (TUN), an inhibitor of protein N-glycosylation that impairing protein synthesis and triggers accumulation of unfolded proteins in the endoplasmic reticulum was selected to induce ER stress response in animals randomly assigned to tunicamycin group. 0.5 mg/kg of tunicamycin in phosphate

buffered saline with 0.67% of DMSO solution was applied intraperitoneal. Blood was collected after 24 h treatment for determination of circulating miRNAs. Tunicamycin group ($n = 3$).

Blood Gas Analysis

Blood gas parameters as lactate (Lac), base excess (ABEc), and bicarbonate (HCO_3^-) were analyzed in heparinized arterial blood samples with a blood gas analyzer ABL800 Flex System (Radiometer Medical A/S, Copenhagen, Denmark) at the end of shock.

Blood Cell Count

Total white blood cells (WBC), neutrophils (NEU), lymphocytes (LYM), monocytes (MONO) were measured 24 h after onset of shock on EDTA-anti-coagulated whole blood using a CELL-DYN 3700 analyzer (Abbott Park, Illinois, U.S.A.).

Pathological Changes in the Blood

The levels of lactate dehydrogenase (LDH), creatine kinase (CK), alanine aminotransferase (ALT), aspartate aminotransferase (AST), urea and creatinine were analyzed from fresh frozen plasma samples with automatic analyzer (Cobas c111; Roche Diagnostics, Vienna, Austria). Cardiac troponin I (cTnI) it was measured using an Ultra-Sensitive Rat Cardiac Troponin-I ELISA kit (Life Diagnostics, Inc., Cat. No. CTNI-2-US). To avoid unintended biasing of the results we performed blind analysis of the samples. Measurements were performed by an investigator unaware of the sample group allocation during the experiment and when assessed its outcome. Pathological changes in the blood (PCB) were analyzed by creating scorings for heart injury (cTnI, CK, LDH), liver injury (ALT and AST), kidney injury (urea and creatinine), cell response [WBC and neutrophil to lymphocyte ratio (NLR)], and tissue hypoxia (lactate and ABEc). Each score was calculated as a sum of the parameters and normalized to the mean value of the THS group and expressed in percent (%). The scores are displayed in **Table 1**.

RNA Extraction and RT-PCR

Ribonucleic acid (RNA) isolation was performed from 200 µl of rat plasma as described previously (41) using the miRNeasy Mini Kit (Qiagen, Germany) together with glycogen to enhance precipitation. The miRCURY RNA Spike-Ins (Qiagen, Germany) were added to the lysis buffer Qiazol prior to RNA isolation. Total RNA was eluted in 30 µl nuclease-free water and frozen at−80°C until further analysis. Reverse transcription was performed using the miRCURY RT Kit (Qiagen, Germany) with 2 µl total RNA input. RT was performed at 42°C for 60 min followed by heat inactivation at 95°C for 2 min. Quantitative polymerase chain reaction (qPCR) was performed on a Roche LightCycler LC480 II with 45 amplification cycles (95°C for 10 s, 60°C for 60 s) followed by melting curve analysis. Cq-Values were calculated using the 2nd derivative maximum method. Data normalization: Equal biofluid volumes were used throughout the analysis. Homogeneous efficiency of all steps in the workflow was confirmed using spike-in controls. RNA spike-in control was used for normalization to adjust for analytical noise using the equation: $Cq = Cq^{(UniSp4)} - Cq^{(miRNA)}$.

RT-qPCR Quality Control

Three types of Spike-In controls were used for monitoring the analytical variability of the workflow assess data quality (**Supplementary Figure 2**). First, a commercial (Qiagen, Germany) non-mammalian RNA spike-In (UniSp 4) was added to each sample prior to RNA extraction. RNA spike-Ins reflect the overall technical variance present in the raw data. Secondly, cel-miR-39, which is a microRNA that is found in C. elegans but not in human or other mammalian species was added to total RNA samples prior to reverse transcription. Cel-miR-39 reflects the variance introduced during reverse transcription and qPCR, and can indicate the presence of enzyme inhibitors. Third, UniSp3 was used, which is a mix of qPCR primers and template that is present on each qPCR plate and used to determine the technical variance of the qPCR reaction.

miRNAs Profiling and Analysis

We have selected and analyzed 91 miRNAs (**Supplementary Table 1**) associated either with organ damage or ER stress based on existing literature using miRBase database (http://www.mirbase.org/). For the Venn diagram we used Venny 2.1 (https://bioinfogp.cnb.csic.es/tools/venny/index.html). Principal component analysis (PCA) was carried out with the XLSTAT software (Microsoft).

Statistics

Statistical analysis was carried out with SPSS15 (Statistical Package for the Social Sciences, version 15.0) and the free software environment for statistical computing and graphics, "R." Kolmogorov–Smirnov test was used to test the distribution of the data. Column analysis was performed using Welch's *t*-test (type 3 *t* test in the EXEL) for Unequal Variances. Volcano plots and Spearman's correlation coefficients were performed R software system using the *EnhancedVolcano* and *corrplot* packages. Significant differences were considered at $p < 0.01$ for the miRNAs analysis, while the criteria for significant correlations was $p < 0.05$.

RESULTS

Tissue Hypoxia, Inflammation, and Organ Damage in THS

A total of 14 animals were used in the THS experiment, of which $n = 4$ rats were randomized to the sham group and $n = 8$ rats to THS group, 2 animals were excluded since they did not survive to the endpoint (24 h). Changes in MAP and heart rate of sham and THS animals are shown in **Supplementary Figures 1B,C**, respectively at baseline, end of shock and, end of reperfusion. For the analysis of PCB induced by THS compared to sham animals, we analyzed the scorings created for the liver, heart, and kidney cumulative damage (**Table 1**). Alterations related to cellular response and tissue hypoxia are also considered in **Table 1**. Neutrophils, which are among the first cells to reach the site of injury had fold change of 1.4 (THS = 46.83%

TABLE 1 | Pathological changes in the blood (PCB) analyzed in THS rat model.

Pathophysiological event	Pathological changes in the blood	THS ($n = 8$)	sham ($n = 4$)	Fold change	*p value*
Heart injury	Cardiac troponin I (ng/mL)	1.150	0.033	34.6	0.1327
	Creatine kinase (U/L)	37499	898	41.8	0.0661
	Lactate dehydrogenase (U/L)	6766	383	17.7	0.0160
	Scoring (cTnI + CK + LDH) **%**	**300**	**10.94**	**27.4**	**0.0063**
Liver injury	Alanine aminotransferase (U/L)	688	153	4.5	0.0082
	Aspartate aminotransferase (U/L)	3279	692	4.7	0.0006
	Scoring (ALT + AST) **%**	**200**	**43.25**	**4.6**	**0.0005**
Kidney injury	Urea (μmol/L)	99	42	2.3	0.0592
	Creatinine (μmol/L)	58.38	34.48	1.7	0.1512
	Scoring (urea + creatinine) **%**	**200**	**101.95**	**2.0**	**0.0859**
Cellular response	White blood cells (K/μl)	9.82	14.85	0.7	0.0273
	Neutrophils (K/μl)	4.36	3.05	1.4	0.0847
	Lymphocytes (K/μl)	5.25	11.11	0.5	0.0390
	Monocytes (K/μl)	0.08	0.21	0.4	0.0584
	Neutrophil to lymphocyte ratio (NLR)	1.07	0.32	3.3	0.0203
	Scoring (WBC + NLR) **%**	**200**	**79.17**	**2.5**	**0.0115**
Tissue hypoxia	Lactate (mg/dL)	34.63	4.50	7.7	<0.00001
	Base excess (mmol/L)	−10.20	−1.03	10.0	<0.00001
	Bicarbonate (mmol/L)	16.54	22.93	0.7	<0.00001
	Scoring (lactate + base excess) **%**	**200**	**23.05**	**8.7**	**<0.00001**

Clinical parameters of animals subjected to THS and sham animals (control group) were collected 24 h upon THS. Biochemical blood parameters as lactate, base excess, and bicarbonate (HCO_{3-}) were determined at the end of shock. The mean values of THS and sham group, fold changes, and p value are displayed. Scorings (bold values) are described in the methods section. Statistical analysis was performed using Welch's t-test.

and sham = 21.95%) 24 h after onset of shock. The overall inflammatory response scoring (WBC and NLR) was elevated by 2.5-fold ($p < 0.05$) in THS. The data showed a significant increase of lactate in THS animals after shock phase which is accompanied by significant changes in base excess and bicarbonate levels ($p < 0.0001$). In general, all parameters had a strong trend to increase but heart injury scoring was the most elevated by 27.4-fold in THS ($p < 0.01$). Liver and kidney injury were elevated by 4.6 and 2.0-fold, respectively.

miRNA Profile of THS Rats

Ninety one miRNAs associated to organ damage and ER stress were selected based on existing literature (**Supplementary Table 1**) and determined their relative expression in plasma samples of THS and sham (control) animals by RT-qPCR. Spike-in quality controls were used to monitor analytical variability and sample quality (**Supplementary Figure 2**). Overall, 40 out of 91 miRNAs were significantly elevated ($p < 0.01$) in the animals subjected to THS compared to the sham group, while none were decreased (**Figure 1**). The full list of the miRNAs induced by THS with a $p < 0.01$ is displayed in **Supplementary Figure 3**. The data showed that miR-638, miR-199a-5p, miR-151a-5p, miR-135b-5p, miR-663a, miR-215-5p, miR-30b-5p, miR-192-5p, miR-221-3p, and miR-346 are the 10 most significantly regulated miRNAs in THS plasma (**Figure 1**). Additionally, several miRNAs such as miR-122-5p ($\log_2$ fold change = 6.41), miR-211-5p ($\log_2$ fold change = 5.76), and miR-135a-5p ($\log_2$ fold change = 5.40) occurred in the blood in particularly high concentrations.

Correlations Between PCB and Circulating miRNAs in THS

Next, it was explored whether the changes in miRNAs in THS are coincident with PCB, which are used in clinical practice. 40 miRNAs induced by THS were selected for performing the correlation analysis with the PCB ($p < 0.01$). **Figure 2** displays all significant Spearman's correlations between miRNAs and PCB ($p < 0.05$). The coefficients (r) between PCB and circulating miRNAs are indicated in **Supplementary Figure 4.** In general, all the miRNAs induced by THS are directly correlated to each other (blue circles). The data did not show an organ-specific miRNA profile but most of the miRNAs were significantly correlated with liver injury (38 out of 40), followed by heart injury and hypoxia (26 out of 40), kidney injury (10 out of 40) and inflammation (4 out of 40) ($p < 0.05$). The data showed a strong correlation between liver injury scoring and miR−122–5p ($r = 0.91$, $p < 0.0001$). Furthermore, miR−135b−5p, miR-668-3p, and miR−146a−5p were found to be associated with all the 5 scorings (liver injury, heart injury, kidney injury, and inflammation, and tissue hypoxia). Additionally, miR−135b−5p, miR−668–3p, miR−146a−5p, and miR−214–3p are the only miRNAs correlated with activation of immune cells (WBC + NLR). Some PCBs are also strongly correlated with each other.

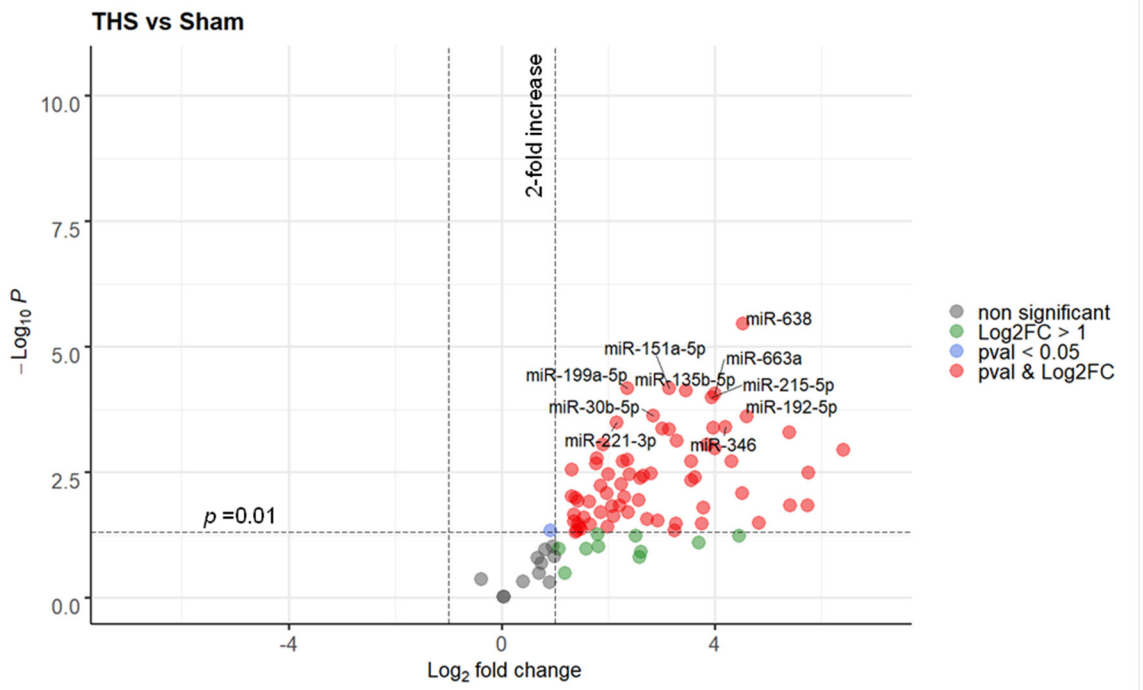

FIGURE 1 | Volcano plot depicting the Log_2-transformed fold change (LogFC, x-axis) of circulating miRNAs in THS compared to controls (sham) in relation to their *p* value (−Log10 (pval), y-axis). In total 90 miRNAs were included in the analysis. The 10 most significantly regulated miRNAs (lowest pval) by THS are labeled. Sham group ($n = 4$ animals); THS group ($n = 8$ animals).

For example, heart injury with inflammation ($r = 0.78$, $p < 0.01$), tissue hypoxia ($r = 0.78$, $p < 0.01$), and kidney injury correlates with tissue hypoxia ($r = 0.69$, $p < 0.05$). Base excess and bicarbonate (HCO_3^-), clinical parameters that reflect shock severity, are negatively correlated with all miRNAs (red circles). Base excess and bicarbonate are also inversely correlated with AST, LDH, CK, urea, creatinine, and lactate. Here, miR-638, miR−135b, miR−135a, miR-668, miR-204, miR−146a, miR−200a, miR−17, miR−30a, and miR−214 were found positively correlated with lactate ($r > 0.7$, $p < 0.05$), negatively with base excess ($r \leq 0.8$, $p < 0.05$) and bicarbonate ($r < -0.8$, $p < 0.05$).

miRNA Profile of Tunicamycin in Rats

In the next step, ER stress response was triggered in rats using a strong and well-known inducer of ER stress, tunicamycin. A total of 3 animals were used in this experiment, all animals were included in the analysis. No animal died due to treatment with tunicamycin. Similar to THS group (24 h), the levels of circulating miRNAs in animals treated with tunicamycin (24 h) were strong upregulated compared to sham group. Overall, 33 out of 91 miRNAs were significantly upregulated ($p < 0.01$), while again, none were decreased. A full list of the miRNAs expressed in response to tunicamycin with a $p < 0.01$ is displayed in **Supplementary Figure 5.** A detailed analysis showed that miR-455-3p, miR-199a-5p, miR-151a-5p, miR-210-3p, let-7g-5p, miR-31-5p, let-7i-5p, let-7f-5p, miR-146b-5p, and miR-486-5 were the 10 most upregulated miRNAs by tunicamycin in our experimental model (**Figure 3**).

A Common miRNA Signature in THS and Upon ER Stress Stimulation With Tunicamycin

Circulating miRNAs released in THS animals were compared to tunicamycin group in relation to sham group (control). The principal component analysis revealed that THS and tunicamycin treatment caused similar miRNA changes compared to sham group (**Figure 4A**). THS and tunicamycin showed a different miRNA profile as well, but more similar to each other than to sham since both groups overlap on PC1 (x-axis, explained 60% variability) but not on PC2 (y-axis, explained 13% variability). Next, a direct comparison of significantly upregulated miRNAs in THS and tunicamycin with a $p < 0.01$ was performed and displayed in **Figure 4B**. The Venn diagram showed that 25 miRNAs were exclusively induced by THS and 18 miRNAs were exclusively induced by tunicamycin treatment. This analysis also identified 15 common miRNAs induced by both, THS and ER stress: miR-199a-5p, miR-151a-5p, miR-221-3p, miR-21-5p, miR-122-5p, let-7g-5p, miR-199a-3p,

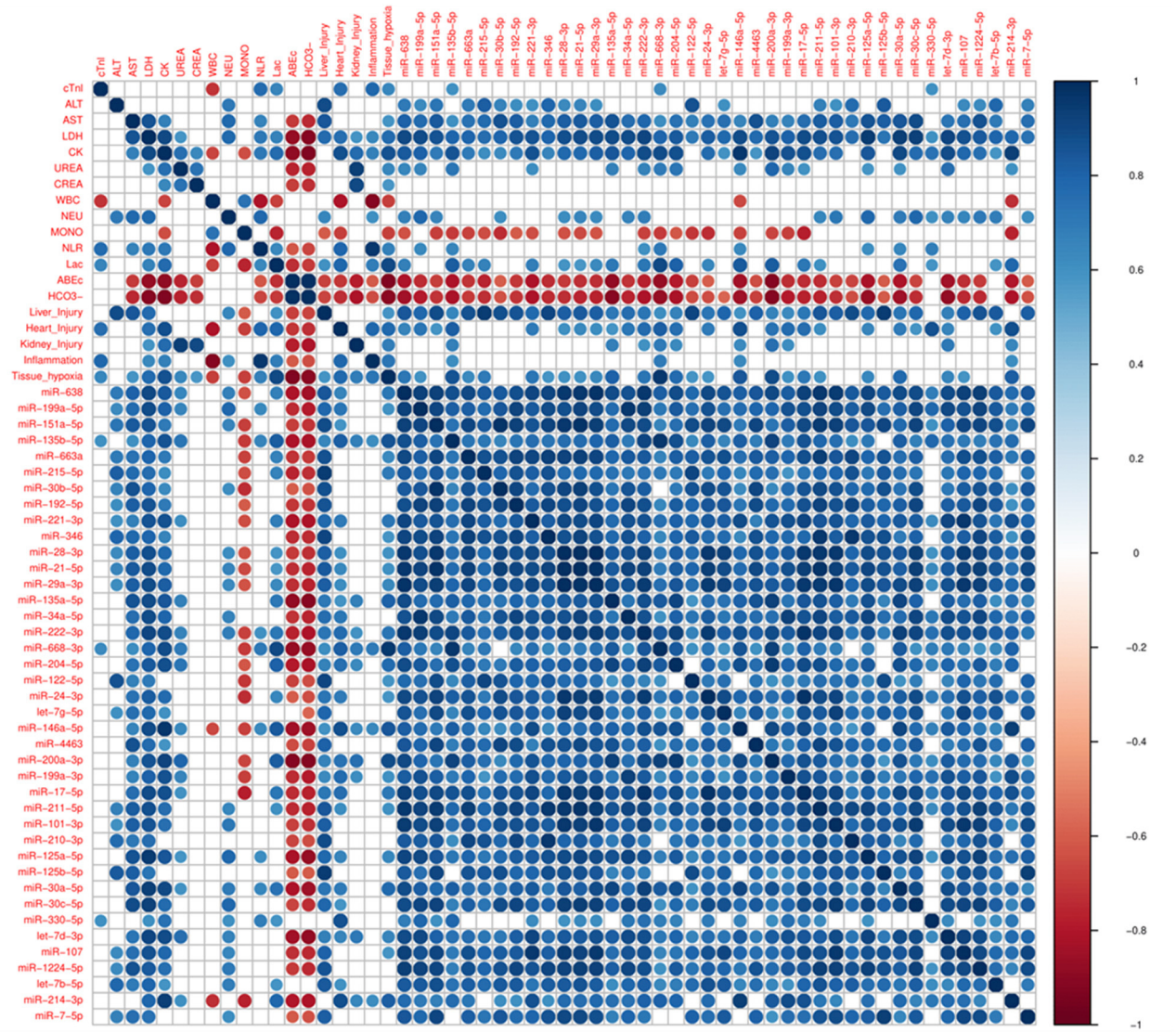

FIGURE 2 | Corrplot with Spearman's correlations between pathological changes in the blood (PCB) and circulating miRNAs induced by THS with $p < 0.01$ ($n = 40$ miRNAs). All significant ($p < 0.05$) correlations are indicated as circle. Positive correlations are displayed in blue and negative correlations in red color. Color intensity and the size of the circle are proportional to the correlation coefficients (r).

miR-17-5p, miR-101-3p, miR-210-3p, miR-125a-5p, miR-125b-5p, miR-107, let-7b-5p, and miR-7-5p. In other words, THS and tunicamycin had an overlap of 25.9% of miRNAs analyzed in our study.

DISCUSSION

MiRNA transcription has previously been reported to be altered in severe trauma patients (31, 42, 43). The role of ER stress following THS is not fully understood but since the ER is responsible for main liver functions as protein synthesis, lipid metabolism, etc., we assumed that ER stress can be a major reason for liver dysfunction contributing to multiple organ failure in THS. However, the relationship between circulating miRNAs, activation of ER stress, and organ damage is very poorly explored. Here, we show that circulating miRNAs upon THS can be used to decipher the role of ER stress in the development of single and/or multiple organ dysfunction. In this study, we determined the major parameters of oxygen deficit during the shock phase, subsequent markers of organ damage, and inflammatory response 24 h after shock. The experimental model simulated a typical situation of clinical trauma. Base excess and bicarbonate were significantly decreased during the shock phase reflecting tissue hypoxia. In line with related literature (44), activation of the innate inflammatory response was characterized by elevated levels of neutrophils and a drop in the absolute number of lymphocytes.

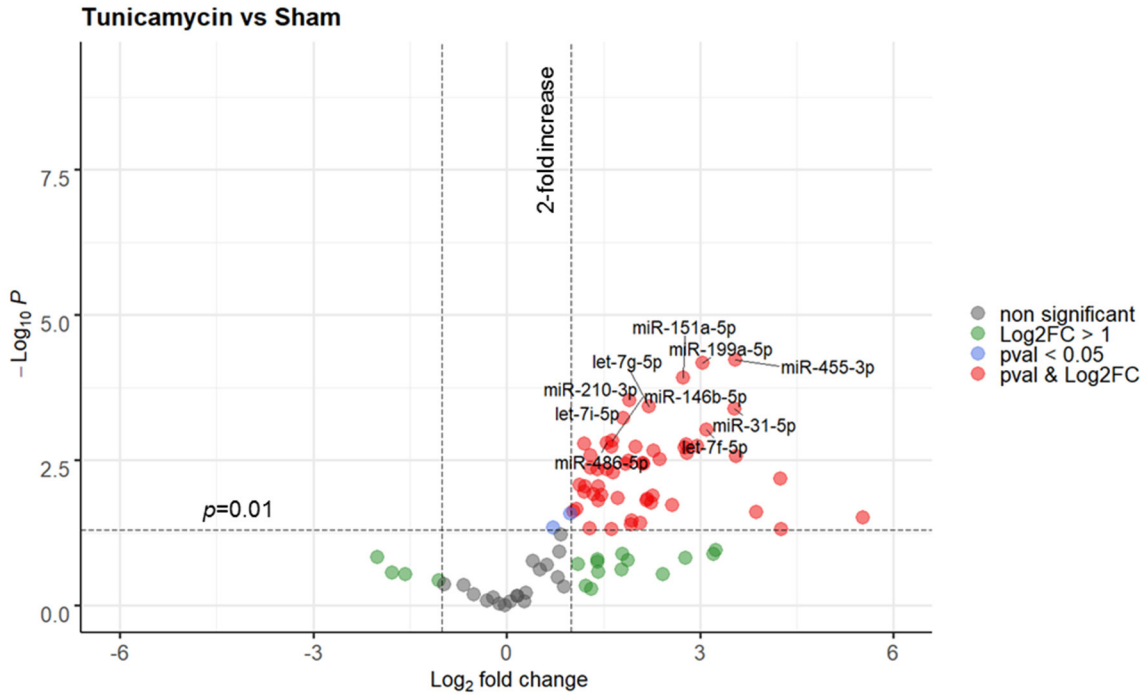

FIGURE 3 | Volcano plot depicting the Log_2-transformed fold change (LogFC, x-axis) of circulating miRNAs induced by tunicamycin compared to controls (sham) in relation to their *p* value [−Log10 (pval), y-axis]. The 10 most significantly regulated miRNAs (lowest pval) by tunicamycin are labeled. Sham group ($n = 4$ animals); Tunicamycin group ($n = 3$ animals).

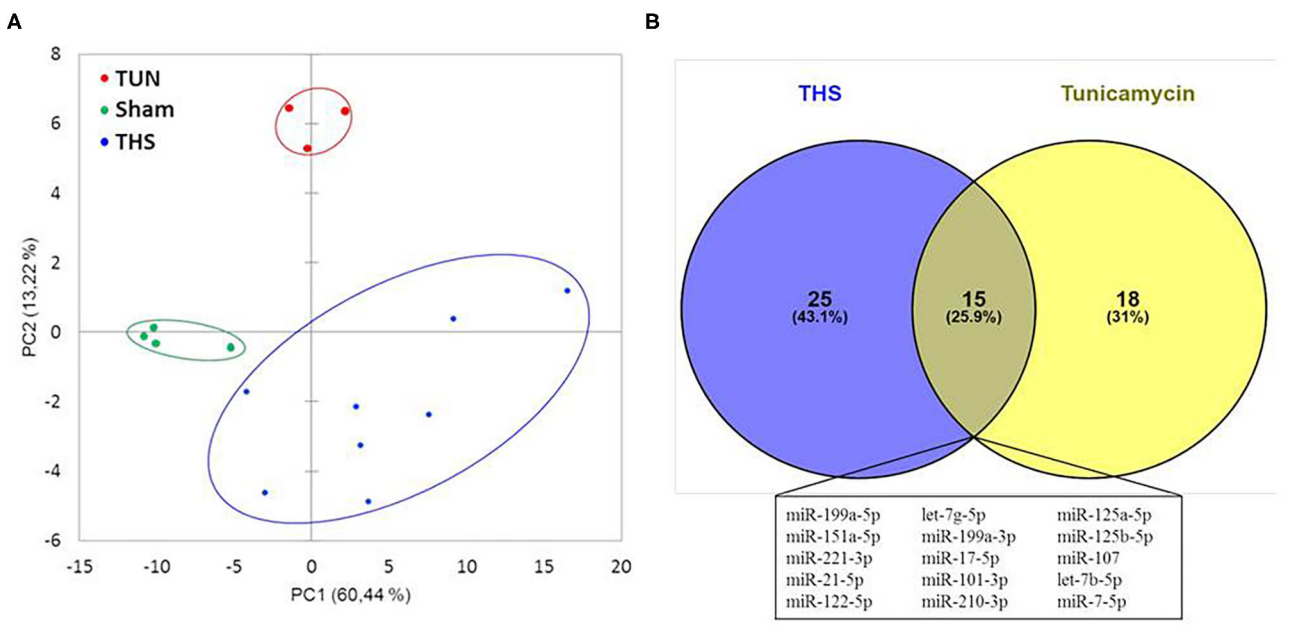

FIGURE 4 | (A) Principal component analysis of miRNAs related to organ injury and ER stress; THS group ($n = 8$); sham group ($n = 4$); tunicamycin (TUN) group ($n = 3$). **(B)** Venn diagram with miRNAs significantly regulated in THS and upon tunicamycin treatment ($p < 0.01$). Blue: 25 miRNAs involved exclusively in THS. Yellow: 18 miRNAs exclusively induced by tunicamycin. Central area: 15 common miRNAs expressed by THS and tunicamycin.

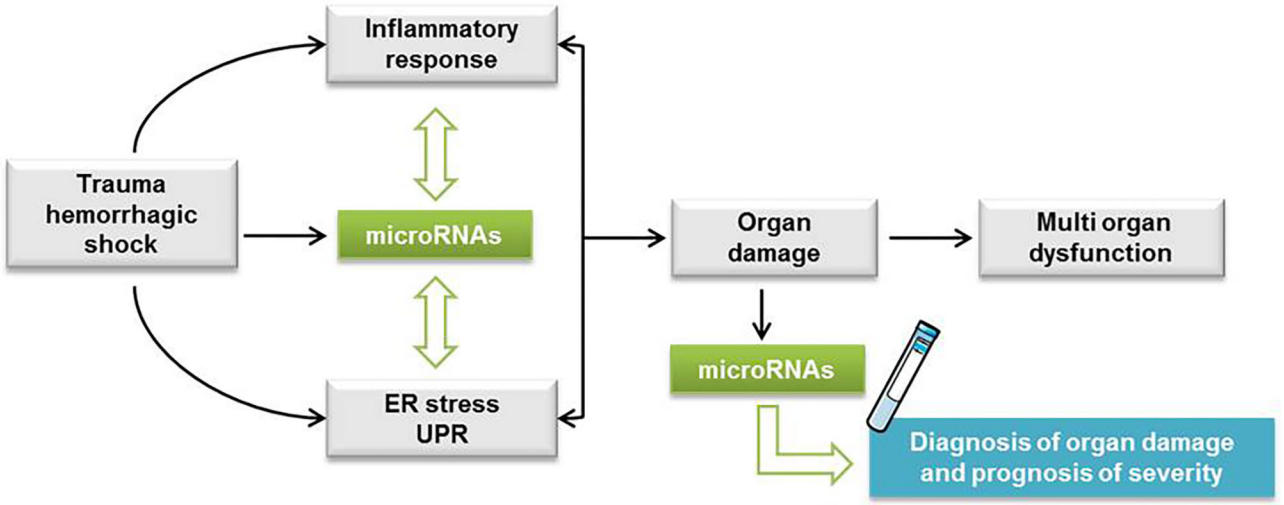

FIGURE 5 | Hypothetic scheme with the interplay between ER stress and miRNAs upon THS. Cellular perturbations resulting from trauma hemorrhagic shock (THS) activate inflammation and endoplasmic reticulum (ER) stress which triggers the unfolded protein response (UPR). At the same time, THS also induces the release of miRNAs in the plasma that fine-tune ER stress/UPR and inflammatory response. The feed-forward loop comprising the activation of inflammation and ER stress is implicated in the development of cell damage followed by single and multiple organ dysfunction.

In this model, we identified 40 miRNAs differently regulated upon THS (all upregulated). MiR-638 was the most significantly upregulated miRNA induced by THS in our study. Overexpression of miR-638 was found to attenuate the effects of hypoxia/reoxygenation in human cardiomyocytes (45). Previously, it was anticipated that in general miRNAs act as pro-adaptive molecules during ER stress and they can be positively and negatively regulated by the UPR (25). Indeed, we found that the most upregulated miRNAs by THS in our study are likely not only involved in organ damage as liver injury (miR-151a-5p), brain injury (miR-135b-5p), and cardiac injury (miR-199a-5p) but there are also miRNAs in this group which are reported to be involved in processes related to ER stress (miR-663a, miR-215-5p) and UPR activities such as cell survival (miR-346) (references are indicated in **Supplementary Table 1**). Considering the marked release of the miRNAs upon THS, we also assume that the miRNA profile obtained may not only reflect regulation of ER stress and organ injury but also possible cellular disruption followed by a passive release of miRNA into the bloodstream, which was previously observed during drug-induced organ damage (46, 47). Furthermore, the upregulation of miR-24-3p ($\log_2$ fold change = 1.79) observed here in the animals subjected to THS ($p < 0.001$) concurs with the overexpression of miR-24-3p reported in trauma patients associated with trauma-induced coagulopathy by preventing the production of coagulation Factor X (42). MiR-24 was also found significantly deregulated under UPR circumstances in H9c2 rat cardiomyoblasts (48).

Based on correlation analysis between miRNAs and PCB, we found that miRNAs are associated with injury of different organs, most importantly liver injury, since 38 out of 40 upregulated miRNAs were correlated to the liver injury score. In addition, we found a strong and direct correlation between liver injury and miR−122-5p ($r = 0.91$, $p < 0.0001$), which confirms previous observations by others (49, 50), and which can be explained not only by passive release but also by the augmentation of miR-122 in the liver. MiR-122 was also found to play a role in the hypoxia responses that regulate glucose and energy metabolism (51). In addition, it was recently reported that ER stress impacts on miR-122 promoter activity (52). We found miR-638, miR−135a-5p, miR−135b-5p, miR-668-3p, miR-204-5p, miR−146a-5p, miR−200a-3p, miR−17-5p, miR−30a-5p, and miR−214-3p strongly correlated with lactate, base excess, and bicarbonate. Base excess is reflected in bicarbonate consumption, which results in acidosis (53). In fact, miR-638, miR−135a, miR-668 were previously associated with hypoxic injury (references are indicated in **Supplementary Table 1**). Thus, our data suggest that these miRNAs could also be explored as markers of tissue hypoxia subsequently to THS. We observed that only a few miRNAs (miR−135b−5p, miR−668–3p, miR−146a−5p, and miR−214–3p) correlated with cellular response scoring (inflammatory response), out of which miR-146a-5p is considered an "inflammamiR" (54, 55). Additionally, in our study, we found several miRNAs strongly increased in the plasma in response to tunicamycin. Of note, tunicamycin may not fully mimic the ER stress response induced by THS, but it's known that the liver is one of the main organs affected by tunicamycin treatment (56). Additionally, since liver dysfunction is also a driver of multiple organ failure in THS, we consider that the choice of tunicamycin as an ER stress model in this study in comparison to the THS model is a suitable approach. And, indeed, miRNAs such as miR-17-5p and miR-125b, which we found to be significantly upregulated in THS and in tunicamycin groups,

are associated with ER stress and UPR. MiR-17 and miR-125b have a role in adaptive UPR signaling by regulating IRE1α (57). Notably, it was found that sustained activation of IRE1α reduced levels of miR-17, miR-34a, miR-96, and miR-125b which are miRNAs that usually inhibit caspase-2 (57). PCA analysis revealed that THS and tunicamycin treatment elicit similar changes in plasma miRNA levels compared to control animals. Indeed, we found a coincidence of 25.9% miRNAs in THS and upon ER stress stimulation. 15 miRNAs (miR-199a-5p, miR-151a-5p, miR-221-3p, miR-21-5p, miR-122-5p, let-7g-5p, miR-199a-3p, miR-17-5p, miR-101-3p, miR-210-3p, miR-125a-5p, miR-125b-5p, miR-107, let-7b-5p, and miR-7-5p) were significantly induced by both THS and tunicamycin. In this list, we highlight miR-122-5p, miR-17-5p, and miR-125b-5p which we discussed above.

We propose that our miRNA profile characterization in THS animals can provide a rationale for the development of bench-to-bedside strategies that target miRNAs. For example, miR-34a, which we found induced by THS ($p < 0.01$) and by tunicamycin ($p < 0.05$) was suppressed in a hemorrhagic shock pregnant rat model. The authors found that suppression of miR-34a alleviates organ damage possibly due to the attenuation of oxidative stress (58). Thus, suppression of specific miRNAs can be explored to treat organ damage caused by THS. In addition, since the miRNAs identified were associated with PCB, they can also be explored to improve the diagnostic toolbox for trauma patients. In fact, it was previously found that miR-106a was dysregulated in hemorrhagic shock patients and appeared to be more downregulated in patients who developed an infection (43). Thus, specific alterations on miRNA levels were suggested to serve as a marker for susceptibility to infection in trauma patients (43). Considering our data, we assumed the following mechanism with respect to the interplay between ER stress and miRNAs upon THS. Cellular perturbations resulting from THS activate inflammation and ER stress which triggers the UPR. At the same time, THS also induces the release of miRNAs in the plasma that fine-tune ER stress/UPR and inflammatory response (**Figure 5**). We recently described a feed-forward loop comprising the activation of inflammation and ER stress in the development of liver damage (59). This cycle can be either beneficial contributing to the restoration of tissue homeostasis or deleterious such as cell and organ dysfunction (59).

Summarized, we show that circulating miRNAs associated with ER stress are increased upon THS, suggesting a relationship between ER stress and the release of miRNAs in the blood. The comparison of the miRNA profiles induced by THS in the blood with specific organ damage markers suggested that miRNAs are predominantly released from the liver. Thus, our data strongly suggest that ER stress is an important pathologic event occurring during THS, but its pathophysiological impact is still unclear. Further studies are required to clarify the pathophysiological role of ER stress upon THS. In addition, as more than half of all hospital deaths associated with THS occur after the first 24 h (60), it is relevant to investigate miRNAs associated with ER stress expressed in the later course of organ failure after trauma. Overall, we consider that the miRNA profile characterized in this study provides a rationale to improve the diagnosis of organ damage and the prognosis of trauma patients (**Figure 5**).

DATA AVAILABILITY STATEMENT

The raw data supporting the conclusions of this article will be made available by the authors, without undue reservation.

ETHICS STATEMENT

The animal protocol was reviewed by the board of the city government of Vienna, Austria and approved for all experimental procedures (GZ: 593334/2016/13). All experiments were conducted in a manner that discomfort, pain, distress and suffering was avoided or minimized and in accordance with the Guide for the Care and Use of Laboratory Animals as defined by the National Institute of Health.

AUTHOR CONTRIBUTIONS

AL, SB, and AK conceived and designed the study. JJ and CK performed the traumatic hemorrhagic shock model in rats. AL and MJ assisted with the experimental performance. AL, AK, and MH contributed to figure creation. AL, MH, JG, and AK contributed to the interpretation and analysis of data. AL and AK drafted the manuscript. All authors read and approved the final version of the manuscript.

FUNDING

This project has received funding from the European Union's Horizon 2020 research and innovation programme under the Marie Skłodowska-Curie grant agreement No 675448.

SUPPLEMENTARY MATERIAL

The Supplementary Material for this article can be found online at: https://www.frontiersin.org/articles/10.3389/fmed.2020.568096/full#supplementary-material

REFERENCES

1. Cannon JW. Hemorrhagic shock. *N Engl J Med.* (2018) 378:371–9. doi: 10.1056/NEJMra1705649
2. Bougié A, Harrois A, Duranteau J. Resuscitative strategies in traumatic hemorrhagic shock. *Ann Intensive Care.* (2013) 3:1–9. doi: 10.1186/2110-5820-3-1
3. Gutierrez G, Reines HD, Wulf-Gutierrez ME. Clinical review: hemorrhagic shock. *Crit Care.* (2004) 8:373–81. doi: 10.1186/cc2851
4. Bahrami A, Jafarmadar M, Redl H, Bahrami S, Jiang JX. TNF-α release capacity is suppressed immediately after hemorrhage and resuscitation. *Chinese J Traumatol.* (2017) 20:207–11. doi: 10.1016/j.cjtee.2016.12.003
5. Johnson D, Mayers I. Multiple organ dysfunction syndrome: a narrative review. *Can J Anaesth.* (2001) 48:502–9. doi: 10.1007/s13398-014-0173-7.2

6. El-Menyar A. Multiple organ dysfunction syndrome (MODS): is it preventable or inevitable? *Int J Clin Med.* (2012) 03:722–30. doi: 10.4236/ijcm.2012.37A127
7. Sauaia A, Moore FA, Moore EE. Postinjury inflammation and organ dysfunction. *Crit Care Clin.* (2017) 33:167–91. doi: 10.1016/j.ccc.2016.08.006
8. Almanza A, Carlesso A, Chintha C, Creedican S, Doultsinos D, Leuzzi B, et al. Endoplasmic reticulum stress signalling - from basic mechanisms to clinical applications. *FEBS J.* (2019) 286:241–78. doi: 10.1111/febs.14608
9. Reverendo M, Mendes A, Argüello RJ, Gatti E, Pierre P. At the crossway of eR-stress and proinflammatory responses. *FEBS J.* (2019) 286:297–310. doi: 10.1111/febs.14391
10. Jian B, Hsieh C-H, Chen J, Choudhry M, Bland K, Chaudry I, et al. Activation of endoplasmic reticulum stress response following trauma-Hemorrhage. *Biochim Biophys Acta.* (2009) 1782:621–6. doi: 10.1002/ar.20849.3D
11. Duvigneau JC, Kozlov A V., Zifko C, Postl A, Hartl RT, Miller I, et al. Reperfusion does not induce oxidative stress but sustained endoplasmic reticulum stress in livers of rats subjected to traumatic-Hemorrhagic shock. *Shock.* (2010) 33:289–98. doi: 10.1097/SHK.0b013e3181aef322
12. Kozlov A V, Duvigneau JC, Hyatt TC, Raju R, Behling T, Hartl RT, et al. Effect of estrogen on mitochondrial function and intracellular stress markers in rat liver and kidney following trauma-hemorrhagic shock and prolonged hypotension. *Mol Med.* (2010) 16:254–61. doi: 10.2119/molmed.2009.00184
13. Hetz C, Chevet E, Oakes SA. Proteostasis control by the unfolded protein response. *Nat Cell Biol.* (2015) 17:829–38. doi: 10.1038/ncb3184
14. Vourc'h M, Roquilly A, Asehnoune K. Trauma-Induced damage-Associated molecular patterns-Mediated remote organ injury and immunosuppression in the acutely ill patient. *Front Immunol.* (2018) 9:1330. doi: 10.3389/fimmu.2018.01330
15. Jiang J, Bahrami S, Leichtfried G, Redl H, Öhlinger W, Schlag G. Kinetics of endotoxin and tumor necrosis factor appearance in portal and systemic circulation after hemorrhagic shock in rats. *Ann Surg.* (1995) 221:100–6. doi: 10.1097/00000658-199501000-00012
16. Andersohn A, Garcia MI, Fan Y, Thompson MC, Akimzhanov AM, Abdullahi A, et al. Aggregated and hyperstable damage-Associated molecular patterns are released during eR stress to modulate immune function. *Front Cell Dev Biol.* (2019) 7:198. doi: 10.3389/fcell.2019.00198
17. Collett GP, Redman CW, Sargent IL, Vatish M. Endoplasmic reticulum stress stimulates the release of extracellular vesicles carrying danger-associated molecular pattern (DAMP) molecules. *Oncotarget.* (2018) 9:6707–17. doi: 10.18632/oncotarget.24158
18. Samali A, FitzGerald U, Deegan S, Gupta S. Methods for monitoring endoplasmic reticulum stress and the unfolded protein response. *Int J Cell Biol.* (2010) 2010:1–11. doi: 10.1155/2010/830307
19. Schultz AM, Oroszlan S. Tunicamycin inhibits glycosylation of precursor polyprotein encoded by env gene of rauscher murine leukemia virus. *Biochem Biophys Res Commun.* (1979) 86:1206–13. doi: 10.1016/0006-291X(79)90245-6
20. Bartel DP. MicroRNAs: target recognition and regulatory functions. *Cell.* (2009) 136:215–33. doi: 10.1016/j.cell.2009.01.002
21. Krol J, Loedige I, Filipowicz W. The widespread regulation of microRNA biogenesis, function and decay. *Nat Rev Genet.* (2010) 11:597–610. doi: 10.1038/nrg2843
22. Byrd AE, Brewer JW. Micro(RNA)managing endoplasmic reticulum stress. *IUBMB Life.* (2013) 65:373–81. doi: 10.1002/iub.1151
23. Maurel M, Chevet E. Endoplasmic reticulum stress signaling: the microRNA connection. *Am J Physiol Cell Physiol.* (2013) 304:C1117–C26. doi: 10.1152/ajpcell.00061.2013
24. Malhi H. MicroRNAs in eR stress: divergent roles in cell fate decisions. *Curr Pathobiol Rep.* (2014) 2:117–22. doi: 10.1007/s40139-014-0046-y
25. Chitnis N, Pytel D, Diehl JA. UPR-inducible miRNAs contribute to stressful situations. *Trends Biochem Sci.* (2013) 38:447–52. doi: 10.1016/j.tibs.2013.06.012
26. De Guire V, Robitaille R, Tétreault N, Guérin R, Ménard C, Bambace N, et al. Circulating miRNAs as sensitive and specific biomarkers for the diagnosis and monitoring of human diseases: promises and challenges. *Clin Biochem.* (2013) 46:846–60. doi: 10.1016/j.clinbiochem.2013.03.015
27. Hackl M, Heilmeier U, Weilner S, Grillari J. Circulating microRNAs as novel biomarkers for bone diseases – complex signatures for multifactorial diseases? *Mol Cell Endocrinol.* (2016) 432:83–95. doi: 10.1016/j.mce.2015.10.015
28. Manna I, Iaccino E, Dattilo V, Barone S, Vecchio E, Mimmi S, et al. Exosome-associated miRNA profile as a prognostic tool for therapy response monitoring in multiple sclerosis patients. *FASEB J.* (2018) 32:4241–6. doi: 10.1096/fj.201701533R
29. Walter E, Dellago H, Grillari J, Dimai HP, Hackl M. Cost-utility analysis of fracture risk assessment using microRNAs compared with standard tools and no monitoring in the austrian female population. *Bone.* (2018) 108:44–54. doi: 10.1016/j.bone.2017.12.017
30. Ludwig N, Leidinger P, Becker K, Backes C, Fehlmann T, Pallasch C, et al. Distribution of miRNA expression across human tissues. *Nucleic Acids Res.* (2016) 44:3865–77. doi: 10.1093/nar/gkw116
31. Uhlich RM, Konie JA, Davis JW, Misfeldt ML, Nelson C, Calaluce R, et al. Novel microRNA correlations in the severely injured. *Surgery.* (2014) 156:834–41. doi: 10.1016/j.surg.2014.06.017
32. Prince JM, Levy RM, Yang R, Mollen KP, Fink MP, Vodovotz Y, et al. Toll-Like receptor-4 signaling mediates hepatic injury and systemic inflammation in hemorrhagic shock. *J Am Coll Surg.* (2006) 202:407–17. doi: 10.1016/j.jamcollsurg.2005.11.021
33. Tsai J-P, Lee C-J, Subeq Y-M, Lee R-P, Hsu B-G. Calcitriol decreases pro-inflammatory cytokines and protects against severe hemorrhagic shock induced-organ damage in rats. *Cytokine.* (2016) 83:262–8. doi: 10.1016/j.cyto.2016.05.008
34. Fan J, Li Y, Vodovotz Y, Billiar TR, Wilson MA. Hemorrhagic shock-activated neutrophils augment tLR4 signaling-induced tLR2 upregulation in alveolar macrophages: role in hemorrhage-primed lung inflammation. *Am J Physiol Lung Cell Mol Physiol.* (2006) 290:L738–L46. doi: 10.1152/ajplung.00280.2005
35. Meng ZH, Dyer K, Billiar TR, Tweardy DJ. Distinct effects of systemic infusion of g-CSF vs. *IL-6 on lung and liver inflammation and injury in hemorrhagic shock. Shock.* (2000) 14:41–8. doi: 10.1097/00024382-200014010-00008
36. Bell E. MicroRNAs and the immune response. *Nat Rev Immunol.* (2007) 7:419–. doi: 10.1038/nri2111
37. O'Neill LA, Sheedy FJ, McCoy CE. MicroRNAs: the fine-tuners of toll-like receptor signalling. *Nat Rev Immunol.* (2011) 11:163–75. doi: 10.1038/nri2957
38. Tahamtan A, Teymoori-Rad M, Nakstad B, Salimi V. Anti-Inflammatory microRNAs and their potential for inflammatory diseases treatment. *Front Immunol.* (2018) 9:1–14. doi: 10.3389/fimmu.2018.01377
39. Bahrami S, Benisch C, Zifko C, Jafarmadar M, Schöchl H, Redl H. Xylazine-/diazepam-ketamine and isoflurane differentially affect hemodynamics and organ injury under hemorrhagic/traumatic shock and resuscitation in rats. *Shock.* (2011) 35:573–8. doi: 10.1097/SHK.0b013e318212266b
40. Fülöp A, Turóczi Z, Garbaisz D, Harsányi L, Szijártó A. Experimental models of hemorrhagic shock: a Review. *Eur Surg Res.* (2013) 50:57–70. doi: 10.1159/000348808
41. Kocijan R, Weigl M, Skalicky S, Geiger E, Ferguson J, Leinfellner G, et al. MicroRNA levels in bone and blood change during bisphosphonate and teriparatide therapy in an animal model of postmenopausal osteoporosis. *Bone.* (2020) 131:115104. doi: 10.1016/j.bone.2019.115104
42. Chen L-J, Yang L, Cheng X, Xue Y-K, Chen L-B. Overexpression of miR-24 is involved in the formation of hypocoagulation state after severe trauma by inhibiting the synthesis of coagulation factor x. *Dis Markers.* (2017) 2017:1–7. doi: 10.1155/2017/3649693
43. Galbraith NJ, O'Brien SJ, Walker SP, Gardner SA, Polk HC, Barnes SL. Temporal expression of circulating miRNA after severe injury. *Surgery.* (2018) 164:665–72. doi: 10.1016/j.surg.2018.05.042
44. Heffernan DS, Monaghan SF, Thakkar RK, Machan JT, Cioffi WG, Ayala A. Failure to normalize lymphopenia following trauma is associated with increased mortality, independent of the leukocytosis pattern. *Crit Care.* (2012) 16:R12. doi: 10.1186/cc11157
45. Zhao P, Zhang BL, Liu K, Qin B, Li ZH. Overexpression of miR-638 attenuated the effects of hypoxia/reoxygenation treatment on cell viability, cell apoptosis and autophagy by targeting aTG5 in the human cardiomyocytes. *Eur Rev Med Pharmacol Sci.* (2018) 22:8462–71. doi: 10.26355/eurrev_201812_16546

46. Laterza OF, Lim L, Garrett-Engele PW, Vlasakova K, Muniappa N, Tanaka WK, et al. Plasma microRNAs as sensitive and specific biomarkers of tissue injury. *Clin Chem.* (2009) 55:1977–83. doi: 10.1373/clinchem.2009.131797
47. Bailey WJ, Glaab WE. Accessible miRNAs as novel toxicity biomarkers. *Int J Toxicol.* (2018) 37:116–20. doi: 10.1177/1091581817752405
48. Read DE, Gupta A, Ladilov Y, Samali A, Gupta S. miRNA signature of unfolded protein response in H9c2 rat cardiomyoblasts. *Cell Biosci.* (2014) 4:1–10. doi: 10.1186/2045-3701-4-56
49. Jopling C. Liver-specific microRNA-122: biogenesis and function. *RNA Biol.* (2012) 9:137–42. doi: 10.4161/rna.18827
50. Shifeng H, Danni W, Pu C, Ping Y, Ju C, Liping Z. Circulating liver-Specific miR-122 as a novel potential biomarker for diagnosis of cholestatic liver injury. *PLoS One.* (2013) 8:e73133. doi: 10.1371/journal.pone.0073133
51. Zeng Y, Lv Y, Tao L, Ma J, Zhang H, Xu H, et al. G6PC3, aLDOA and cS induction accompanies mir-122 down-regulation in the mechanical asphyxia and can serve as hypoxia biomarkers. *Oncotarget.* (2016) 7:74526–36. doi: 10.18632/oncotarget.12931
52. Aydin Y, Kurt R, Song K, Lin D, Osman H, Youngquist B, et al. Hepatic stress response in hCV infection promotes sTAT3-mediated inhibition of hNF4A-miR-122 feedback loop in liver fibrosis and cancer progression. *Cancers (Basel).* (2019) 11:407. doi: 10.3390/cancers11101407
53. Wagner PD. The physiological basis of pulmonary gas exchange: implications for clinical interpretation of arterial blood gases. *Eur Respir J.* (2015) 45:227–43. doi: 10.1183/09031936.00039214
54. Bhaumik D, Scott GK, Schokrpur S, Patil CK, Orjalo A V., Rodier F, et al. MicroRNAs miR-146a/b negatively modulate the senescence-associated inflammatory mediators iL-6 and iL-8. *Aging (Albany NY).* (2009) 1:402–11. doi: 10.18632/aging.100042
55. Russo A, Bartolini D, Mensà E, Torquato P, Albertini MC, Olivieri F, et al. Physical activity modulates the overexpression of the inflammatory miR-146a-5p in obese patients. *IUBMB Life.* (2018) 70:1012–22. doi: 10.1002/iub.1926
56. Foufelle F, Fromenty B. Role of endoplasmic reticulum stress in drug-induced toxicity. *Pharmacol Res Perspect.* (2016) 4:e00211. doi: 10.1002/prp2.211
57. Upton J-P, Wang L, Han D, Wang ES, Huskey NE, Lim L, et al. IRE1α cleaves select microRNAs during eR stress to derepress translation of proapoptotic caspase-2. *Science.* (2012) 338:818–22. doi: 10.1126/science.1226191
58. Qin LB, Li ZY, Li H, Fan XQ, Liu HG, Dong XM, et al. Inhibitive effects of microRNA-34a on protecting against ischemia-reperfusion injury of vital organs in hemorrhagic shock pregnant mice. *Eur Rev Med Pharmacol Sci.* (2018) 22:1812–8. doi: 10.26355/eurrev_201803_14600
59. Duvigneau JC, Luís A, Gorman AM, Samali A, Kaltenecker D, Moriggl R, et al. Crosstalk between inflammatory mediators and endoplasmic reticulum stress in liver diseases. *Cytokine.* (2019) 124:154577. doi: 10.1016/j.cyto.2018.10.018
60. Brohi K, Gruen RL, Holcomb JB. Why are bleeding trauma patients still dying? *Intensive Care Med.* (2019) 45:709–11. doi: 10.1007/s00134-019-05560-x

Conflict of Interest: MH is employed by the company TAmiRNA GmbH, Vienna, Austria, and JG is a co-founder and shareholder of TAmiRNA.

The remaining authors declare that the research was conducted in the absence of any commercial or financial relationships that could be construed as a potential conflict of interest.

frontiers in Medicine

ORIGINAL RESEARCH
published: 02 October 2020
doi: 10.3389/fmed.2020.562904

Ethyl Pyruvate Reduces Systemic Leukocyte Activation via Caspase-1 and NF-κB After Blunt Chest Trauma and Haemorrhagic Shock

*Scott Dieteren[1,2], Niklas Franz[2], Kernt Köhler[3], Aleksander Nowak[1], Sabrina Ehnert[4], Alexey Surov[5], Marcus Krüger[6], Ingo Marzi[2], Nils Wagner[2] and Borna Relja[1]**

[1] Experimental Radiology, Department of Radiology and Nuclear Medicine, Otto von Guericke University, Magdeburg, Germany, [2] Department of Trauma, Hand and Reconstructive Surgery, University Hospital of the Goethe University Frankfurt, Frankfurt, Germany, [3] Institute of Veterinary Pathology, Justus Liebig University Giessen, Giessen, Germany, [4] Department of Trauma and Reconstructive Surgery, BG Trauma Center Tuebingen, Siegfried Weller Research Institute, Eberhard Karls University Tuebingen, Tübingen, Germany, [5] Department of Radiology and Nuclear Medicine, Otto von Guericke University, Magdeburg, Germany, [6] Department of Microgravity and Translational Regenerative Medicine, Clinic for Plastic, Aesthetic and Hand Surgery, Otto von Guericke University, Magdeburg, Germany

OPEN ACCESS

Edited by:
Mihály Boros,
University of Szeged, Hungary

Reviewed by:
Andrey V. Kozlov,
Institute for Experimental and Clinical Traumatology (LBG), Austria
Petra Hartmann,
University of Szeged, Hungary

***Correspondence:**
Borna Relja
info@bornarelja.com

Specialty section:
This article was submitted to Intensive Care Medicine and Anesthesiology, a section of the journal Frontiers in Medicine

Received: *16 May 2020*
Accepted: *28 August 2020*
Published: *02 October 2020*

Citation:
Dieteren S, Franz N, Köhler K, Nowak A, Ehnert S, Surov A, Krüger M, Marzi I, Wagner N and Relja B (2020) Ethyl Pyruvate Reduces Systemic Leukocyte Activation via Caspase-1 and NF-κB After Blunt Chest Trauma and Haemorrhagic Shock. Front. Med. 7:562904. doi: 10.3389/fmed.2020.562904

Background: Blunt chest (thoracic) trauma (TxT) and haemorrhagic shock with subsequent resuscitation (H/R) induce strong systemic and local inflammatory response, which is closely associated with apoptotic cell loss and subsequently impaired organ function. The underlying mechanisms are not completely understood, therefore, the treatment of patients suffering from TxT+H/R is challenging. In our recent studies, we have demonstrated local anti-inflammatory effects of ethyl pyruvate (EtP) in lung and liver after TxT+H/R. Here, the therapeutic potential of a reperfusion regime with EtP on the early post-traumatic systemic inflammatory response and apoptotic changes after TxT followed by H/R were investigated.

Methods: Female Lewis rats underwent TxT followed by haemorrhagic shock (60 min). Resuscitation was performed with own blood transfusion and either lactated Ringers solution (LR) or LR supplemented with EtP (50 mg/kg). Sham group underwent the surgical procedures. After 2 h blood as well as lung and liver tissues were obtained for analyses. Systemic activation of neutrophils (expression of CD11b and CD62L), leukocyte phagocytosis, apoptosis (caspase-3/7 activation), pyroptosis (caspase-1 activation) and NF-κB p65 activity were assessed. $p < 0.05$ was considered significant.

Results: TxT+H/R-induced systemic activation of neutrophils (increased CD11b and reduced CD62L expression) was significantly reduced by EtP. Trauma-induced delayed neutrophil apoptosis was further reduced by EtP reperfusion but remained unaltered in monocytes. Reperfusion with EtP significantly increased the phagocytizing capacity of granulocytes. Trauma-induced inflammasome activation, which was observed in monocytes and not in neutrophils, was significantly reduced by EtP in both cell entities. NF-κB p65 activation, which was increased in neutrophils and monocytes was significantly decreased in monocytes.

Conclusion: TxT+H/R-induced systemic activation of both neutrophils and monocytes concomitant with increased systemic inflammation was reduced by a reperfusion with EtP and was associated with a down-regulation of NF-κB p65 activation.

Keywords: ethyl pyruvate, leukocytes, inflammation, NF-κB, trauma

INTRODUCTION

Trauma is the sixth leading cause of death and the leading cause of mortality in individuals under 35 years of age (1). Notably patients with blunt chest trauma, severe traumatic brain injuries (56.6%) and/or bleeding (18.5%) are at high risk for mortality; of which the last is responsible for 80% of all deaths that occur within the first hour (1). Patients who initially survive their injuries suffer from a dysfunctional post-traumatic inflammatory response with excessive systemic and local leukocyte activation which leads to tissues damage, acute lung and liver injury, multiple organ failure (MOF) and delayed mortality (2–4). MOF following haemorrhagic shock and resuscitation extends the intensive care and still remains one of the most significant contributors to late post-injury mortality (5).

Due to post-injury hypoperfusion with concomitant microcirculatory disturbances, endothelial damage, and tissue injury induce an extensive release of Pathogen-associated molecular patterns (PAMP) and/or Damage-associated molecular patterns (DAMP) (4, 6). Those stimulate, activate and recruit effector cells of the innate immune system e.g., granulocytes and monocytes to the sites of injury, which exert their defense strategies i.e. production, activation and/or release of proinflammatory mediators, proteases (neutrophil elastase), or reactive oxygen species (ROS) (3, 4, 6). During the post-traumatic priming of those cells, their phenotypic and functional shifts and changes occur, including the activation of adhesion molecules and diminished apoptosis (7). Trauma-associated activation of circulating granulocytes with a significant increase in CD11b expression (8, 9), which is promoting the adhesion of activated neutrophils to inflamed endothelia, and a decrease in CD62L expression, which plays an important role in tethering and rolling along postcapillary venules (10) has been shown. The increased pulmonary infiltration with activated polymorphonuclear leukocytes (PMNL) initiates the early state of post-traumatic acute respiratory distress syndrome (11, 12). Concomitant trauma is associated with delayed apoptosis of systemic neutrophils, which is mediated by Caspase-3/7, thus lowered apoptosis rates extending their live span (8, 13, 14). Maianski et al. demonstrated that apoptosis in neutrophils is linked to caspase-3 activation (15). Furthermore, the decreased apoptosis of circulating neutrophils persisted until 9 days after injury in traumatized patients (14). On the other hand, increasing neutrophil apoptosis early after trauma-haemorrhagic shock as well as inhibiting caspase-3 dependent apoptosis after shock resulted in tissue protective effects and protection from infection and organ failure (16, 17). Thus, this alteration suggests a prolonged presence of PMNL in tissues which may exaggerate the local post-traumatic proinflammatory response and cause tissue damage (13, 18). Conflictive data are provided regarding systemic activity of monocytes, which on the one hand is diminished by reduced inflammasome activation with caspase-1 as its key player in trauma patients (19, 20), and on the other hand an increase due to trauma and shock-induced pyroptosis in circulating monocytes (21, 22). Inflammasome activation and subsequent proinflammatory cell death so-called pyroptosis involve the activation of NF-κB, which is a central contributor in the production of proinflammatory cytokines, leukocyte recruitment, and cell survival (18, 23, 24). Oxidative burst in trauma-primed neutrophils correlate with elevated NF-κB p65 phosphorylation mediating the inflammatory response and tissue damage as well (24).

Ethyl pyruvate (EtP) is a stable ester formed from ethanol linked to pyruvate, which has demonstrated anti-inflammatory potential with tissue protective effects in several *in vivo* models of acute inflammation (25–27). Ethyl pyruvate ameliorated the inflammatory and apoptotic effects of cytokine- as well as trauma-induced inflammation in lung tissue and lung cells *in vivo* and *in vitro* (28–32). Its anti-inflammatory influence was associated with induced activation of the inflammasome, thus reduced caspase-1 activity and lower levels of interleukin (IL)-1β in endotoxin-primed macrophages (33). In ischemia models, a resuscitation with EtP reduced the local proinflammatory tumor necrosis factor (TNF) expression in liver, and improved survival by reducing mucosal hyperpermeability (34–36). In our recent studies, we have demonstrated tissue-protective effects of EtP with diminished levels of proinflammatory cytokines and reduced NF-κB p65 phosphorylation in lung and liver as well as reduced neutrophilic infiltration into those organs (32, 37). Thus, we studied the influence of a reperfusion regime with EtP on systemic inflammatory and apoptotic changes in leukocytes in our clinically relevant double-hit model of hemorrhage and blunt chest trauma.

Abbreviations: APC, allophycocyanin; CD, cluster of differentiation; DAMP, damage-associated molecular patterns; EtP, ethyl pyruvate; FACS, fluorescence-activated cell sorter; fig., figure; g, earth's gravitational acceleration; $Gran^+$, RP-1 positive granulocytes; h, hour; H&E, hematoxylin-eosin; Hg, mercury; H/R, haemorrhagic shock with subsequent resuscitation; HS, haemorrhagic shock; IL, interleukin; kg, kilogram; LR, lactated Ringers solution; MABP, mean arterial blood pressure; MFU, mean fluorescence units; mg, milligram; min, minute; ml, milliliter; mm, millimeter; MOF, multiple organ failure; NF-κB, nuclear factor kappa-light-chain-enhancer of activated B-cells; *p*, *p*-value; PAMP, pathogen-associated molecular patterns; PBS, phosphate-buffered saline; PMNL, polymorphonuclear leukocytes; ROS, reactive oxygen species; RT, room temperature; sem, standard error of the mean; TLR, Toll-like receptor; TNF, tumor necrosis factor; TxT, blunt thoracic chest trauma; U, unit; °C, Celsius; %, percent.

MATERIALS AND METHODS

Animals and Experimental Model

This study was approved by the veterinary department of the regional council in Darmstadt, Germany (Hessen, Germany; "Regierungspraesidium Darmstadt, Veterinaerswesen," Hessen, Germany; Nr. of the ethical approval: FK/1028) and assigned in accordance with the ARRIVE guidelines (38). Only members with the certificate of the Federation of European Laboratory Animal Science Association treated and handed the animals. In the experiments, female LEWIS rats (190–240 g, Janvier Labs, France) were anesthetized with isoflurane (1.2–3.0%), buprenorphine (0.05 mg/kg body weight), and local anesthesia (0.25% Carbostesin) were applied. In detail, during anesthesia initiation (mask anesthesia), a 3.0% isoflurane oxygen mixture was used. The vessels were cannulated with a 1.2–2.5% isoflurane oxygen mixture depending on individual responses to pain stimulation. Trauma was performed with a concentration of 2% isoflurane following a short stabilization period and in the reperfusion period. At the end of experimentation, the isoflurane concentration was reduced in a step-by-step manner. The animals breathed spontaneously and were not intubated. The abdomen, chest, right inguinal and the neck of the animals were shaved and marked for surgical preparation. The right femoral artery was cannulated with polyethylene tubing for continuous blood pressure measurement. For the bilateral lung contusion the animals placed and a standardized air blast wave was directed to the thorax (TxT) of the animals as described before (39). After a short stabilization phase, the left jugular vein and the right carotid artery were cannulated. Then haemorrhagic shock (HS) by withdrawing stepwise blood via the carotid artery until a mean arterial blood pressure (MABP) of 35 ± 3 mm Hg was initiated. Over a period of 60 min the MABP was monitored by a blood pressure analyzer (Siemens AG), and if necessary was kept constant by further withdrawal or recirculation of withdrawn blood (40, 41). At the end of the haemorrhagic shock, reperfusion (H/R) was carried out via the jugular vein. Resuscitation was either performed by reperfusion with 60% of the shed blood plus 50% Ringer's lactated solution (LR) or 60% blood plus 50% LR supplemented with EtP (Sigma Aldrich, 50 mg/kg body weight). After an observation and stabilization phase of 30 min the catheters were removed, the vessels were occluded and the wounds closed. A continuous temperature monitoring in the colon maintaining 37°C was carried out. The animals always had free access to food and water. Two hours after the end of experiments sampling was performed. Briefly, the sacrifice was performed by withdrawing blood *via* the aorta using the same isoflurane oxygen concentration as during the preparation period and flushing the organs with LR.

Group Allocation

Thirty animals were randomly assigned to sham, TxT+H/R_LR and TxT+H/R_EtP groups. The sham groups underwent all the surgical procedures without inducing TxT+H/R. The trauma groups were resuscitated either with LR solution or LR solution supplemented with EtP.

Measurement of Antigen Expression by Flow Cytometry

Blood samples were collected from the aorta in pyrogen-free heparinized tubes for cytometric flow analyses. Blood samples (50 µl) were transferred into polystyrene fluorescence-activated cell sorter (FACS) tubes (BD Pharmingen™) and incubated with mouse anti-rat Granulocytes (RP-1, gran$^+$) (Bio Legend, conjugated to Mix-n-Stain CF405 Antibody Labeling Kit from Sigma-Aldrich), anti-rat CD62L allophycocyanin (APC) (Bio Legend), and mouse anti-rat CD11b fluorescein isothiocyanate (BD Pharmingen™) antibodies. For the settings, control stainings with the corresponding isotype antibodies were applied. After 30 min at room temperature (RT) one ml of the FACS Lysing Solution (BD Pharmingen™) was added for additional 10 min (RT). Then samples were centrifuged at 400 g for 7 min and washed twice with two ml FACS buffer. After removal of the supernatants, cells were diluted in 400 µl FACS buffer and subjected to flow cytometric analyses. Either granulocytes or monocytes were defined by gating the corresponding forward and side scatter scan. The granulocyte population was additionally gated by the RP-1 positive cells in the corresponding forward and sideward scatter scan (**Figures 1A,B**). From each sample a minimum of 30,000 cells was measured. The percentage of positive cells and the MFU were determined.

Phagocytosis of Staphylococcus Aureus Bioparticles

A single vial of lyophilized pHrodo *Staphylococcus* (*S.*) *aureus* Red BioParticles Conjugate (Life Technologies, Paisley, UK) was resuspended as suggested by the provider, and the suspension was added to 100 µl of whole blood and treated according to the manufacturer's instructions for 1 h at 37°C and 5% CO_2. A negative control without BioParticles was included. Then, red blood cells were removed using FACS Lysing Solution diluted with distilled water (1:10, Biosciences, Heidelberg, Germany) for 10 min. Two ml phosphate-buffered saline (PBS) were added and the cells were centrifuged at 400 g for 7 min at room temperature. Thereafter, the cells were washed with 3 ml FACS buffer (PBS w/o Ca_2^+/Mg^{2+} supplemented with 0.5% bovine serum albumin). After the centrifugation, the supernatants were removed and the cells were diluted in 400 µl FACS buffer. The phagocytizing activity of granulocytes and monocytes, respectively, was quantified as a percentage of phagocytizing cells as well as their capacity by determining the mean fluorescence units (MFU) using a BD FACS Canto 2™ and FACS DIVA™ software (BD). Either granulocytes or monocytes were defined by gating the corresponding forward and side scatter scan. From each sample a minimum of 30,000 cells was measured.

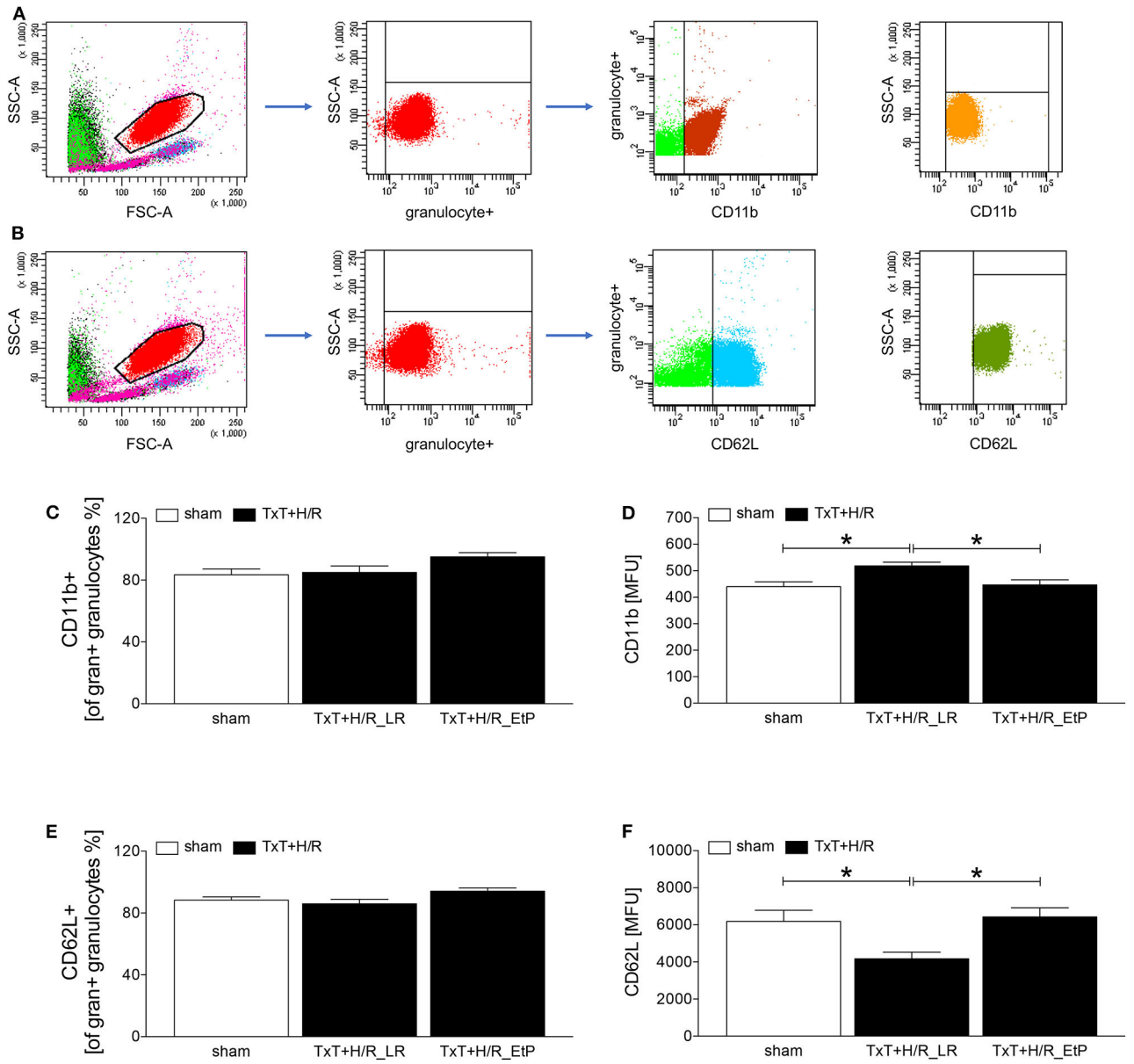

FIGURE 1 | Flow cytometric analysis of cellular adhesion molecule CD11b and CD62L on circulating neutrophils after blunt thoracic trauma (TxT) followed by haemorrhagic shock and resuscitation (H/R). Two hours after resuscitation flow cytometric analysis of CD11b or CD62L expression on circulating granulocytes **(A-F)** was performed. Sham operated animals underwent all surgical procedures without induction of TxT and H/R. TxT+H/R_LR animals received lactated Ringers solution (LR) and TxT+H/R_EtP animals were resuscitated with LR supplemented with ethyl pyruvate (EtP). **(A)** Gating strategy for CD11b positive granulocyte. **(B)** Gating strategy for CD62L positive granulocytes. **(C)** Percentage of $CD11b^+$ cells out of all $gran^+$ granulocytes. **(D)** Mean fluorescence units (MFU) of $CD11b^+$ on $gran^+$ granulocytes. **(E)** Percentage of $CD62L^+$ cells out of all $gran^+$ granulocytes. **(F)** MFU of $CD62L^+$ on $gran^+$ granulocytes. Data are given as mean ± standard error of the mean, $^*p < 0.05$ vs. indicated, $n = 10$.

Caspase-3/7 and Caspase-1 Activation Assay

Active caspases were quantified by using a FAM-DEVD-FLICA caspase-3/7 kit and FAM-YVAD-FMK 660 caspase-1 detection kit (ImmunoChemistry Technologies) according to the manufacturer's guidelines. MFU of the cells were quantified by flow cytometry (using unstained cells to set the gate) by BD FACS Canto 2™ and FACS DIVA™ software. Each cell population was defined by gating the corresponding forward and side scatter scan.

Measurement of NF-κB p65 (Phospho) Expression by Flow Cytometry

Blood samples (50 μl) were transferred into polystyrene FACS tubes (BD Pharmingen™) and incubated with mouse anti-rat Granulocytes (RP-1) (Bio Legend, conjugated to Mix-n-Stain CF405 Antibody Labeling Kit from Sigma-Aldrich), and mouse anti-rat CD68 Alexa Fluor 700 (Abd Serotec) antibodies. After 30 min at RT the samples were washed with 4 ml FACS buffer. Then, supernatants were removed and the samples were incubated with 100 μl Fix & Perm Solution A (FIX&PERM Kit, An Der Grub) for 15 min at RT. After another washing procedure with PBS, the supernatants were removed and samples were incubated with 100 μl Fix & Perm Solution B, and anti NF-κB p65 (Abcam, conjugated with APC/Cy7 Conjugation Kit from Abcam) anti phospho NF-κB p65/Ser536 (Abcam, conjugated with Mix-n-Stain CF488A Antibody Labeling Kit from Sigma-Aldrich) antibodies for 30 min at RT. Subsequently, 2 ml of FACS lysing solution (FACS Lysing Solution, BD Pharmingen™) were added for additional 10 min and the samples were centrifuged at 400 g for 5 min. Another washing procedure with 4 ml FACS buffer followed. After removal of the supernatants, cells were diluted in 400 μl FACS buffer and subjected to flow cytometric analyses and gated as described above.

Lung and Liver Preparation

After collecting blood samples flushing with 20 ml LR followed. *Via* the portal vein 10% buffered formalin solution was infused as it was done into the lung lobe itself. Then, the samples were embedded in paraffin and subsequently sectioned and stained with hematoxylin-eosin (H&E). The histological examination of the tissue morphology in both organs was performed by an independent pathologist who allocated the H&E-stained sections to the different experimental groups in a blinded manner as described before (32, 37).

Statistical Analysis

Normality distribution was assessed by Kolmogorov-Smirnov test with Dallal-Wilkinson-Lilliefor *P*-value. Non-parametric Kruskal-Wallis test was applied to study the differences between the groups. For *post-hoc* corrections Dunn's multiple comparison test was applied. Data are given as mean ± standard error of the mean (sem). A p-value below 0.05 was considered statistically significant. All statistical analyses were performed using GraphPad Prism 6 (Graphpad Software, Inc., San Diego, CA).

RESULTS

Granulocyte Activity After Blunt Thoracic Trauma Followed by Hemorrhage and Resuscitation

Two hours after resuscitation CD11 and CD62L expression levels on granulocytes were assessed to evaluate the impact of EtP on neutrophil activation after TxT+H/R (**Figures 1A–F**). The proportion of CD11b positive of all granulocyte$^+$ gated granulocytes was not significantly changed between the groups, however, a trend to an increase was observed in the TxT+H/R_EtP group (**Figure 1C**). CD11b expression on granulocytes was significantly increased in TxT+H/R_LR group as compared to the sham group (518.10 ± 14.36 vs. 440.00 ± 318.19 MFU, respectively, $p < 0.05$, **Figure 1D**). Resuscitation with EtP diminished CD11b expression significantly in relation to the TxT+H/R_LR group (446.40 ± 19.19 vs. 518.10 ± 14.36 MFU, respectively, $p < 0.05$, **Figure 1D**). CD11b expression levels in the EtP group were comparable to those in the sham group ($p < 0.05$, **Figure 1D**).

Similar to the CD11b data, the proportion of CD62L positive of all granulocyte$^+$ gated granulocytes exerted a trend to an increase in the TxT+H/R_EtP group, however, this was not significant (**Figure 1E**). CD62L expression significantly decreased in TxT+H/R_LR group compared to the sham group (4174.00 ± 355.80 vs. 6186.00 ± 599.70 MFU, respectively, $p < 0.05$, **Figure 1F**). Resuscitation with EtP significantly increased the CD62L expression on granulocytes compared to the TxT+H/R_LR group (6427.00 ± 497.60 vs. 4174.00 ± 355.80 MFU, respectively, $p < 0.05$, **Figure 1F**). The CD62L expression levels in the EtP group were comparable to the sham group.

Systemic Leukocyte Phagocytosis After Blunt Thoracic Trauma Followed by Hemorrhage and Resuscitation

The proportion of phagocytizing granulocytes did not show significant changes (**Figure 2A**). However, the phagocytizing capacity was significantly reduced in the TxT+H/R_LR vs. TxT+H/R_EtP group (3169.00 ± 156.10 vs. 3864.00 ± 175.00 MFU, $p < 0.05$, **Figure 2B**). Comparing the proportion of phagocytizing monocytes, there were no significant changes between the groups, however, some trends were observed (**Figures 2C,D**).

Systemic Leukocyte Apoptosis After Blunt Thoracic Trauma Followed by Hemorrhage and Resuscitation

Monocyte and granulocyte apoptosis were assessed by measuring the level of activated caspase-3/7 2 h after resuscitation (**Figures 3A,B**). In granulocytes TxT+H/R significantly reduced caspase-3/7 activation in the LR group compared to the sham group (1076.00 ± 70.79 vs. 1445.00 ± 168.30 MFU, $p < 0.05$, **Figure 3A**). Moreover, resuscitation with EtP significantly diminished caspase-3/7 activation in granulocytes after TxT+H/R compared to both TxT+H/R_LR as well as to the sham group (854.40 ± 30.78 vs. 1076.00 ± 70.79 and 1445.00 ± 168.30 MFU, respectively, $p < 0.05$, **Figure 3A**).

In monocytes, no significant changes in caspase-3/7 activation were detected between the groups (**Figure 3B**).

Systemic Leukocyte Pyroptosis After Blunt Thoracic Trauma Followed by Hemorrhage and Resuscitation

Monocyte and granulocyte pyroptosis were assessed by measuring the activity of caspase-1 2 h after resuscitation (**Figures 4A,B**). In granulocytes, no significant changes

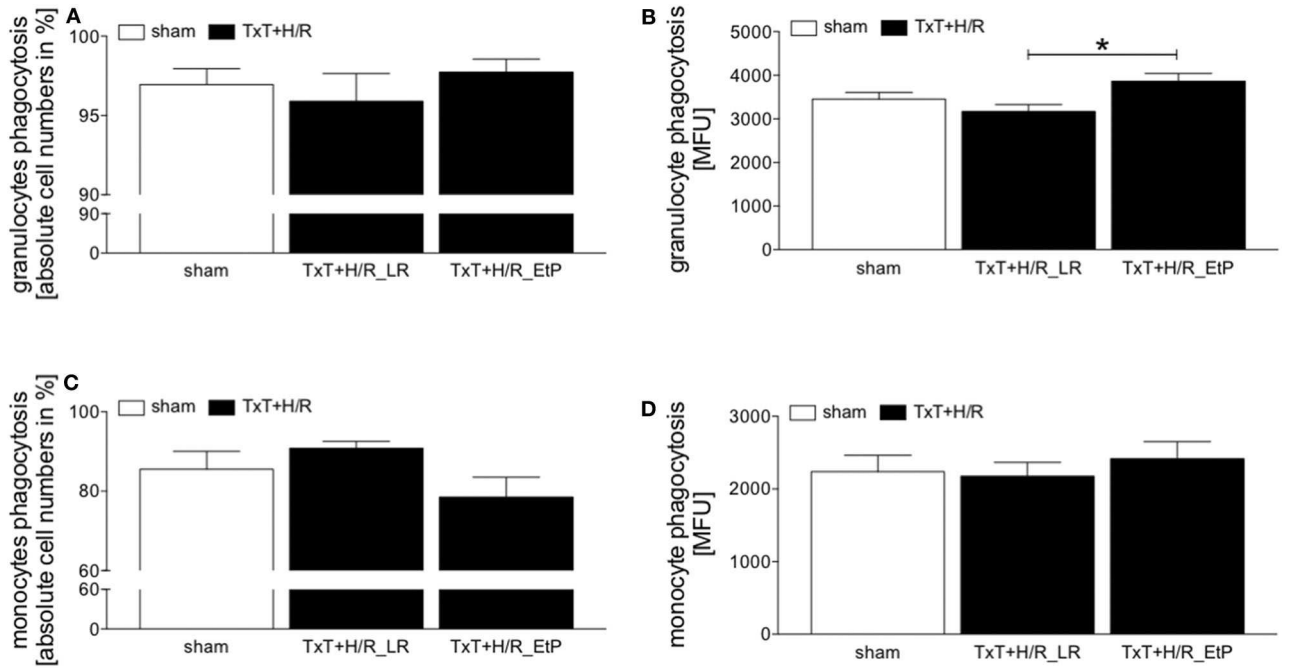

FIGURE 2 | Flow cytometric analysis of granulocyte and monocyte phagocytosis after blunt thoracic trauma (TxT) followed by haemorrhagic shock and resuscitation (H/R). Two hours after resuscitation flow cytometric analysis of phagocytosis in circulating granulocytes and monocytes was performed. Sham operated animals underwent all surgical procedures without induction of TxT and H/R. TxT+H/R_LR animals received lactated Ringers solution (LR) and TxT+H/R_EtP animals were resuscitated with LR supplemented with ethyl pyruvate (EtP). **(A)** Percentage of phagocytizing granulocytes in absolute cell numbers. **(B)** Mean fluorescence units (MFU) of phagocytizing granulocytes. **(C)** Percentage of phagocytizing monocytes in absolute cell numbers. **(D)** MFU of phagocytizing monocytes. Data are given as mean ± standard error of the mean, $^*p < 0.05$ vs. indicated, $n = 10$.

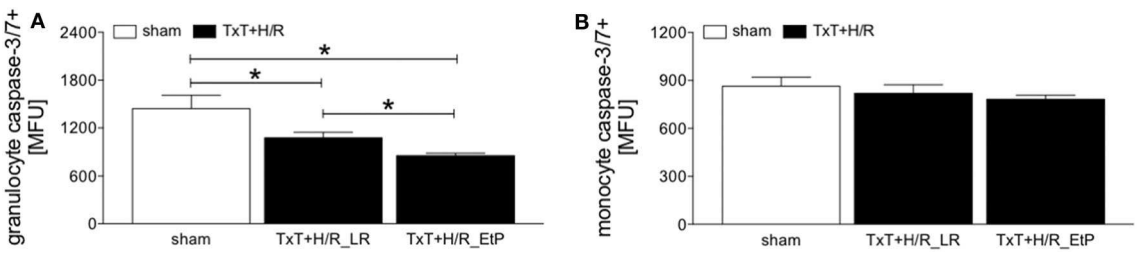

FIGURE 3 | Caspase-3/7 activation after blunt thoracic trauma (TxT) followed by haemorrhagic shock and resuscitation (H/R) in granulocytes and monocytes. Two hours after resuscitation flow cytometric analysis of apoptosis (caspase-3/7 activation) in circulating granulocytes **(A)** and monocytes **(B)** was performed. Sham operated animals underwent all surgical procedures without induction of TxT and H/R. TxT+H/R_LR animals received lactated Ringers solution (LR) and TxT+H/R_EtP animals were resuscitated with LR supplemented with ethyl pyruvate (EtP). **(A)** Mean fluorescence units (MFU) of caspase-3/7 positive granulocytes and **(B)** monocytes. Data are given as mean ± standard error of the mean, $^*p < 0.05$ vs. indicated, $n = 10$.

were observed between the sham and TxT+H/R_LR group. However, there was a significant decrease in pyroptosis in the TxT+H/R_EtP group compared to both sham and TxT+H/R_LR (1414.00 ± 102.60 vs. 2444.00 ± 293.00 and 2267.00 ± 137.00 MFU, respectively, $p < 0.05$, **Figure 4A**).

In monocytes caspase-1 activity was significantly increased after TxT+H/R compared to the sham group (1880.00 ± 296.20 vs. 1033.00 ± 44.22, $p < 0.05$, **Figure 4B**). TxT+H/R followed by resuscitation with EtP significantly decreased the caspase-1 activation compared with the TxT+H/R_LR group to the levels comparable to those of the sham animals (1074.00 ± 52.12 vs. 1880.00 ± 296.20, $p < 0.05$, **Figure 4B**).

Analysis of NF-κB p65 Phosphorylation in Systemic Leukocytes After Blunt Thoracic Trauma Followed by Hemorrhage and Resuscitation

The ratio of the expression of NF-κB p65 phosphorylated protein to the total p65 protein in granulocytes and monocytes

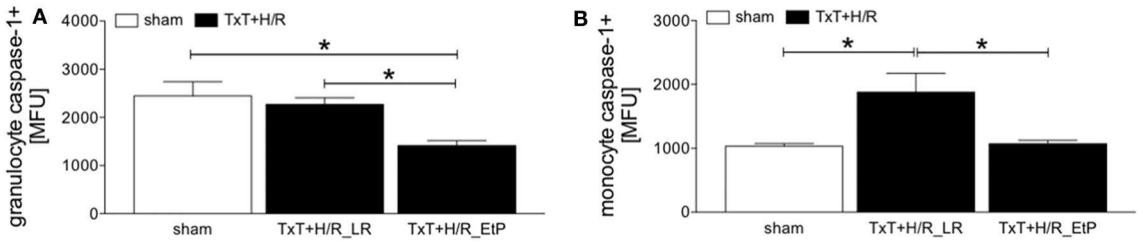

FIGURE 4 | Caspase-1 activation after blunt thoracic trauma (TxT) followed by haemorrhagic shock and resuscitation (H/R) in granulocytes and monocytes. Two hours after resuscitation flow cytometric analysis of pyroptosis (caspase-1 activation) in circulating granulocytes **(A)** and monocytes **(B)** was performed. Sham operated animals underwent all surgical procedures without induction of TxT and H/R. TxT+H/R_LR animals received lactated Ringers solution (LR) and TxT+H/R_EtP animals were resuscitated with LR supplemented with ethyl pyruvate (EtP). **(A)** Mean fluorescence units (MFU) of caspase-1 positive granulocytes and **(B)** monocytes. Data are given as mean ± standard error of the mean, $^*p < 0.05$ vs. indicated, $n = 10$.

2 h after resuscitation was evaluated (**Figures 5A,B**). There were no significant changes in the ratio of NF-κB p65 phosphorylated/total NF-κB p65 protein, however, there was a trend to an increase after TxT+H/R in the LR group compared with both sham as well as TxT+H/R_EtP groups in granulocytes (**Figure 5A**).

TxT+H/R_LR induced a significant increase in the expression of NF-κB p65 phosphorylated/total NF-κB p65 protein in monocytes compared to sham as well as to the TxT+H/R_EtP group ($p < 0.05$, **Figure 5B**).

Histomorphological Changes in Lung and Liver

Both lung and liver showed prominent organ damage in the TxT+H/R_LR group (data not shown). In lungs, alveolar wall thickening with disruption and cellular infiltrates compared to the sham groups were detected. TxT+H/R-induced changes were markedly reduced in the TxT+H/R_EtP group. Liver sections from the TxT+H/R_LR group revealed large areas of necrosis compared to the sham group (data not shown). TxT+H/R-induced changes were markedly reduced in the TxT+H/R_EtP group with less necrotic areas in liver sections. No tissue damage or necrosis were observed in the sham group. The representative and detailed analyses of the local effects of a EtP-reperfusion on lungs and liver in the underlying model of TxT and H/R are shown in our referred studies (32, 37).

DISCUSSION

In our previous studies, we have shown significant local anti-inflammatory and organ-protective effects of ethyl pyruvate after trauma (32, 37), which has been confirmed as a safe drug to use in cardiac surgery in a phase II multicentre study (42). Here, we investigated if the reperfusion with EtP will affect systemic inflammatory response in leukocytes induced by a double-hit model of blunt chest trauma and haemorrhagic shock. The anti-inflammatory potential of EtP is associated with reduced systemic inflammation of neutrophils and local organ damage as shown before in *in vitro* and *in vivo* studies (43, 44). Endotoxin-induced acute lung injury was attenuated by EtP due to the inhibition of cytokine production of IL-6 and TNF-α (44). However, although there are diverse studies demonstrating anti-inflammatory effects of EtP, the applied models do not mimic often occurring clinical situation with traumatic insult of blunt chest trauma concomitant with haemorrhagic shock, as it has been applied in the underlying study.

Trauma-induced release of PAMPs and/or DAMPs into circulation primes systemic neutrophils inciting non-specific organ damage (3, 45). Those activated circulating cells may cause dysfunctions of endothelial barriers due to increased migratory and functional capacity with enhanced release of ROS and elastases which damage the endothelia in critically ill trauma patients. Samples from traumatized patients who develop pneumonia show increased migratory potential of circulating neutrophils *via* elevated Mac-1 and reduced L-selectin levels (46). CD11b and CD62L play an important role in tethering and rolling along endothelia and transmigration into sites of inflammation (8, 47). During neutrophil activation, rolling and transmigration to sites of inflammation, CD62L can be shedded as soluble L-selectin from the cell surface into the circulation (48, 49). In our study, we also show upregulated CD11b and reduced CD62L levels on circulating neutrophils, indicating at an enhanced activation of neutrophil after trauma and hemorrhage in our model. In line with our findings Visser et al. have shown that the transient activation of neutrophils and mobilization of young neutrophils into the circulation was accompanied by decreased CD62L expression in a model of blunt chest injury (10). According to Mommsen et al. CD62L shedding from the surface of neutrophils may be a protective mechanism against inflammation after surgical trauma (50). The elevated levels of soluble L-selectin may interfere with L-selectin-mediated migration by competing for ligand binding, resulting in decreased leucocyte delivery to sites of inflammation (51, 52). In contrast to this, CD62L shedding is proposed to modulate the ability of leukocytes to migrate and enter sites of inflammation (51). Thus, CD62L shedding is required for activated leukocytes to detach from endothelia before their extravasation into tissues (51). This is in line with our findings showing decreased CD62L levels on circulating neutrophils after TxT+H/R. Adjacent to CD62, CD11b is responsible for mediating neutrophil adhesion to vascular endothelia (8). Traumatic brain injury

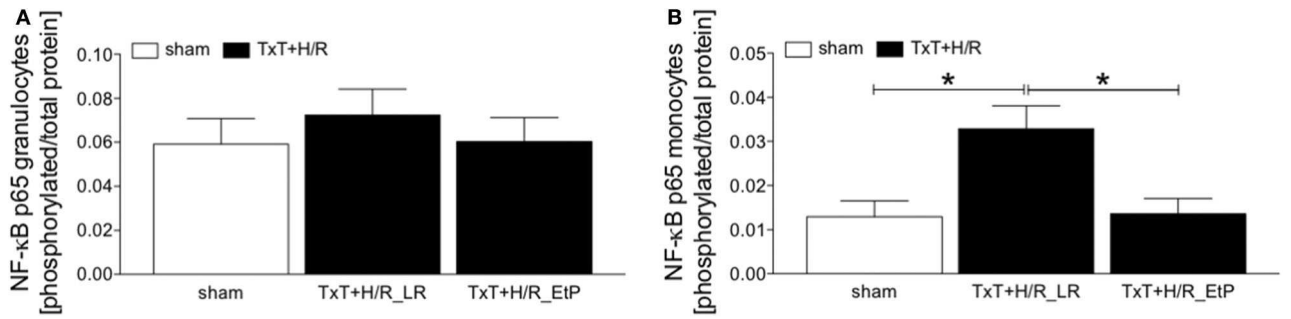

FIGURE 5 | Flow cytometric analysis of NF-κB p65 phosphorylation after blunt thoracic trauma (TxT) followed by haemorrhagic shock and resuscitation (H/R). Two hours after resuscitation flow cytometric analysis of phosphorylated NF-κB p65 in circulating granulocytes **(A)** and monocytes **(B)** was performed. Sham operated animals underwent all surgical procedures without induction of TxT and H/R. TxT+H/R_LR animals received lactated Ringers solution (LR) and TxT+H/R_EtP animals were resuscitated with LR supplemented with ethyl pyruvate (EtP). The ratio of phosphorylated to total NF-κB protein in granulocytes **(A,B)** monocytes is given. Data are given as mean ± standard error of the mean, $*p < 0.05$ vs. indicated, $n = 10$.

was accompanied by significantly elevated CD11b expression on circulating neutrophils and increased neutrophil infiltration into tissue after injury (53). In line with these reports, the double-hit as applied in our model induced CD11b. Moreover, the combination of decreased CD62L and increased CD11b expression on circulating neutrophils after trauma is in line with results of Hazeldine et al. (54). With regard to monocytes, in traumatized patients with sepsis and acute respiratory distress syndrome a similar systemic activation of peripheral blood mononuclear cells as well as their pyroptosis and apoptosis compared to those patients without complications has been shown (55). In terms of functional analyses, next to their activation, trauma induces modulations in neutrophils such as increased life-span which is caused by lowered apoptosis rates (8, 14). Interestingly, it has been shown that decreased apoptosis in circulating neutrophils persisted until 9 days after injury in trauma patients, contributing to organ dysfunction due to prolonged neutrophil hyperactivity (14). Maianski et al. demonstrated that apoptosis in neutrophils is linked to caspase-3 activation (15).The inhibited neutrophil apoptosis and prolonged live span promoted local inflammation in lung tissue (56). The data are in line with our observations demonstrating reduced caspase-3/7 activation after double-hit trauma and showing prolonged live span in our model. Anne Morrison et al. indicated that early increased neutrophil apoptosis in trauma-haemorrhagic shock may prevent from developing subsequent infection and MOF (16). Similarly, in a rat model of haemorrhagic shock, inhibition of caspase-3 dependent apoptosis resulted in tissue protective effects (17). Furthermore, major trauma leads to rapid recruitment of circulating monocytes, that serve as phagocytizing cells and executors of tissue healing and of an effective inflammatory response (57). Here, notably pyroptosis, a specific form of inflammasome- and inflammation-induced cell death can amplify the inflammatory response (58). Inflammasomes are promoting inflammation by processing and thus activation of proinflammatory cytokines notably IL-1β or IL-18 *via* i.e., caspase-1 (59). Our data show increased pyroptosis *via* elevated caspase-1 levels in circulating monocytes after TxT+H/R indicating at trauma-induced proinflammatory effects on circulating monocytes. In terms of pathomechanistical pathways, Nolan has shown that reduced apoptosis in systemic neutrophils after trauma may be NF-κB dependent (18). NF-κB plays a central role in the initiation and regulation of systemic and local immune response after trauma (23, 60, 61). In our study, TxT+H/R significantly increased NF-κB p65 phosphorylation in circulating monocytes. This is in line with increased NF-κB activity in monocytes of multiply injured trauma patients in the early post-traumatic phase (61, 62).

Our results and data from others indicate that organ-protective effects of EtP may be caused by a decreased systemic activation of leukocytes. Decreased CD62L levels on circulating neutrophils after TxT+H/R were significantly increased by EtP. Thus, the data suggest, that TxT+H/R-induced systemic activation can be diminished by EtP, subsequently reducing the transmigration of neutrophils to sites of inflammation upon a traumatic insult. Moreover, in a model of *E. coli*-induced sepsis, treatment with EtP significantly diminished inflammation by reduced systemic leukocyte rolling, adherence and migration in the mesenteric microcirculation (63). In the present study, resuscitation with EtP reduced the expression of CD11b on circulating neutrophils, indicating at an anti-inflammatory effect *via* inhibition of systemic activation of leukocytes. Intriguing data have been found after resuscitation with EtP which further reduced caspase-3/7 activity in circulating granulocytes, effects that can be associated with diminished tissue damage in liver and lung as shown in our previous studies (32, 37). This is in contrast to above described findings, where tissue-protective effects were demonstrated by restoring apoptotic capacity in neutrophils. Tissue-protective effects of EtP are potentially caused by a diminished ability of neutrophils to transmigrate into sites of inflammation and additionally inhibiting apoptosis *via* caspase-3 in tissues. This is in line with the results of Sharma et al. in a model of haemorrhagic shock, where liver protective by an EtP resuscitation were linked to the inhibition of caspase-3 induced cell apoptosis (17). In our study resuscitation with EtP had no significant

effect on apoptosis of circulating monocytes. Resuscitation with EtP significantly diminished the inflammasome activity in monocytes to levels comparable to those of the untreated sham group. This is in line with Li et al. who has shown that EtP reduced IL-1β expression in macrophages *via* inhibiting caspase-1 activation through inflammasome (33). Interestingly, also in neutrophils EtP reduced the caspase-1 activity to levels below sham and trauma groups, data which might indicate at a general effect of EtP on pyroptosis in circulating immune cells. Furthermore, Yang et al. provided the first clear evidence that EtP exerts its anti-inflammatory effects *via* decreasing the activation of NF-κB, which is then followed by a downregulated expression of proinflammatory genes in liver and colon mucosa (36). In an *in vitro* experiment with macrophage like RAW and kidney cells, EtP directly targets the p65 subunit of the transcription factor, modifying the cysteine 38 and inhibiting NF-κB signaling (64). In a model of traumatic brain injury, multiple injections with EtP significantly inhibited NF-κB p65 presence in the nucleus of damaged microglia cells, improving blood brain barrier and inflammatory response (65). Anti-inflammatory effects in ischemia/reperfusion model of the kidney with a pre- and post-treatment with EtP diminished NF-κB phosphorylation and reduced levels of High mobility group box 1 protein, Toll-like receptor (TLR)2 and TLR4, resulting in renal protection (66). In line with these findings, resuscitation with EtP markedly inhibited the phosphorylation of the p65 subunit, possibly thereby diminishing inflammation-inducing effects of TxT+H/R. In conclusion, during acute inflammation EtP may exert protective effects by reducing the systemic activation of inflammatory leukocytes ending in previously described diminished local tissue damage.

There are several limitations of our study that remain to be considered when interpreting the results. We investigated only one endpoint, which is 2 h post resuscitation, while clinical outcome with regard to systemic and local inflammation after trauma should be investigated in the later course. Furthermore, next to observed acute changes after TxT+H/R investigations of overall survival, organ failure and MOF require larger study groups and prolonged observational periods. While we included female LEWIS rats, based on recent literature, differences between age and gender should be considered as important confounding factors in the immune response to traumatic insult and post-traumatic outcomes, and thus those remain to be further investigated in future studies. Regarding the dose- and time-dependent effects of EtP, that have been demonstrated before, our study is limited to one applied dose (50 mg/kg). Specific dose- and time-dependent influence of EtP on the post-traumatic inflammation and outcomes have to be further evaluated. Furthermore, the findings should be correlated to histological evaluations, e.g., the effect of reduced CD11b but elevated CD62L expression in response to EtP treatment on neutrophil infiltration may be investigated by histology. Similarly, biochemical assays of oxidative damage would demonstrate the net effect of increased phagocyte activity and delayed apoptosis of neutrophils on tissues. Thus, the correlation of systemic modulations with local changes should be assessed in future studies.

DATA AVAILABILITY STATEMENT

The raw data supporting the conclusions of this article will be made available by the authors, without undue reservation.

ETHICS STATEMENT

The animal study was reviewed and approved by the veterinary department of the regional council in Darmstadt, Germany (Hessen, Germany).

AUTHOR CONTRIBUTIONS

BR designed the study and obtained the grant. SD, NF, and NW performed the experiments. SD wrote the first draft of the manuscript. KK performed the histological evaluations. BR, NW, and AS performed the statistical analysis and revised the manuscript. AN, SE, MK, and IM made important intellectual contributions to the study. All authors contributed to the article and approved the submitted version.

FUNDING

This study was supported by grants from the DFG RE 3304/5-1.

ACKNOWLEDGMENTS

We thank Kerstin Kontradowitz, Katrin Jurida, and Alexander Schaible for outstanding technical assistance. Parts of this study were presented at the XVII. Congress of the European Shock Society held in Paris, France (September 13–15, 2017) with the abstract titled: *Ethylpyruvate reduces local inflammation and systemic leukocyte activation via NF-κB, protecting from organ damage after blunt chest trauma and haemorrhagic shock*.

REFERENCES

1. Alberdi F, Garcia I, Atutxa L, Zabarte M, Trauma, Neurointensive Care Work Group of the S. Epidemiology of severe trauma. *Med Intensiva.* (2014) 38:580–8. doi: 10.1016/j.medine.2014.06.002
2. Makley AT, Goodman MD, Friend LA, Deters JS, Johannigman JA, Dorlac WC, et al. Resuscitation with fresh whole blood ameliorates the inflammatory response after hemorrhagic shock. *J Trauma.* (2010) 68:305–11. doi: 10.1097/TA.0b013e3181cb4472
3. Relja B, Mors K, Marzi I. Danger signals in trauma. *Eur J Trauma Emerg Surg.* (2018) 44:301–16. doi: 10.1007/s00068-018-0962-3
4. Wutzler S, Lustenberger T, Relja B, Lehnert M, Marzi I. Pathophysiology of multiple trauma : intensive care medicine and timing of treatment. *Chirurg.* (2013) 84:753–8. doi: 10.1007/s00104-013-2477-0
5. Dewar D, Moore FA, Moore EE, Balogh Z. Postinjury multiple organ failure. *Injury.* (2009) 40:912–8. doi: 10.1016/j.injury.2009.05.024
6. Lord JM, Midwinter MJ, Chen YF, Belli A, Brohi K, Kovacs EJ, et al. The systemic immune response to trauma: an overview of pathophysiology

and treatment. *Lancet.* (2014) 384:1455–65. doi: 10.1016/S0140-6736(14)60687-5
7. Miralda I, Uriarte SM, McLeish KR. Multiple phenotypic changes define neutrophil priming. *Front Cell Infect Microbiol.* (2017) 7:217. doi: 10.3389/fcimb.2017.00217
8. Hazeldine J, Hampson P, Lord JM. The impact of trauma on neutrophil function. *Injury.* (2014) 45:1824–33. doi: 10.1016/j.injury.2014.06.021
9. Johansson J, Sjogren F, Bodelsson M, Sjoberg F. Dynamics of leukocyte receptors after severe burns: an exploratory study. *Burns.* (2011) 37:227–33. doi: 10.1016/j.burns.2010.08.015
10. Visser T, Hietbrink F, Groeneveld KM, Koenderman L, Leenen LP. Isolated blunt chest injury leads to transient activation of circulating neutrophils. *Eur J Trauma Emerg Surg.* (2011) 37:177–84. doi: 10.1007/s00068-010-0041-x
11. Hauser CJ. Preclinical models of traumatic, hemorrhagic shock. *Shock.* (2005) 24(Suppl. 1):24–32. doi: 10.1097/01.shk.0000191387.18818.43
12. Botha AJ, Moore FA, Moore EE, Fontes B, Banerjee A, Peterson VM. Postinjury neutrophil priming and activation states: therapeutic challenges. *Shock.* (1995) 3:157–66. doi: 10.1097/00024382-199503000-00001
13. Weckbach S, Hohmann C, Braumueller S, Denk S, Klohs B, Stahel PF, et al. Inflammatory and apoptotic alterations in serum and injured tissue after experimental polytrauma in mice: distinct early response compared with single trauma or "double-hit" injury. *J Trauma Acute Care Surg.* (2013) 74:489–98. doi: 10.1097/TA.0b013e31827d5f1b
14. Paunel-Gorgulu A, Kirichevska T, Logters T, Windolf J, Flohe S. Molecular mechanisms underlying delayed apoptosis in neutrophils from multiple trauma patients with and without sepsis. *Mol Med.* (2012) 18:325–35. doi: 10.2119/molmed.2011.00380
15. Maianski NA, Mul FP, van Buul JD, Roos D, Kuijpers TW. Granulocyte colony-stimulating factor inhibits the mitochondria-dependent activation of caspase-3 in neutrophils. *Blood.* (2002) 99:672–9. doi: 10.1182/blood.V99.2.672
16. Anne Morrison C, Moran A, Patel S, Vidaurre Mdel P, Carrick MM, Tweardy DJ. Increased apoptosis of peripheral blood neutrophils is associated with reduced incidence of infection in trauma patients with hemorrhagic shock. *J Infect.* (2013) 66:87–94. doi: 10.1016/j.jinf.2012.10.001
17. Sharma P, Mongan PD. Hypertonic sodium pyruvate solution is more effective than Ringer's ethyl pyruvate in the treatment of hemorrhagic shock. *Shock.* (2010) 33:532–40. doi: 10.1097/SHK.0b013e3181cc02b3
18. Nolan B, Collette H, Baker S, Duffy A, De M, Miller C, et al. Inhibition of neutrophil apoptosis after severe trauma is NFkappabeta dependent. *J Trauma.* (2000) 48:599–604; discussion −5. doi: 10.1097/00005373-200004000-00004
19. Relja B, Horstmann JP, Kontradowitz K, Jurida K, Schaible A, Neunaber C, et al. Nlrp1 inflammasome is downregulated in trauma patients. *J Mol Med.* (2015) 93:1391–400. doi: 10.1007/s00109-015-1320-0
20. Kany S, Horstmann JP, Sturm R, Mors K, Relja B. Reduced NLRP3 gene expression limits the IL-1beta cleavage via inflammasome in monocytes from severely injured trauma patients. *Mediators Inflamm.* (2018) 2018:1752836. doi: 10.1155/2018/1752836
21. Mariathasan S, Weiss DS, Newton K, McBride J, O'Rourke K, Roose-Girma M, et al. Cryopyrin activates the inflammasome in response to toxins and ATP. *Nature.* (2006) 440:228–32. doi: 10.1038/nature04515
22. Ogura Y, Sutterwala FS, Flavell RA. The inflammasome: first line of the immune response to cell stress. *Cell.* (2006) 126:659–62. doi: 10.1016/j.cell.2006.08.002
23. Lawrence T. The nuclear factor NF-kappaB pathway in inflammation. *Cold Spring Harb Perspect Biol.* (2009) 1:a001651. doi: 10.1101/cshperspect.a001651
24. Shih HC, Huang MS, Lee CH. Polymorphonuclear cell priming associated with NF-kB activation in patients with severe injury is partially dependent on macrophage migration inhibitory factor. *J Am Coll Surg.* (2010) 211:791–7. doi: 10.1016/j.jamcollsurg.2010.07.028
25. Kao KK, Fink MP. The biochemical basis for the anti-inflammatory and cytoprotective actions of ethyl pyruvate and related compounds. *Biochem Pharmacol.* (2010) 80:151–9. doi: 10.1016/j.bcp.2010.03.007
26. Fink MP. Ethyl pyruvate: a novel treatment for sepsis. *Curr Drug Targets.* (2007) 8:515–8. doi: 10.2174/138945007780362791
27. Fink MP. Ethyl pyruvate. *Curr Opin Anaesthesiol.* (2008) 21:160–7. doi: 10.1097/ACO.0b013e3282f63c2e
28. Relja B, Omid N, Kontradowitz K, Jurida K, Oppermann E, Stormann P, et al. Decreased inflammatory responses of human lung epithelial cells after ethanol exposure are mimicked by ethyl pyruvate. *Mediators Inflamm.* (2014) 2014:781519. doi: 10.1155/2014/781519
29. Relja B, Omid N, Schaible A, Perl M, Meier S, Oppermann E, et al. Pre- or post-treatment with ethanol and ethyl pyruvate results in distinct anti-inflammatory responses of human lung epithelial cells triggered by interleukin-6. *Mol Med Rep.* (2015) 12:2991–8. doi: 10.3892/mmr.2015.3764
30. Cai B, Brunner M, Wang H, Wang P, Deitch EA, Ulloa L. Ethyl pyruvate improves survival in awake hemorrhage. *J Mol Med.* (2009) 87:423–33. doi: 10.1007/s00109-009-0441-8
31. Nguyen BN, Albadawi H, Oklu R, Crawford RS, Fink MP, Cambria RP, et al. Ethyl pyruvate modulates delayed paralysis following thoracic aortic ischemia reperfusion in mice. *J Vasc Surg.* (2016) 64:1433–43. doi: 10.1016/j.jvs.2015.06.214
32. Relja B, Wagner N, Franz N, Dieteren S, Mors K, Schmidt J, et al. Ethyl pyruvate reduces acute lung damage following trauma and hemorrhagic shock via inhibition of NF-kappaB and HMGB1. *Immunobiology.* (2018) 223:310–8. doi: 10.1016/j.imbio.2017.10.037
33. Li S, Liang F, Kwan K, Tang Y, Wang X, Tang Y, et al. Identification of ethyl pyruvate as a NLRP3 inflammasome inhibitor that preserves mitochondrial integrity. *Mol Med.* (2018) 24:8. doi: 10.1186/s10020-018-0006-9
34. Uchiyama T, Delude RL, Fink MP. Dose-dependent effects of ethyl pyruvate in mice subjected to mesenteric ischemia and reperfusion. *Intensive Care Med.* (2003) 29:2050–8. doi: 10.1007/s00134-003-1966-x
35. Tawadrous ZS, Delude RL, Fink MP. Resuscitation from hemorrhagic shock with Ringer's ethyl pyruvate solution improves survival and ameliorates intestinal mucosal hyperpermeability in rats. *Shock.* (2002) 17:473–7. doi: 10.1097/00024382-200206000-00006
36. Yang R, Gallo DJ, Baust JJ, Uchiyama T, Watkins SK, Delude RL, et al. Ethyl pyruvate modulates inflammatory gene expression in mice subjected to hemorrhagic shock. *Am J Physiol Gastrointest Liver Physiol.* (2002) 283:G212–21. doi: 10.1152/ajpgi.00022.2002
37. Wagner N, Dieteren S, Franz N, Kohler K, Mors K, Nicin L, et al. Ethyl pyruvate ameliorates hepatic injury following blunt chest trauma and hemorrhagic shock by reducing local inflammation, NF-kappaB activation and HMGB1 release. *PLoS ONE.* (2018) 13:e0192171. doi: 10.1371/journal.pone.0192171
38. Kilkenny C, Browne WJ, Cuthill IC, Emerson M, Altman DG. Improving bioscience research reporting: the arrive guidelines for reporting animal research. *PLoS Biol.* (2010) 8:e1000412. doi: 10.1371/journal.pbio.1000412
39. Wagner N, Franz N, Dieteren S, Perl M, Mors K, Marzi I, et al. Acute alcohol binge deteriorates metabolic and respiratory compensation capability after blunt chest trauma followed by hemorrhagic shock - a new research model. *Alcohol Clin Exp Res.* (2017) 41:1559–67. doi: 10.1111/acer.13446
40. Relja B, Henrich D, Wetzel G, Sander AL, Jakob H, Maraslioglu M, et al. Effects of acute ethanol gavage on intestinal integrity after hemorrhage/resuscitation. *Scand J Gastroenterol.* (2013) 48:448–58. doi: 10.3109/00365521.2013.772228
41. Relja B, Tottel E, Breig L, Henrich D, Schneider H, Marzi I, et al. Effects of green tea catechins on the pro-inflammatory response after haemorrhage/resuscitation in rats. *Br J Nutr.* (2011) 105:1791–7. doi: 10.1017/S000711451000560X
42. Bennett-Guerrero E, Swaminathan M, Grigore AM, Roach GW, Aberle LG, Johnston JM, et al. A phase II multicenter double-blind placebo-controlled study of ethyl pyruvate in high-risk patients undergoing cardiac surgery with cardiopulmonary bypass. *J Cardiothorac Vasc Anesth.* (2009) 23:324–9. doi: 10.1053/j.jvca.2008.08.005
43. Cai B, Deitch EA, Grande D, Ulloa L. Anti-inflammatory resuscitation improves survival in hemorrhage with trauma. *J Trauma.* (2009) 66:1632–9 doi: 10.1097/TA.0b013e3181a5b179
44. Zhu Q, Wang H, Wang H, Luo Y, Yu Y, Du Q, et al. Protective effects of ethyl pyruvate on lipopolysaccharideinduced acute lung injury through inhibition of autophagy in neutrophils. *Mol Med Rep.* (2017) 15:1272–8. doi: 10.3892/mmr.2017.6118
45. Zhang Q, Raoof M, Chen Y, Sumi Y, Sursal T, Junger W, et al. Circulating mitochondrial DAMPs cause inflammatory responses to injury. *Nature.* (2010) 464:104–7. doi: 10.1038/nature08780

46. Relja B, Taraki R, Teuben MP, Mors K, Wagner N, Wutzler S, et al. Sera from severe trauma patients with pneumonia and without infectious complications have differential effects on neutrophil biology. *BMC Pulm Med.* (2016) 16:171. doi: 10.1186/s12890-016-0329-7
47. Smalley DM, Ley K. L-selectin: mechanisms and physiological significance of ectodomain cleavage. *J Cell Mol Med.* (2005) 9:255–66. doi: 10.1111/j.1582-4934.2005.tb00354.x
48. Venturi GM, Tu L, Kadono T, Khan AI, Fujimoto Y, Oshel P, et al. Leukocyte migration is regulated by L-selectin endoproteolytic release. *Immunity.* (2003) 19:713–24. doi: 10.1016/S1074-7613(03)00295-4
49. Liu Z, Yago T, Zhang N, Panicker SR, Wang Y, Yao L, et al. L-selectin mechanochemistry restricts neutrophil priming *in vivo*. *Nat Commun.* (2017) 8:15196. doi: 10.1038/ncomms15196
50. Mommsen P, Barkhausen T, Hildebrand F, Zeckey C, Krettek C, van Griensven M. Regulation of L-selectin expression by trauma-relevant cytokines. *Pathol Res Pract.* (2011) 207:142–7. doi: 10.1016/j.prp.2010.12.003
51. Tu L, Poe JC, Kadono T, Venturi GM, Bullard DC, Tedder TF, et al. A functional role for circulating mouse L-selectin in regulating leukocyte/endothelial cell interactions *in vivo*. *J Immunol.* (2002) 169:2034–43. doi: 10.4049/jimmunol.169.4.2034
52. Ferri LE, Swartz D, Christou NV. Soluble L-selectin at levels present in septic patients diminishes leukocyte-endothelial cell interactions in mice *in vivo*: a mechanism for decreased leukocyte delivery to remote sites in sepsis. *Crit Care Med.* (2001) 29:117–22. doi: 10.1097/00003246-200101000-00024
53. Junger WG, Rhind SG, Rizoli SB, Cuschieri J, Baker AJ, Shek PN, et al. Prehospital hypertonic saline resuscitation attenuates the activation and promotes apoptosis of neutrophils in patients with severe traumatic brain injury. *Shock.* (2013) 40:366–74. doi: 10.1097/SHK.0000000000000038
54. Hazeldine J, Naumann DN, Toman E, Davies D, Bishop JRB, Su Z, et al. Prehospital immune responses and development of multiple organ dysfunction syndrome following traumatic injury: a prospective cohort study. *PLoS Med.* (2017) 14:e1002338. doi: 10.1371/journal.pmed.1002338
55. Wang YC, Liu QX, Liu T, Xu XE, Gao W, Bai XJ, et al. Caspase-1-dependent pyroptosis of peripheral blood mononuclear cells predicts the development of sepsis in severe trauma patients: a prospective observational study. *Medicine.* (2018) 97:e9859. doi: 10.1097/MD.0000000000009859
56. Daigle I, Simon HU. Critical role for caspases 3 and 8 in neutrophil but not eosinophil apoptosis. *Int Arch Allergy Immunol.* (2001) 126:147–56. doi: 10.1159/000049506
57. Peiseler M, Kubes P. Macrophages play an essential role in trauma-induced sterile inflammation and tissue repair. *Eur J Trauma Emerg Surg.* (2018) 44:335–49. doi: 10.1007/s00068-018-0956-1
58. Baroja-Mazo A, Martin-Sanchez F, Gomez AI, Martinez CM, Amores-Iniesta J, Compan V, et al. The NLRP3 inflammasome is released as a particulate danger signal that amplifies the inflammatory response. *Nat Immunol.* (2014) 15:738–48. doi: 10.1038/ni.2919
59. Martinon F, Mayor A, Tschopp J. The inflammasomes: guardians of the body. *Annu Rev Immunol.* (2009) 27:229–65. doi: 10.1146/annurev.immunol.021908.132715
60. Zhang Q, Lenardo MJ, Baltimore D. 30 years of NF-kappaB: a blossoming of relevance to human pathobiology. *Cell.* (2017) 168:37–57. doi: 10.1016/j.cell.2016.12.012
61. Li J, Li NP, Gu YF, Yang X, Lu XB, Cong JN, et al. Dynamic activity of NF-kappaB in multiple trauma patients and protective effects of ulinastain. *Chin J Traumatol.* (2011) 14:354–8.
62. Biberthaler P, Stegmaier J, Mayer V, Kirchhoff C, Neth P, Mussack T, et al. Initial posttraumatic translocation of NF-kappaB and TNF-alpha mRNA expression in peripheral blood monocytes of trauma patients with multiple injuries: a pilot study. *Shock.* (2004) 22:527–32. doi: 10.1097/01.shk.0000142819.68823.14
63. Guarda IF, Correia CJ, Breithaupt-Faloppa AC, Ferreira SG, Moreno AC, Martinez MB, et al. Effects of ethyl pyruvate on leukocyte-endothelial interactions in the mesenteric microcirculation during early sepsis treatment. *Clinics.* (2015) 70:508–14. doi: 10.6061/clinics/2015(07)08
64. Han Y, Englert JA, Yang R, Delude RL, Fink MP. Ethyl pyruvate inhibits nuclear factor-kappaB-dependent signaling by directly targeting p65. *J Pharmacol Exp Ther.* (2005) 312:1097–105. doi: 10.1124/jpet.104.079707
65. Shi H, Wang HL, Pu HJ, Shi YJ, Zhang J, Zhang WT, et al. Ethyl pyruvate protects against blood-brain barrier damage and improves long-term neurological outcomes in a rat model of traumatic brain injury. *CNS Neurosci Ther.* (2015) 21:374–84. doi: 10.1111/cns.12366
66. Jun JH, Song JW, Shin EJ, Kwak YL, Choi N, Shim JK. Ethyl pyruvate is renoprotective against ischemia-reperfusion injury under hyperglycemia. *J Thorac Cardiovasc Surg.* (2018) 155:1650–8. doi: 10.1016/j.jtcvs.2017.10.069

Conflict of Interest: The authors declare that the research was conducted in the absence of any commercial or financial relationships that could be construed as a potential conflict of interest.

frontiers in Medicine

ORIGINAL RESEARCH
published: 22 October 2020
doi: 10.3389/fmed.2020.567260

Methane Exhalation Can Monitor the Microcirculatory Changes of the Intestinal Mucosa in a Large Animal Model of Hemorrhage and Fluid Resuscitation

Anett Bársony[1], Noémi Vida[2], Ámos Gajda[2], Attila Rutai[2], Árpád Mohácsi[3], Anna Szabó[4], Mihály Boros[2], Gabriella Varga[2†] and Dániel Érces[2†]*

[1] Department of Surgery, University of Szeged, Szeged, Hungary, [2] Institute of Surgical Research, University of Szeged, Szeged, Hungary, [3] MTA–SZTE Research Group on Photoacoustic Spectroscopy, Szeged, Hungary, [4] Department of Optics and Quantum Electronics, Faculty of Science and Informatics, University of Szeged, Szeged, Hungary

OPEN ACCESS

Edited by:
Raghavan Pillai Raju,
Augusta University, United States

Reviewed by:
Johanna Catharina Duvigneau,
University of Veterinary Medicine Vienna, Austria
Wolfgang Weihs,
Medical University of Vienna, Austria

***Correspondence:**
Dániel Érces
erces.daniel@med.u-szeged.hu

[†]These authors have contributed equally to this work

Specialty section:
This article was submitted to Intensive Care Medicine and Anesthesiology, a section of the journal Frontiers in Medicine

Received: 29 May 2020
Accepted: 11 September 2020
Published: 22 October 2020

Citation:
Bársony A, Vida N, Gajda Á, Rutai A, Mohácsi Á, Szabó A, Boros M, Varga G and Érces D (2020) Methane Exhalation Can Monitor the Microcirculatory Changes of the Intestinal Mucosa in a Large Animal Model of Hemorrhage and Fluid Resuscitation. Front. Med. 7:567260. doi: 10.3389/fmed.2020.567260

Background: Internal hemorrhage is a medical emergency, which requires immediate causal therapy, but the recognition may be difficult. The reactive changes of the mesenteric circulation may be part of the earliest hemodynamic responses to bleeding. Methane is present in the luminal atmosphere; thus, we hypothesized that it can track the intestinal circulatory changes, induced by hemorrhage, non-invasively. Our goal was to validate and compare the sensitivity of this method with an established technique using sublingual microcirculatory monitoring in a large animal model of controlled, graded hemorrhage and the early phase of following fluid resuscitation.

Materials and Methods: The experiments were performed on anesthetized, ventilated Vietnamese minipigs (approval number: V/148/2013; $n = 6$). The animals were gradually bled seven times consecutively of 5% of their estimated blood volume (BV) each, followed by gradual fluid resuscitation with colloid (hydroxyethyl starch; 5% of the estimated BV/dose) until 80 mmHg mean arterial pressure was achieved. After each step, macrohemodynamic parameters were recorded, and exhaled methane level was monitored continuously with a custom-built photoacoustic laser-spectroscopy unit. The microcirculation of the sublingual area, ileal serosa, and mucosa was examined by intravital videomicroscopy (Cytocam-IDF, Braedius).

Results: Mesenteric perfusion was significantly reduced by a 5% blood loss, whereas microperfusion in the oral cavity deteriorated after a 25% loss. A statistically significant correlation was found between exhaled methane levels, superior mesenteric artery flow ($r = 0.93$), or microcirculatory changes in the ileal serosa ($\rho = 0.78$) and mucosa ($r = 0.77$). After resuscitation, the ileal mucosal microcirculation increased rapidly [De Backer score (DBS): 2.36 ± 0.42 vs. 8.6 ± 2.1 mm^{-1}], whereas serosal perfusion changed gradually and with a lower amplitude (DBS: 2.51 ± 0.48 vs. 5.73 ± 0.75). Sublingual perfusion correlated with mucosal ($r = 0.74$) and serosal ($r = 0.66$) mesenteric microperfusion during the hemorrhage phase but not during the resuscitation phase.

Conclusion: Detection of exhaled methane levels is of diagnostic significance during experimental hemorrhage as it indicates blood loss earlier than sublingual microcirculatory changes and in the early phase of fluid resuscitation, the exhaled methane values change in association with the mesenteric perfusion and the microcirculation of the ileum.

Keywords: exhaled methane, diagnostic significance, small intestinal microcirculation, hemorrhage, resuscitation

INTRODUCTION

The manifestation of internal bleeding varies, with the signs and symptoms usually not easily recognized; thus, a diagnosis can be difficult (1–5). Hemodynamic changes or alterations within simple laboratory parameters are often not present during the early stage of bleeding, and advanced imaging possibilities, such as CT angiography and catheter angiography, which are able to identify the presence and location of a hemorrhage, are frequently inaccessible and unsuitable for continuous monitoring (6). Nevertheless, it is recognized that the mortality rate for postoperative internal bleeding is significantly increased if higher transfusion volumes are required; therefore, the earliest possible diagnosis is necessary.

As part of the redistribution of circulation, the reduction of mesenteric perfusion is among the first homeostatic responses, and therefore a continuous, direct monitoring of blood flow in the superior mesenteric artery (SMA) and downstream intestinal microperfusion would be a highly useful, early warning tool. Today, such observations at the patient's bedside, however, are impossible. Nevertheless, non-invasive techniques with indirect monitoring options, such as sublingual capnometry and intravital microscopy methods, were developed and are in clinical use with variable success (7, 8).

We hypothesized that measurement of exhaled methane concentrations may also offer a solution to this problem. Methane in the human body originates from several sources, but it is widely accepted that it is produced by anaerobic methanogenic microorganisms, colonizing the mammalian gastrointestinal (GI) tract (9). Due to its physicochemical properties, methane is distributed evenly across membrane barriers, traverses the mucosa, and enters the mesenteric microcirculation freely (10). For continuous methane detection, near-infrared diode lasers are very effective tools for high-sensitivity photoacoustic spectroscopy (PAS) (11), and we have already provided evidence that a PAS-based breath analysis device can successfully replace gas chromatography (GC) (12).

In our earlier proof of principle study, we provided evidence that the exhaled methane levels change in association with changes in superior mesenteric arterial blood flow (13). It has been demonstrated that arterial occlusions and reperfusions and the accompanying mucosal microcirculatory cycles correlated significantly with parallel changes in methane concentration in the exhaled air (13). Therefore, the aim of the present study was to investigate the diagnostic value of real-time detection of exhaled methane levels to recognize internal bleeding in a clinically-relevant large animal model. Further aims were to examine whether continuous breath methane output monitoring can provide information on the condition of the mesenteric vascular beds during fluid resuscitation and to compare the efficacy of the technique with intravital sublingual microcirculatory analysis, a diagnostic method already in clinical use (14, 15).

MATERIALS AND METHODS

Animals

The experiments were performed on male outbred Vietnamese minipigs ($n = 6$; 40 ± 3 kg bw) in accordance with the National Institutes of Health guidelines on the handling of and care for experimental animals and EU Directive 2010/63 on the protection of animals used for scientific purposes (approval number: V/148/2013). The animals were obtained from a local, officially licensed breeder and were kept in the animal house of the institute for an acclimatization period of 7–10 days with natural circadian light and free access to water and food. Prior to the experiments, the animals were fasted for 12 h with free access to tap water.

Surgical Preparations

Male outbred Vietnamese minipigs ($n = 6$; weighing 40 ± 3 kg) were used. Anesthesia was induced with a mixture of tiletamine zolazepam (5 mg kg^{-1} *im*; Virbac, Carros, France) and xylazine (2 mg kg^{-1} *im*; Produlab Pharma, Raamsdonksveer, The Netherlands). The animals were placed in supine position on a warming pad with body temperature kept at $37.5 \pm 0.4^{\circ}$C. After endotracheal intubation, mechanical ventilation was started with a tidal volume of 8–10 ml kg^{-1}, and the respiratory rate was adjusted to maintain the end-tidal pressure of carbon dioxide in the 35–45 mmHg range. Anesthesia was maintained with a continuous infusion of propofol (6 mg kg^{-1} h^{-1} *iv*; Fresenius Kabi, Bad Homburg, Germany), midazolam (1.2 mg kg^{-1} h^{-1}; Torrex Chiesi Pharma, Vienna, Austria), and fentanyl (0.02 mg kg^{-1} h^{-1}; Richter Gedeon, Budapest, Hungary). Ringer's lactate (RL) infusion was administered at a rate of 10 ml kg^{-1} h^{-1} until bleeding was started. The depth of anesthesia was regularly controlled by monitoring the jaw tone and the absence of interdigital reflex.

The left jugular vein was cannulated with a 7F, three lumen catheter (Smiths Medical, Kirchseeon, Germany) for fluid and drug administration, as was the left femoral artery for invasive monitoring of mean arterial pressure (MAP) (PICCO Plus; PULSION Medical Systems, Feldkirchen, Germany). The left carotid artery was cannulated with a 13G single lumen catheter

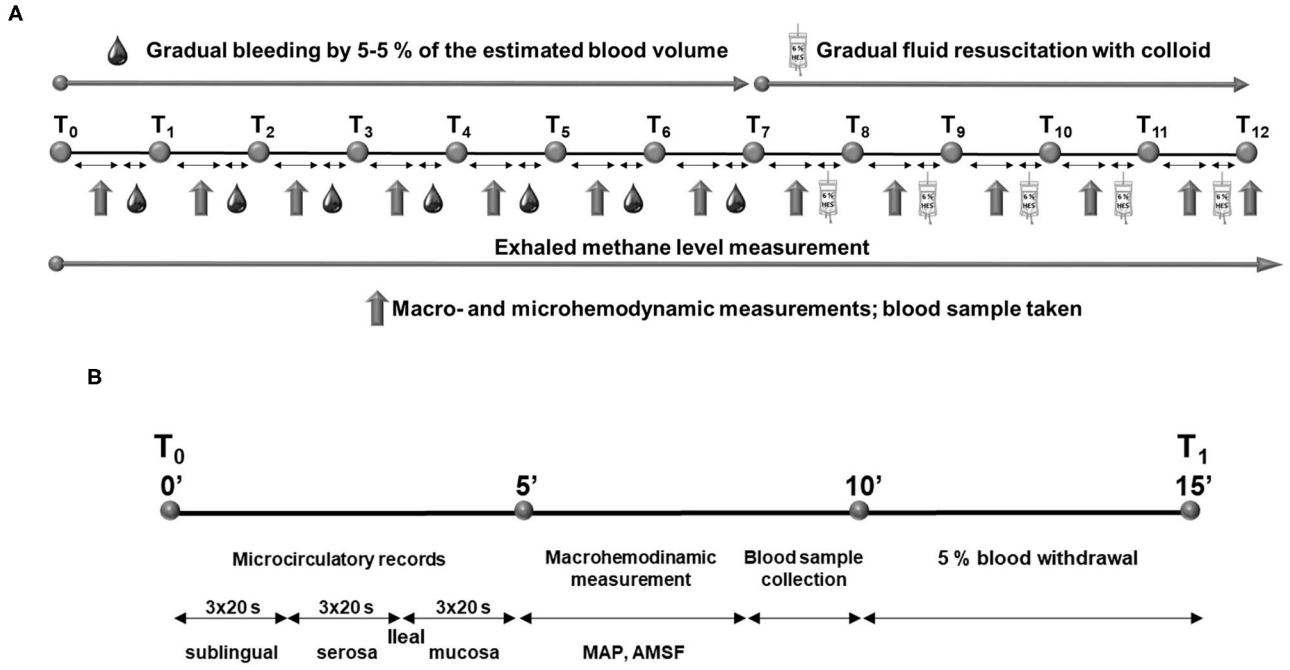

FIGURE 1 | Experimental protocol **(A)** and timeline of the measurement period during the experiment **(B)**.

(Balton, Warsaw, Poland) for blood withdrawal. After median laparotomy, the SMA was dissected free, and a flow probe (Transonic Systems Inc., Ithaca, NY, USA) was placed around it to measure SMA flow. The wound in the abdominal wall had then been temporarily closed with clips until the microcirculatory investigations were started.

Experimental Protocol

After the surgical preparation, a 30-min stabilizing period was provided, followed by baseline measurements. Gradual bleeding was then started. The protocol was divided into seven steps with hemorrhage (T_0-T_6), followed by gradual fluid resuscitation in five steps (T_7-T_{12}), until 80% of the baseline MAP value was reached (**Figure 1A**). The total blood volume (BV) was set as 65 ml kg^{-1}, 5% of the estimated BV was withdrawn (129 ± 8 ml) by the end of each bleeding step, and an equal volume of hydroxyethyl starch (HES; Voluven 6%, 130/0.4; Fresenius Kabi, Bad Homburg, Germany) was administered during each resuscitation step.

Every bleeding or resuscitation interval was started with microcirculatory recordings at the ileal mucosal and serosal surfaces and at the sublingual area. The terminal ileum was positioned on a purpose-built investigation stand. To provide access to the ileal mucosa, a 5-cm antimesenteric incision was made with diathermy 15 cm orally from the ileo-cecal junction. The serosal and mucosal surfaces of the exteriorized ileal section were continuously rinsed with saline. At each location, three, 20-s video recordings were made. Following the intravital videomicroscopic investigations, MAP and SMA flow were recorded, and finally blood samples were taken for lactate, total hemoglobin (tHb), and hematocrit (Hct) determinations. Methane values were continuously recorded throughout the observation period. At the end of the experiments, the animals were sacrificed with an overdose of pentobarbital sodium (120 mg kg^{-1} iv; Sigma-Aldrich Inc., St. Louis, MO, USA). The timeline of measurement intervals is summarized in **Figure 1B**.

Exhaled CH_4 Analysis

We employed a near-infrared laser technique-based PS apparatus (12). PS is a subclass of optical absorption spectroscopy that measures optical absorption indirectly via the conversion of absorbed light energy into acoustic waves due to the thermal expansion of absorbing gas samples. The amplitude of the generated sound is directly proportional to the concentration of the absorbing gas component. The gas sample passes through the photoacoustic cell, in which signal generation takes place, and a microphone then detects the photoacoustic signal produced. The gas samples were taken continuously from the exhalation outlet of the ventilator at a 150 ml min^{-1} rate during the experiments. The baseline exhaled CH_4 values were determined, and the values were thereafter subtracted from the test values. The online-detected methane values were averaged for 60-s periods to be identical with the parallel, 3 × 20-s periods of the microcirculatory analyses.

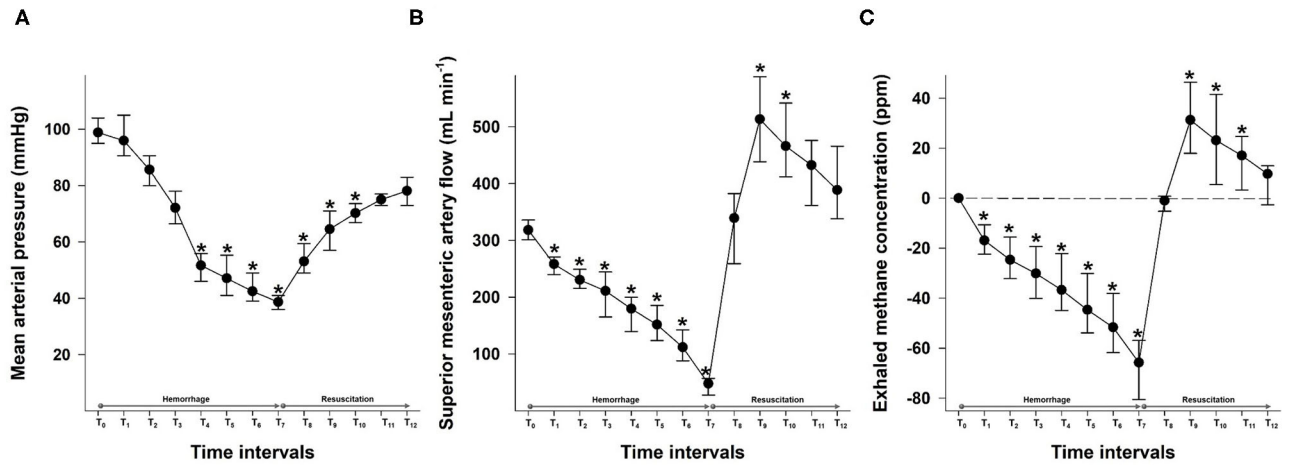

FIGURE 2 | Changes in mean arterial pressure (mmHg) **(A)**, the superior mesenteric artery flow (ml min^{-1}) **(B)**, and exhaled methane levels (ppm) **(C)** during the hemorrhage and resuscitation phases. The plots demonstrate the median and the 25th (lower whisker) and 75th (upper whisker) percentiles. *$p < 0.05$ within group vs. baseline values.

Measurements of Lactate Level, Total Hemoglobin Concentration, and Hematocrit

Changes in tHb, Hct, and lactate concentration were analyzed with a cooximetry blood gas analyzer (Cobas b 123; Roche Ltd., Basel, Switzerland) from the arterial blood samples.

Microcirculation Measurements

The Cytocam-Incident Dark Field (IDF) imaging technique (CytoCam Video Microscope System; Braedius Medical, Huizen, The Netherlands) was used to visualize and evaluate the microcirculation of the ileal serosal and mucosal layers and the sublingual area. IDF imaging is optimized to visualize the hemoglobin-containing structures by illuminating the organ surface with linearly polarized light (16).

Images of empty ileum segment microcirculation (serosal and mucosal surfaces) and sublingual microcirculation were recorded in three, 20-s, high-quality video clips per location by the same investigator, and records were saved as digital AVI-DV files to a hard drive. Every video clip was evaluated offline using analyzing software (AVA 3.0; Automated Vascular Analysis, Academic Medical Center, University of Amsterdam).

The capillaries (with diameter $<20\,\mu m$) were categorized by sight as capillaries with no flow, sluggish flow, or continuous flow. The number of intersections of capillaries with at least sluggish flow with three equidistant horizontal and three equidistant vertical lines was counted and was manually entered in the corresponding tool in the analyzing software to calculate the De Backer score (DBS). The microvascular flow index (MFI) was determined in four quadrants of a record according to the score system defined by the MFI evaluation tool in the analyzing software: no flow (1), sluggish flow (2), or continuous flow (3). The final MFI value of a record was the average for the MFI of the four quadrants. The microvascular heterogeneity index (HI) was calculated as the difference between the highest and lowest MFIs of the three records divided by the mean MFI value of the same three videos (17). Blinded evaluation was performed by two investigators (NV and AG).

Statistical Analysis

Data analysis was performed with a statistical software package (SigmaStat for Windows; Jandel Scientific, Erkrath, Germany). Normality of data distribution was analyzed with the Shapiro–Wilk test. The Friedman on ranks or one-way repeated measures analysis of variance (ANOVA) was applied within groups. Time-dependent differences from the baseline for each group were assessed with Dunn's method or the Bonferroni *t*-test. Differences among groups were analyzed with the Kruskal–Wallis one-way ANOVA on ranks, followed by Dunn's method. Median values and 75th and 25th percentiles are provided in the figures; *p* values < 0.05 were considered significant. Correlations between two variables were examined using Pearson's correlation coefficient (r) or Spearman's rank correlation coefficient (ρ); regression lines and 95% confidence intervals are provided in the figures.

RESULTS

Systemic Effects of Gradual Bleeding and Resuscitation: Changes in MAP

After the bleeding, MAP significantly decreased by T_3 (20% of blood loss) and remained significantly lower until the end of the hemorrhage phase. During the resuscitation period, it remained significantly lower than the control values until T_{10}, at which the volume of fluid replacement was equal to 15% of the estimated BV. By the end of the resuscitation phase, MAP reached 80% of the baseline value, as planned (**Figure 2A**).

The plasma lactate level was increased significantly by T_6 (30% blood loss) and remained significantly higher than the baseline value until T_{11}. The bleeding and fluid resuscitation caused a continuous decrease in both tHb and Hct values. A significant

TABLE 1 | The effects of the hemorrhage and resuscitation phases on blood lactate (mmol L^{-1}), Hct (%), and tHb (g dl^{-1}).

	Parameters	Lactate	tHb	Hct
Hemorrhage phase				
T_0	Median	2.25	11.92	33.25
	p25; p75	1.97; 2.43	9.7; 13.4	27.75; 38.1
T_1	Median	2.69	11.8	33.7
	p25; p75	2.2; 2.83	9.45; 12.9	28.25; 36.78
T_2	Median	2.91	11.13	32.1
	p25; p75	2.73; 3.2	9.0; 12.4	26.9; 35.2
T_3	Median	3.11	11.04	31.4
	p25; p75	2.77; 3.5	9.02; 12.02	25.7; 33.8
T_4	Median	3.675	10.58	29.89
	p25; p75	3.438; 4.03	8.8; 11.45	25.5; 32.68
T_5	Median	4.41	10.36	29.1
	p25; p75	4.27; 4.53	8.55; 11.3	24.9; 31.6
T_6	Median	5.42*	10.11*	26.1*
	p25; p75	4.65; 6.05	8.28; 10.85	23.38; 29.63
Resuscitation phase				
T_7	Median	6.71*	8.66*	23.68*
	p25; p75	5.88; 7.3	7.43; 10.48	20.9; 28.82
T_8	Median	6.33*	7.99*	21.97*
	p25; p75	5.63; 7.0	7.05; 10.23	19.45; 27.97
T_9	Median	5.4*	7.5*	20.56*
	p25; p75	5.13; 6.1	6.58; 9.68	18.57; 26.2
T_{10}	Median	4.65*	7.29*	18.8*
	p25; p75	4.425; 5.4	6.6; 8.98	16.55; 24.0
T_{11}	Median	4.418*	6.9*	17.38*
	p25; p75	3.9; 4.85	5.85; 8.2	15.43; 21.88
T_{12}	Median	3.95	6.75*	16.37*
	p25; p75	3.55; 4.85	5.7; 7.87	14.4; 20.77

The table demonstrates the median values and the 25th and 75th percentiles.
$^*p < 0.05$ vs. baseline values.

difference from the baseline values was observed at T_6 in the case of both parameters. tHb was raised by more than 3 g dl^{-1} until the end of the hemorrhage phase (M = 11.92; p25 = 9.7; p75 = 13.4 g dl^{-1} vs. M = 8.66; p25 = 7.43; p75 = 10.48 g dl^{-1}), which indicates severe bleeding (**Table 1**).

Mesenteric Macrohemodynamics

The SMA flow decreased continuously during the hemorrhage phases. An early, significant drop was already noted at a 5% loss (T_1) of the estimated BV. After fluid resuscitation, the MAP started to increase steeply and reached its peak value at the second resuscitation step at T_8. During the following parts of the resuscitation phase, it decreased gradually to the level of the baseline values (**Figure 2B**).

Changes in Exhaled Methane Levels

The average for baseline exhaled methane was 60.9–90.1 ppm, which corresponds to the higher range of values measured in methane-producing humans (9). The individual baseline data were subtracted from the test values to increase the comparability of measurements even in the case of larger individual variances (13).

The exhaled methane concentration decreased significantly after 5% blood loss, already at T_1, similarly to the SMA flow changes. After resuscitation was started, breath methane level rapidly increased to a significantly higher level than the baseline and reached a peak after a fluid volume equal to 10% of the estimated BV, administered at the T_8 period (**Figure 2C**).

Changes in Sublingual and Ileal Microcirculation

The DBS values decreased significantly as the bleeding progressed. The serosal DBS was lower than the baseline value from a 10% blood loss (T_2). This was followed by a deterioration of mucosal DBS from the loss of 20% of the estimated BV (T_4), whereas the decrease of DBS in the sublingual area was statistically significant from a 25% blood loss only (T_5). Moreover, the sublingual DBS was significantly higher than the values in the ileal regions from T_5 to T_7, which marks the end of the hemorrhage phase and a loss of 35% of BV. When fluid resuscitation started, the mucosal DBS increased rapidly and was significantly higher than the serosal and sublingual values after fluid replacement with a volume equal to 5% of BV (T_8), reaching the highest value at T_{10}. The serosal DBS values increased more gradually with a maximum at T_{12} (**Figure 3A**).

Bleeding caused a decrease in the MFI in all three locations, and the first to reach significance was the MFI in the sublingual area at T_3. This was followed by a significant decrease in serosal MFI from T_4 and in mucosal MFI from T_5. The fluid resuscitation resulted in a significant improvement of the MFI in all investigated locations. Sublingual MFI was significantly higher than the MFI in the ileal mucosa and serosa from T_{10} (**Figure 3B**).

The heterogeneity of the microcirculation increased during the hemorrhage phase as shown by the HI. The most important difference between the sublingual and ileal regions is that while the sublingual HI was restored during resuscitation, the HI in both the ileal mucosa and serosa remained significantly higher than the baseline and the sublingual values until the end of the experiments (**Figure 3C**).

Link Between Changes in Exhaled Methane Concentration and Mesenteric Macro- and Microperfusion

We compared the changes in the exhaled methane concentration during the whole observation period with SMA flow data (r = 0.93; **Figure 4A**). Moreover, we investigated the association separately in the hemorrhage phase (r = 0.82; **Figure 4B**) and in the resuscitation phase as well (r = 0.79; **Figure 4C**). When the possible links between the changes in exhaled methane levels and the DBS values of the two components of the ileal microcirculation during the hemorrhage and resuscitation were investigated, the DBS in the serosa correlated significantly with the exhaled methane values during the experiments (ρ = 0.78; **Figure 5A**). When separately investigated, the correlation could be shown in both the bleeding phase (r = 0.79; **Figure 5B**) and

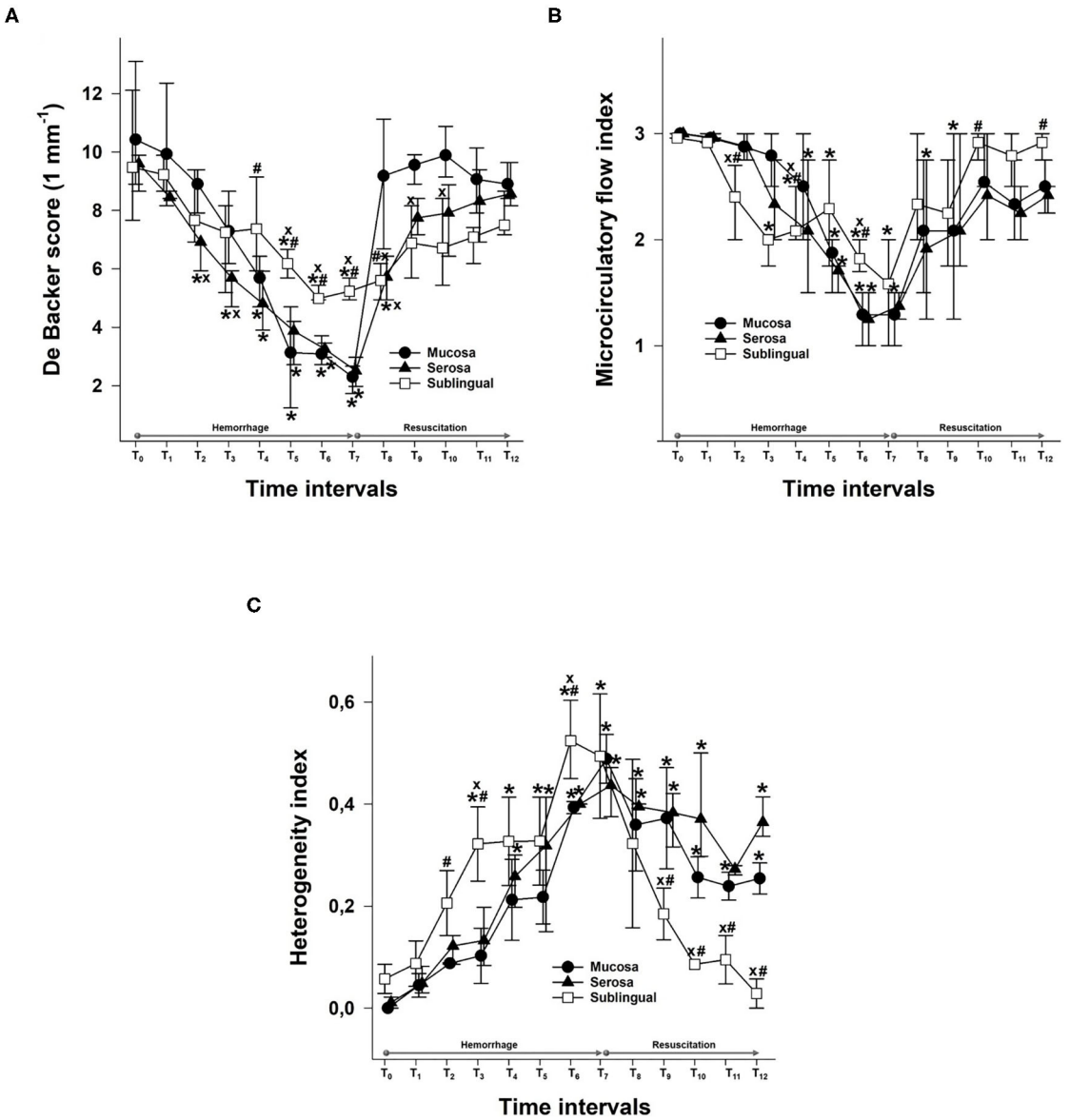

FIGURE 3 | Changes in De Backer score (1 mm^{-1}) values **(A)**, the microvascular flow index **(B)**, and the heterogeneity index **(C)** for the mucosa (black circles) and serosa in the ileum (black triangle) and sublingual area (empty square) during the hemorrhage and resuscitation phases. The plots demonstrate the median values and the 25th (lower whisker) and 75th (upper whisker) percentiles. $^{x}p < 0.05$ mucosa or sublingual values vs. serosa values; $^{\#}p < 0.05$ serosa or sublingual values vs. mucosa values; $^{*}p < 0.05$ vs. baseline values.

the fluid resuscitation period ($\rho = 0.52$; **Figure 5C**). Similarly, a significant correlation was present in the case of the mucosal DBS values when the whole data set was analyzed ($r = 0.77$; **Figure 6A**) and also when data were separated to the hemorrhage ($r = 0.82$; **Figure 6B**) and resuscitation phases ($\rho = 0.63$; **Figure 6C**). Phases are shown to demonstrate the changes in exhaled methane concentrations and the DBS of the ileal mucosa on an original methane registration curve of a single animal and the simultaneous changes in the SMA flow and mucosal DBS in the same animal during hemorrhage and resuscitation (**Figure 7**).

Correlations Between Sublingual and Ileal Mucosal or Serosal Microcirculation

Significant correlations were detected during the hemorrhage phase between the sublingual DBS and the serosal or mucosal DBS values ($r = 0.74$ and $r = 0.66$, respectively; **Figures 8A,B**).

DISCUSSION

We used continuous, real-time detection of exhaled methane concentration to investigate the link to the macro- and

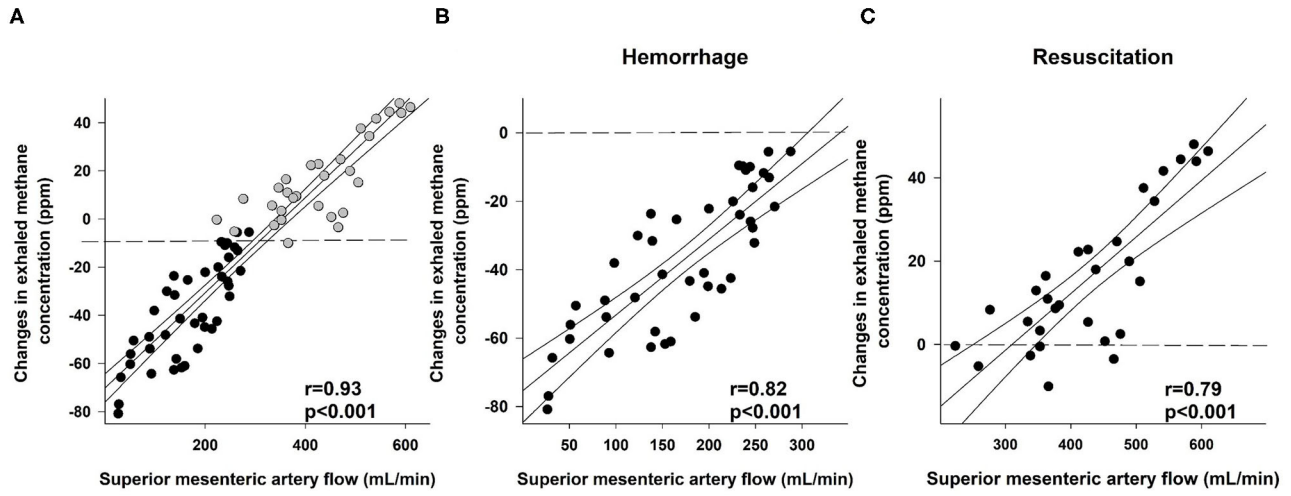

FIGURE 4 | Correlation between superior mesenteric artery flow (ml min^{-1}) and changes in exhaled methane concentration (ppm) during the whole course of experiments (**A**; black scatters show the data collected during bleeding, and gray scatters show the data recorded during resuscitation), the hemorrhage (**B**; black scatters) and resuscitation phases (**C**; black scatters). The plot demonstrates the regression line (black line) and corresponding *r* values as indicators of the strength of the linear correlation and *p* significance values.

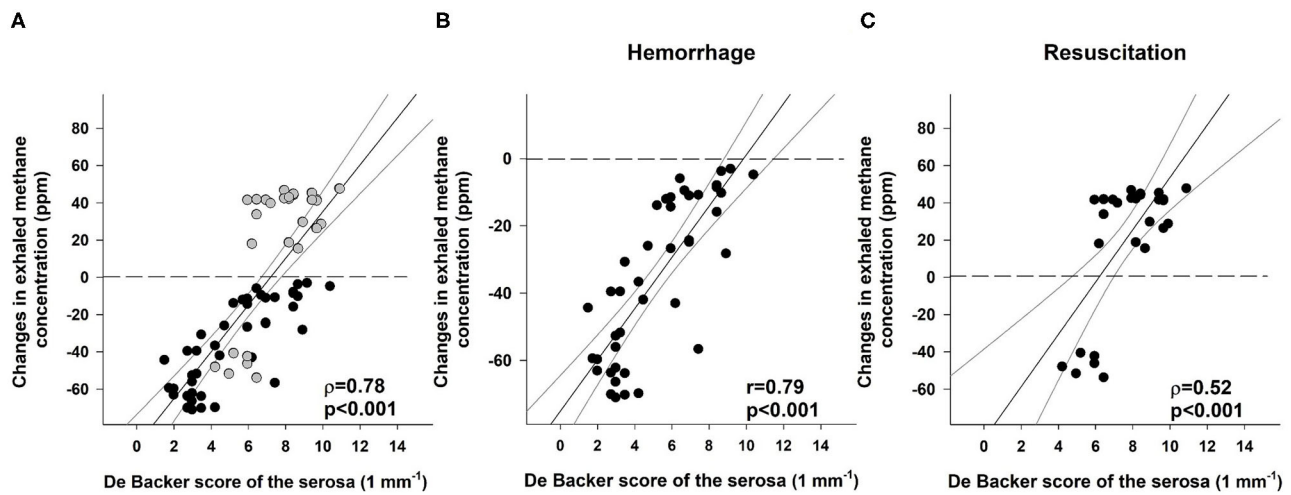

FIGURE 5 | Correlation between the De Backer score (1 mm^{-1}) for the serosa and changes in exhaled methane concentration (ppm) during the whole course of experiments (**A**; black scatters show the data collected during bleeding, and gray scatters show the data recorded during resuscitation), the hemorrhage (**B**; black scatters) and resuscitation phases (**C**; black scatters). The plot demonstrates the regression line (black line) and corresponding *r* and ρ values as indicators of the strength of the linear correlation and p significance values.

microvascular components of the mesenteric circulation during and after hemorrhage. The changes in SMA flow developed earlier than systemic hemodynamic or Hct responses, and the changes in exhaled methane levels strictly followed the mesenteric alterations. Therefore, we propose that monitoring methane in the exhaled air may be an early warning tool to recognize internal hemorrhage. Moreover, exhaled methane monitoring can provide information to estimate the condition of the microcirculatory part of the mesenteric region during bleeding, and it is capable of following the sudden changes during the very early phase of fluid resuscitation. Nonetheless, we are aware that an important limitation is the detection of baseline values in certain clinical situations. Here, it should be noted that real-time breath methane monitoring technique may increase the diagnostic potential of previous, traditional methods. This approach is based on dynamic, constant tracking instead of detection static values in a given time. Any observation (increase or decrease) can direct the attention toward a possible disturbance of the mesenteric circulation.

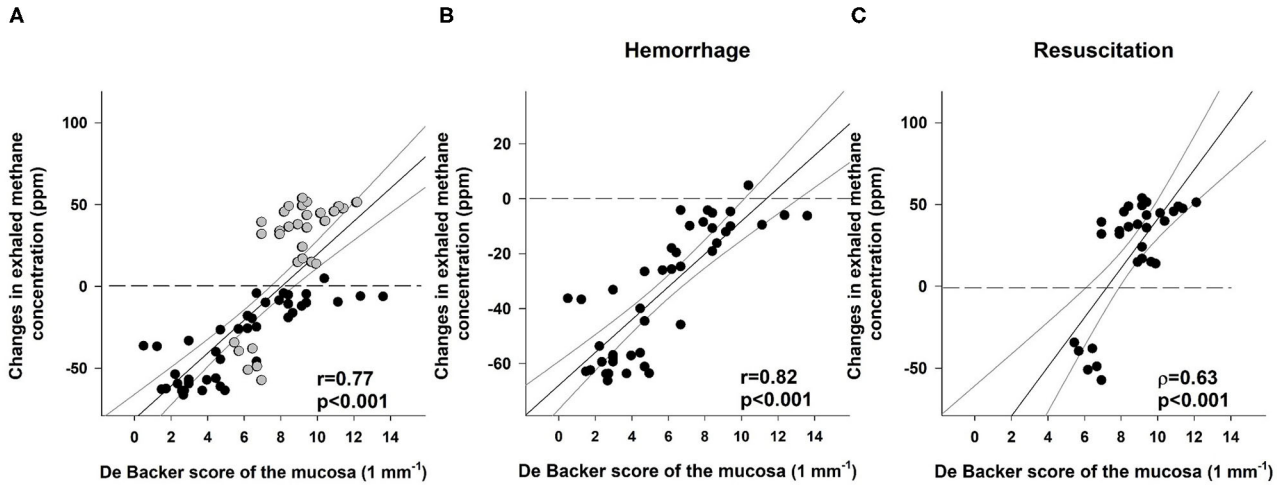

FIGURE 6 | Correlation between the De Backer score (1 mm^{-1}) for the mucosa and changes in exhaled methane concentration (ppm) during the whole course of experiments (**A**; black scatters show the data collected during bleeding, and gray scatters show the data recorded during resuscitation), the hemorrhage (**B**; black scatters) and resuscitation phases (**C**; black scatters). The plot demonstrates the regression line (black line) and corresponding **r** and ρ values as indicators of the strength of the linear correlation and p significance values.

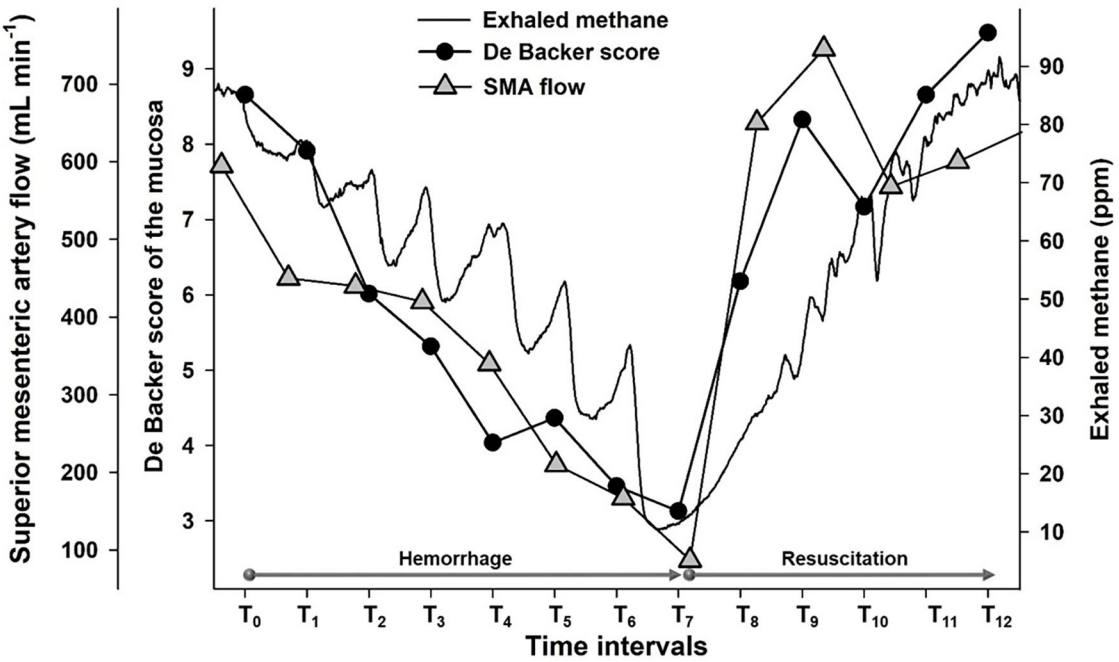

FIGURE 7 | Original tracings representing changes in exhaled methane levels (ppm) (continuous black line), the De Backer score (1 mm^{-1}) for ileal mucosa (black circles) and superior mesenteric artery flow (ml min^{-1}) (gray triangle) of an individual animal.

The methane breath test is already used to diagnose certain GI disorders. In human clinical laboratory practice, breath methane levels are usually determined by a lactulose test and sampling of breath air in gas-tight bags, which are then analyzed by GC, equipped with either flame ionization, thermal conductivity, or mass spectrometry detectors (18). Here, it should be noted that the sampling frequency of these traditional methods is limited. Our approach is somehow different; in contrast to the GC technique, PAS provides the option to follow real-time changes at a sensitivity threshold <1 ppm compared with the 3 ppm sensitivity threshold of the presently available GC instruments. With this method, the dynamics of exhaled methane

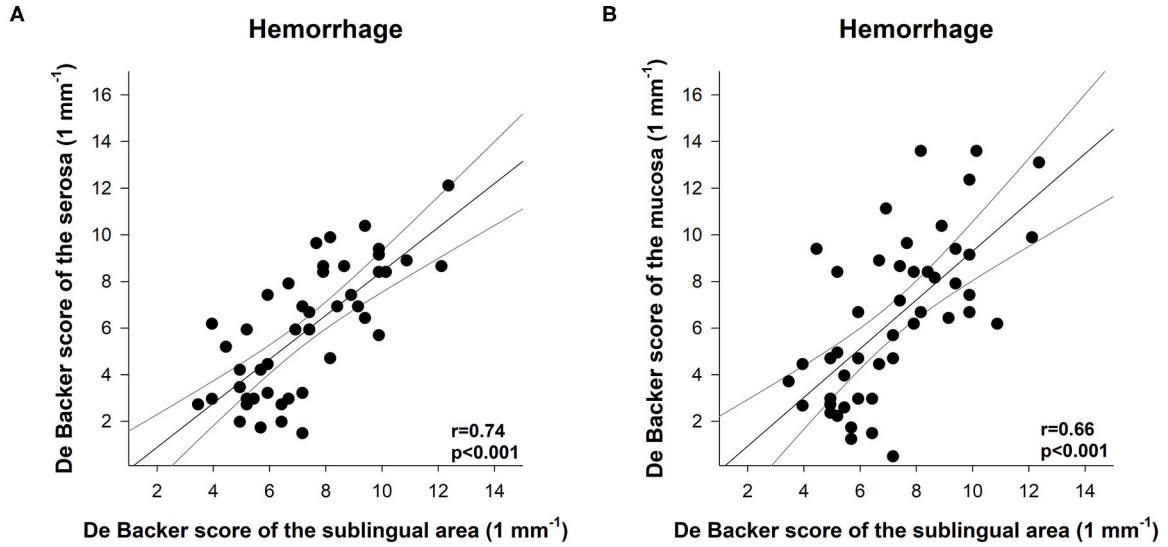

FIGURE 8 | Correlation between the De Backer score (1 mm^{-1}) for the serosa **(A)** or mucosa **(B)** and the De Backer score (1 mm^{-1}) for the sublingual area during the hemorrhage phase. The plot demonstrates the regression line (gray line) and corresponding (black scatters) *r* values as an indicator of the strength of the linear correlation and *p* significance values.

concentrations can also be followed in single breath sample analyses (12).

We used an anesthetized, acute pig model for a gradual, relatively low rate (5% loss of BV in each step), but severe hemorrhage was followed by a controlled, gradual and restricted (80% of the baseline MAP) fluid resuscitation. The total BV loss was set at 35%, which resulted in an approximately 3 g dl^{-1} loss of tHB, confirming the severity of the bleeding. The low rate provided a good temporal resolution with the possibility of seven measurement intervals during the hemorrhage phase and five intervals until the goal MAP was reached in the resuscitation phase. We decided to use HES as resuscitation fluid, as it was expected to provide pronounced macrohemodynamic changes and was also capable of restoring intestinal microcirculation (19).

As expected, the SMA blood flow was affected very early, already significantly decreased after 5% blood was withdrawn. Changes in the exhaled methane concentration followed the decrease with the same dynamics. Significant changes in the DBS of the serosal and mucosal components of the ileal microcirculation occurred slightly later, after a 10 or 20% blood loss, respectively. The difference between the mesenteric macro- and microcirculation might be explained by a possible autoregulation of mesenteric microperfusion (20), whereas the delay between the mucosal and serosal microcirculatory changes may be a result of the phenomenon of microcirculatory redistribution, which supports the oxygenation of the mucosa at the price of reduced serosal perfusion (21). The earlier decrease of the exhaled methane level might indicate a reduced absolute volume of the perfused blood, without the decrease of perfused capillary density.

At the beginning of the resuscitation phase (T_7-T_8), a sudden increase in the SMA flow and mucosal DBS and a rise in exhaled methane levels were observed. However, by the end of the experiments, the exhaled methane and SMA flow values decreased, and no significant difference could be detected compared with the baseline values. The DBS of both the mucosal and serosal areas remained steady during the whole resuscitation phase, and no decrease was observed in the last two resuscitation intervals. Nonetheless, the HI was increased by the end of the hemorrhage phase and remained elevated during the entire resuscitation phase, which suggests that the microcirculation was not completely restored by the fluid replacement and might explain the methane decrease after the initial peak.

The microcirculation of the sublingual area is frequently investigated, as it is considered a suitable GI region for non-invasive approaches, assuming that the changes might indicate the condition of the microcirculation in more distal sections, such as the ileum. Indeed, earlier studies demonstrated that tissue carbon dioxide pressure in the sublingual area is tied to changes in the small intestinal microcirculation in a hemorrhagic shock and fluid resuscitation model (22). In the present study, we could not detect a correlation between the sublingual microcirculation and the serosal or mucosal components of ileal microperfusion in the resuscitation phase, and this finding highlights the difference between the two methods. An investigation of the sublingual area is capable of following the GI microcirculatory changes in a wider timeframe only, and this is not affected by an increase in the sampling frequency because of the inertia between the sublingual and more distal microcirculatory regions. On the other hand, the dynamics of the changes in the exhaled methane concentrations were similar to those of the changes in the mesenteric circulation. Real-time monitoring of exhaled methane level was capable

of following the sudden changes observed at the very early resuscitation phase.

However, the changes of methane levels increased with a slightly lower rate following the microcirculatory changes during the resuscitation phase than in the hemorrhage period. The lower correlation coefficients between exhaled methane levels and serosal or mucosal DBS values also refer to the role of the characteristics of the changes of the mesenteric perfusion. The different kinetics of the relationship of exhaled methane levels and microcirculatory changes might be explained by the rapid improvement of the microperfusion at the early phase of resuscitation. We suggest a two-compartment model, in which the lumen and the wall of the intestines is one of the components, and the circulating blood is the other part. In this case, the disproportionate increase in the blood flow and methane access to the circulatory compartment may explain the lower than expected exhaled methane output during the resuscitation phase.

In conclusion, changes in exhaled methane concentration may indicate bleeding at an early stage and follow changes in mesenteric perfusion during hemorrhage and resuscitation as well, with a diagnostic value comparable to the monitoring of the sublingual microcirculatory area. It might be a useful, additional non-invasive tool in cases where hemorrhagic complications might be expected; however, even in its current form, the technique might contribute to acquiring additional information on the mesenteric circulation in experimental setups.

DATA AVAILABILITY STATEMENT

The raw data supporting the conclusions of this article will be made available by the authors, without undue reservation.

ETHICS STATEMENT

The animal study was reviewed and approved by National Scientific Ethical Committee on Animal Experimentation (National Competent Authority of Hungary).

AUTHOR CONTRIBUTIONS

AB, GV, MB, and DÉ performed experiments and wrote the manuscript. AR performed experiments and figures. NV and ÁG prepared figures and evaluated microcirculatory records. GV, DÉ, and MB supervised and edited the manuscript. AS and ÁM designed and constructed the photoacoustic spectroscopy device and supervised the manuscript. All authors contributed to the article and approved the submitted version.

FUNDING

This study was supported by the Hungarian National Research, Development and Innovation Office grants NKFIH-K120232 and NKFIH-K116861 as well as GINOP-2.3.2-15-2016-00015 and EFOP-3.6.2-16-2017-00006. University of Szeged Open Access Fund 4749 and FIKP programme grant (TUDFO/47138-1/2019-ITM).

ACKNOWLEDGMENTS

The authors are grateful to Andrea Bús, Csilla Mester, Nikolett Beretka, Bence Gyorfi, and Péter Sárkány for their skillful assistance.

REFERENCES

1. Kassavin DS, Kuo Y-H, Ahmed N. Initial systolic blood pressure and ongoing internal bleeding following torso trauma. *J Emerg Trauma Shock.* (2011) 4:37–41. doi: 10.4103/0974-2700.76833
2. Kumar Y, Hooda K, Li S, Goyal P, Gupta N, Adeb M. Abdominal aortic aneurysm: pictorial review of common appearances and complications. *Ann Transl Med.* (2017) 5: doi: 10.21037/atm.2017.04.32
3. Lim C, Dokmak S, Farges O, Aussilhou B, Sauvanet A, Belghiti J. Reoperation for post-hepatectomy hemorrhage: increased risk of mortality. *Langenbecks Arch Surg.* (2014) 399:735–40. doi: 10.1007/s00423-014-1189-3
4. Stollman N, Metz DC. Pathophysiology and prophylaxis of stress ulcer in intensive care unit patients. *J Crit Care.* (2005) 20:35–45. doi: 10.1016/j.jcrc.2004.10.003
5. Tasu J-P, Vesselle G, Herpe G, Ferrie J-C, Chan P, Boucebci S, et al. Postoperative abdominal bleeding. *Diagn Int Imaging.* (2015) 96:823–31. doi: 10.1016/j.diii.2015.03.013
6. Kim BSM, Li BT, Engel A, Samra JS, Clarke S, Norton ID, et al. Diagnosis of gastrointestinal bleeding: a practical guide for clinicians. *World J Gastrointest Pathophysiol.* (2014) 5:467–78. doi: 10.4291/wjgp.v5.i4.467
7. Chung KK, Ryan KL, Rickards CA, Hinojosa-Laborde C, Pamplin JC, Patel SS, et al. Progressive reduction in central blood volume is not detected by sublingual capnography. *Shock.* (2012) 37:586–91. doi: 10.1097/SHK.0b013e318252da82
8. Edul VSK, Ince C, Navarro N, Previgliano L, Risso-Vazquez A, Rubatto PN, et al. Dissociation between sublingual and gut microcirculation in the response to a fluid challenge in postoperative patients with abdominal sepsis. *Ann Intens Care.* (2014) 4:39. doi: 10.1186/s13613-014-0039-3
9. Levitt MD, Furne JK, Kuskowski M, Ruddy J. Stability of human methanogenic flora over 35 years and a review of insights obtained from breath methane measurements. *Clin Gastroenterol Hepatol.* (2006) 4:123–9. doi: 10.1016/j.cgh.2005.11.006
10. Szabó A, Unterkofler K, Mochalski P, Jandacka M, Ruzsanyi V, Szabó G, et al. Modeling of breath methane concentration profiles during exercise on an ergometer. *J Breath Res.* (2016) 10:017105. doi: 10.1088/1752-7155/10/1/017105
11. Ngai AKY, Persijn ST, Basum G von, Harren FJM. Automatically tunable continuous-wave optical parametric oscillator for high-resolution spectroscopy and sensitive trace-gas detection. *Appl Phys B.* (2006) 85:173–80. doi: 10.1007/s00340-006-2362-3
12. Tuboly E, Szabó A, Eros G, Mohácsi Á, Szabó G, Tengölics R, et al. Determination of endogenous methane formation by photoacoustic spectroscopy. *J Breath Res.* (2013) 7:046004. doi: 10.1088/1752-7155/7/4/046004
13. Szucs S, Bari G, Ugocsai M, Lashkarivand RA, Lajkó N, Mohácsi Á, et al. Detection of intestinal tissue perfusion by real-time breath methane analysis in rat and pig models of mesenteric circulatory distress. *Crit Care Med.* (2019) 47:e403. doi: 10.1097/CCM.0000000000003659
14. Ince C, Boerma EC, Cecconi M, De Backer D, Shapiro NI, Duranteau J, et al. Second consensus on the assessment of sublingual microcirculation in critically ill patients: results from a task force of the European Society of Intensive Care Medicine. *Intens Care Med.* (2018) 44:281–299. doi: 10.1007/s00134-018-5070-7

15. Scheuzger JD, Zehnder A, Yeginsoy D, Siegemund M. Sublingual microcirculation: a case report. *J Med Case Reports.* (2019) 13:179. doi: 10.1186/s13256-019-2118-4
16. Aykut G, Veenstra G, Scorcella C, Ince C, Boerma C. Cytocam-IDF (incident dark field illumination) imaging for bedside monitoring of the microcirculation. *ICMx.* (2015) 3:4. doi: 10.1186/s40635-015-0040-7
17. De Backer D, Hollenberg S, Boerma C, Goedhart P, Büchele G, Ospina-Tascon G, et al. How to evaluate the microcirculation: report of a round table conference. *Crit Care.* (2007) 11:R101. doi: 10.1186/cc6118
18. Costello BPJ de L, Ledochowski M, Ratcliffe NM. The importance of methane breath testing: a review. *J Breath Res.* (2013) 7:024001. doi: 10.1088/1752-7155/7/2/024001
19. Wu C-Y, Chan K-C, Cheng Y-J, Yeh Y-C, Chien C-T, on behalf of the NTUH Center of Microcirculation Medical Research (NCMMR). Effects of different types of fluid resuscitation for hemorrhagic shock on splanchnic organ microcirculation and renal reactive oxygen species formation. *Crit Care.* (2015) 19:434. doi: 10.1186/s13054-015-1135-y
20. Pestel GJ, Fukui K, Kimberger O, Hager H, Kurz A, Hiltebrand LB. Hemodynamic parameters change earlier than tissue oxygen tension in hemorrhage. *J Surg Res.* (2010) 160:288–93. doi: 10.1016/j.jss.2008.11.002
21. Hiltebrand LB, Krejci V, tenHoevel ME, Banic A, Sigurdsson GH. Redistribution of microcirculatory blood flow within the intestinal wall during sepsis and general anesthesia. *Anesthesiology.* (2003) 98:658–69. doi: 10.1097/00000542-200303000-00014
22. Palágyi P, Kaszaki J, Rostás A, Érces D, Németh M, Boros M, et al. Monitoring microcirculatory blood flow with a new sublingual tonometer in a porcine model of hemorrhagic shock. *BioMed Res Int.* (2015) 2015:e847152. doi: 10.1155/2015/847152

Conflict of Interest: The authors declare that the research was conducted in the absence of any commercial or financial relationships that could be construed as a potential conflict of interest.

frontiers in Medicine

REVIEW
published: 27 October 2020
doi: 10.3389/fmed.2020.585638

Resuscitation After Hemorrhagic Shock in the Microcirculation: Targeting Optimal Oxygen Delivery in the Design of Artificial Blood Substitutes

Carlos Munoz[1†], *Federico Aletti*[1*†], *Krianthan Govender*[1], *Pedro Cabrales*[1] *and Erik B. Kistler*[2,3]

[1] *Department of Bioengineering, University of California, San Diego, La Jolla, CA, United States,* [2] *Department of Anesthesiology and Critical Care, University of California, San Diego, La Jolla, CA, United States,* [3] *Department of Anesthesiology and Critical Care, Veterans Affairs San Diego Healthcare System, San Diego, CA, United States*

OPEN ACCESS

Edited by:
Mihály Boros,
University of Szeged, Hungary

Reviewed by:
Andrea Szabó,
University of Szeged, Hungary
Tommaso Tonetti,
University of Bologna, Italy

***Correspondence:**
Federico Aletti
faletti@eng.ucsd.edu

[†] *These authors have contributed equally to this work and share first authorship*

Specialty section:
This article was submitted to Intensive Care Medicine and Anesthesiology, a section of the journal Frontiers in Medicine

Received: *21 July 2020*
Accepted: *18 September 2020*
Published: *27 October 2020*

Citation:
Munoz C, Aletti F, Govender K, Cabrales P and Kistler EB (2020) Resuscitation After Hemorrhagic Shock in the Microcirculation: Targeting Optimal Oxygen Delivery in the Design of Artificial Blood Substitutes. Front. Med. 7:585638. doi: 10.3389/fmed.2020.585638

Microcirculatory preservation is essential for patient recovery from hemorrhagic shock. In hemorrhagic shock, microcirculatory flow and pressure are greatly reduced, creating an oxygen debt that may eventually become irreversible. During shock, tissues become hypoxic, cellular respiration turns to anaerobic metabolism, and the microcirculation rapidly begins to fail. This condition requires immediate fluid resuscitation to promote tissue reperfusion. The choice of fluid for resuscitation is whole blood; however, this may not be readily available and, on a larger scale, may be globally insufficient. Thus, extensive research on viable alternatives to blood has been undertaken in an effort to develop a clinically deployable blood substitute. This has not, as of yet, achieved fruition, in part due to an incomplete understanding of the complexities of the function of blood in the microcirculation. Hemodynamic resuscitation is acknowledged to be contingent on a number of factors other than volume expansion. The circulation of whole blood is carefully regulated to optimize oxygen delivery to the tissues *via* shear stress modulation through blood viscosity, inherent oxygen-carrying capacity, cell-free layer variation, and myogenic response, among other variables. Although plasma expanders can address a number of these issues, hemoglobin-based oxygen carriers (HBOCs) introduce a method of replenishing the intrinsic oxygen-carrying capacity of blood. There continue to be a number of issues related to HBOCs, but recent advances in the next-generation HBOCs show promise in the preservation of microcirculatory function and limiting toxicities. The development of HBOCs is now focused on viscosity and the degree of microvascular shear stress achieved in order to optimize vasoactive and oxygen delivery responses by leveraging the restoration and maintenance of physiological responses to blood flow in the microcirculation. Blood substitutes with higher viscous properties tend to improve oxygen delivery compared to those with lower viscosities. This review details current concepts in blood substitutes, particularly as they relate to trauma/hemorrhagic shock, with a specific focus on their complex interactions in the microcirculation.

Keywords: hemorrhagic shock, resuscitation, microcirculation, blood substitutes, viscosity, oxygen delivery, shear stress

INTRODUCTION

Strategies for reperfusion after hemorrhage are typically aimed at the restoration of systemic hemodynamic indices such as blood pressure, heart rate, and venous return. Commensurate improvements in organ function such as mental status and urine output serve as crude confirmation that end-organ perfusion is preserved. However, the mechanisms that determine survival and recovery after hemorrhagic shock ultimately occur in the microcirculation, a milieu of which there is little understanding and no direct ability to control or modulate. There exists, therefore, a disconnect between the clinical interventions that are applied to treat hemorrhagic shock and the downstream consequences of these interventions in the microcirculation (1).

Microvascular dysfunction associated with hemorheological alterations results in oxidative stress, release of proinflammatory cytokines (2), and disruption of endothelial integrity (specifically the endothelial glycocalyx). Given the importance and delicate nature of the endothelium integrity and its physiological function in the microcirculation, its protection may prove a promising target in critical care settings. Previous *in vitro* studies showed that shear significantly increased glycosaminoglycan synthesis in endothelial cells (3). Fluid shear stress on the endothelium modifies the organization of inter-endothelial junctions (4) and can alter the barrier properties of the endothelium by activating intracellular signaling events (3–5). The glycocalyx represents a major barrier against the extravasation of fluids and colloids; sieving and binding of intravascular colloids from the plasma restrict transport of other plasma molecules (6). Thus, the endothelial glycocalyx is better preserved when the appropriate fluid is used during resuscitation from hemorrhagic shock (HS).

Fluid resuscitation is used to restore/preserve blood volume. Colloidal resuscitation fluids stabilize hydrostatic capillary pressure, which is required to preserve functional capillary density (FCD) (7). FCD determines the serum lactate levels and acid–base balance and is critical for tissue survival after HS (8). We demonstrated that the maintenance of adequate FCD is directly related to capillary pressure, which can be preserved by increasing plasma viscosity using high-viscosity resuscitation fluids (9). Hemodilution with high-viscosity resuscitation fluids (with viscosities of 4 cP) does not increase diluted blood viscosity above that of undiluted whole blood, but it increases plasma viscosity and endothelial wall shear stress, thus promoting the production of shear stress-mediated vascular autocoids [e.g., nitric oxide (NO) and prostaglandins] (10). These autocoids cause vasodilation and increase microvascular blood flow, which increases oxygen (O_2) delivery without increasing the O_2-carrying capacity (11).

The cornerstone for resuscitation after hemorrhage is blood, either whole blood as is now increasingly being practiced in both military and civilian trauma settings (low-titer type O-positive whole blood) or, more commonly, blood component therapy in the form of packed red blood cells (PRBCs), fresh frozen plasma (FFP), and platelets. The critical issue with the use of blood as the first line of treatment in trauma and hemorrhagic shock (T/HS) is its availability from donors. In an effort to develop usable alternatives, artificial blood substitutes—tacitly defined as alternatives to red blood cells (RBCs), not plasma or platelets—have been studied for many years. A major barrier to progress in this area has been the lack of a mechanistic understanding of the processes associated with oxygen transport by blood and the physiological interaction of blood and the tissue as a system in the microcirculation.

Blood substitutes have the potential to be engineered in such a way as to replicate or even optimize the critical biophysical parameters of circulating blood, enabling the production of life-sustaining product for critical patient needs. In order to develop a successful blood substitute for T/HS, however, an improved understanding of the role of blood is necessary.

The most important biophysical parameter of the interaction between blood and tissues at the microvascular level is blood viscosity, which is significantly altered in hemorrhagic shock because of hemodilution and reduced hematocrit, with a direct impact on microvascular function.

In order to design efficient blood substitutes able to fulfill the metabolic demands of tissues during resuscitation, key alterations induced in the microcirculation by T/HS should be analyzed from the point of view of their impact on viscosity. Therefore, optimizing viscosity should become the new paradigm in the design of next-generation blood substitutes.

TRANSFUSION MEDICINE: MIMICKING THE BLOOD TO PRESERVE OXYGEN DELIVERY TO THE TISSUES

Demand for whole blood and components is presently satisfied by donor blood, a source that is projected to become increasingly scarce and ultimately insufficient for healthcare needs as the proportion of older individuals increases in the United States and worldwide (12). Advances in recombinant technology and stem cell manipulation may be able to correct some of the projected deficits in blood product inventories; however, the technology required to produce a useable product in the quantities needed is not presently available at costs affordable by the health care system (13).

Although component therapy is much more versatile than whole blood resuscitation, which is hampered by shorter storage times (21–35 days depending on anticoagulant, e.g., citrate phosphate dextrose vs. citrate phosphate dextrose adenine) because of the necessary dilution of blood factors for storage, resuscitation at the recommended 1:1:1 ratio (PRBCs/FFP/platelets) results in a resuscitation fluid diluted to a hematocrit (Hct) of ∼29%, platelet concentration of 88,000/mcl, and 65% of the normal coagulation factor activity, all substantially inferior to component concentrations in whole blood. Of potential importance is that the viscosity, as well as the oxygen-carrying capacity of the 1:1:1 ratio, is markedly reduced compared to that of whole blood.

Blood substitutes are engineered as resuscitation fluids which ideally mimic the main functions of biological blood to target hypoxic tissue caused by shock. Because oxygen delivery to tissues has historically been considered to be the goal of blood substitutes, most research done on blood alternatives has been

hemoglobin (Hb) based. Blood substitutes that leverage Hb as the method to sustain the oxygen-carrying capacity (O_2CC) are known as hemoglobin-based oxygen carriers (HBOCs). However, circulating cell-free Hb has been associated with a number of adverse outcomes, including inflammation, thrombosis, oxygen free radical generation via its heme moiety, kidney failure through glomerular compromise, and hypertension and vessel constriction NO scavenging (14). In fact, the U.S. Food and Drug Administration (FDA) stipulates that any proposed blood substitutes specifically address the issue of NO scavenging as part of their approval process.

To circumvent limitations inherent using free Hb as a blood substitute, several different variations of HBOCs have been designed, including alpha-alpha cross-linked Hb (ααHb) (15), polyethylene glycol-bound Hb (PEG-Hb) (16), and polymerized hemoglobin (polyHb) (17). However, none of these has been proven effective as a replacement for blood or blood products. Non-Hb-containing modalities have been studied as well, such as perfluorocarbons (PFCs), a class of compounds that readily bind both oxygen and carbon dioxide. The discovery that PFCs could dissolve a comparatively large amount of oxygen, albeit at high oxygen partial pressures, suggested using this vehicle as blood substitute. PFCs have a number of potential advantages over HBOCs, most notably their lack of potential infectivity and their ability to be mass produced as synthetic compounds (18). However, the use of PFC-based blood replacement fluids has not materialized, in part because of the lack of definitive experimental studies on the physiology related to altered blood physical properties and changes in the distribution of oxygen partial pressures in the circulation.

To date, there are virtually no viable alternatives to hemoglobin for oxygen transport from the lungs to the tissues because of the ability of hemoglobin to bind a large amount of oxygen *via* a chemical reaction. Thus, hemoglobin is still the key constituent of presently designed oxygen-carrying blood substitutes. Various modifications and formulations continue to optimize its performance and have largely eliminated inherent toxicities, but continued development of HBOCs requires addressing the underlying issues of microcirculatory dysfunction, especially during T/HS.

MICROVASCULAR PATHOPHYSIOLOGY IN HEMORRHAGIC SHOCK

The blood that circulates through the body conducts a number of functions that are essential for survival, such as perfusing tissues with oxygen, collecting waste products of metabolism, and maintaining an acceptable pH via CO_2 offloading. In the event of severe blood loss, the intrinsic O_2CC of the microcirculation begins to falter as the concentration of RBCs declines. The drop in blood pressure caused by hemorrhage results in a fall of the hydrostatic pressure at the arteriolar end of the capillaries. This reduced pressure head affects fluid movement across the capillary bed, promoting reabsorption. With the pooling of fluid in the vasculature to maintain fluid flow, the concentration of RBCs is further diluted. A myogenic response takes place, causing an inward remodeling of the vessels and vasoconstriction (9). There are many local regulatory mechanisms that respond during hypovolemic shock in a tissue-dependent manner. For example, adenosine and prostanoids together are responsible for most of the dilation in femoral resistance vessels (19), while the myogenic response is dominant in other tissues like the kidney (20). While local flow regulatory mechanisms are important determinants of blood flow to individual organs, the central nervous system also exerts an important influence through sympathetic nerves in most organs (21). Some of the most striking changes seen at the tissue level due to severe shock are a reduction in O_2CC, a decrease in blood viscosity, a decrease in vessel wall shear stress (WSS), shedding of the protective glycocalyx barrier (22), and pathologic hyperfibrinolysis and diffuse coagulopathy (23–25).

T/HS also takes a toll at the cellular level. With the decrease in tissue perfusion, anaerobic metabolism becomes the key source of energy production. Diminished O_2 delivery to cells results in the shunting of pyruvate to increase lactate production at the expense of oxidative phosphorylation. Since cellular respiration is the key metabolic process that produces ATP to fuel tissues and a lack of oxygen shunts energy production anaerobically, a primary metabolite is lactate, whose plasma levels rise in consequence of this metabolic alteration. Inadequate aerobic cellular respiration ultimately leads to mitochondrial dysfunction (26). As ATP supplies dwindle, cellular homeostasis ultimately fails, and cell death ensues through necrosis from membrane rupture, apoptosis, or necroptosis.

Oxygen Debt

The decreased rate of O_2 delivery results in tissue "oxygen debt" (24). If this debt is not "paid," the tissue will not survive. Therefore, at the microvascular and cell level, three principles must be considered to devise an effective microcirculation-targeted resuscitation strategy: (1) prevention of "oxygen debt" accumulation, (2) repayment of "oxygen debt," and (3) minimization of the time to "oxygen debt" resolution (27).

A major challenge of resuscitation is determining oxygen delivery to the tissues (DO_2) and oxygen consumption by the tissues (VO_2). Serial lactate measurements coupled with central venous oxygen saturation (SVO_2) can aid in this determination on the macro level. However, these parameters do not distinguish between microcirculatory arterial–venous shunting and true increases in perfusion or between lactate generation vs. uptake. At present, there is no reliable method to clinically measure regional tissue oxygenation, particularly in organs that are not amenable to direct examination (28–30).

Microcirculation Analysis as a Tool to Design Novel Resuscitation Strategies

Systemic parameters such as heart rate and blood pressure have historically been used to monitor recovery from shock. However, if we consider the idea of "oxygen debt" and the use of DO_2/VO_2 to aid in our understanding of the reoxygenation of previously ischemic tissue, it becomes apparent that there must be a focus on the microcirculation in addition to the restoration of systemic indices. Microcirculatory integrity is the principal determinant

for tissue oxygenation, nutrient supply, organ function at the tissue level, and adequate immunological function (31).

Hamster Models for the Analysis of Microcirculation in Hemorrhagic Shock

There are a variety of animal models used to understand the microcirculation in shock; one of the most common is the hamster model (32). Hamsters have a low central partial pressure of oxygen (PaO_2) of ∼57 mmHg, corresponding to a Hb O_2 saturation of 84% (32). Because the baseline arteriolar partial pressure of oxygen (pO_2) is so low, calculation of the pre-microvascular oxygen consumption shows that this species is very efficient at delivering oxygen to the tissues, and very little oxygen leaves the circulation before delivery to the microcirculation, with the change in blood saturation of only about 3% (33).

While in clinical practice the sublingual area has been typically used to measure microvascular performance using dark-field microscopy, observation of the microcirculation in hamsters is commonly achieved via intravital microscopy of the dorsal skin flap: the skin is lifted, creating a skin fold, which is supported by two titanium frames with 12-mm circular openings. One frame is sutured on one side of the skin fold. The opposite skin layer is removed following the outline of the window, leaving only a thin layer of retractor muscle, connective tissue, and intact skin. The exposed tissue is then sealed with a glass cover held by the other frame, creating an environment to make optical measurements of the microcirculation *in vivo* (33–35). Two vessels are generally cannulated, the carotid artery for monitoring blood pressure and the femoral or jugular vein for the infusion of fluids and dyes. Intravital microscopy enables better understanding of the inputs that determine the cellular and subcellular processes within multiple organs. While this type of microscopy can only be implemented in hamsters and other rodents, and does not directly translate to humans, the observed intrinsic regulatory processes at the tissue level do not differ between humans and rodents. This experimental setup allows for microhemodynamic measurements of blood velocity using the photodiode cross-correlation technique and vessel diameters *via* video image shearing (36, 37). The study of flow in the microcirculation enables an improved understanding of the mechanisms underlying oxygen delivery (38). Microvascular pressure and the perfusion of blood in the tissues can be quantified by FCD or the number of perfused capillaries per unit area (9). Capillaries are considered functional if RBCs transit though the capillary segments during a prescribed unit of time. Capillary perfusion is necessary for the oxygenation of the tissues and, perhaps as importantly, the removal of metabolic waste. High-resolution microvascular pO_2 measurements can be made using phosphorescence quenching microscopy (PQM) or hyperspectral imaging. PQM is a technique based on oxygen-dependent quenching of phosphorescence emitted by an albumin-bound metalloporphyrin complex after light excitation (39). Hyperspectral imaging is a technique that utilizes the spectra differences in oxyhemoglobin and deoxyhemoglobin to determine oxygen saturation in the microcirculation (40).

Figure 1 shows a typical example of tissue perfusion in the skin pouch of a Golden Syrian hamster during experimental hemorrhage obtained using hyperspectral imaging. The experiments were approved by the Institutional Animal Care and Use Committee of the University of California, San Diego, and performed following the NIH Guide for the Care and Use of Laboratory Animals, 8th edition (2011). The images were acquired using a Pika-L hyperspectral imaging system with a linear translation stage (Resonon, Bozeman, MT) with a spectral range of 390–1,020 nm, a spectral resolution of 2.1 nm, and a spatial resolution of 900 pixels per line. Each image consisted of a 2,900 × 900 × 300 hypercube. After the acquisition, the images were truncated and resampled in the spectral domain between 500 and 590 nm. Calculation of the relative deoxygenated and oxygenated hemoglobin abundances were completed based on a calibration standard for hemoglobin using Beer's law.

When quantifying microcirculatory dysfunction resulting from hemorrhagic shock, there are several variables that must be considered: the dynamic changes in flow, vasoactive responses, the tissue pO_2 in the microcirculation, lactate concentration, etc. Regardless of the hemorrhagic shock model (fixed pressure vs. fixed volume), microcirculatory parameters are used as barometers of successful resuscitation interventions (41–43). However, there is no consensus on a quantitative definition of "recovery." The literature commonly refers to three schools of thought in defining microvascular recovery after hemorrhagic shock: (1) increased microvascular viscosity (33–35), (2) increased microvascular pressure (44, 45), and (3) improved hemodynamics in the microvasculature (46). Arguments have been made for each parameter individually, but they all hinge on what is defined as "recovery," which should be taken into consideration for the optimization of blood substitutes design.

LOCAL REGULATION OF BLOOD FLOW AND OXYGEN DELIVERY

Engineering any type of blood substitute requires an understanding of the complex interactions between oxygen consumption, changes in the composition of blood and its viscosity, and the oxygen dissociation curve for hemoglobin. A decrease in O_2CC due to hemodilution induces vasodilation, and the restoration of the lost RBCs with an oxygen carrier can produce additional signals depending on whether the carrier has a high or low affinity for oxygen. Facilitated release of oxygen from blood is a property defined by the value of pO_2 at which blood is 50% saturated (P_{50}). A high oxygen affinity (low P_{50}) results in oxygen being preferentially unloaded in the capillaries, and vice versa (32).

An important consideration when designing blood substitutes that will necessarily unload oxygen in the microcirculation is oxygen consumption by the vessel wall itself. Several studies have concluded that oxygen consumption may be extraordinarily high at the vessel wall and increases during vasoconstriction (47, 48). The marked uptake of oxygen at the vessel wall by vascular smooth muscle is somewhat analogous to the significant increases in oxygen use by the skeletal muscle during exercise;

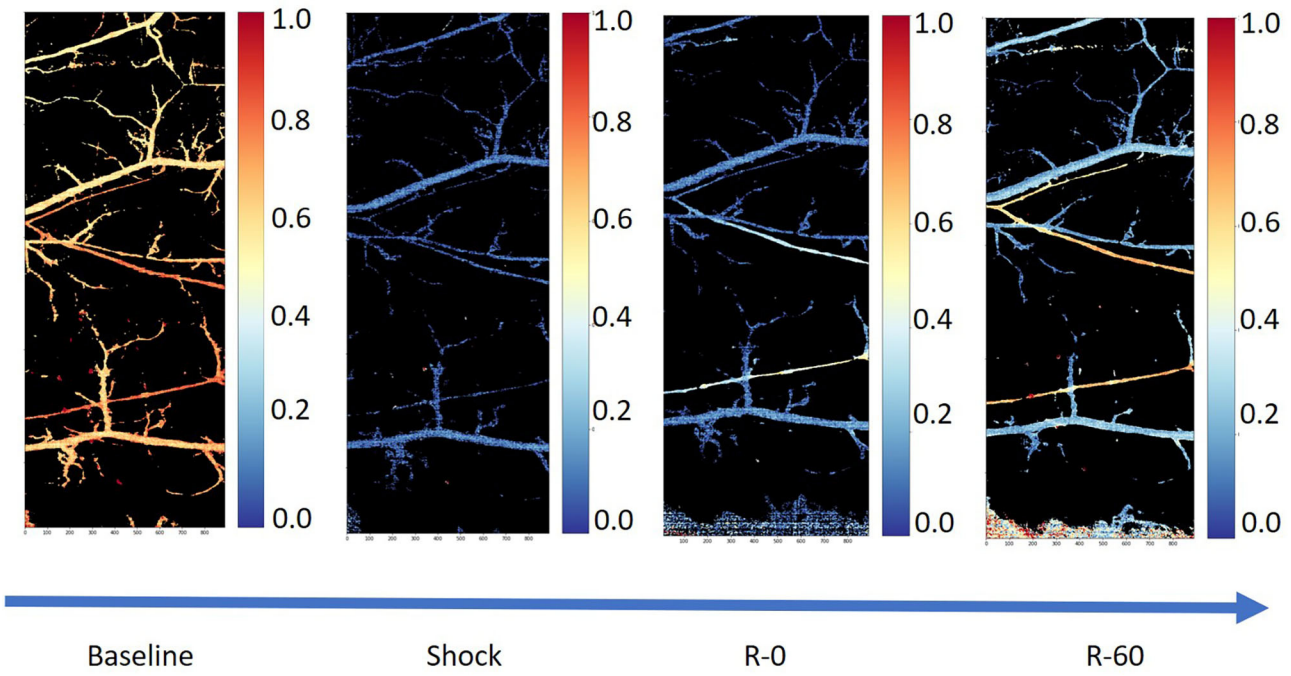

FIGURE 1 | Tissue perfusion in the microcirculation using hyperspectral images from the skin pouch of a Golden Syrian hamster following hemorrhage (50% total blood volume) and a resuscitation using whole blood (25% total blood volume in 5% albumin; Sigma-Aldrich, Saint Louis, MO). The first image (from left to right) is the microcirculation at baseline, the second one is the microcirculation in shock, the third one is the microcirculation immediately after the completion of resuscitation, and the fourth and final image is the microcirculation 60 min post-resuscitation.

vasoconstriction of vessel beds necessarily requires energy and, thus, increased oxygen consumption.

In a reciprocal fashion, increases in circulating pO_2 result in increased vessel vasoconstriction. The reasons for this are unclear, but changes in vessel wall oxygen uptake (and thus vascular tone) in response to circulating pO_2 suggest that the purpose of vasoconstriction in the presence of elevated circulating pO_2 is to limit tissue pO_2 to within a fairly narrow range. This phenomenon further complicates the engineering of effective HBOCs for treatment during T/HS as shock induces vasoconstriction, indicating a potential need to satisfy the vessel wall's oxygen debt before oxygen can enter the tissue beds.

Blood substitute design is often tested using extreme hemodilution, a condition in which systemic Hct is reduced to the point where oxygen delivery becomes dependent on the intrinsic oxygen-carrying capacity of the circulation. This approach allows evaluating blood substitutes characterized by high-affinity hemoglobin products such as 4% Mal–PEG–hemoglobin (MP4) (Hemospan, Sangart Inc., San Diego, CA) or low-affinity bovine-derived PolyBvHb (PBH) (Biopure Inc., Boston, MA) (**Table 1**).

The goal of high-affinity Hb-based blood substitutes is to create a reservoir of oxygen that only unloads oxygen when the circulating blood arrives at tissue regions where the pO_2 is very low, promoting oxygen delivery through diffusion. However, if the affinity for oxygen is too high, the inability to release oxygen may become problematic, leaving the tissue hypoxic. On the other hand, in low-affinity Hb-based blood substitutes, a rightward shift in the O_2 dissociation curve should theoretically increase O_2 extraction and improve maximal O_2 uptake. This manipulation of the P_{50} offers the opportunity to vary O_2 delivery to the tissues without altering blood flow or arterial O_2 content, promoting oxygen delivery *via* convection rather than diffusion.

TABLE 1 | Typical properties of hemoglobin (Hb)-based oxygen carriers vs. blood/plasma.

	Concentration (g/dl)	Viscosity (cp)	COP (mmHg)	P_{50} (mmHg)
Hemospan[a] (MP4)	4.2	2.5	55	6
Oxyglobin[b] (PBH)	13.2	1.8	40	54
Blood		4.2	20	32
Plasma		1.2	20	

COP, colloid osmotic pressure; P_{50}, pO_2 at which blood is 50% saturated.
[a] Polyethylene glycol-conjugated Hb, Sangart Inc., San Diego, CA.
[b] Polymerized bovine hemoglobin, Biopure Corp., Boston, MA.

Blood viscosity is a critical determinant of tissue perfusion because of its direct influence on vascular resistance. Blood viscosity depends primarily on RBC concentration (hematocrit) and secondarily on the viscosity of plasma. Restoration of viscosity in the initial resuscitation period is a common method for assessing recovery in the microcirculation after hypovolemic

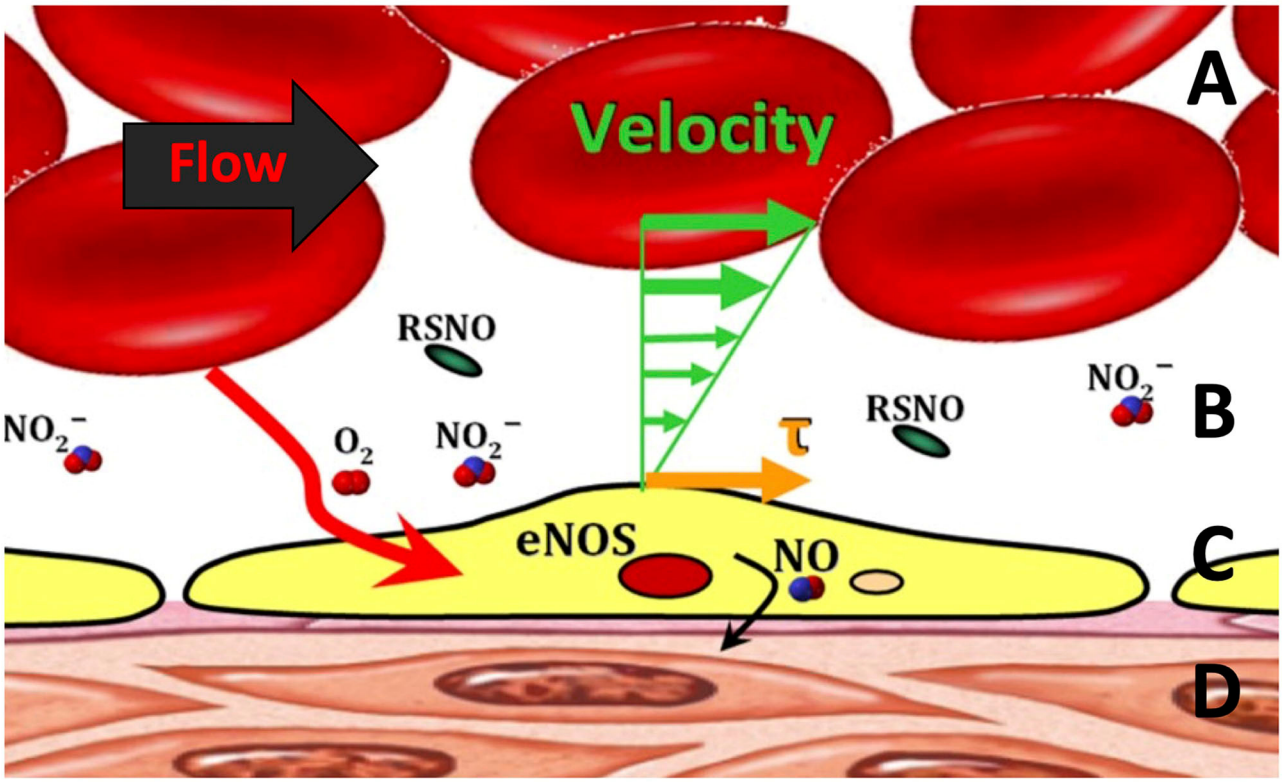

FIGURE 2 | Blood flow through the microcirculation. **(A)** The bulk of red blood cell (RBC) flow, which is related to the shear stress (τ). **(B)** Cell-free layer in the microcirculation. **(C)** Endothelial cell lining generating endothelial nitric oxide synthase (eNOS), *S*-nitrosothiols (RSNO), and nitric oxide (NO) *via* mechanotransduction. **(D)** Smooth muscle layer encapsulating the entire vessel.

shock (33, 42, 43); it is not, however, widely studied clinically. As an alternative to oxygen-carrying modalities, restitution of blood loss with non-oxygen-carrying plasma expanders (PEs) can be effectively and safely accomplished after up to a 50% loss of the RBC mass using fluids with plasma-like viscosity, which induce a compensatory increase in cardiac output aimed at maintaining oxygen delivery (49). Additionally, interventions that increase the viscosity of circulating blood after shock can mitigate the effects that reduced viscosity have on mechanical transduction of the endothelium, potentially preserving the native myogenic responses that normally regulate microvascular flow and pressure (50). Large-molecular-diameter HBOCs play a similar role to PEs, increasing blood and plasma viscosity and preserving microvascular perfusion (51).

Microvascular perfusion and FCD are controlled in part through shear-mediated factors. For example, shear stress exerted on the blood moving near the endothelial surface releases dilatory autocoids (7, 52, 53). Increasing the shear stress on the endothelial surface promotes the expression of anti-inflammatory, antiproliferative, anti-apoptotic, and antioxidative genes, all of which reduce the effects of systemic inflammation associated with hemorrhage shock (54). Recent studies have demonstrated a new, microscopic area of the cell-free layer (CFL) which appears to be the critical focal point of the interaction between blood and microcirculation (**Figure 2**) (55). The CFL regulates oxygen transport and capillary perfusion as it determines the distance between the circulating oxygen supply and the tissue as well as the degree of shear stress on the endothelial wall caused by the passing blood.

Formation of a wider cell-free layer reduces effective blood viscosity near the vessel wall and, thus, the amount of shear experienced by the endothelium, a principal stimulus for release of the potent vasodilator NO (56, 57). However, the CFL has been shown to act as a barrier to NO scavenging, potentially mitigating the effects of reduced shear (58). The CFL is also an important determinant of the rate of oxygen diffusion from the red cells to the tissues. The radial diffusion gradient of oxygen from the hemoglobin carried by RBCs transits from blood to the parenchymal cells through several barriers including plasma, the endothelial layer, and interstitial fluid. Due to the low solubility of oxygen in plasma, the width of the cell-free plasma layer barrier significantly limits oxygen delivery (59, 60). Thus, the interplay between the CFL and the microcirculation serves to regulate vascular perfusion via changes in NO scavenging and oxygen delivery to the tissues. The initial response of the vasculature during T/HS is to vasoconstrict, thus reducing the CFL and thereby potentially increasing NO bioavailability and oxygen delivery to the tissue.

An improved understanding of the fundamental role of the CFL in the microcirculation has contributed to assessing how the circulation responds to small (±10%) changes in Hct and blood viscosity (61). A novel methodology to measure the CFL width (62–64) has been recently developed. This technique is based on high-speed video recording (up to 30,000 frames/second) and a thresholding algorithm that converts the interface between blood and plasma into a black and white image, defining the stochastic surface of the RBC column and identifying the location of the plasma/vessel wall interface. Studies of the trajectories of RBCs at the blood column/plasma interface have identified several features of relevance, particularly the RBC exclusion zone which outlines the glycocalyx. Studies using this technique have led to conclude that CFL width is a function of Hct (65). CFL thickness is an important feature of blood flow in the microcirculation and is proportional to the shear stress and the thickness of the endothelial glycocalyx. Hemorrhage alters glycocalyx structure and function, and changes in the CFL thickness can reflect glycocalyx shedding (64).

Further, small changes in Hct result in large changes in the CFL, significantly affecting arteriolar wall NO bioavailability and wall shear stress (WSS) (**Figure 3**) (61). This relationship between Hct and CFL, described by mathematical modeling, confirms previous assumptions that (1) NO bioavailability in hemodilution increases by decreasing CFL width; (2) hemodilution decreases Hct and plasma viscosity, lowering WSS and increasing CFL width; and (3) FCD is directly proportional to WSS in hemodilution.

Previous studies measuring CFL width changes after 40% hemodilution using low-viscosity PEs (e.g., albumin solutions) demonstrate small but measurable decreases in CFL width. It is hypothesized that this effect is significantly reduced with high-viscosity PEs because of their comparatively large hydrodynamic radius compared to albumin. Furthermore, mathematical modeling of the CFL width effects suggests the hypothesis that the width is in part determined by the type of colloid used (61). One of the relevant processes may be shear-dependent dilation, which provides a dispersive lateral force to the direction of flow. The assumption is that this force acts on the flowing RBCs, thus confirming the importance of viscosity in microcirculation hemodynamics and function.

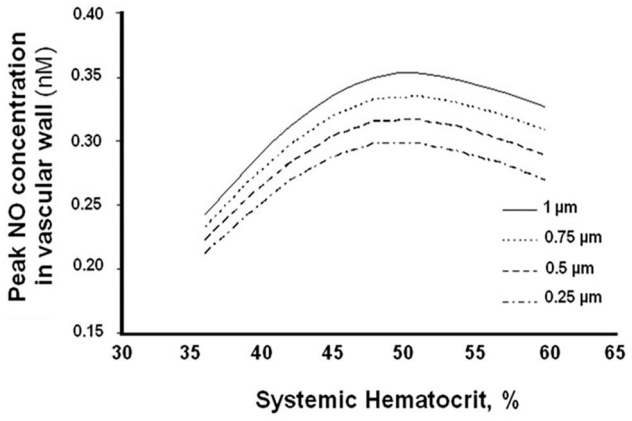

FIGURE 3 | Arteriolar wall nitric oxide bioavailability as a function of systemic hematocrit percentage for different cell-free layer (CFL) widths.

MICROCIRCULATION FUNCTION AND BLOOD SUBSTITUTE VISCOSITY

Survival in hemorrhage after ensuing extreme hemodilution is primarily dependent on the maintenance of FCD and secondarily on tissue O_2. In the previous section, CFL width was introduced as the key parameter of wall shear stress modulation in the microcirculation. As the bioavailability of NO is inversely proportional to CFL width, NO-induced vasodilation is the main determinant of FCD and microvascular perfusion. Based on these observations, increasing wall shear stress in the CFL after T/HS should improve perfusion by the combination of three effects: (1) decreasing plasma CFL width; (2) increasing plasma viscosity; and (3) increasing blood vessel flow velocity. Solely increasing plasma viscosity has potential limitations because, in conditions of extreme hemodilution after hemorrhage, resuscitation with a high-viscosity plasma expander increases the workload of the heart while a simultaneously lower Hct limits O_2 delivery. It is assumed, however, that this intervention can increase the width of the blood column and (moderately) the resistance to plasma fluid flow in the glycocalyx, which would decrease effective CFL width. Current understanding of this complex dynamic suggests that developed blood substitutes should thus be of high viscosity (51).

Microvascular Pressure

Modulating microvascular pressure following hemorrhagic shock directly relates to FCD, a key determinant of survival from T/HS. During shock, the microvascular pressure plummets, resulting in a sharp decrease in the number of perfused capillaries with implications for the surrounding tissue. Adequate perfusion of the capillary bed is thus vital as it is associated with oxygen delivery (diffusion) to the tissue from the systemic circulation as well as the continuous washout of metabolites (31). As tissues become hypoxic, they also become acidotic and lactate is accumulated. This, in turn, negatively affects systemic pH and base excess. The severity of the changes seen in arterial blood gas measurements (including pH, PaO_2, $PaCO_2$, base excess/deficit, and lactate) can be used to assess the extent of shock (34, 66). Increasing FCD restores flow to the tissues, alleviating local as well as systemic acidosis as oxygen diffusion into the tissue increases, shifting metabolic processes once again toward aerobic metabolism. Increasing the microvascular pressure may be accomplished systemically by the use of resuscitation fluids that increase plasma viscosity or have high colloid osmotic pressure (COP) and are therefore able to draw fluid into the microvasculature.

Microvascular Flow

Peripheral hemodynamics are a typical measure of recovery in experimental T/HS (31). In the quiescent state, microcirculatory

hemodynamics are equilibrated to the point where RBC velocity ensures the optimal diffusion of oxygen to the tissues through convective processes. In shock, flow can be significantly impaired and reduced dramatically, resulting in inadequate tissue oxygenation. Thus, increasing the intravascular microcirculatory volume *via* resuscitation fluid will enhance flow and tissue (re)oxygenation (67). Regardless of the mechanism for reperfusion, microvascular recovery following shock is contingent on how well oxygen delivery to previously hypoxic tissues can be achieved.

CONCLUSIONS

Plasma expansion and blood transfusion are major medical interventions in T/HS, and even minor improvements in their efficacy will have significant healthcare repercussions. Advancements from current research will help to guide the development of fluids that are safe and effective blood substitutes. These may then lead to the development of transfusion protocols that include O_2 transport indices and blood viscosity as targets of an effective microcirculation-targeted resuscitation.

Experimental results from microcirculation studies modeling blood loss and blood transfusion suggest that the present focus on restoring blood volume and O_2-carrying capacity should be redirected toward using fluids that trade the requirement for O_2-carrying capacity with the enhancement of microcirculatory O_2 delivery. It then follows from this hypothesis that the development of artificial blood substitutes, which are presently aimed at restoring the blood O_2-carrying capacity, should rather be designed to restore blood viscosity. This corresponds to a fundamental change in the perception of what blood has to accomplish in the circulation, which includes the maintenance of a shear stress environment conducive to adequate bioavailability of NO as a function of Hct with a proportional relationship to the CFL. In this new view, artificial blood substitutes for resuscitation after hemorrhagic shock should be optimally designed with the following priorities in mind: restoration of circulating (1) volume, (2) viscosity, and, lastly, (3) O_2-carrying capacity.

A potential clinical implication might revolve around the question "What is the patient's blood viscosity?" in the assessment of a hemorrhaging victim, with the answer to this question used as a guide to the fluid treatment strategy. Theoretically, demand for rapid and reliable blood viscometry would be expanded, and the use of blood transfusions substantially diminished, to eventually be relegated to extreme conditions. Determining the blood viscosity that optimizes systemic and microvascular function when Hb is reduced beyond the transfusion trigger is a challenge. We have extensive experience in the analysis of shock resuscitation using a variety of blood substitutes, besides blood (32, 33, 41, 42, 65, 68–81). However, the definitive test of the viscogenic hypothesis requires its verification in T/HS, one of its most likely areas of application.

Hemorrhagic shock entails a complex series of cascading events that have synergistic pathophysiologic effects, from the cellular level up to the entire cardiovascular circuit as a whole. Theories that revolve around rheology, functional physiology, and hemodynamics have been proposed regarding the optimal way to successfully treat a patient in shock. Vasopressor and inotrope therapies have been explored as part of the resuscitation strategy from hemorrhagic shock, either as main treatments or simultaneously in combination with fluid support, with mixed success. While vasopressors and inotropes could improve systemic hemodynamic metrics representative of the effectiveness of resuscitation (for instance mean arterial pressure), their benefit to the blood flow in the microcirculation is questionable. Indeed, they could have a limited beneficial effect or even contribute to jeopardize further the long-term recovery of the microcirculation from hemorrhagic shock, especially during severe hypovolemia, when venous return is insufficient to support systemic O_2 requirements. All of these hypotheses relate back to replenishing the pool of oxygen that was depleted in the tissues. Arguments can be made for each of these hypotheses. However, artificial blood substitutes must satisfy all three hypotheses to be a viable alternative to blood transfusion. In order to provide adequate oxygen delivery to tissues, high-viscosity HBOC solutions must have the ability to reversibly bind oxygen (18). Increases in viscosity using these solutions should promote vasodilation *via* mechanical transduction on the endothelium and increase functional capillary density (34), which in turn would lead to an increase in microvascular pressure and subsequently in blood flow. Whether the postulated benefits of artificial blood substitutes with these design constraints are eventually realized and enter routine clinical use hinge on the optimization of ideal viscosity in addition to the restoration of blood volume, but the outlined strategies represent promising steps toward a clinically translatable solution to the ever-growing problem of blood shortage for transfusions in T/HS and other acute and chronic pathologies.

AUTHOR CONTRIBUTIONS

CM, FA, KG, PC, and EK reviewed the literature and drafted the manuscript. All authors contributed to the article and approved the submitted version.

FUNDING

Department of Defense award W81XWH-17-2-0047.

REFERENCES

1. Tsai AG, Cabrales P, Intaglietta M. Microvascular perfusion upon exchange transfusion with stored RBCs in normovolemic anemic conditions. *Transfusion*. (2004) 44:1626–34. doi: 10.1111/j.0041-1132.2004.04128.x
2. Saldanha C. Physiological role of erythrocyte nitric oxide. *Clin Hemorheol Microcirc*. (2016) 64:517–20. doi: 10.3233/CH-168028
3. Leiman PG, Chipman PR, Kostyuchenko VA, Mesyanzhinov VV, Rossmann MG. Three-dimensional rearrangement of proteins in the tail of bacteriophage T4 on infection of its host. *Cell*. (2004) 118:419–29. doi: 10.1016/j.cell.2004.07.022

4. Liu Y, Li D, Chen J, Xie J, Bandyopadhyay S, Zhang D, et al. Inhibition of atherogenesis in LDLR knockout mice by systemic delivery of adeno-associated virus type 2-hIL-10. *Atherosclerosis*. (2006) 188:19–27. doi: 10.1016/j.atherosclerosis.2005.10.029
5. Tateishi O, Shouda T, Sakai T, Honda Y, Mochizuki S, Machida K. Apnea-related heart rate variability in congestive heart failure patients. *Clin Exp Hypertens*. (2003) 25:183–9. doi: 10.1081/CEH-120019150
6. Ghinea N, Milgrom E. A new function for the LH/CG receptor: transcytosis of hormone across the endothelial barrier in target organs. *Semin Reprod Med*. (2001) 19:97–101. doi: 10.1055/s-2001-13916
7. Tsai AG, Acero C, Nance PR, Cabrales P, Frangos JA, Buerk DG, et al. Elevated plasma viscosity in extreme hemodilution increases perivascular nitric oxide concentration and microvascular perfusion. *Am J Physiol-Heart Circ Physiol*. (2005) 288:H1730–9. doi: 10.1152/ajpheart.00998.2004
8. Kimmoun A, Novy E, Auchet T, Ducrocq N, Levy B. Hemodynamic consequences of severe lactic acidosis in shock states: from bench to bedside. *Crit Care*. (2015) 19:175. doi: 10.1186/s13054-015-0896-7
9. Cabrales P, Tsai AG, Intaglietta M. Microvascular pressure and functional capillary density in extreme hemodilution with low- and high-viscosity dextran and a low-viscosity Hb-based O_2 carrier. *Am J Physiol Heart Circ Physiol*. (2004) 287:H363–73. doi: 10.1152/ajpheart.01039.2003
10. Pyke KE, Tschakovsky ME. The relationship between shear stress and flow-mediated dilatation: implications for the assessment of endothelial function. *J Physiol*. (2005) 568:357–69. doi: 10.1113/jphysiol.2005.089755
11. Doss DN, Estafanous FG, Ferrario CM, Brum JM, Murray PA. Mechanism of systemic vasodilation during normovolemic hemodilution. *Anesth Analg*. (1995) 81:30–4. doi: 10.1213/00000539-199507000-00006
12. National Research Council (US) Panel on Statistics for an Aging Population, National Research Council Staff, Gilford DM, Shapiro S, Division of Behavioral and Social Sciences and Education, Committee on National Statistics, et al. *The Aging Population in the Twenty-First Century: Statistics for Health Policy*. Washington, DC: National Academies Press (US) (1988). Available online at: http://www.ncbi.nlm.nih.gov/books/NBK217737/ (accessed July 20, 2020)
13. Gunsilius E, Gastl G, Petzer AL. Hematopoietic stem cells. *Biomed Pharmacother*. (2001) 55:186–94. doi: 10.1016/S0753-3322(01)00051-8
14. Chen J-Y, Scerbo M, Kramer G. A review of blood substitutes: examining the history, clinical trial results, and ethics of hemoglobin-based oxygen carriers. *Clinics*. (2009) 64:803–13. doi: 10.1590/S1807-59322009000800016
15. Buehler PW, Mehendale S, Wang H, Xie J, Ma L, Trimble CE, et al. Resuscitative effects of polynitroxylated αα-cross-linked hemoglobin following severe hemorrhage in the rat. *Free Radic Biol Med*. (2000) 29:764–74. doi: 10.1016/S0891-5849(00)00383-X
16. Meng F, Kassa T, Jana S, Wood F, Zhang X, Jia Y, et al. Comprehensive biochemical and biophysical characterization of hemoglobin-based oxygen carrier therapeutics: all HBOCs are not created equally. *Bioconjug Chem*. (2018) 29:1560–75. doi: 10.1021/acs.bioconjchem.8b00093
17. S Jahr J, Sadighi Akha A, Holtby RJ. Crosslinked, polymerized, and PEG-conjugated hemoglobin-based oxygen carriers: clinical safety and efficacy of recent and current products. *Curr Drug Discov Technol*. (2012) 9:158–65. doi: 10.2174/157016312802650742
18. Cabrales P, Intaglietta M. Blood substitutes: evolution from non-carrying to oxygen and gas carrying fluids. *ASAIO J*. (2013) 59:337–54. doi: 10.1097/MAT.0b013e318291fbaa
19. Ray CJ, Abbas MR, Coney AM, Marshall JM. Interactions of adenosine, prostaglandins and nitric oxide in hypoxia-induced vasodilatation: *in vivo* and *in vitro* studies. *J Physiol*. (2002) 544:195–209. doi: 10.1113/jphysiol.2002.023440
20. Roman RJ. P-450 metabolites of arachidonic acid in the control of cardiovascular function. *Physiol Rev*. (2002) 82:131–185. doi: 10.1152/physrev.00021.2001
21. Chien S. Role of the sympathetic nervous system in hemorrhage. *Physiol Rev*. (1967) 47:214–88. doi: 10.1152/physrev.1967.47.2.214
22. Cannon JW. Hemorrhagic shock. *N Engl J Med*. (2018) 378:370–9. doi: 10.1056/NEJMra1705649
23. Chang R, Cardenas JC, Wade CE, Holcomb JB. Advances in the understanding of trauma-induced coagulopathy. *Blood*. (2016) 128:1043–9. doi: 10.1182/blood-2016-01-636423
24. White NJ, Ward KR, Pati S, Strandenes G, Cap AP. Hemorrhagic blood failure: oxygen debt, coagulopathy and endothelial damage. *J Trauma Acute Care Surg*. (2017) 82:S41. doi: 10.1097/TA.0000000000001436
25. Cohen MJ. Towards hemostatic resuscitation: the changing understanding of acute traumatic biology, massive bleeding, and damage-control resuscitation. *Surg Clin North Am*. (2018) 92:877–91. doi: 10.1016/j.suc.2012.06.001
26. Rhodes RS, DePalma RG. Mitochondrial dysfunction of the liver and hypoglycemia in hemorrhagic shock. *Surg Gynecol Obstet*. (1980) 150:347–52.
27. Barbee RW, Reynolds PS, Ward KR. Assessing shock resuscitation strategies by oxygen debt repayment. *Shock*. (2010) 33:113–22. doi: 10.1097/SHK.0b013e3181b8569d
28. Convertino VA, Moulton SL, Grudic GZ, Rickards CA, Hinojosa-Laborde C, Gerhardt RT, et al. Use of advanced machine-learning techniques for noninvasive monitoring of hemorrhage. *J Trauma Acute Care Surg*. (2011) 71:S25–32. doi: 10.1097/TA.0b013e3182211601
29. Scalea TM, Maltz S, Yelon J, Trooskin SZ, Duncan AO, Sclafani SJ. Resuscitation of multiple trauma and head injury: role of crystalloid fluids and inotropes. *Crit Care Med*. (1994) 22:1610–5. doi: 10.1097/00003246-199422100-00017
30. Abou-Khalil B, Scalea TM, Trooskin SZ, Henry SM, Hitchcock R. Hemodynamic responses to shock in young trauma patients: need for invasive monitoring. *Crit Care Med*. (1994) 22:633–9. doi: 10.1097/00003246-199404000-00020
31. Munoz CJ, Lucas A, Williams AT, Cabrales P. A review on microvascular hemodynamics: the control of blood flow distribution and tissue oxygenation. *Crit Care Clin*. (2020) 36:293–305. doi: 10.1016/j.ccc.2019.12.011
32. Tsai AG, Cabrales P, Intaglietta M. Mechanisms of oxygen transport in the microcirculation: effects of cell-free oxygen carriers. In: *Blood Substitutes*. San Diego, CA: Elsevier (2006). p. 84–92. doi: 10.1016/B978-012759760-7/50013-5
33. Cabrales P, Intaglietta M, Tsai AG. Transfusion restores blood viscosity and reinstates microvascular conditions from hemorrhagic shock independent of oxygen carrying capacity. *Resuscitation*. (2007) 75:124–34. doi: 10.1016/j.resuscitation.2007.03.010
34. Wettstein R, Tsai AG, Erni D, Winslow RM, Intaglietta M. Resuscitation with polyethylene glycol-modified human hemoglobin improves microcirculatory blood flow and tissue oxygenation after hemorrhagic shock in awake hamsters. *Crit Care Med*. (2003) 31:1824–30. doi: 10.1097/01.CCM.0000069340.16319.F2
35. Cabrales P, Tsai AG, Intaglietta M. Increased plasma viscosity prolongs microhemodynamic conditions during small volume resuscitation from hemorrhagic shock. *Resuscitation*. (2008) 77:379–86. doi: 10.1016/j.resuscitation.2008.01.008
36. Lipowsky HH, Zweifach BW. Application of the "two-slit" photometric technique to the measurement of microvascular volumetric flow rates. *Microvasc Res*. (1978) 15:93–101. doi: 10.1016/0026-2862(78)90009-2
37. Intaglietta M, Tompkins WR. Microvascular measurements by video image shearing and splitting. *Microvasc Res*. (1973) 5:309–12. doi: 10.1016/0026-2862(73)90042-3
38. Pittman RN. Oxygen transport. In: Nei Granger D, LSU Health Sciences Center, Granger JP, editors. *Regulation of Tissue Oxygenation*. San Rafael, CA: Morgan & Claypool Life Sciences (2011). p. 19–30. Available online at: https://www.ncbi.nlm.nih.gov/books/NBK54103/ (accessed July 23, 2019).
39. Torres Filho IP, Intaglietta M. Microvessel PO_2 measurements by phosphorescence decay method. *Am J Physiol-Heart Circ Physiol*. (1993) 265:H1434–8. doi: 10.1152/ajpheart.1993.265.4.H1434
40. Lucas A. *Use of Hyperspectral Imaging for the Study of Hemoglobin Oxygen Saturation in the Microcirculation*. (2019). Available online at: https://escholarship.org/uc/item/21m251cb (accessed July 10, 2020).
41. Wettstein R, Tsai AG, Erni D, Lukyanov AN, Torchilin VP, Intaglietta M. Improving microcirculation is more effective than substitution of red blood cells to correct metabolic disorder in experimental hemorrhagic shock. *Shock*. (2004) 21:235–40. doi: 10.1097/01.shk.0000114301.36496.ea
42. Cabrales P, Intaglietta M, Tsai AG. Increase plasma viscosity sustains microcirculation after resuscitation from hemorrhagic shock and continuous

bleeding. *Shock*. (2005) 23:549–55. Available online at: https://journals.lww.com/shockjournal/fulltext/2005/06000/increase_plasma_viscosity_sustains.12.aspx
43. Villela NR, Tsai AG, Cabrales P, Intaglietta M. Improved resuscitation from hemorrhagic shock with ringer's lactate with increased viscosity in the hamster window chamber model. *J Trauma Acute Care Surg*. (2011) 71:418–24. doi: 10.1097/TA.0b013e3181fa2630
44. Wang P, Hauptman JG, Chaudry IH. Hemorrhage produces depression in microvascular blood flow which persists despite fluid resuscitation. *Circ Shock*. (1990) 32:307–18.
45. Nakayama S, Sibley L, Gunther RA, Holcroft JW, Kramer GC. Small-volume resuscitation with hypertonic saline (2,400 mOsm/liter) during hemorrhagic shock. *Circ Shock*. (1984) 13:149–59.
46. Tsai AG, Cabrales P, Acharya AS, Intaglietta M. Resuscitation from hemorrhagic shock: recovery of oxygen carrying capacity or perfusion?: efficacy of new plasma expanders. *Transfus Altern Transfus Med*. (2007) 9:246–53. doi: 10.1111/j.1778-428X.2007.00086.x
47. Ye J-M, Colquhoun EQ, Clark MG. A comparison of vasopressin and noradrenaline on oxygen uptake by perfused rat hindlimb, kidney, intestine and mesenteric arcade suggests that it is in part due to contractile work by blood vessels. *Gen Pharmacol Vasc Syst*. (1990) 21:805–10. doi: 10.1016/0306-3623(90)91037-R
48. Friesenecker B, Tsai AG, Dunser MW, Mayr AJ, Martini J, Knotzer H, et al. Oxygen distribution in microcirculation after arginine vasopressin-induced arteriolar vasoconstriction. *Am J Physiol-Heart Circ Physiol*. (2004) 287:H1792–800. doi: 10.1152/ajpheart.00283.2004
49. Tsai AG, Sakai H, Wettstein R, Kerger H, Intaglietta M. An effective blood replacement fluid that targets oxygen delivery, increases plasma viscosity, and has high oxygen affinity. *Transfus Altern Transfus Med*. (2004) 5:507–13. doi: 10.1111/j.1778-428X.2004.tb00089.x
50. Fukumura D, Jain RK. Role of nitric oxide in angiogenesis and microcirculation in tumors. *Cancer Metastasis Rev*. (1998) 17:77–89. doi: 10.1023/A:1005908805527
51. Williams AT, Lucas A, Muller CR, Bolden-Rush C, Palmer AF, Cabrales P. Balance between oxygen transport and blood rheology during resuscitation from hemorrhagic shock with polymerized bovine hemoglobin. *J Appl Physiol*. (2020) 129:97–107. doi: 10.1152/japplphysiol.00016.2020
52. Cooke JP, Rossitch E, Andon NA, Loscalzo J, Dzau VJ. Flow activates an endothelial potassium channel to release an endogenous nitrovasodilator. *J Clin Invest*. (1991) 88:1663–71. doi: 10.1172/JCI115481
53. Frangos JA, Huang TY, Clark CB. Steady shear and step changes in shear stimulate endothelium via independent mechanisms—superposition of transient and sustained nitric oxide production. *Biochem Biophys Res Commun*. (1996) 224:660–5. doi: 10.1006/bbrc.1996.1081
54. Cunningham KS, Gotlieb AI. The role of shear stress in the pathogenesis of atherosclerosis. *Lab Investig J Tech Methods Pathol*. (2005) 85:9–23. doi: 10.1038/labinvest.3700215
55. Kim S, Ong PK, Yalcin O, Intaglietta M, Johnson PC. The cell-free layer in microvascular blood flow. *Biorheology*. (2009) 46:181–9. doi: 10.3233/BIR-2009-0530
56. Busse R, Fleming I. Regulation of endothelium-derived vasoactive autacoid production by hemodynamic forces. *Trends Pharmacol Sci*. (2003) 24:24–9. doi: 10.1016/S0165-6147(02)00005-6
57. Koller A, Kaley G. Prostaglandins mediate arteriolar dilation to increased blood flow velocity in skeletal muscle microcirculation. *Circ Res*. (1990) 67:529–34. doi: 10.1161/01.RES.67.2.529
58. Liao JC, Hein TW, Vaughn MW, Huang K-T, Kuo L. Intravascular flow decreases erythrocyte consumption of nitric oxide. *Proc Natl Acad Sci USA*. (1999) 96:8757–61. doi: 10.1073/pnas.96.15.8757
59. Lamkin-Kennard KA, Jaron DOV, Buerk DG. Impact of the fåhraeus effect on NO and O_2 biotransport: a computer model. *Microcirculation*. (2004) 11:337–49. doi: 10.1080/10739680490437496
60. Maeda N, Shiga T. Velocity of oxygen transfer and erythrocyte rheology. *Physiology*. (1994) 9:22–7. doi: 10.1152/physiologyonline.1994.9.1.22
61. Sriram K, Salazar Vazquez BY, Yalcin O, Johnson PC, Intaglietta M, Tartakovsky DM. The effect of small changes in hematocrit on nitric oxide transport in arterioles. *Antioxid Redox Signal*. (2010) 14:175–85. doi: 10.1089/ars.2010.3266
62. Kim S, Kong RL, Popel AS, Intaglietta M, Johnson PC. A computer-based method for determination of the cell-free layer width in microcirculation. *Microcirculation*. (2006) 13:199–207. doi: 10.1080/10739680600556878
63. Kim S, Kong RL, Popel AS, Intaglietta M, Johnson PC. Temporal and spatial variations of cell-free layer width in arterioles. *Am J Physiol Heart Circ Physiol*. (2007) 293:H1526–35. doi: 10.1152/ajpheart.01090.2006
64. Yalcin O, Jani VP, Johnson PC, Cabrales P. Implications enzymatic degradation of the endothelial glycocalyx on the microvascular hemodynamics and the arteriolar red cell free layer of the rat cremaster muscle. *Front Physiol*. (2018) 9:168. doi: 10.3389/fphys.2018.00168
65. Yalcin O, Choi C, Chatpun S, Intaglietta M, Johnson PC. The dependence of cell-free layer thickness in arterioles on systemic hematocrit level. *FASEB J*. (2009) 23:949. doi: 10.1096/fasebj.23.1_supplement.949.7
66. Cabrales P, Nacharaju P, Manjula BN, Tsai AG, Acharya SA, Intaglietta M. Early difference in tissue pH and microvascular hemodynamics in hemorrhagic shock resuscitation using polyethylene glycol-albumin- and hydroxyethyl starch-based plasma expanders. *Shock*. (2005) 24:66–73. doi: 10.1097/01.shk.0000167111.80753.ef
67. Tsai AG, Vázquez BYS, Hofmann A, Acharya SA, Intaglietta M. Supra-plasma expanders–the future of treating blood loss and anemia without red cell transfusions? *J Infus Nurs Off Publ Infus Nurses Soc*. (2015) 38:217. doi: 10.1097/NAN.0000000000000103
68. Kerger H, Torres Filho IP, Rivas M, Winslow RM, Intaglietta M. Systemic and subcutaneous microvascular oxygen tension in conscious Syrian golden hamsters. *Am J Physiol-Heart Circ Physiol*. (1995) 268:H802–10. doi: 10.1152/ajpheart.1995.268.2.H802
69. Cabrales P, Tsai AG, Ananda K, Acharya SA, Intaglietta M. Volume resuscitation from hemorrhagic shock with albumin and hexaPEGylated human serum albumin. *Resuscitation*. (2008) 79:139–46. doi: 10.1016/j.resuscitation.2008.04.020
70. Cabrales P, Tsai AG, Intaglietta M. Hemorrhagic shock resuscitation with carbon monoxide saturated blood. *Resuscitation*. (2007) 72:306–18. doi: 10.1016/j.resuscitation.2006.06.021
71. Cabrales P, Tsai AG, Intaglietta M. Hyperosmotic-hyperoncotic vs. hyperosmotic-hyperviscous small volume resuscitation in hemorrhagic shock. *Shock*. (2004) 22:431–7. doi: 10.1097/01.shk.0000140662.72907.95
72. Cabrales P, Tsai AG, Intaglietta M. Is resuscitation from hemorrhagic shock limited by blood oxygen-carrying capacity or blood viscosity? *Shock*. (2007) 27:380–9. doi: 10.1097/01.shk.0000239782.71516.ba
73. Cabrales P, Tsai AG, Intaglietta M. Polymerized bovine hemoglobin can improve small-volume resuscitation from hemorrhagic shock in hamsters. *Shock*. (2009) 31:300–7. doi: 10.1097/SHK.0b013e318180ff63
74. Cabrales P, Tsai AG, Intaglietta M. Resuscitation from hemorrhagic shock with hydroxyethyl starch and coagulation changes. *Shock*. (2007) 28:461–7. doi: 10.1097/shk.0b013e31804880a1
75. Kerger H, Tsai AG, Saltzman DJ, Winslow RM, Intaglietta M. Fluid resuscitation with O_2 vs. non-O_2 carriers after 2 h of hemorrhagic shock in conscious hamsters. *Am J Physiol*. (1997) 272:H525–37. doi: 10.1152/ajpheart.1997.272.1.H525
76. Kerger H, Waschke KF, Ackern KV, Tsai AG, Intaglietta M. Systemic and microcirculatory effects of autologous whole blood resuscitation in severe hemorrhagic shock. *Am J Physiol*. (1999) 276(6 Pt 2):H2035–43. doi: 10.1152/ajpheart.1999.276.6.H2035
77. Sakai H, Hara H, Tsai AG, Tsuchida E, Johnson PC, Intaglietta M. Changes in resistance vessels during hemorrhagic shock and resuscitation in conscious hamster model. *Am J Physiol*. (1999) 276:H563–71. doi: 10.1152/ajpheart.1999.276.2.H563
78. Sakai H, Takeoka S, Wettstein R, Tsai AG, Intaglietta M, Tsuchida E. Systemic and microvascular responses to hemorrhage shock and resuscitation with Hb vesicles. *Am J Physiol Heart Circ Physiol*. (2002) 283:H1191–9. doi: 10.1152/ajpheart.00080.2002
79. Villela NR, Salazar Vazquez BY, Intaglietta M. Microcirculatory effects of intravenous fluids in critical illness: plasma expansion

beyond crystalloids and colloids. *Curr Opin Anaesthesiol*. (2009) 22:163–7. doi: 10.1097/ACO.0b013e328328d304

80. Wettstein R, Cabrales P, Erni D, Tsai AG, Winslow RM, Intaglietta M. Resuscitation from hemorrhagic shock with MalPEG-albumin: comparison with MalPEG-hemoglobin. *Shock*. (2004) 22:351–7. doi: 10.1097/01.shk.0000135253.14076.d9
81. Wettstein R, Erni D, Intaglietta M, Tsai AG. Rapid restoration of microcirculatory blood flow with hyperviscous and hyperoncotic solutions lowers the transfusion trigger in resuscitation from hemorrhagic shock. *Shock*. (2006) 25:641–6. doi: 10.1097/01.shk.0000209532.15317.15

Conflict of Interest: The authors declare that the research was conducted in the absence of any commercial or financial relationships that could be construed as a potential conflict of interest.

frontiers in Medicine

ORIGINAL RESEARCH
published: 12 November 2020
doi: 10.3389/fmed.2020.566388

Comparison Between Two Pharmacologic Strategies to Alleviate Rewarming Shock: Vasodilation vs. Inodilation

Brage Håheim[1], *Timofei Kondratiev*[1], *Erik Sveberg Dietrichs*[1,2] *and Torkjel Tveita*[1,3]*

[1] *Anesthesia and Critical Care Research Group, Department of Clinical Medicine, UiT, The Arctic University of Norway, Tromsø, Norway,* [2] *Experimental and Clinical Pharmacology Research Group, Department of Medical Biology, UiT, The Arctic University of Norway, Tromsø, Norway,* [3] *Division of Surgical Medicine and Intensive Care, University Hospital of North Norway, Tromsø, Norway*

Rewarming from hypothermia is often challenged by coexisting cardiac dysfunction, depressed organ blood flow (OBF), and increased systemic vascular resistance. Previous research shows cardiovascular inotropic support and vasodilation during rewarming to elevate cardiac output (CO). The present study aims to compare the effects of inodilatation by levosimendan (LS) and vasodilation by nitroprusside (SNP) on OBF and global oxygen transport during rewarming from hypothermia. We used an *in vivo* experimental rat model of 4 h 15°C hypothermia and rewarming. A stable isotope-labeled microsphere technique was used to determine OBF. Cardiac and arterial pressures were monitored with fluid-filled pressure catheters, and CO was measured by thermodilution. Two groups were treated with either LS ($n = 7$) or SNP ($n = 7$) during the last hour of hypothermia and throughout rewarming. Two groups served as hypothermic ($n = 7$) and normothermic ($n = 6$) controls. All hypothermia groups had significantly reduced CO, oxygen delivery, and OBF after rewarming compared to their baseline values. After rewarming, LS had elevated CO significantly more than SNP (66.57 ± 5.6/+30% vs. 54.48 ± 5.2/+14%) compared to the control group (47.22 ± 3.9), but their ability to cause elevation of brain blood flow (BBF) was the same (0.554 ± 0.180/+81 vs. 0.535 ± 0.208/+75%) compared to the control group (0.305 ± 0.101). We interpret the vasodilator properties of LS and SNP to be the primary source to increase organ blood flow, superior to the increase in CO.

Keywords: hypothermia, nitroprusside, levosimendan, rewarming shock, targeted therapeutic strategies, microcirculation

OPEN ACCESS

Edited by:
Mihály Boros,
University of Szeged, Hungary

Reviewed by:
Peter Paal,
Krankenhaus der Barmherzigen Brüder Wien, Austria
Denise Battaglini,
University of Barcelona, Spain

***Correspondence:**
Torkjel Tveita
torkjel.tveita@uit.no

Specialty section:
This article was submitted to Intensive Care Medicine and Anesthesiology, a section of the journal Frontiers in Medicine

Received: *27 May 2020*
Accepted: *05 October 2020*
Published: *12 November 2020*

Citation:
Håheim B, Kondratiev T, Dietrichs ES and Tveita T (2020) Comparison Between Two Pharmacologic Strategies to Alleviate Rewarming Shock: Vasodilation vs. Inodilation. Front. Med. 7:566388. doi: 10.3389/fmed.2020.566388

INTRODUCTION

Clinical presentation of accidental hypothermia and rewarming is associated with hypotension, hypoperfusion, and vital organ injury (1, 2). Coined *rewarming shock*, this unstable hemodynamic state (3–5) contributes to the lethality of 28–35% in accidental hypothermia patients (6, 7). The underlying mechanisms of rewarming shock are yet not fully understood. Clinical experience and experimental studies have identified hypothermia-induced cardiac dysfunction and elevated systemic vascular resistance (SVR) as fundamental mechanisms (5, 8). Hypothermia-induced

cardiac dysfunction has been linked to inotropic failure and dysregulation of myocardial beta-receptors. The current European guidelines for resuscitation during hypothermia focus on mechanical circulatory support in unstable patients and restrictive adrenergic intervention, significantly below 30°C (9). Thus, experimental studies are needed to improve our understanding of rewarming shock and identify possible pharmacological treatment options.

A combination of positive inotropy and vasodilation, i.e., inodilation, with levosimendan (LS), or vasodilation only with sodium nitroprusside (SNP), have both demonstrated to elevate cardiac output (CO) and reduce SVR in experimental models of hypothermia and rewarming (8, 10, 11). The results show LS and SNP to elevate CO by +166 and +77%, respectively (8, 10). LS increases Ca^{2+} sensitivity of the cardiac contractile apparatus and open ATP-dependent K^{+}-channels in smooth muscle, resulting in elevated cardiac inotropy and vasodilation. LS also inhibits phosphodiesterase-3, elevating cyclic adenosine monophosphate (cAMP), promoting additional positive inotropy and vasodilation (12). SNP vasodilates by activating smooth muscle cyclic guanosine monophosphate (cGMP) (13), and *in vivo* studies show no changes in cardiac contractility (14).

Organ blood flow (OBF) and oxygen transport (DO_2) are essential factors in the treatment of critical care patients (15). The pharmacological elevation of OBF improves short-term organ function and reduce mortality of patients in circulatory shock (16, 17). While studies conducted during normothermic conditions have shown elevated OBF by both LS and SNP (18–20), little knowledge exists on their effects during rewarming from hypothermia. It is therefore vital to assess if their beneficial effects on global hemodynamic function translate into improved OBF (8, 10). With this in mind, we hypothesize that the combined inotropic and vasodilatory effects of LS improve OBF more than isolated vasodilation by SNP after rewarming from hypothermia. To test our hypothesis, we used an *in vivo* rat model instrumented for measurements of hemodynamic function and OBF during cooling, 3 h stable hypothermia, and rewarming. Pharmacologic interventions were instituted 1 h before rewarming and continued throughout the rewarming process.

MATERIALS AND METHODS

Experimental Design

The main aim of this study was to investigate if the beneficial effects of LS and SNP on cardiac function translate into improved organ perfusion during hypothermia and rewarming. Four experimental groups were included: control (n = 7), Levosimendan (n = 7), Nitroprusside (n = 7), and Normothermic control (n = 6).

Abbreviations: SVR, systemic vascular resistance; LS, levosimendan; SNP, sodium nitroprusside; CO, cardiac output; OBF, organ blood flow; DO_2, oxygen transport; HR, heart rate; SV, stroke volume; CI, cardiac index; SaO_2, oxygen saturation; Hb, hemoglobin; CaO_2, Arterial blood oxygen content; CvO_2, venous blood oxygen content; VO_2, oxygen consumption; MAP, mean arterial pressure; BBF, brain blood flow; MBF, myocardial blood flow; RBF, renal blood flow; SBF, stomach blood flow.

Control (n = 7)

The animals were cooled to and kept at 15°C for 3 h. After 2 h, the animals received a bolus dose of 0.33 ml of 5% glucose over 10 min, followed by a continuous infusion of 0.5 ml/h during the last hour of hypothermia and until rewarming was completed at 37°C.

Levosimendan (n = 7)

The animals were cooled to and kept at 15°C for 3 h. After 2 h, the animals received a bolus dose of 24 μg/kg/min levosimendan over 10 min, followed by a continuous 0.6 μg/kg/min infusion during the last hour of hypothermia and throughout rewarming (10).

Nitroprusside (n = 7)

The animals were cooled to and kept at 15°C for 3 h. After 2 h, an infusion of nitroprusside was started at 0.625 μg/kg/min. During rewarming, the dose was titrated to reduce mean arterial pressure (MAP) by 30% compared to historical controls (8). On average, each rat received 0.178 mg of nitroprusside.

Normothermic Control (n = 6)

The animals were kept at 37°C for 5 h. After 2.5 h, the animals received a 10-min bolus infusion of 2.0 ml/h glucose (5%), followed by a 0.5 ml/h infusion lasting throughout the remaining experiment.

Hemodynamic Data

Arterial pressure was obtained with a fluid-filled 22G cannula inserted in the left femoral artery and connected to a fluid manometer. Left ventricular pressure was obtained with a fluid-filled catheter inserted into the right carotid artery and advanced to the left ventricle under pressure guidance and connected to a manometer.

CO was measured with the thermodilution method, by injecting 0.15 ml of precooled (5°C) 0.9% saline through the jugular vein (21). The rapid change in temperature was recorded by a thermocouple, inserted into the left femoral artery, and advanced to the ascending aortic arch. Thermodilution curves were recorded and analyzed in LabChart 8.0. In the hypothermia groups, CO was measured at 37, 30, 22, and 15°C during cooling and rewarming. In the normothermia group, CO was measured at baseline ($37°C_{BL}$) and, after that, hourly till final recording ($37°C_{5h}$). Heart rate (HR) was calculated based on the femoral pressure signal, and SVR, stroke volume (SV), and cardiac index (CI) were calculated using the following formulas: SVR = MAP/CO, SV = CO/HR, and CI = CO/9.83*[body weight$^{(2/3)}$].

To investigate organ blood flow, we applied the stable isotope microsphere technique (22). A volume of 0.5 ml, containing 250,000 microspheres/ml (BioPal Mi, USA), labeled with either lutetium or samarium, was injected into the left ventricle using the catheter. Simultaneously, a reference sample, 0.5 ml/min, was drawn from the left femoral artery (2, 23, 24). After euthanasia, the brain and cerebellum, heart, kidneys, liver, and stomach were harvested, washed in SanSaline (BioPal), weighed, and dried. Quantification of microspheres in tissue and blood samples was done by BioPal (Mi, USA). Later, OBF was calculated by

normalizing organ microsphere concentration (disintegration per minute/g) with the microsphere concentration of the reference sample (disintegration per minute/ml/min) (22). In the hypothermia groups, OBF was measured during rewarming at 30 and 37°C. In the normothermia group (37°C), OBF was measured at baseline.

Biochemical Data

Arterial blood was analyzed for pO_2, pCO_2, oxygen saturation (SaO_2), pH, hemoglobin (Hb), hematocrit, and lactate. HCO_3^- and base excess were automatically calculated based on the measured data (Rapidlab 800, Chiron Diagnostics). Blood gases were analyzed at 37°C and not corrected for core temperature (25). In the hypothermia groups, arterial blood gas analyses were obtained at baseline, during cooling at the start of stable hypothermia (15°C_0), during rewarming at 30°C (30°C_{RW}), and after rewarming (37°C_{RW}). At 37°C_{RW}, a venous blood gas was also sampled. In the normothermia group, arterial blood gases were analyzed at 37°C_{BL}, and finally, after 5 h, also venous blood gases were analyzed. Arterial and venous blood oxygen content (CaO_2 and CvO_2), DO_2, and oxygen consumption (V_{O2}) were calculated using the following formulas: CaO_2 and $CvO_2 = (Hb \times 1.34 \times SaO_2/100) + (pO_2 \times 0.0031 \times 7.5)$, $D_{O2} = CaO_2 \times CO$ and $V_{O2} = CO \times (CaO_2 - CvO_2)$.

Levosimendan and Nitroprusside

Levosimendan was purchased from Orion pharma as SIMDAX® (2.5 mg/ml). On the day of the experiment, it was diluted in 5% glucose (10). Dilution was calculated in each experiment to adjust for body weight.

Nitroprusside was purchased from Hospira as NITROPRESS® (25 mg/ml). On the day of the experiment, it was diluted to 0.125 mg/ml (1:200) in 5% glucose (8).

Statistical Analyses

All statistical analysis were performed using SigmaPlot 13.0 (SAS).

The sample size was calculated with three independent sample size analysis. The first two used the expected difference between myocardial blood flow and mean arterial pressure after rewarming in the three group thermic groups. The third used the expected change in myocardial blood flow after rewarming compared to baseline.

Based on these sample size analyses, we concluded that a total of 27 animals were needed to attain a statistical power >0.8.

Hemodynamic results were analyzed with a two-way repeated measure ANOVA analysis. *Post hoc* analysis and all group comparisons were performed using a Holm–Sidak method.

Within-group comparisons of organ blood flow and blood gas data were done using repeated measure one-way ANOVA. *Post hoc* analyses were performed using a Holm–Sidak method. Between-group analyses at baseline, during, and after rewarming were done using a one-way ANOVA. *Post hoc* analyses were performed using a Holm–Sidak method.

RESULTS

Organ Blood Flow

Figure 1 compared to 37°C_{BL}, blood flow in the brain, stomach, right, and left kidney was reduced in all groups at 30°C_{RW}. No difference in blood flow of other organs was found between the three groups.

At 37°C_{RW}, the control and LS-treated groups demonstrated significant reductions in blood flow to all organs, except for the liver, compared to 37°C_{BL} Similar results were found in the SNP group. However, heart blood flow was not reduced at 37°C_{RW}

At 37°C_{RW}, both LS and SNP elevated brain blood flow compared to the control group. Blood flow in the heart was elevated in the SNP-treated group compared to both the control group and LS. Blood flow in the stomach was elevated in the SNP group compared to the control group. No difference was found between the three groups in kidneys or liver blood flow.

Hemodynamic Results

Table 1 and **Figure 2** no differences were found in any of the hemodynamic variables between the three hypothermia groups at baseline (37°C_{BL}).

At 30°C during rewarming (30°C_{RW}), all three groups, independent of intervention, showed depressed MAP, CI, CO, and HR when compared to 37°C_{BL}.

At 30°C_{RW}, CI, CO, and SV were significantly higher in the LS group compared to the control. Further, SVR was reduced in both SNP and LS groups compared to the control. No differences were found between SNP and LS in any of the other hemodynamic variables.

Compared to 37°C_B, SV was depressed in both the control and the SNP group at 37°C after rewarming (37°C_{RW}). SVR was elevated only in the control group at 37°C_{RW} compared to 37°C_{BL}. At 37°C_{RW}, MAP, CI, and CO were all depressed in all three groups, while SV was depressed only in the SNP and control groups compared to 37°C_{BL}.

At 37°C_{RW}, CO, CI, and SV were significantly higher and SVR significantly lower in the LS-treated group compared to the control. Compared to the control group, SNP significantly elevated CO and CI and reduced MAP and SVR. CO, CI, and MAP were significantly higher with LS than SNP.

Blood Gas Results

Table 2 no differences were found in arterial blood gases between the three hypothermia groups at 37°C_{BL}.

Compared to 37°C_{BL}, Hb), hematocrit and lactate were significantly elevated at 30°C_{RW} in all groups. SaO_2 was elevated in the control group, and pCO_2 was elevated in the SNP group. Further, D_{O2}, pH, base excess, and HCO_3^- were significantly reduced in all groups at 30°C_{RW}. In addition, SaO_2 was decreased in the control group.

At 30°C_{RW}, D_{O2} was significantly higher in the LS group than in the control. Further, plasma lactate levels were elevated in the SNP group compared to both control and LS groups. No other between-group differences were found at 30°C_{RW}.

At 37°C_{RW} Hb, hematocrit, pO_2, and lactate were elevated in all groups compared to 37°C_{BL}. Further, D_{O2}, pH, base excess,

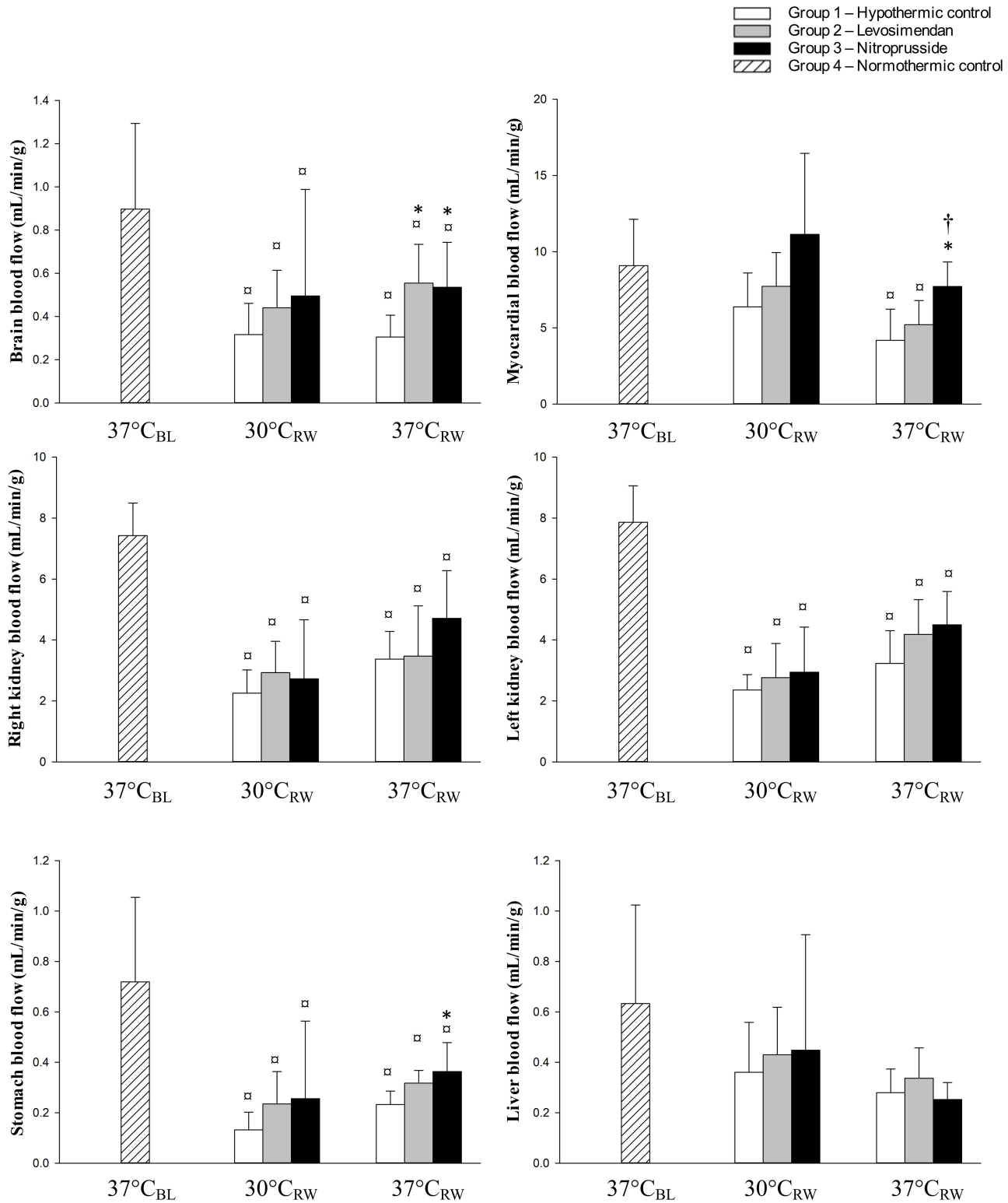

FIGURE 1 | Organ blood flow at baseline (37°C$_{BL}$), during and after rewarming (30 and 37°C$_{RW}$) from hypothermia in untreated and treated rats with levosimendan or nitroprusside (each group $n = 7$). Values are mean ± SD. *$P < 0.05$ vs. control group at corresponding temperatures, †$P < 0.05$ vs. levosimendan group at corresponding temperatures, ¤$P < 0.05$ vs. 37°C$_{BL}$ (Holm–Sidak method).

TABLE 1 | Heart rate (HR), mean arterial pressure (MAP), stroke volume (SV), cardiac output (CO), cardiac index (CI), and systemic vascular resistance (SVR) at baseline (37°C_{BL}), during and after rewarming (30 and 37°C_{RW}) from hypothermia in untreated and treated rats with levosimendan or nitroprusside (each group $n = 7$).

Parameter	Group	37°C_{BL}	30°C_{RW}	37°$_{RW}$
HR (beats/min)	Control	433 ± 27	312 ± 23¤	411 ± 39
	Levosimendan	435 ± 34	296 ± 41¤	428 ± 63
	Nitroprusside	449 ± 24	284 ± 41¤	417 ± 26
MAP (mmHg)	Control	115.1 ± 8.8	94.2 ± 17.1¤	80.8 ± 13.5¤
	Levosimendan	118.4 ± 13.8	81.5 ± 12.5¤	86.7 ± 10.3¤
	Nitroprusside	115.3 ± 12.6	71.3 ± 5.2¤*	69.6 ± 12.7¤†
SV (μL)	Control	186 ± 19	129 ± 27¤	116 ± 11¤
	Levosimendan	192 ± 16	180 ± 33*	159 ± 31*
	Nitroprusside	182 ± 13	167 ± 69¤	131 ± 8¤
CO (mL/min)	Control	80.41 ± 6.5	40.03 ± 8.1¤	47.22 ± 3.9¤
	Levosimendan	83.09 ± 5.8	52.24 ± 4.8¤*	66.57 ± 5.6¤*
	Nitroprusside	81.47 ± 6.1	45.28 ± 10.7¤	54.48 ± 5.2¤†
CI (mL/min/g)	Control	0.18 ± 0.02	0.09 ± 0.01¤	0.10 ± 0.01¤
	Levosimendan	0.19 ± 0.02	0.12 ± 0.01¤*	0.15 ± 0.01¤*
	Nitroprusside	0.19 ± 0.01	0.10 ± 0.02¤	0.12 ± 0.01¤*†
SVR (mmHg/mL/min)	Control	1.44 ± 0.17	2.37 ± 0.26¤	1.71 ± 0.20 ¤
	Levosimendan	1.43 ± 0.20	1.57 ± 0.26*	1.31 ± 0.18*
	Nitroprusside	1.42 ± 0.14	1.64 ± 0.31*	1.27 ± 0.12*

Values are mean ± SD.
**P < 0.05 vs. control group at corresponding temperatures.*
†P < 0.05 vs. levosimendan group at corresponding temperatures.
¤P < 0.05 vs. 37°C_{BL} within-group (Holm–Sidak method).

and HCO_3^- were significantly reduced in all groups at 37°C_{RW}. In addition, SaO_2 was reduced in the control group.

At 37°C_{RW}, D_{O2}, and V_{O2} were significantly elevated in the LS-treated group than in the SNP and control. No differences were found between groups in other variables at 37°C_{RW}.

DISCUSSION

The main findings of this study are that LS and SNP equally improved blood flow to the brain, despite elevating cardiac output to different levels. When comparing the effects of two different pharmacologic interventions during rewarming, vasodilation by SNP vs. inotropic support plus vasodilation by LS, we find that, although LS is superior to SNP to restore global hemodynamic function, OBF is equally or better preserved after intervention with SNP. This finding indicates that increased vascular resistance is a central element in the complex pathophysiology of cardiac dysfunction and reduced OBF after rewarming from hypothermia.

The aim of this experiment was to verify if the documented effects that both LS and SNP to elevate OBF during normothermic conditions (18–20) are valid also during rewarming from hypothermia. As a surrogate for monitoring organ microcirculatory variables, in clinical practice, we usually pay attention to variables such as CO, HR, MAP, and SVR. The specific aim was to test our hypotheses that the combined inotropic and vasodilatory effects of LS would improve OBF over that of the isolated vasodilation offered by SNP after rewarming from hypothermia. However, this experiment indicates that, during rewarming, peripheral vasodilation is superior to CO to increase OBF. To emphasize this, we present and discuss our data related to the different organs.

Brain Blood Flow

A mismatch between brain blood flow (BBF) and cerebral metabolic rate of oxygen during hypothermia is a much-discussed topic (2, 26–29). Other studies state that, while the cerebral metabolic rate of oxygen is normalized, BBF remains reduced after rewarming. This indicates the existence of maintained dysfunctional cerebral autoregulation (26, 30, 31). Evidence of faulty cerebral autoregulation after rewarming is reported and supports the presence of a concomitant change in cerebral vascular function and hemodynamics (32–35). Under non-pathological, normothermic conditions, neither SNP nor LS will affect BBF (18, 36). In the present experiment, a 42% reduction in CO corresponds to a 75% reduction of BBF in the control group after rewarming. For comparison, studies during normothermic conditions on healthy humans report that a 30% reduction in CO would reduce BBF by only 10% (37). If we return to the present experiment, different from the non-treated control group, both SNP and LS elevated BBF similarly, 75 vs. 81%. However, at the same time, SNP managed to elevated CO by only 14%, compared to 30% with LS. Thus, we interpret our findings to disclose alterations of cerebral autoregulation after rewarming, possibly due to elevated cerebral vascular resistance (32, 33). To speculate, we suggest that differences in the effects of SNP and LS

TABLE 2 | Hemoglobin (Hb), hematocrit, oxygen saturation (SaO_2), oxygen saturation (pO_2), arterial oxygen content (CaO_2), venous oxygen content (CvO_2), oxygen delivery, (D_{O2}); oxygen consumption, (V_{O2}), at baseline (37°C_{BL}), during and after rewarming (30°C_{RW}, and 37°C_{RW}) from hypothermia in untreated and treated rats with levosimendan or nitroprusside (each group $n = 7$).

Parameter	Group	37°C_{BL}	30°C_{RW}	37°C_{RW}
Hb (g/dL)	Control	12.56 ± 0.96	14.69 ± 0.25¤	13.27 ± 0.84¤
	Levosimendan	12.86 ± 1.18	14.29 ± 0.36¤	13.01 ± 0.88¤
	Nitroprusside	12.13 ± 0.71	14.04 ± 0.32¤	12.77 ± 0.62¤
Hct (%)	Control	38.63 ± 2.93	45.04 ± 0.74¤	40.80 ± 2.55¤
	Levosimendan	39.59 ± 3.53	43.80 ± 1.10¤	39.99 ± 2.73¤
	Nitroprusside	37.37 ± 2.12	43.13 ± 0.97¤	39.29 ± 1.85¤
SaO_2 (%)	Control	86.29 ± 8.93	95.10 ± 0.77¤	91.80 ± 4.17¤
	Levosimendan	88.46 ± 3.46	91.66 ± 2.53	92.13 ± 3.71
	Nitroprusside	91.67 ± 2.98	94.76 ± 0.55	91.17 ± 4.28
pO_2 (kPa)	Control	9.77 ± 2.39	17.38 ± 1.41	12.22 ± 2.54¤
	Levosimendan	9.55 ± 1.01	15.28 ± 2.38	11.12 ± 1.87¤
	Nitroprusside	12.16 ± 0.70	17.61 ± 0.85	12.31 ± 0.73¤
CaO_2 (mg/dL)	Control	14.71 ± 1.61	18.98 ± 0.39	16.58 ± 0.74
	Levosimendan	15.49 ± 1.89	17.92 ± 0.79	16.32 ± 1.35
	Nitroprusside	15.16 ± 0.70	18.25 ± 0.48	15.88 ± 1.03
D_{O2} (mg/min)	Control	1,180 ± 142	766 ± 54¤	784.5 ± 89¤
	Levosimendan	1,281 ± 117	935 ± 51¤*	1083 ± 81¤*
	Nitroprusside	1,235 ± 103	820 ± 68¤	866 ± 111¤†
V_{O2} (mg/min)	Control	–	–	465 ± 40
	Levosimendan	–	–	586 ± 109*
	Nitroprusside	–	–	521 ± 110 †
pH	Control	7.35 ± 0.03	7.22 ± 0.03¤	7.30 ± 0.04¤
	Levosimendan	7.35 ± 0.04	7.22 ± 0.01¤	7.33 ± 0.03¤
	Nitroprusside	7.38 ± 0.02	7.20 ± 0.02¤	7.28 ± 0.03¤
pCO_2 (kPa)	Control	5.01 ± 0.88	5.01 ± 0.42	4.11 ± 0.56¤
	Levosimendan	5.07 ± 0.26	5.50 ± 0.22	4.31 ± 0.38¤
	Nitroprusside	4.52 ± 0.49	5.50 ± 0.17¤	4.63 ± 0.34
Lactate (mmol/L)	Control	0.90 ± 0.51	2.97 ± 0.23¤	3.64 ± 0.84¤
	Levosimendan	0.87 ± 0.51	3.01 ± 0.41¤	3.26 ± 0.67¤
	Nitroprusside	0.63 ± 0.19	3.93 ± 0.31¤†*	4.10 ± 0.52¤
BE (mmol)	Control	−4.60 ± 2.31	−11.80 ± 0.57¤	−10.16 ± 1.96¤
	Levosimendan	−3.94 ± 2.22	−10.23 ± 0.68¤	−8.41 ± 1.12¤
	Nitroprusside	−4.93 ± 1.45	−11.11 ± 0.67¤	−9.57 ± 1.07¤
HCO_3^- (mmol/L)	Control	20.44 ± 1.52	15.00 ± 0.58¤	16.54 ± 1.46¤
	Levosimendan	21.02 ± 1.87	15.82 ± 0.46¤	17.80 ± 0.90¤
	Nitroprusside	20.53 ± 1.01	15.25 ± 0.53¤	16.72 ± 0.84¤

Values are mean ± SD.
$P < 0.05$ vs. control group at corresponding temperatures.
†$P < 0.05$ vs. levosimendan group at corresponding temperatures.*
¤$P < 0.05$ vs. 37°C_{BL} within-group (Holm–Sidak method).*

to elevate BBF over those to increase CO are due to increased cerebral vascular resistance. This increased vascular resistance appears not to be expedient, and the vasodilator properties of SNP and LS are the primary driving forces to improved BBF in this study.

Myocardial Blood Flow

Aortic pressure and coronary resistance strongly regulate myocardial blood flow (MBF) by myocardial metabolic demand (38). While MBF is depressed after hypothermia, the autoregulatory properties of the coronaries appear to be unaltered. In this study, only the vasodilatory effects of SNP caused the elevation of MBF. This is in concordance with findings reported during normothermic conditions (18, 39).

Investigators have demonstrated a reduced MBF during hypothermia with spontaneous circulation (2, 40–43). Further, Berne revealed that the coronary regulation of flow is changed in hypothermia. He argued that the coronary vessels are

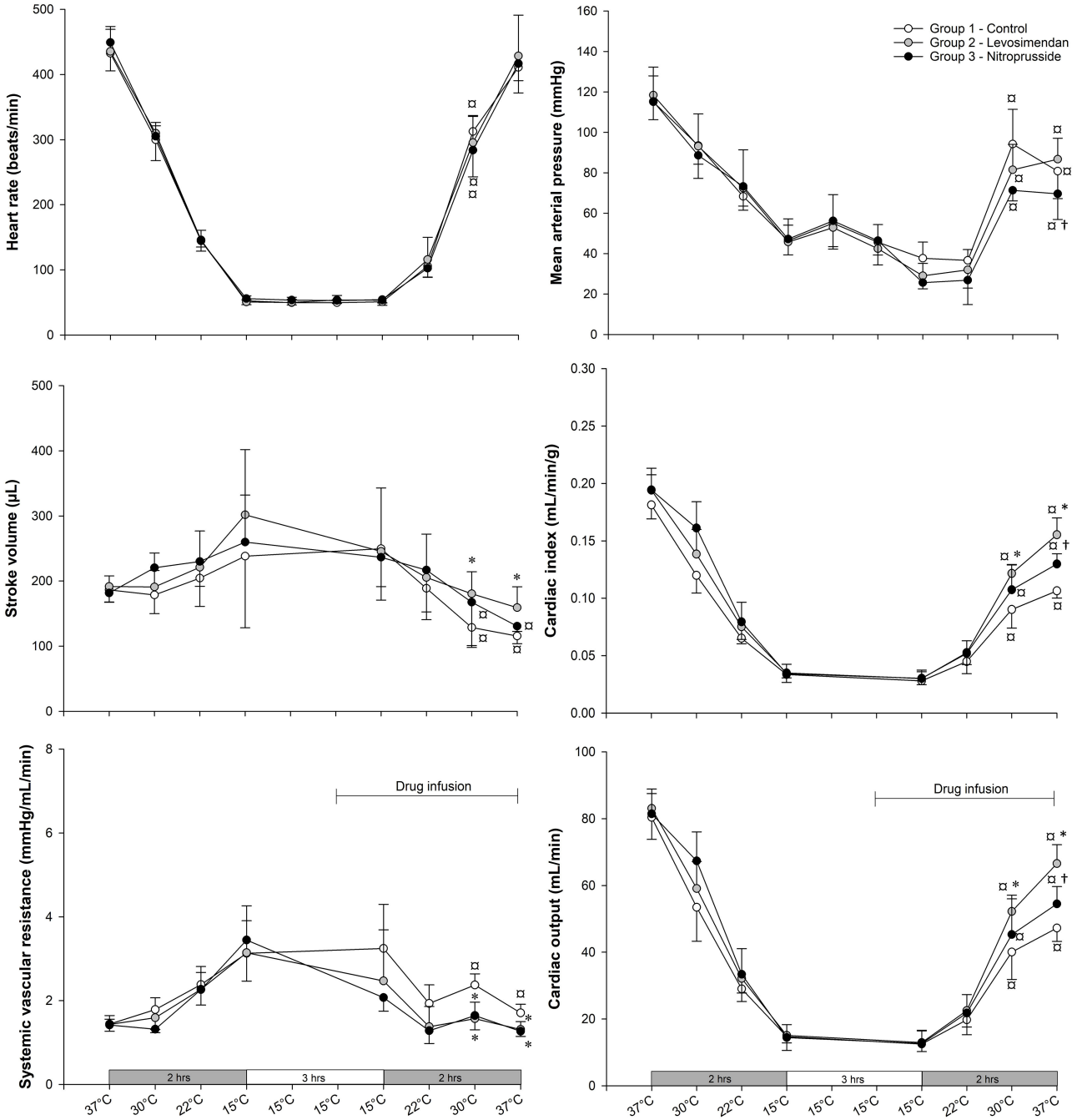

FIGURE 2 | Heart rate (HR), mean arterial pressure (MAP), stroke volume (SV), cardiac output (CO), cardiac index (CI), and systemic vascular resistance (SVR) at baseline, during and after rewarming from hypothermia in untreated and treated rats with levosimendan or nitroprusside (each group $n = 7$). Values are mean ± SD. *$P < 0.05$ vs. control group at 37°C_{BL}, 30°C_{RW}, and 37°C_{RW}; †$P < 0.05$ vs. levosimendan group at corresponding temperatures; ¤$P < 0.05$ vs. 37°C_{BL} within-group (Holm–Sidak method).

relatively vasodilated during hypothermia, as the relative reduction in MBF is lower than the change in aortic perfusion pressure (41, 44). He stated that the effects of hypothermia on coronary smooth muscle are relaxation and that this is the main explanation for vasodilation, which causes a high ratio between MBF and myocardial oxygen consumption (41, 44).

In concordance with previous studies, the present study also shows a reduced MBF during and after rewarming (2, 40–43). Previously, we reported that the coronary vasculature

has reduced sensitivity to endothelium-dependent and *independent* vasodilation but normalized after rewarming (45). This might indicate functioning vascular regulation after rewarming. Although this study made no attempts to investigate endothelium-dependent vasodilation in this study, we show that SNP-induced endothelium-independent vasodilation resulted in elevated MBF after rewarming from hypothermia.

Myocardial Function

A study from our group demonstrated LS to improve cardiac contractility and CO after rewarming from hypothermia (10) after using the present intact animal model. In the present study, LS improved cardiac function without elevating MBF, as demonstrated using the same model and dosage of LS. Elevated cardiac contractility should elevate myocardial oxygen consumption (46). Our findings might indicate that MBF matches cardiac metabolic demands and that regulation of MBF is preserved after rewarming. A similar conclusion was made in earlier studies (25, 47). Lastly, in another study, LS did not increase plasma cardiac troponin I, compared to non-treated animals during rewarming. As the release of cardiac troponin is a marker of myocardial damage, we understand this to indicate the absence of further damaging factors such as hypoxia or apoptosis (10).

Renal and Stomach Blood Flow

Previous studies have reported depressed renal blood flow (RBF) following rewarming (2, 48). As both LS and SNP failed to elevate RBF in response to elevated CO, the depressed flow likely stems from other mechanisms than low CO. Hypothermia and rewarming is associated with activation of the renin–aldosterone–angiotensin system (RAAS) in both humans and rats (49, 50). Broome et al. demonstrated that SNP did not affect RBF during targeted vasoconstriction with angiotensin II infusion (19). They interpreted that the vasoconstrictive effects of angiotensin II supersede the vasodilatory effects of SNP in the kidney. In the presented study, SNP failed to elevate RBF. As in the experiment with Broome et al., the elevation of the renin–aldosterone–angiotensin system might explain our findings (49, 50).

In contrast to the RBF, Broome et al. found SNP to have a vasodilating effect on stomach blood flow (SBF) during angiotensin II-induced vasoconstriction (19). In the presented study, SNP also elevated SBF. To speculate, our findings might indicate that activation of the renin–aldosterone–angiotensin system hormones as possible mediators of poor RBF and SBF. Our results and reports from other investigators may support these ideas, as they show that SNP only affects SBF and not RBF, as well as increased renin–aldosterone–angiotensin during hypothermia (49, 50). Further, studies from an identical model, as presented, show renal tubular necrosis after rewarming (51). Severe tubular necrosis is associated with renal vasoconstriction and reduced RBF and explains why SNP and LS failed to elevate RBF.

Clinical Significance

The physiological message this study brings to the clinical table is to focus on the mismatch between organ perfusion/microcirculation and global perfusion in the hypothermia/rewarming setting. Routine bedside intensive care lacks tools to assess organ perfusion and microcirculation changes, continually and accurately, in response to treatment. This highlights the need to be cautious in translating variables related to global circulation into changes that are important for organ blood flow and microcirculation, in this case, during rewarming from hypothermia.

This experiment, describing both LS and SNP's pharmacologic effects to alleviate post-hypothermic circulatory dysfunction and OBF in a rodent model, may encourage further research in large animal models before clinical applications can be suggested.

Limitations

SNP is a known cyanide donor (52, 53). Enzymatic breakdown of cyanide is done by the enzyme thiosulfate sulfurtransferase (54). In critically ill patients, SNP-induced cyanide breakdown is higher than production at SNP infusion rates below 2 μg/kg/min (55). However, studies have reported elevated cyanide levels at lower infusion rates during hypothermia, possibly due to low enzymatic activity. Therefore, investigators have advocated for caution when using high doses or prolonged use of SNP (56). Animals in this study received, on average, 2.9 μg/kg/min SNP and are, therefore, possible victims of high cyanide levels, affecting the results. We do see possible evidence of cyanide in the presented data. Both elevated venous O_2 and serum lactate are present in the SNP group, although not significantly. Other investigators have toned down the importance of cyanide poisoning by SNP, also during hypothermia and cardiopulmonary bypass. Interestingly enough, the SNP-treated animals, despite possible cyanide toxicity, had improved hemodynamic and blood flow parameters compared to the control group (52, 53).

CONCLUSIONS

From critical care reports, we know that efforts to elevate OBF will improve end-organ function and patient survival. The present findings indicate potential beneficial effects on organ function by combining cardiac inotropic support and reducing peripheral organ vascular resistance (15–17). In more detail, our results demonstrate the beneficial effects of vasodilation to increase CO and OBF, in general, and BBF, in particular. While the inotropic effects of LS are shown to improve CO, its relative weak additional vasodilator properties fail to improve peripheral organ circulation. We, therefore, interpret the vasodilator properties of LS and SNP to be the primary source to increase organ blood flow, superior to the increase in CO.

DATA AVAILABILITY STATEMENT

The raw data supporting the conclusions of this article will be made available by the authors, without undue reservation.

ETHICS STATEMENT

The animal study was reviewed and approved by Norwegian Animal Research Authority.

AUTHOR CONTRIBUTIONS

BH has contributed with research ideas, protocol development, experimental work, data analysis, and manuscript. TK has contributed with experimental work and data analysis. ED has contributed with research ideas, data analysis, and manuscript. TT has contributed with research ideas, protocol development, data analysis, and manuscript. All authors contributed to the article and approved the submitted version.

FUNDING

This study was supported by The Laerdal Foundation (grant no. 3272) and Norwegian Research Council.

ACKNOWLEDGMENTS

This study would not be possible without the funding from The Laerdal Foundation, and we greatly appreciate their support.

REFERENCES

1. Danzl DF, Pozos RS. Accidental hypothermia. *N Engl J Med.* (1994) 331:1756–60. doi: 10.1056/NEJM199412293312607
2. Tveita T, Ytrehus K, Skandfer M, Oian P, Helset E, Myhre ES, et al. Changes in blood flow distribution and capillary function after deep hypothermia in rat. *Can J Physiol Pharmacol.* (1996) 74:376–81. doi: 10.1139/y96-028
3. Tveita T, Mortensen E, Hevroy O, Refsum H, Ytrehus K. Experimental hypothermia: effects of core cooling and rewarming on hemodynamics, coronary blood flow, and myocardial metabolism in dogs. *Anesth Analg.* (1994) 79:212–8. doi: 10.1213/00000539-199408000-00002
4. Han Y-S, Tveita T, Kondratiev TV, Prakash YS, Sieck GC. Changes in cardiovascular beta-adrenoceptor responses during hypothermia. *Cryobiology.* (2008) 57:246–50. doi: 10.1016/j.cryobiol.2008.09.006
5. Tveita T, Ytrehus K, Myhre ES, Hevroy O. Left ventricular dysfunction following rewarming from experimental hypothermia. *J Appl Physiol.* (1998) 85:2135–9. doi: 10.1152/jappl.1998.85.6.2135
6. van der Ploeg G-J, Goslings JC, Walpoth BH, Bierens JJLM. Accidental hypothermia: rewarming treatments, complications and outcomes from one university medical centre. *Resuscitation.* (2010) 81:1550–5. doi: 10.1016/j.resuscitation.2010.05.023
7. Mégarbane B, Axler O, Chary I, Pompier R. Hypothermia with indoor occurrence is associated with a worse outcome. *J Intensive Care Med.* (2000) 26:1843–9. doi: 10.1007/s001340000702
8. Håheim B, Kondratiev T, Dietrichs ES, Tveita T. The beneficial hemodynamic effects of afterload reduction by sodium nitroprusside during rewarming from experimental hypothermia. *Cryobiology.* (2017) 77:75–81. doi: 10.1016/j.cryobiol.2017.05.002
9. Soar J, Perkins GD, Abbas G, Alfonzo A, Barelli A, Bierens JJLM, et al. European resuscitation council guidelines for resuscitation 2010 section 8. Cardiac arrest in special circumstances: Electrolyte abnormalities, poisoning, drowning, accidental hypothermia, hyperthermia, asthma, anaphylaxis, cardiac surgery, trauma, pregnancy, electrocution. *Resuscitation.* (2010) 81:1400–33. doi: 10.1016/j.resuscitation.2010.08.015
10. Dietrichs ES, Håheim B, Kondratiev T, Sieck GC, Tveita T. Cardiovascular effects of levosimendan during rewarming from hypothermia in rat. *Cryobiology.* (2014) 69:402–10. doi: 10.1016/j.cryobiol.2014.09.007
11. Dietrichs ES, Kondratiev T, Tveita T. Milrinone ameliorates cardiac mechanical dysfunction after hypothermia in an intact rat model. *Cryobiology.* (2014) 69:361–6. doi: 10.1016/j.cryobiol.2014.09.002
12. Pathak A, Lebrin M, Vaccaro A, Senard JM, Despas F. Pharmacology of levosimendan: inotropic, vasodilatory and cardioprotective effects. *J Clin Pharm Ther.* (2013) 38:341–9. doi: 10.1111/jcpt.12067
13. Mohan P, Brutsaert DL, Paulus WJ, Sys SU. Myocardial contractile response to nitric oxide and cGMP. *Circulation.* (1996) 93:1223–9. doi: 10.1161/01.CIR.93.6.1223
14. Thompson RB, Bos EJ, Esposito DJ. The effects of acute afterload change on systolic ventricular function in conscious dogs with normal vs. failing hearts. *Eur J Heart Fail.* (2003) 5:741–9. doi: 10.1016/S1388-9842(03)00152-1
15. Spronk PE, Zandstra DF, Ince C. Bench-to-bedside review: sepsis is a disease of the microcirculation. *Crit Care.* (2004) 8:462–8. doi: 10.1186/cc2894
16. Trzeciak S, McCoy JV, Phillip Dellinger R, Arnold RC, Rizzuto M, Abate NL, et al. Early increases in microcirculatory perfusion during protocol-directed resuscitation are associated with reduced multi-organ failure at 24 h in patients with sepsis. *Intensive Care Med.* (2008) 34:2210–7. doi: 10.1007/s00134-008-1193-6
17. Tuchschmidt J, Fried J, Astiz M, Rackow E. Elevation of cardiac output and oxygen delivery improves outcome in septic shock*. *Chest.* (2006) 102:216–20. doi: 10.1378/chest.102.1.216
18. Pagel PS, Hettrick DA, Warltier DC. Influence of levosimendan, pimobendan, and milrinone on the regional distribution of cardiac output in anaesthetized dogs. *Br J Pharmacol.* (1996) 119:609–15. doi: 10.1111/j.1476-5381.1996.tb15716.x
19. Broomé M, Åneman A, Haney M, HÄggmark S, Johansson G, Biber B. Angiotensin II mesenteric and renal vasoregulation: dissimilar modulatory effects with nitroprusside. *Acta Anaesthesiol Scand.* (2000) 44:1238–45. doi: 10.1034/j.1399-6576.2000.441009.x
20. Rowe GG, Henderson RH. Systemic and coronary hemodynamic effects of sodium nitroprusside. *Am Heart J.* (1974) 87:83–7. doi: 10.1016/0002-8703(74)90394-9
21. Kondratiev TV, Myhre ESP, Simonsen O, Nymark TB, Tveita T. Cardiovascular effects of epinephrine during rewarming from hypothermia in an intact animal model. *J Appl Physiol.* (2006) 100:457–64. doi: 10.1152/japplphysiol.00356.2005
22. Reinhardt CP, Dalhberg S, Tries MA, Marcel R, Leppo JA. Stable labeled microspheres to measure perfusion: validation of a neutron activation assay technique. *Am J Physiol Heart Circ Physiol.* (2001) 280:H108–16. doi: 10.1152/ajpheart.2001.280.1.H108
23. Ishise S, Pegram BL, Yamamoto J, Kitamura Y, Frohlich ED. Reference sample microsphere method: cardiac output and blood flows in conscious rat. *Am J Physiol.* (1980) 239:443–9. doi: 10.1152/ajpheart.1980.239.4.H443
24. Valkov S, Mohyuddin R, Nilsen JH, Schanche T, Kondratiev TV, Sieck GC, et al. Organ blood flow and O2 transport during hypothermia (27°C) and rewarming in a pig model. *Exp Physiol.* (2019) 104:50–60. doi: 10.1113/EP087205
25. Kondratiev TV, Flemming K, Myhre ESP, Sovershaev MA, Tveita T. Is oxygen supply a limiting factor for survival during rewarming from profound hypothermia? *Am J Physiol Heart Circ Physiol.* (2006) 291:H441–50. doi: 10.1152/ajpheart.01229.2005
26. Michenfelder JD, Milde JH. The effect of profound levels of hypothermia (below 14 C) on canine cerebral metabolism. *J Cereb Blood Flow Metab*. (1992) 12:877–80. doi: 10.1038/jcbfm.1992.120
27. Yenari MA, Wijman CAG, Steinberg GK. Effects of Hypothermia on Cerebral Metabolism, Blood Flow, and Autoregulation. In: Mayer SA, Sessler DI, editors. *Therapeutic Hypothermia* (Marcel Dekker) (2005). p. 141–79.
28. Polderman KH. Application of therapeutic hypothermia in the ICU: opportunities and pitfalls of a promising treatment modality. Part 1: indications evidence. *Intens Care Med.* (2004) 30:556–75. doi: 10.1007/s00134-003-2152-x

29. Polderman KH. Application of therapeutic hypothermia in the intensive care unit. *Intensive Care Med.* (2004) 30:757–69. doi: 10.1007/s00134-003-2151-y
30. Michenfelder JD, Milde JH. The relationship among canine brain temperature, metabolism, and function during hypothermia. *Anesthesiology.* (1991) 75:130–6. doi: 10.1097/00000542-199107000-00021
31. Murkin JM, Farrar JK, Tweed WA, McKenzie FN, Guiraudon G. Cerebral autoregulation and flow/metabolism coupling during cardiopulmonary bypass: the influence of PaCO2. *Anesth Analg.* (1987) 66:825–32. doi: 10.1213/00000539-198709000-00003
32. Johnston WE, Vinten-Johansen J, DeWitt DS, O'Steen WK, Stump DA, Prough DS. Cerebral perfusion during canine hypothermic cardiopulmonary bypass: effect of arterial carbon dioxide tension. *Ann Thorac Surg.* (1991) 52:479–89. doi: 10.1016/0003-4975(91)90909-A
33. Mezrow CK, Sadeghi AM, Gandsas A, Shiang HH, Levy D, Green R, et al. Cerebral blood flow and metabolism in hypothermic circulatory arrest. *Ann Thorac Surg.* (1992) 54:609–16. doi: 10.1016/0003-4975(92)91002-Q
34. Hansen TN, Dawson PE, Brockbank K. Effects of hypothermia upon endothelial cells: mechanisms and clinical importance. *Cryobiology.* (1994) 31:101–6. doi: 10.1006/cryo.1994.1013
35. Wagerle LC, Russo P, Dahdah NS, Kapadia N, Davis DA. Endothelial dysfunction in cerebral microcirculation during hypothermic cardiopulmonary bypass in newborn lambs. *J Thorac Cardiovasc Surg.* (1998) 115:1047–54. doi: 10.1016/S0022-5223(98)70404-0
36. Crockard HA, Brown FD, Mullan JF. Effects of trimethaphan and sodium nitroprusside on cerebral blood-flow in rhesus-monkeys. *Acta Neurochir.* (1976) 35:85–9. doi: 10.1007/BF01405936
37. Lassen NA. Cerebral blood flow and oxygen consumption in man. *Physiol Rev.* (1959) 39:183–238. doi: 10.1152/physrev.1959.39.2.183
38. Rubio R, Berne RM. Regulation of coronary blood flow. *Prog Cardiovasc Dis.* (1975) 18:105–22. doi: 10.1016/0033-0620(75)90001-8
39. Hoffman WE, Satinover I, Miletich DJ, Albrecht RF, Gans BJ. Cardiovascular changes during sodium nitroprusside or adenosine triphosphate infusion in the rat. *Anesth Analg.* (1982) 61:99–103. doi: 10.1213/00000539-198202000-00006
40. Anzai T, Turner MD, Gibson WH, Neely WA. Blood flow distribution in dogs during hypothermia and posthypothermia. *Am J Physiol.* (1978) 234:H706–10. doi: 10.1152/ajpheart.1978.234.6.H706
41. Berne RM. Cardiodynamics and the coronary circulation in hypothermia. *Ann N Y Acad Sci.* (1959) 80:365–83. doi: 10.1111/j.1749-6632.1959.tb49217.x
42. Edwards WS, Tuluy S, Reber WE, Siegel A, Bing RJ. Coronary blood flow and myocardial metabolism in hypothermia. *Ann Surg.* (1954) 139:275. doi: 10.1097/00000658-195403000-00003
43. Burlington RF, Dean MS, Jones SB. Coronary autoregulation and metabolism in hypothermic rat and ground squirrel hearts. *Am J Physiol Regul Integr Comp Physiol.* (1989) 256:R357–65. doi: 10.1152/ajpregu.1989.256.2.R357
44. Berne RM. The effect of immersion hypothermia on coronary blood flow. *Circ Res.* (1954) 2:236–42. doi: 10.1161/01.RES.2.3.236
45. Tveita T, Hevroy O, Refsum H, Ytrehus K. Coronary endothelium-derived vasodilation during cooling and rewarming of the in situ heart. *Can J Physiol Pharmacol.* (1999) 77:56–63. doi: 10.1139/y98-149
46. Graham TP, Covell JW, Sonnenblick EH, Ross J, Braunwald E. Control of myocardial oxygen consumption: relative influence of contractile state and tension development. *J Clin Invest.* (1968) 47:375–85. doi: 10.1172/JCI105734
47. Tveita T, Skandfer M, Refsum H, Ytrehus K. Experimental hypothermia and rewarming: changes in mechanical function and metabolism of rat hearts. *J Appl Physiol.* (1996) 80:291–7. doi: 10.1152/jappl.1996.80.1.291
48. Karim F, Reza H. Effect of induced hypothermia and rewarming on renal hemodynamics in anesthetized dogs. *Life Sci.* (1970) 9:1153–63. doi: 10.1016/0024-3205(70)90148-7
49. Kuroda T, Shida H, Inokawak K, Morimoto M, Ikeda Y, Tsugana J, et al. Significance of renin-angiotensin system during and after surface-induced simple hypothermia in open-heart surgery. *Jap Circ J.* (1983) 47:400–5. doi: 10.1253/jcj.47.400
50. Munday KA, Noble AR. Renin secretion in the hypothermic dog. *J Physiol.* (1970) 206:38–9P.
51. Tveita T, Johansen K, Lien AH, Myklebust R, Lindal S. Morphologic changes in tubular cells from in situ kidneys following experimental hypothermia and rewarming. *APMIS.* (2005) 113:13–20. doi: 10.1111/j.1600-0463.2005.apm1130103.x
52. Undquist PL, Rosling H, Tydén H. Cyanide release from sodium nitroprusside during coronary bypass in hypothermia. *Acta Anaesthesiol Scand.* (1989) 33:686–8. doi: 10.1111/j.1399-6576.1989.tb02992.x
53. Thomas C, Svehla L, Moffett BS. Sodium-nitroprusside-induced cyanide toxicity in pediatric patients. *Expert Opin Drug Saf.* (2009) 8:599–602. doi: 10.1517/14740330903081717
54. Smith RP, Kruszyna H. Nitroprusside produces cyanide poisoning via a reaction with hemoglobin. *J Pharmacol Exp Ther.* (1974) 191:557–63.
55. Johanning RJ, Zaske DE, Tschida SJ, Johnson SV, Hoey LL, Vance-Bryan K. A retrospective study of sodium nitroprusside use and assessment of the potential risk of cyanide poisoning. *Pharmacotherapy.* (1995) 15:773–7.
56. Friederich JA, Butterworth JF. Sodium nitroprusside: twenty years and counting. *Anesth Analg.* (1995) 81:152–62. doi: 10.1097/00000539-199507000-00031

Conflict of Interest: The authors declare that the research was conducted in the absence of any commercial or financial relationships that could be construed as a potential conflict of interest.

frontiers in Medicine

ORIGINAL RESEARCH
published: 27 November 2020
doi: 10.3389/fmed.2020.566582

Divergent Effects of the N-Methyl-D-Aspartate Receptor Antagonist Kynurenic Acid and the Synthetic Analog SZR-72 on Microcirculatory and Mitochondrial Dysfunction in Experimental Sepsis

László Juhász[1†], Attila Rutai[1†], Roland Fejes[1], Szabolcs P. Tallósy[1], Marietta Z. Poles[1], Andrea Szabó[1], István Szatmári[2], Ferenc Fülöp[2], László Vécsei[3,4], Mihály Boros[1] and József Kaszaki[1]*

[1] Faculty of Medicine, Institute of Surgical Research, University of Szeged, Szeged, Hungary, [2] Research Group for Stereochemistry, Institute of Pharmaceutical Chemistry, Hungarian Academy of Sciences, University of Szeged, Szeged, Hungary, [3] Department of Neurology, Interdisciplinary Excellence Centre, Faculty of Medicine, University of Szeged, Szeged, Hungary, [4] Hungarian Academy of Sciences (MTA)-University of Szeged (SZTE), Neuroscience Research Group, Szeged, Hungary

OPEN ACCESS

Edited by:
Andrey V. Kozlov,
Institute for Experimental and Clinical Traumatology (LBG), Austria

Reviewed by:
Johanna Catharina Duvigneau,
University of Veterinary Medicine Vienna, Austria
Balázs Hauser,
Semmelweis University Budapest, Hungary

***Correspondence:**
József Kaszaki
kaszaki.jozsef@med.u-szeged.hu

[†] These authors have contributed equally to this work

Specialty section:
This article was submitted to Intensive Care Medicine and Anesthesiology, a section of the journal Frontiers in Medicine

Received: 28 May 2020
Accepted: 28 October 2020
Published: 27 November 2020

Citation:
Juhász L, Rutai A, Fejes R, Tallósy SP, Poles MZ, Szabó A, Szatmári I, Fülöp F, Vécsei L, Boros M and Kaszaki J (2020) Divergent Effects of the N-Methyl-D-Aspartate Receptor Antagonist Kynurenic Acid and the Synthetic Analog SZR-72 on Microcirculatory and Mitochondrial Dysfunction in Experimental Sepsis. Front. Med. 7:566582. doi: 10.3389/fmed.2020.566582

Introduction: Sepsis is a dysregulated host response to infection with macro- and microhemodynamic deterioration. Kynurenic acid (KYNA) is a metabolite of the kynurenine pathway of tryptophan catabolism with pleiotropic cell-protective effects under pro-inflammatory conditions. Our aim was to investigate whether exogenously administered KYNA or the synthetic analog SZR-72 affects the microcirculation and mitochondrial function in a clinically relevant rodent model of intraabdominal sepsis.

Methods: Male Sprague–Dawley rats ($n = 8$/group) were subjected to fecal peritonitis (0.6 g kg^{-1} feces ip) or a sham operation. Septic animals were treated with sterile saline or received ip KYNA or SZR-72 (160 μmol kg^{-1} each) 16 and 22 h after induction. Invasive monitoring was performed on anesthetized animals to evaluate respiratory, cardiovascular, renal, hepatic and metabolic dysfunctions (PaO_2/FiO_2 ratio, mean arterial pressure, urea, AST/ALT ratio and lactate levels, respectively) based on the Rat Organ Failure Assessment (ROFA) score. The ratio of perfused vessels (PPV) of the ileal serosa was quantified with the intravital imaging technique. Complex I- and II-linked (CI; CII) oxidative phosphorylation capacities (OXPHOS) and mitochondrial membrane potential ($\Delta\Psi$mt) were evaluated by High-Resolution FluoRespirometry (O2k, Oroboros, Austria) in liver biopsies. Plasma endothelin-1 (ET-1), IL-6, intestinal nitrotyrosine (NT) and xanthine oxidoreductase (XOR) activities were measured as inflammatory markers.

Results: Sepsis was characterized by an increased ROFA score (5.3 ± 1.3 vs. 1.3 ± 0.7), increased ET-1, IL-6, NT and XOR levels, and decreased serosal PPV (65 ± 12% vs. 87 ± 7%), $\Delta\Psi$mt and CI–CII-linked OXPHOS (73 ± 16 vs. 158 ± 14, and 189 ± 67 vs. 328 ± 81, respectively) as compared to controls. Both KYNA and SZR-72 reduced systemic inflammatory activation; KYNA treatment decreased serosal perfusion

heterogeneity, restored PPV (85 ± 11%) and complex II-linked OXPHOS (307 ± 38), whereas SZR-72 improved both CI- and CII-linked OXPHOS (CI: 117 ± 18; CII: 445 ± 107) without effects on PPV 24 h after sepsis induction.

Conclusion: Treatment with SZR-72 directly modulates mitochondrial respiration, leading to improved conversion of ADP to ATP, while administration of KYNA restores microcirculatory dysfunction. The results suggest that microcirculatory and mitochondrial resuscitation with KYNA or the synthetic analog SZR-72 might be an appropriate supportive tool in sepsis therapy.

Keywords: polymicrobial sepsis, kynurenic acid, N-methyl-D-aspartate receptor antagonist, microcirculation, mitochondrial respiration, organ dysfunction

INTRODUCTION

Treatment of sepsis-induced multi-organ failure (MOF) is one of the most challenging tasks in intensive care therapy (1). According to current knowledge, the key problem in sepsis is the oxygen extraction deficit, which can originate from either insufficient oxygen delivery to the cells or inability of the cells to utilize oxygen. The poorly functioning microvasculature reduces delivery of oxygen to the tissue. In addition, as the mitochondrial electron transport system (ETS) is insufficient, it is unable to use oxygen efficiently; the switch to anaerobic pathways thus causes an energy deficit and eventual cell death (2, 3). These processes are intimately linked and finally lead to microcirculatory and mitochondrial distress syndrome (MMDS), which is believed to mediate end-organ damage (4). Therefore, the cornerstone of current organ-protective therapies is to prevent and treat oxygen debt globally by increasing oxygen uptake and transport, providing an adequate supply to meet subcellular oxygen demand (5). However, currently used respiratory- and circulatory-supportive modalities cannot always improve sepsis-induced alterations at the later stages (6).

Given this background, the major goal of our study was to find a novel, clinically applicable maneuver for microcirculatory recruitment and mitochondrial resuscitation to minimize the energy deficit of the organs. The metabolites and end-products of the tryptophan–L-kynurenine pathway have already been implicated in several ischemic and inflammatory disorders in the central nervous system (7). This pathway generates excitotoxic, N-methyl-D-aspartate receptor (NMDA-R) agonist quinolinic acid and the glutamate receptor antagonist kynurenic acid (KYNA). Interestingly, sepsis-induced tissue hypoxia is also associated with the activation of NMDA-R, which can lead to glutamate excitotoxicity and oxidative/nitrosative stress-mediated cell damage (8). Further, elevated plasma KYNA levels have been reported in association with pro-inflammatory cytokines and increased lactate concentrations in septic shock patients (9).

Excessive NMDA-R activation has been documented in various experimental models of inflammatory bowel diseases (10). Apart from neurons, the expression of receptor subunits was confirmed in peripheral organs, including the heart, small intestine, pancreas, and liver (11), where the activation of cellular NMDA-Rs may initiate oxidative stress, mitochondrial dysfunction, and apoptosis through calcium (Ca^{2+})- and reactive oxygen species (ROS)-mediated pathways (12).

Based on these findings, we hypothesized that KYNA via the inhibition of NMDA-R or other mechanisms might be a therapeutic tool to reduce microcirculatory and mitochondrial disturbances in sepsis. KYNA has a high affinity for the glycine co-agonist site on NMDA-R, binds to orphan G protein-coupled receptor GPR35 and aryl hydrocarbon receptor (13), and therefore takes part in the modulation of glutamatergic neurotransmission and alleviates adaptive immune response. Despite these properties and pleiotropic effects, its role in the regulation of the circulatory system is still unclear, and KYNA is considered a non-receptor-specific molecule (14). To address this issue, we set out to characterize and compare the microcirculatory and mitochondrial effects of KYNA and its blood–brain barrier (BBB)-permeable synthetic analog, SZR-72 (15, 16), on sepsis-induced microcirculatory and mitochondrial abnormalities and organ failure in a clinically-relevant rodent model of intra-abdominal sepsis.

MATERIALS AND METHODS

Animals

Male Sprague–Dawley rats ($n = 32$; 350 ± 30 g) were used. The animals were housed in plastic cages (21–23°C) with a 12/12 h dark/light cycle and access to standard rodent food and water *ad libitum*. The experiments were performed in accordance with the National Institutes of Health guidelines on the handling and care of experimental animals and the EU Directive 2010/63 for the protection of animals used for scientific purposes (approval number V/175/2018).

Sepsis Induction

Polymicrobial sepsis was induced with 3 ml intraperitoneally (ip)-administered fecal inoculum as described before (17). Briefly, fresh feces was collected from different animals and suspended in physiological saline. The concentration of the microorganisms in the suspension was determined before injection in 0.6 g kg^{-1} final doses.

Experimental Protocol

The animals were randomly divided into sham-operated ($n = 8$) and sepsis ($n = 24$) groups. Septic animals were subjected to fecal peritonitis (0.6 g kg^{-1} feces ip) or a sham operation (sterile saline ip). After 6 and 16 h from sepsis induction, all the animals received balanced crystalloid solution (Ringerfundin, 1.5 ml kg^{-1}; B. Braun, Melsungen, Germany) and analgesics (Buprenorphine, 15 μg kg^{-1}; Richter Pharma, Hungary) subcutaneously. Septic animals were divided further into KYNA- (Sigma-Aldrich Inc., St. Louis, MO, USA; 160 μmol kg^{-1} ip; $n = 8$) or SZR-72- [2-(2-N,N-dimethylaminoethyl-amine-1-carbonyl)-1H-quinolin-4-one hydrochloride, synthesized by the Institute of Pharmaceutical Chemistry, University of Szeged, Hungary; 160 μmol kg^{-1} ip; $n = 8$] treated and vehicle-treated control (saline ip; $n = 8$) groups. Treatments were performed in two steps (80 μmol kg^{-1}; in 1 ml kg^{-1} saline each) 16 and 22 h after sepsis induction.

To follow the progression of sepsis, the health status of the animals was monitored with a standardized well-being scoring system originally described for mice (18, 19). At the 22nd hour of the study, all the animals were anesthetized (ip ketamine 45.7 mg kg^{-1} and xylazine 9.12 mg kg^{-1}) and placed on a heating pad to maintain normal core body temperature (37°C). A tracheostomy was performed to facilitate spontaneous breathing, and the right jugular vein was cannulated for fluid resuscitation (Ringerfundin, 10 ml^{-1} kg^{-1} h^{-1}; B. Braun, Melsungen, Germany) and for the maintenance of continuous anesthesia (ketamine 12 mg kg^{-1} h^{-1}, xylazine 2.4 mg kg^{-1} h^{-1}, and diazepam 0.576 mg kg^{-1} h^{-1} iv). The left carotid artery was cannulated to monitor heart rate (HR) and mean arterial pressure (MAP) (SPEL Advanced Cardiosys 1.4; Experimetria Ltd., Budapest, Hungary).

After surgery and a 30-min stabilization, MAP and HR monitoring was performed every 15 min for 60 min. Arterial and venous blood gas analyses (Cobas b123; Roche Ltd., Basel, Switzerland) were performed at the 0th and 60th min of the monitoring period. Simplified oxygen extraction (O_2ER) was calculated from arterial and venous oxygen saturation based on a standard formula ($SaO_2 - SvO_2)/SaO_2$). The degree of lung injury was determined by using the arterial partial pressure of oxygen to fractional inspired oxygen (PaO_2/FiO_2) ratio. After the 60-min hemodynamic monitoring period, a median laparotomy was performed to observe the microcirculation of the ileal serosa (see below). Thereafter, a liver tissue biopsy was taken to evaluate mitochondrial respiratory functions. Samples from the terminal ileum were harvested, followed by blood sampling from the inferior vena cava for biochemical measurements (see below). After tissue samplings, animals were sacrificed under deep anesthesia (**Figure 1**).

Measurements of Metabolic, Inflammatory, and Organ Function-Related Markers

Whole blood lactate levels were measured from venous blood samples (Accutrend Plus Kit; Roche Diagnostics Ltd., Rotkreuz, Switzerland) to determine metabolic imbalance. After the liver sampling, blood samples were collected from the inferior caval vein into precooled, EDTA-containing tubes (1 mg ml^{-1}), centrifuged (1,200*g* at 4°C for 10 min), and stored at −70°C. Plasma endothelin-1 (ET-1) and interleukin-6 (IL-6) levels were determined with standard ELISA kits (Cusabio Biotechnology Ltd., Wuhan, China and Biomedica Ltd., Vienna, Austria, respectively) following the manufacturer's instructions. Kidney injury was determined from plasma urea level, whereas liver dysfunction was assessed by measuring plasma alanine aminotransferase (ALT) and aspartate aminotransferase (AST) levels, using a Roche/Hitachi 917 analyzer (F. Hoffmann-La Roche AG, Switzerland). The De Ritis ratio (AST/ALT ratio) was calculated as a marker of hepatocellular damage. All analyses were performed on coded samples in a blinded fashion.

Evaluation of Ileal Xanthine Oxidoreductase Activity and Nitrotyrosine Levels

The same snap frozen tissues were used for these measurements. Ileum biopsies kept on ice were homogenized with a rotor stator homogenizer in a phosphate buffer (pH 7.4) containing 50 mmol l^{-1} Tris–HCl, 0.1 mmol l^{-1} EDTA, 0.5 mmol l^{-1} dithiothreitol, 1 mmol l^{-1} phenylmethylsulfonyl fluoride, 10 μg ml^{-1} soybean trypsin inhibitor, and 10 μg ml^{-1} leupeptin. Homogenates were then centrifuged at 4°C for 10 min at 15,000*g*, and the supernatant was then divided into one ultra-filtered part and one unfiltered one, which were used for xanthine oxidoreductase (XOR) activity and nitrotyrosine determination, respectively.

XOR activity was measured in the ultra-filtered supernatant (Amicon Ultra-0.5 Centrifugal Filter) with a fluorometric kinetic assay on the basis of the conversion of pterin to isoxanthopterin in the presence (total XOR) or absence (xanthine oxidase activity) of the electron acceptor methylene blue (20). XOR activity was calculated and expressed in μmol min^{-1} mg $protein^{-1}$.

Free nitrotyrosine as a marker of peroxynitrite generation was measured from unfiltered supernatant by enzyme-linked immunosorbent assay (Cayman Chemical, Ann Arbor, MI, USA). The supernatants were incubated overnight with anti-nitrotyrosine rabbit IgG and nitrotyrosine acetylcholinesterase tracer in precoated (mouse anti-rabbit IgG) microplates, followed by development with Ellman's reagent, and measured spectrophotometrically at 405 and 420 nm. Tissue nitrotyrosine content was calculated in ng mg^{-1} protein. Protein content was assessed by Lowry's method.

Rat Organ Failure Score Assessment

The severity of organ failure was determined by using a scoring system adapted for rats (Rat Organ Failure Assessment—ROFA) considering the principles of the Sepsis-3 international consensus (**Table 1**). ROFA components were scored between 0 and 4 based on threshold values of different parameters (21). The cardiovascular (MAP values) and respiratory components (the PaO_2/FiO_2 ratio) of ROFA were determined from readings of

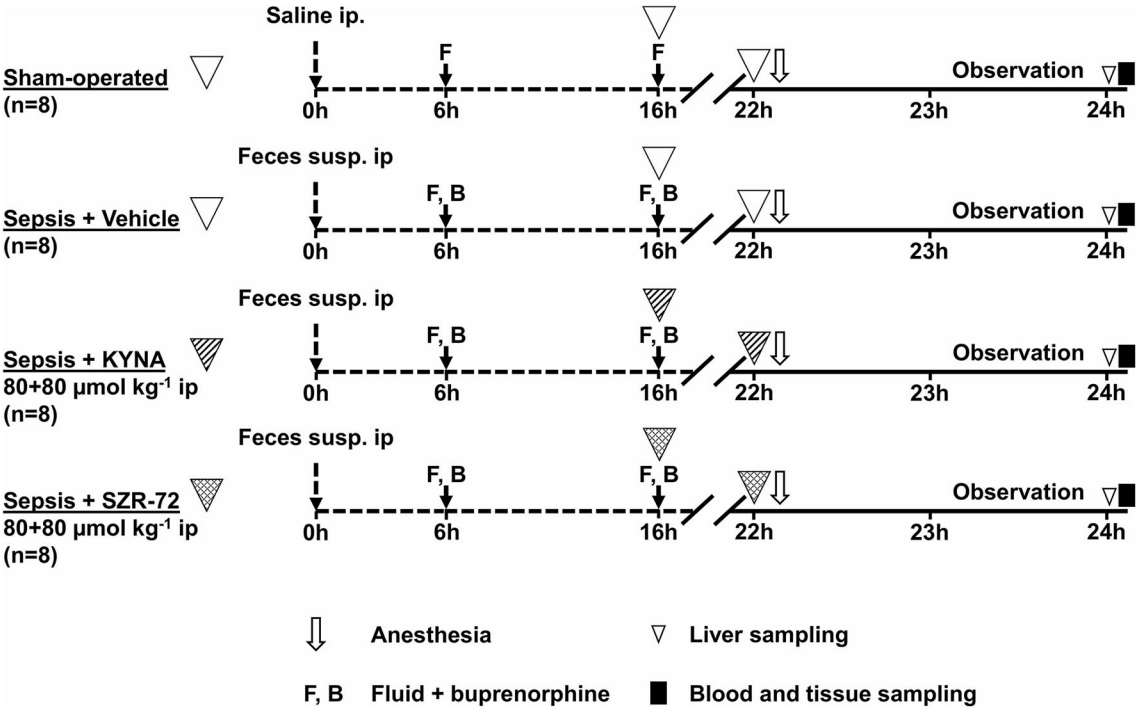

FIGURE 1 | The experimental scheme. The animals were randomly assigned into the sham-operated and sepsis groups. Sixteen hours after sepsis induction, animals were randomly divided into three subgroups: treated with vehicle, KYNA (80 + 80 μmol kg^{-1} ip), or SZR-72 (80 + 80 μmol kg^{-1} ip), respectively.

hemodynamic and blood gas monitoring, respectively. Sepsis-induced liver damage was determined by calculating the AST/ALT ratio (De Ritis ratio) (22). Renal dysfunction was characterized by determining plasma urea levels. The ROFA scoring system was supplemented by scoring the degree of blood lactate level (indicative of metabolic disturbances caused by tissue hypoxia). The ROFA values were calculated by summing up the scores in each element of the scoring system. Septic status was defined as a ROFA score above 2.

Microcirculatory Measurements

The Incident Dark Field (IDF) imaging technique (CytoCam Video Microscope System; Braedius Medical, Huizen, the Netherlands) was used for non-invasive evaluation of the serosal microcirculation of the ileum. IDF imaging is optimized for visualization of hemoglobin-containing structures by illuminating the organ surface with linearly polarized light, where the filtered light reflected from the tissues is detected by a computer-controlled sensor (23). Images from an ileum segment were recorded in six, 50-frame-long, high-quality video clips (spatial resolution 14 megapixels; temporal resolution 60 fps). The video was recorded at separate locations of the terminal ileum by the same investigator. The records were saved as digital AVI-DV files to a hard drive and analyzed with an off-line software-assisted system (AVA 3.0, Automated Vascular Analysis, Academic Medical Center, University of Amsterdam). The screens recorded with the IDF imaging technique were divided into four equal quadrants, as recommended. The proportion of perfused vessels (PPV) was defined as the ratio of the perfused vessel lengths to total vessel lengths. The PPV values were calculated in all quadrants, and the software (Automated Vascular Analysis 3.0) for the device provided four individual PPV values, Q1 PPV, Q2 PPV, Q3 PPV, and Q4 PPV, respectively. The average of these individual values (Q1PPV–Q4PPV) is shown as % PPV in the illustrations.

TABLE 1 | Threshold values of the Rat Organ Failure Assessment (ROFA) scoring system for the individual organ dysfunction parameters.

		ROFA score				
Organ dysfunction	**Parameters**	**0**	**1**	**2**	**3**	**4**
Respiratory system	PaO_2/FiO_2 ratio	≥400	<400	<300	<200	<100
Cardiovascular system	MAP (mmHg)	≥75	65–75	55–65	<55	–
Renal function	Urea (mmol l^{-1})	<7.5	7.5–21	>21	–	–
Liver function	AST/ALT ratio	<1.7	1.7–2.5	>2.5	–	–
Metabolism	Lactate (mmol l^{-1})	<1.64	1.64–3	3–4	4–5	>5

ROFA, Rat Organ Failure Assessment; MAP, mean arterial pressure; ALT, alanine aminotransferase; AST, aspartate aminotransferase.

The median PPV values for the four quadrants were used as a reference (median values for Q1–4) in calculating microvascular heterogeneity (MVH). Heterogeneity was defined as the average difference of the PPV values (%) between each quadrant and the reference value (the differences are given in absolute values) for each record using the following formula:

$$MVH = [|(M_{\sum QPPV} - Q1PPV)| + |(M_{\sum QPPV} - Q2PPV)| + |(M_{\sum QPPV} - Q3PPV)| + |(M_{\sum QPPV} - Q4PPV)|]/\text{number of quadrants}$$

$\mathbf{M}$ = median
$\mathbf{M}_{\sum QPPV}$ = median of the total PPV in the four quadrants
QxPPV = PPV value for each individual quadrant.

This calculation provides numerical values for perfusion heterogeneity (24, 25).

Measurement of Mitochondrial Respiration and Membrane Potential

Mitochondrial O_2 consumption and mitochondrial membrane potential ($\Delta\Psi$mt) were assessed from liver homogenates using High-Resolution FluoRespirometry (Oxygraph-2k; Oroboros Instruments, Innsbruck, Austria). Measurements were performed in a Mir05 respiration medium under continuous magnetic stirring at 37°C. Changes in $\Delta\Psi$mt were assessed with safranin dye using Blue Fluorescence Sensor (Sigma Aldrich, St. Louis, MO, USA). DatLab software (Oroboros Instruments, Innsbruck, Austria) was employed for online display, respirometry data acquisition, and analysis. A detailed description of the FluoRespirometry protocol used can be found in the **Supplementary Data 1**.

Statistical Analysis

Data analysis was performed with a statistical software package (SigmaStat for Windows; Jandel Scientific, Erkrath, Germany). Normality of data distribution was analyzed with the Shapiro–Wilk test. The Friedman analysis of variance on ranks was applied within groups. Time-dependent differences from the baseline for each group were assessed with Dunn's method. In this study, differences between groups were analyzed with the Kruskal–Wallis one-way analysis of variance on ranks, followed by Dunn's method. Median values and 75th and 25th percentiles are provided in the figures; $P < 0.05$ were considered significant.

RESULTS

Hemodynamics and Oxygen Dynamics

Sepsis resulted in significant hypotension during the observation period, which was not altered by the treatments (**Figure 2A**). HR increased significantly in two time points (the 0th and 30th min of the monitoring period) in the SZR-72-treated group (**Figure 2B**). As compared with sham-operated animals, a decreased PaO_2/FiO_2 ratio was observed in the vehicle-treated sepsis group, whereas no significant changes were found in the other groups (**Figure 2C**). Sepsis reduced O_2ER values as compared with the sham-operated group, whereas both KYNA and SZR-72 resulted in a significant improvement in this parameter (**Figure 2D**).

Changes in Metabolic and Organ Dysfunction Markers

In the vehicle-treated sepsis group, plasma urea levels significantly increased, but urea levels in both treated groups were similar to those seen in the sham animals (**Figure 3A**). Hepatic cellular damage as indicated by the De Ritis ratio was evident in the vehicle-treated and SZR-72-treated sepsis groups, whereas this ratio did not differ between the sham-operated and KYNA-treated animals (**Figure 3B**). When ALT and AST values were evaluated separately (**Supplementary Figures 1A,B**), these changes were not influenced by the treatments. In comparison with the sham-operated group, all of the groups challenged with sepsis showed a similar extent of elevation in blood lactate levels (**Figure 3C**). The ROFA score was significantly higher in the vehicle-treated and SZR-72-treated sepsis groups than in the sham-operated group. The ROFA values in the KYNA-treated group were not significantly different from those in the septic group (**Figure 3D**).

Changes in Inflammatory and Oxidative/Nitrosative Stress Markers

Sepsis led to significant elevations in ET-1, IL-6, nitrotyrosine levels, and XOR activity (**Figures 4A–D**). All of these parameters remained, however, at the levels seen in the sham group in both the sepsis + KYNA and sepsis + SZR-72 groups.

Microcirculatory Changes

Sepsis-induced microcirculatory perfusion disorders manifested in lower levels of capillary perfusion and increased perfusion heterogeneity as compared with those in the sham group (**Figures 5A,B**). The values of these parameters did not differ between the sepsis and sepsis + SZR-72 groups and between the sham and sepsis + KYNA groups. KYNA was significantly more effective in ameliorating sepsis-related changes than SZR-72.

Changes in Mitochondrial Respiration

Baseline respiration without external substrate (BLresp) and respiration following the oxidation of complex I- and complex II-linked substrates ($LEAK_{GM}$ and $LEAK_S$) were significantly decreased in sepsis (**Figures 6A,B**). KYNA administration did not modify sepsis-induced changes in BLresp, $LEAK_{GM}$, and $LEAK_S$. In this respect, treatment with SZR-72 preserved mitochondrial respiration with and without NADH- and $FADH_2$-linked substrates (**Figures 6A,B**). In addition, sepsis significantly decreased complex I- and complex II-linked OXPHOS. Both KYNA and SZR-72 increased complex II-linked OXPHOS capacity, whereas SZR-72 was able to restore complex I-linked OXPHOS completely (**Figure 6A**). As a result of septic insult, respiratory acceptor control ratios (RCR I and RCR II) were markedly decreased. These parameters were significantly improved by KYNA and completely reversed by SZR-72 treatment (**Figures 6A,B**).

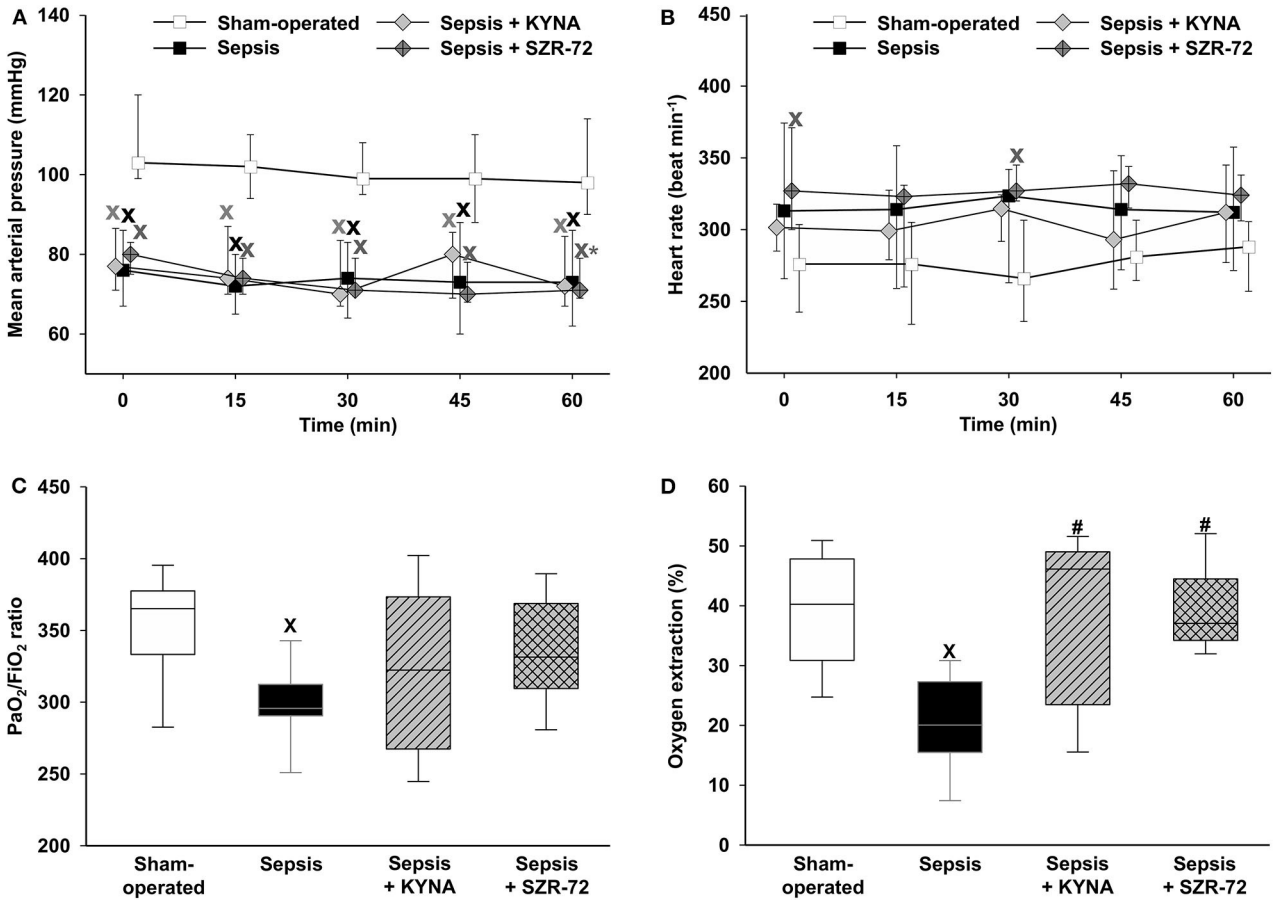

FIGURE 2 | Time-dependent changes in mean arterial pressure **(A)**, heart rate **(B)**, PaO_2/FiO_2 ratio **(C)**, and oxygen extraction **(D)** in the sham-operated group (empty box) and in the different sepsis groups treated with the saline vehicle (black box), KYNA (gray diamond/striped gray box), and SZR-72 (dark gray diamond with cross/checked gray box). The plots demonstrate the median values (horizontal line in box plots) and the 25th (lower whisker) and 75th (upper whisker) percentiles. $^{x}P < 0.05$ vs. sham-operated; $^{\#}P < 0.05$ vs. vehicle-treated sepsis; $^{*}P < 0.05$ vs. 0 min.

Changes in Mitochondrial Membrane Potential ($\Delta\Psi$mt)

The addition of complex II substrate resulted in a sharp decrease in fluorescence signal (F_{LEAK}) within 90 s, indicating an increase of $\Delta\Psi$mt (succinate-induced hyperpolarization) (**Figure 7A**). As a result of the septic insult, there was a comparatively lower decrease in safranin fluorescence after succinate (**Figure 7B**), reflecting a significant decrease in $\Delta\Psi$mt. Treatment with KYNA markedly improved, whereas SZR-72 completely restored the sepsis-induced decrease in $\Delta\Psi$mt. Stimulation with CCCP resulted in depolarization and collapse of $\Delta\Psi$mt at a critical uncoupler concentration. These changes were characterized as (I) stepwise increases in safranin fluorescence (depolarization) and (II) stabilization of fluorescence signal (loss of $\Delta\Psi$mt).

In comparison with the sham-operated group, CCCP-mediated loss of $\Delta\Psi$mt was obtained at lower uncoupler concentration in the vehicle-treated septic group (**Figure 7B**). KYNA and SZR-72 therapies significantly increased the concentration of CCCP used for $\Delta\Psi$mt disruption. Among these treatments, SZR-72 had a more profound effect on $\Delta\Psi$mt preservation (**Figures 7A,B**).

DISCUSSION

The present study demonstrates the distinct effects of KYNA and its synthetic analog on microcirculation and mitochondrial function in experimental sepsis. Proper analgesia, fluid resuscitation, and assessment of organ failure were conducted according to the standards in the Minimum Quality Threshold in Pre-clinical Sepsis Studies (MQTiPSS) guidelines (19). The clinical relevance of this model was confirmed by the presence of hypotension, impaired pulmonary function and oxygen extraction, and elevations in lactate levels and in oxidative/nitrosative stress as well as microcirculatory and mitochondrial dysfunctions. Sepsis-induced organ injuries were characterized by a newly developed, rat-specific organ failure (ROFA) scoring system based on threshold values adopted from the relevant literature (21). The scoring system included the following: (I–II) cardiovascular and respiratory dysfunctions

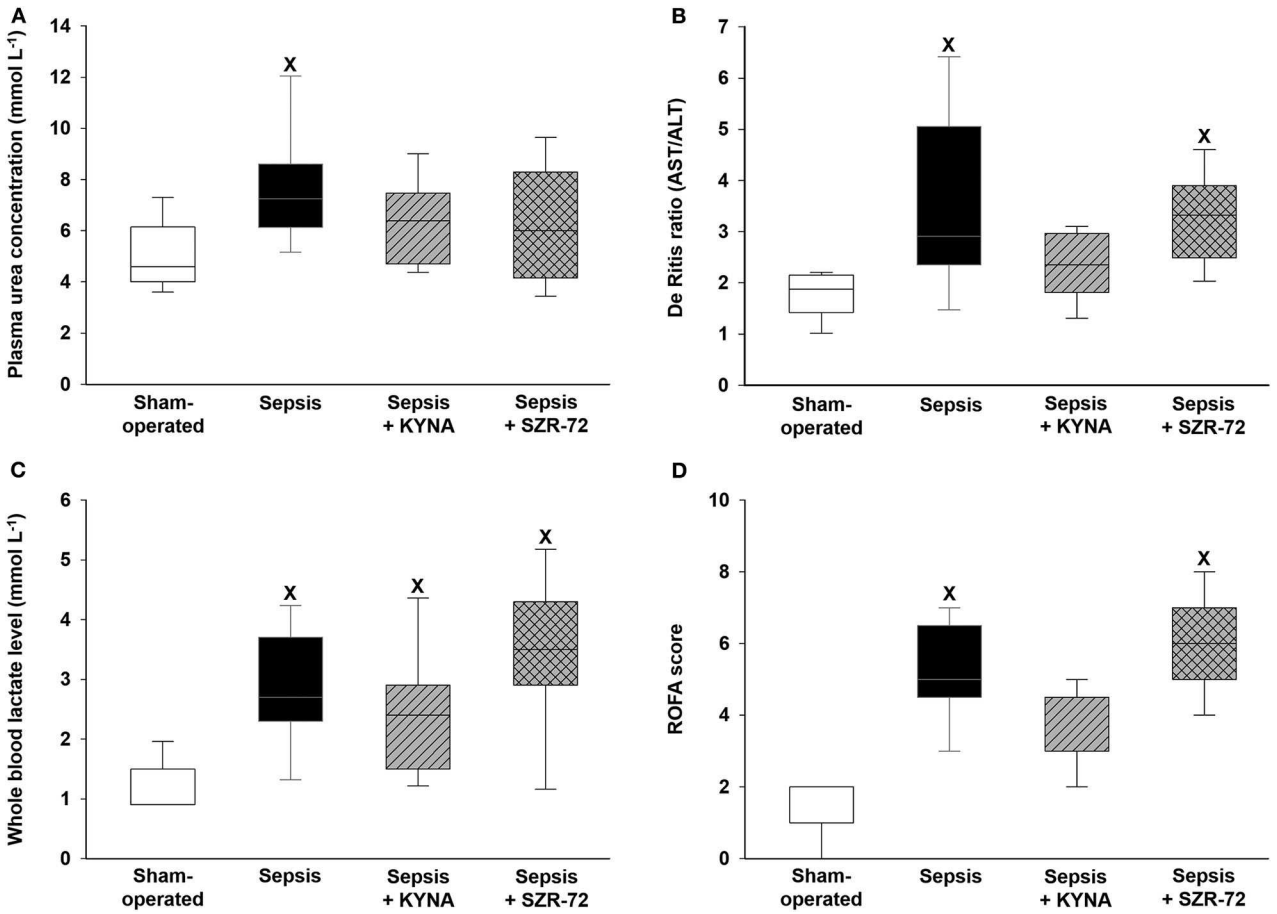

FIGURE 3 | Changes in plasma urea **(A)**, De Ritis ratio (AST/ALT) **(B)**, whole blood lactate levels **(C)**, and ROFA score values **(D)** in the sham-operated group (empty box) and in the different sepsis groups treated with the saline vehicle (black box), KYNA (striped gray box), and SZR-72 (checked gray box). The plots demonstrate the median (horizontal line in the box) and the 25th (lower whisker) and 75th (upper whisker) percentiles. Between groups: Kruskal–Wallis test and Dunn's *post-hoc* test. $^{x}P < 0.05$ vs. sham-operated.

were determined by MAP and PaO_2/FiO_2 values, respectively. (In MAP scoring, anesthesia-related effects were also taken into account, whereas PaO_2/FiO_2 was used in accordance with clinical practice.) (III) The AST/ALT ratio was considered to assess hepatocellular damage based on the observation that AST depicts liver-related injury more specifically than ALT (22). (IV) Renal damage was characterized by plasma urea changes (26) based on threshold values suggested by Zhai et al. (21). (V) The ROFA score was supplemented with consideration of lactate values (indicative of cellular hypoxia) according to Zhai et al. (21). This novel, rat-specific scoring system was applicable to trace development of MOF in this rat sepsis model and indicated differences between the efficacy of KYNA and SZR-72. Both treatments reduced lung and kidney dysfunctions to a similar extent due to the decreased level of inflammatory markers and their enhanced antioxidant/anti-nitrosative effect. However, only KYNA treatment reduced hypoxia-sensitive ET-1 levels, also displaying a tendency toward amelioration of liver injury and ROFA score values.

Deteriorating tissue perfusion is a key element in sepsis pathophysiology and in the development of MOF (4). We observed that both KYNA and SZR-72 prevented a sepsis-induced decrease in oxygen extraction to the same extent, but only KYNA ameliorated sepsis-related microcirculatory perfusion deficit (reduction in capillary perfusion and an increase in perfusion heterogeneity) significantly. This distinct effect of compounds is possibly due to their different structure- and receptor-related characteristics (27).

The potential direct microcirculatory effects of KYNA in the ileum are unknown, but it has been shown to increase global and cortical renal blood flow (and to improve renal excretion) under physiological conditions and to reduce renal oxidative stress during ischemia–reperfusion injury (28, 29). Based on our results, some of these micro-hemodynamic effects can also be linked to a reduced ET-1 release elicited by KYNA.

NMDA receptor-related microcirculation improvement can be explained by many mechanisms. Firstly, antagonism of NMDA receptors expressed on the surface of smooth muscle cells brings about reduced intracellular Ca^{2+} levels (30), resulting in

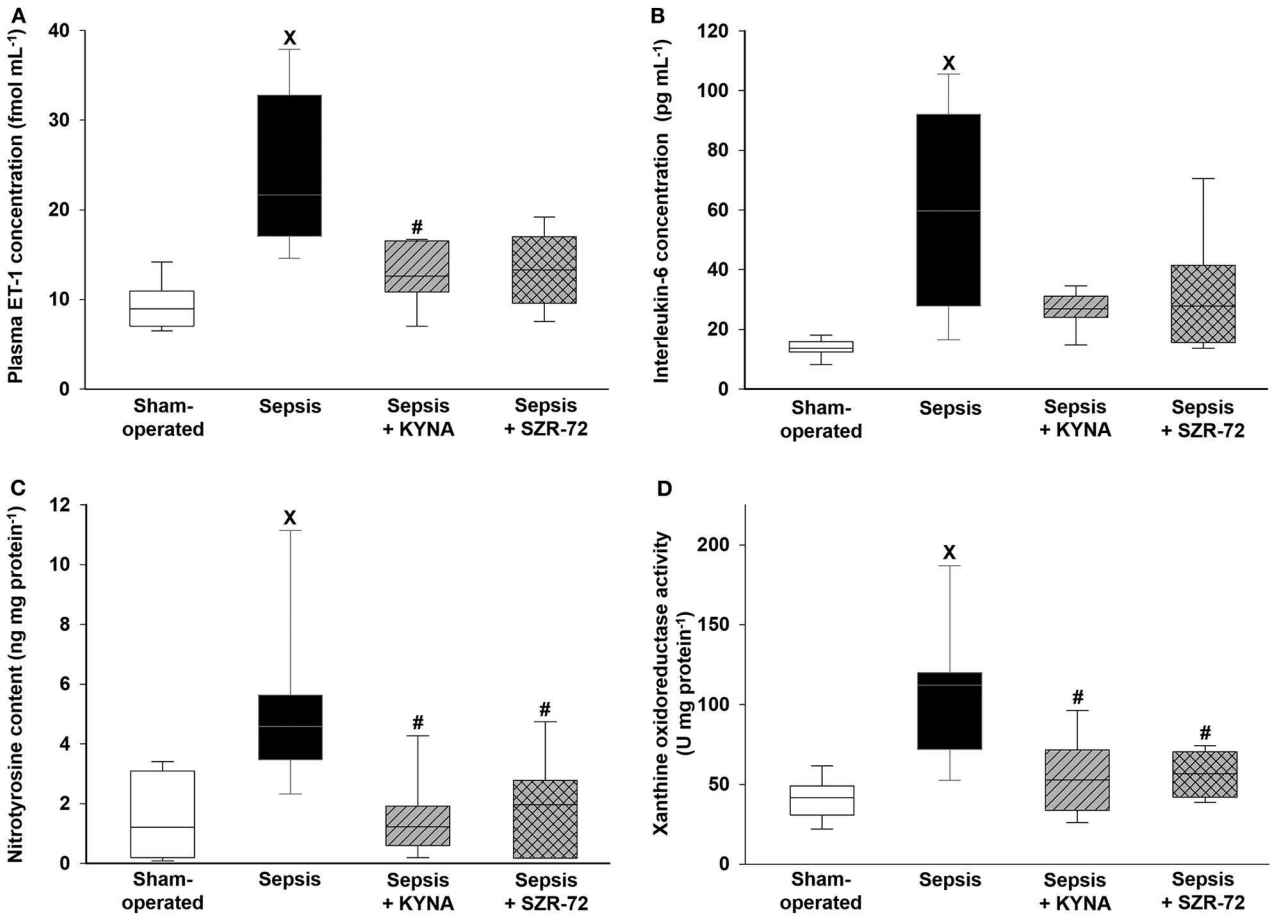

FIGURE 4 | Changes in plasma endothelin-1 (ET-1) **(A)**, interleukin-6 (IL-6) **(B)**, ileal nitrotyrosine levels **(C)**, and xanthine oxidoreductase (XOR) activity **(D)** in the sham-operated group (empty box) and in the different sepsis groups treated with saline (black box), KYNA (striped gray box), and SZR-72 (checked gray box). The plots demonstrate the median (horizontal line in the box) and the 25th (lower whisker) and 75th (upper whisker) percentiles. Between groups: Kruskal–Wallis test and Dunn's *post-hoc* test. $^{x}P < 0.05$ vs. sham-operated; $^{\#}P < 0.05$ vs. vehicle-treated sepsis.

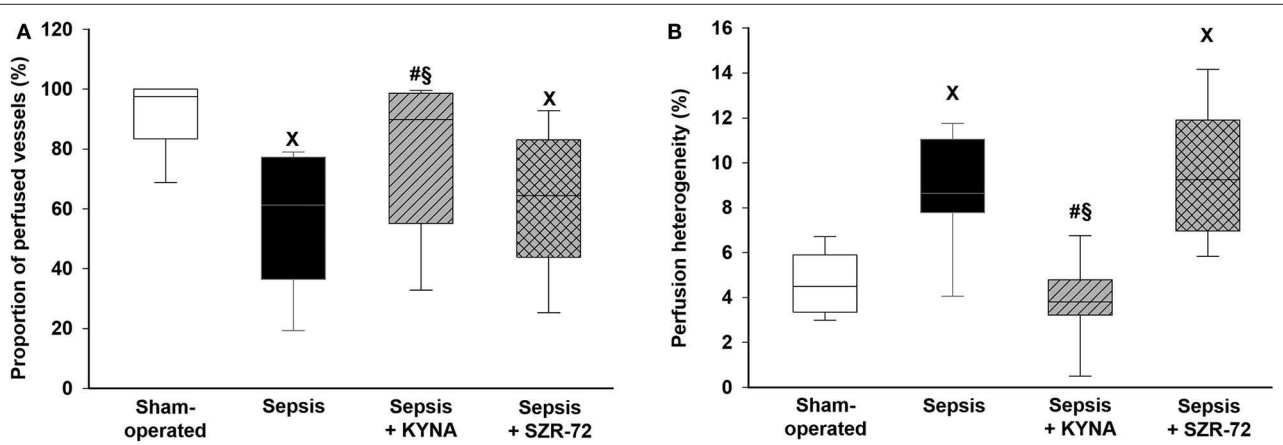

FIGURE 5 | Changes in the proportion of perfused vessels **(A)** and in perfusion heterogeneity values **(B)** in the serosal layer of the ileum in the sham-operated group (empty box) and in the different sepsis groups treated with saline (black box), KYNA (striped gray box), and SZR-72 (checked gray box). The plots demonstrate the median (horizontal line in the box) and the 25th (lower whisker) and 75th (upper whisker) percentiles. Between groups: Kruskal–Wallis test and Dunn's *post-hoc* test. $^{x}P < 0.05$ vs. sham-operated; $^{\#}P < 0.05$ vs. vehicle-treated sepsis; $^{\S}P < 0.05$ sepsis + KYNA vs. sepsis + SZR-72.

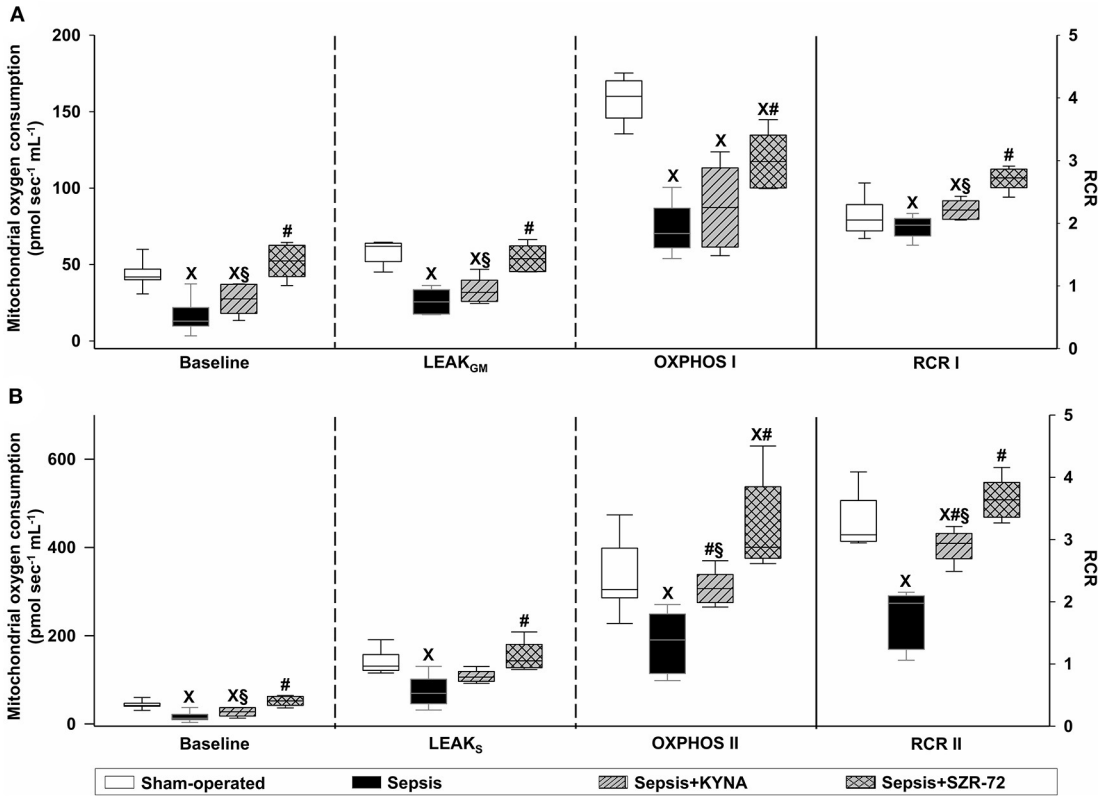

FIGURE 6 | Baseline respiration, substrate oxidation ($LEAK_{GM}$ and $LEAK_S$), complex I- **(A)** and complex II-linked **(B)** OXPHOS capacities (OXPHOS I and OXPHOS II; left axis), and respiratory acceptor control ratios (CI, CII RCR; right axis) in the sham-operated group (empty box) and in the different sepsis groups treated with the saline vehicle (black box), KYNA (striped gray box), and SZR-72 (checked gray box). The plots illustrate the median (horizontal line in the box) and the 25th (lower whisker) and 75th (upper whisker) percentiles. $^{X}P < 0.05$ vs. sham-operated; $^{\#}P < 0.05$ vs. vehicle-treated sepsis; $^{\S}P < 0.05$ sepsis + KYNA vs. sepsis + SZR-72.

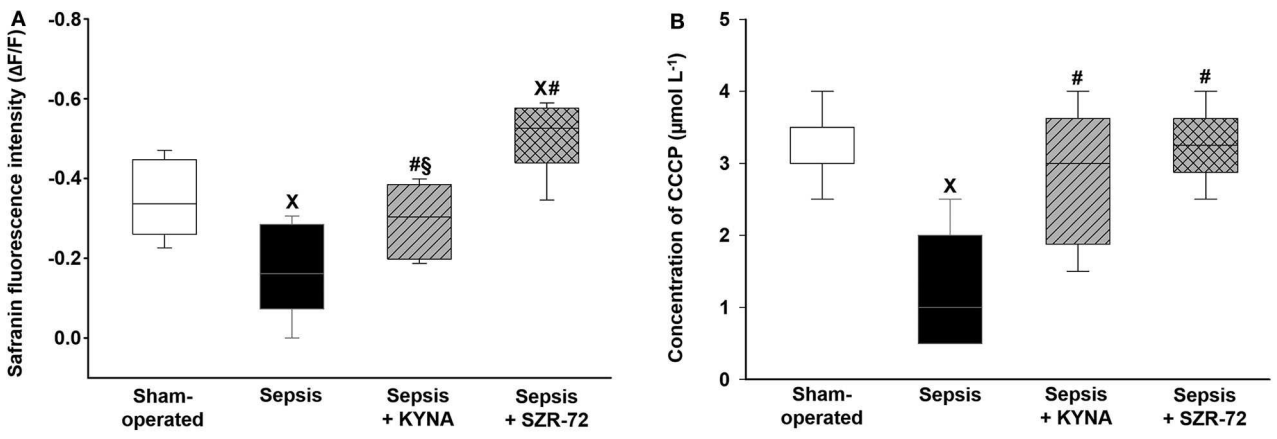

FIGURE 7 | Succinate-induced hyperpolarization **(A)** and CCCP-induced loss of mitochondrial membrane potential **(B)** in the sham-operated group (empty box) and in the different sepsis groups treated with the saline vehicle (black box), KYNA (striped box), and SZR-72 (checked box). The plots illustrate the median (horizontal line in the box) and the 25th (lower whisker) and 75th (upper whisker) percentiles. $^{x}P < 0.05$ vs. sham-operated; $^{\#}P < 0.05$ vs. vehicle-treated sepsis; $^{\S}P < 0.05$ sepsis + KYNA vs. sepsis + SZR-72.

smooth muscle relaxation (31). On the other hand, a reduction of the levels of pro-inflammatory IL-6, XOR activity, and ROS-sensitive vasoconstrictor ET-1 release by KYNA may attenuate the cytokine- and ROS-induced vasoconstriction of microvessels. Although the use of vasodilator therapy in sepsis is debated (6, 32, 33), a reduction of circulating ET-1 levels through a

combined ET_A/ET_B receptor-targeted treatment regimen has been demonstrated to ameliorate microcirculatory deficit in sepsis (17).

Further, KYNA may also act as an agonist for the orphan receptor GPR35 and reduce inflammation independently of the NMDA receptors. This receptor is expressed at high levels in intestine and immune cells (34), and the concentrations of KYNA required to induce effects differ between NMDA-R and GPR35. Compared with NMDA-R, lower concentrations of KYNA are able to elicit a response when binding to GPR35 (35). Taking into account that (1) KYNA is an endogenous ligand for GPR35 and that (2) only KYNA, but not the synthetic analog, was able to restore the perfusion disturbances in the ileum, a GPR35-mediated mechanism cannot be ruled out.

The KYNA- and its analog-based treatments also had different effects on mitochondrial function, with the ameliorating effects of SZR-72 being more pronounced. A considerable decrease in substrate- and ADP-stimulated respirations was accompanied by a decrease in RCR and $\Delta\Psi$mt after sepsis insult (17). A decrease of $\Delta\Psi$mt may originate in complex metabolic, functional, and membrane integrity changes within the organelle and may explain the decline in mitochondrial O_2 consumption and lower interdependence (coupling) of ATP synthesis with ETS. Although an O_2-independent glycolytic pathway for ATP production has been documented, this alternate route may not be effective for energy production in sepsis. Of note, ATP depletion is not a unique component of sepsis-induced mitochondrial dysfunction; organellar ROS production, elevated mitochondrial DNA level, transition pore opening-mediated apoptosis, and necrosis are fundamental mitochondrial events, which lead to cellular injury (36, 37). In addition, the release of mitochondrial components of damage-associated molecular patterns to the extracellular space may further aggravate an inflammatory response (38). Taken together, all these processes are intimately involved in the progression of sepsis and contribute to MOF.

The role of endogenous KYNA on mitochondrial physiology is still unmapped; however, exogenous KYNA was able to improve OXPHOS II and $\Delta\Psi$mt without affecting OXPHOS I. This difference in complex activities may arise from the fact that complex I is more susceptible to cellular injury than complex II. Oxidation of glutamate requires pyridine nucleotides, and these with other cofactors may be lost during sepsis (39).

Our findings are in agreement with the study by Ferreira et al. (40), in which KYNA ameliorated several aspects of mitochondrial function in a neurodegeneration model. Similar to our results, KYNA administration significantly improved succinate dehydrogenase activity and $\Delta\Psi$mt. In addition, KYNA preserved mitochondrial mass, enhanced antioxidant enzyme levels, and reduced ROS production after quinolinic acid-induced cell injury (40). In adipose tissue, KYNA modulated energy utilization (increased lipid metabolism and mitochondrial respiration) via a GPR35 pathway (41).

In our experiments, administration of SZR-72 markedly improved the key indices of mitochondrial function. Previous studies with the KYNA analog revealed a more pronounced anti-inflammatory response in animal models of colitis and neuro-inflammation than that seen with KYNA (10, 16, 42), but both KYNA and SZR-72 reduced oxidative/nitrosative stress marker levels [XOR, nitric oxide synthase (NOS), and myeloperoxidase (MPO) activities] (10) and attenuated glutamate expression (42). Compared with KYNA, the effects of SZR-72 were more pronounced in this sepsis model, and a remarkable increase in ADP-stimulated respirations (OXPHOS I and II), RCR, and $\Delta\Psi$mt was found in liver homogenate after sepsis induction. Preservation of these parameters is fundamental for better O_2 utilization (less ETS-linked ROS is generated), maintenance of ATP production, and provision of $\Delta\Psi$mt for mitochondrial transport.

Several hypotheses may explain the mechanism behind the more advantageous mitochondrial effects of SZR-72. First, the physico-chemical properties of KYNA and SZR-72 are different, thus possibly influencing crossing through the BBB and membranes (16). There is evidence that KYNA only crosses the BBB poorly, whereas SZR-72 is BBB-permeable due to a water-soluble side chain with an extra cationic center (7, 43). Apart from BBB, a facilitated membrane crossing of SZR-72 may affect intracellular signaling, including the activation of antioxidative/anti-apoptotic pathways.

A second scenario is a distinct molecule binding at the NMDA-R glycine site. More recently, NMDA-Rs were shown to be present in the inner mitochondrial membrane (mtNMDA-R) (44), where they may play a regulative role in (1) Ca^{2+} transport, (2) ROS production, and (3) metabolic switching during hypoxia (45). Under these circumstances, it may well be that SZR-72 has a much higher affinity for either plasma membrane or mtNMDA-R than KYNA. In addition, a protein–protein interaction between NMDA-R and an ND2 subunit of complex I was found through an Src adapter protein (12). It cannot be ruled out that KYNA and SZR-72 influence this interaction and regulate mitochondrial homeostasis differently.

The influence of sepsis on NMDA-R expression and glutamate levels is incompletely characterized. We did not examine changes in NMDA-R subunits due to technical limitations, but other laboratories have found a marked increase in lung NR1 and NR2A contents in a cecal ligation and puncture (CLP) sepsis model. Furthermore, treatment with the NMDA-R antagonist MK-801 lowered lactate dehydrogenase and oxidative damage and improved survival 144 h after sepsis induction in rats (46). Similarly, survival was markedly increased (by 80%), and markers of inflammation were reduced in MK-801-treated mice 48 h after lipopolysaccharide (LPS) stimuli (47). In this model, LPS also raised the glutamate level in bronchoalveolar lavage fluid. Based on these findings and the fact that KYNA is a natural antagonist, a similar, NMDA-R-linked mechanism, at least in part, cannot be ruled out in our polymicrobial sepsis model.

Our study has limitations. Firstly, the observation timeline was relatively short, and therefore longer end points, such as mortality, with longer pharmacological effects should also be examined in follow-up studies. Our newly described ROFA score also seems to be a potentially useful tool for this purpose, but it will be necessary to validate the system under other experimental

conditions as well. The effect of the ketamine-containing anesthesia on the results cannot be disregarded. Similarly, despite our intention to follow all of the recommendations in the MQTiPSS guidelines, antimicrobial therapy was excluded from the protocol due to the known influence on mitochondrial respiration (48).

In conclusion, both treatments with KYNA and its synthetic analog attenuated the deleterious consequences of oxidative/nitrosative stress and resulted in lower inflammatory mediator release. Administration of SZR-72 may directly regulate mitochondrial respiration and ATP synthesis, whereas treatment with KYNA primarily ameliorates microcirculatory dysfunction and consequently restores organelle function. Further experiments are surely needed to clarify the exact mechanism behind these compounds, but these results suggest that therapies with KYNA or its synthetic analog, SZR-72, against MMDS might be a supportive intervention in the treatment of sepsis.

DATA AVAILABILITY STATEMENT

The raw data supporting the conclusions of this article will be made available by the authors, without undue reservation.

ETHICS STATEMENT

The animal study was reviewed and approved by National Competent Authority of Hungary.

AUTHOR CONTRIBUTIONS

LJ, AR, RF, ST, MP, and JK performed experiments and wrote the manuscript. ST and AS prepared figures. FF and IS contributed to new KYNA analog. AS, JK, MB, and LV supervised and edited the manuscript. All authors contributed to the article and approved the submitted version.

FUNDING

Sources of funding: NKFIH K116689, GINOP-2.3.2-15-2016-00034, EFOP-3.6.2-16-2017-00006, TUDFO/47138-1/2019-ITM, and University of Szeged Open Access Fund (grant number: 4748). This research was conducted with the support of the Szeged Scientists Academy under the sponsorship of the Hungarian Ministry of Human Capacities (EMMI:13725-2/2018/INTFIN).

ACKNOWLEDGMENTS

We appreciate the excellent technical assistance from Csilla Mester and Annamária Kócsó.

SUPPLEMENTARY MATERIAL

The Supplementary Material for this article can be found online at: https://www.frontiersin.org/articles/10.3389/fmed.2020.566582/full#supplementary-material

REFERENCES

1. Singer M, Deutschman CS, Seymour CW, Shankar-Hari M, Annane D, Bauer M, et al. The Third International Consensus Definitions for Sepsis and Septic Shock (Sepsis-3). *JAMA.* (2016) 315:801. doi: 10.1001/jama.2016.0287
2. De Backer D, Orbegozo Cortes D, Donadello K, Vincent J-L. Pathophysiology of microcirculatory dysfunction and the pathogenesis of septic shock. *Virulence.* (2014) 5:73–79. doi: 10.4161/viru.26482
3. Arulkumaran N, Deutschman CS, Pinsky MR, Zuckerbraun B, Schumacker PT, Gomez H, et al. Mitochondrial function in sepsis. *Shock.* (2016) 45:271–81. doi: 10.1097/SHK.0000000000000463
4. Balestra GM, Legrand M, Ince C. Microcirculation and mitochondria in sepsis: getting out of breath. *Curr Opin Anaesthesiol.* (2009) 22:184–90. doi: 10.1097/ACO.0b013e328328d31a
5. Armstrong BA, Betzold RD, May AK. Sepsis and septic shock strategies. *Surg Clin North Am.* (2017) 97:1339–79. doi: 10.1016/j.suc.2017.07.003
6. Moore JPR, Dyson A, Singer M, Fraser J. Microcirculatory dysfunction and resuscitation: why, when, and how. *Br J Anaesth.* (2015) 115:366–75. doi: 10.1093/bja/aev163
7. Vécsei L, Szalárdy L, Fülöp F, Toldi J. Kynurenines in the CNS: recent advances and new questions. *Nat Rev Drug Discov.* (2013) 12:64–82. doi: 10.1038/nrd3793
8. Rameaut GA, Chiu LY, Ziff EB. Bidirectional regulation of neuronal nitric-oxide synthase phosphorylation at serine 847 by the N-methyl-D-aspartate receptor. *J Biol Chem.* (2004) 279:14307–14. doi: 10.1074/jbc.M311103200
9. Dabrowski W, Kocki T, Pilat J, Parada-Turska J, Malbrain MLNG. Changes in plasma kynurenic acid concentration in septic shock patients undergoing continuous veno-venous haemofiltration. *Inflammation.* (2014) 37:223–34. doi: 10.1007/s10753-013-9733-9
10. Kaszaki J, Érces D, Varga G, Szabó A, Vécsei L, Boros M. Kynurenines and intestinal neurotransmission: the role of N-methyl-d-aspartate receptors. *J Neural Transm.* (2012) 119:211–23. doi: 10.1007/s00702-011-0658-x
11. Hogan-Cann AD, Anderson CM. Physiological roles of non-neuronal NMDA receptors. *Trends Pharmacol Sci.* (2016) 37:750–67. doi: 10.1016/j.tips.2016.05.012
12. Gingrich JR, Pelkey KA, Fam SR, Huang Y, Petralia RS, Wenthold RJ, et al. Unique domain anchoring of Src to synaptic NMDA receptors via the mitochondrial protein NADH dehydrogenase subunit 2. *Proc Natl Acad Sci USA.* (2004) 101:6237–42. doi: 10.1073/pnas.0401413101
13. Tanaka M, Bohár Z, Vécsei L. Are kynurenines accomplices or principal villains in dementia? Maintenance of kynurenine metabolism. *Molecules.* (2020) 25:564. doi: 10.3390/molecules25030564
14. Walczak K, Wnorowski A, Turski WA, Plech T. Kynurenic acid and cancer: facts and controversies. *Cell Mol Life Sci.* (2020) 77:1531–50. doi: 10.1007/s00018-019-03332-w
15. Fülöp F, Szatmári I, Vámos E, Zádori D, Toldi J, Vécsei L. Syntheses, transformations and pharmaceutical applications of kynurenic acid derivatives. *Curr Med Chem.* (2009) 16:4828–42. doi: 10.2174/092986709789909602
16. Knyihar-Csillik E, Mihaly A, Krisztin-Peva B, Robotka H, Szatmari I, Fulop F, et al. The kynurenate analog SZR-72 prevents the nitroglycerol-induced increase of c-fos immunoreactivity in the rat caudal trigeminal nucleus: comparative studies of the effects of SZR-72 and kynurenic acid. *Neurosci Res.* (2008) 61:429–32. doi: 10.1016/j.neures.2008.04.009
17. Rutai A, Fejes R, Juhász L, Tallósy SP, Poles MZ, Földesi I, et al. Endothelin A and B receptors. *Shock.* (2019) 54:87–95. doi: 10.1097/SHK.0000000000001414
18. Rademann P, Weidinger A, Drechsler S, Meszaros A, Zipperle J, Jafarmadar M, et al. Mitochondria-targeted antioxidants SkQ1 and MitoTEMPO failed to

exert a long-term beneficial effect in murine polymicrobial sepsis. *Oxid Med Cell Longev.* (2017) 2017:6412682. doi: 10.1155/2017/6412682
19. Osuchowski MF, Ayala A, Bahrami S, Bauer M, Boros M, Cavaillon J-M, et al. Minimum quality threshold in pre-clinical sepsis studies (MQTiPSS). *Shock.* (2018) 50:377–80. doi: 10.1097/SHK.0000000000001212
20. Beckman JS, Parks DA, Pearson JD, Marshall PA, Freeman BA. A sensitive fluorometric assay for measuring xanthine dehydrogenase and oxidase in tissues. *Free Radic Biol Med.* (1989) 6:607–15. doi: 10.1016/0891-5849(89)90068-3
21. Zhai X, Yang Z, Zheng G, Yu T, Wang P, Liu X, et al. Lactate as a potential biomarker of sepsis in a rat cecal ligation and puncture model. *Mediators Inflamm.* (2018) 2018:8352727. doi: 10.1155/2018/8352727
22. Botros M, Sikaris KA. The De Ritis ratio: the test of time. *Clin Biochem Rev.* (2013) 34:117–30.
23. Aykut G, Veenstra G, Scorcella C, Ince C, Boerma C. Cytocam-IDF (incident dark field illumination) imaging for bedside monitoring of the microcirculation. *Intens Care Med Exp.* (2015) 3:40. doi: 10.1186/s40635-015-0040-7
24. De Backer D, Hollenberg S, Boerma C, Goedhart P, Büchele G, Ospina-Tascon G, et al. How to evaluate the microcirculation: report of a round table conference. *Crit Care.* (2007) 11:R101. doi: 10.1186/cc6118
25. Massey MJ, Shapiro NI. A guide to human in vivo microcirculatory flow image analysis. *Crit Care.* (2016) 20:35. doi: 10.1186/s13054-016-1213-9
26. Wang K, Xie S, Xiao K, Yan P, He W, Xie L. Biomarkers of sepsis-induced acute kidney injury. *Biomed Res Int.* (2018) 2018:6937947. doi: 10.1155/2018/6937947
27. Mándi Y, Endrész V, Mosolygó T, Burián K, Lantos I, Fülöp F, et al. The opposite effects of kynurenic acid and different kynurenic acid analogs on tumor necrosis factor-α (TNF-α) production and tumor necrosis factor-stimulated gene-6 (TSG-6) expression. *Front Immunol.* (2019) 10:1406. doi: 10.3389/fimmu.2019.01406
28. Badzyńska B, Zakrocka I, Sadowski J, Turski WA, Kompanowska-Jezierska E. Effects of systemic administration of kynurenic acid and glycine on renal haemodynamics and excretion in normotensive and spontaneously hypertensive rats. *Eur J Pharmacol.* (2014) 743:37–41. doi: 10.1016/j.ejphar.2014.09.020
29. Pundir M, Arora S, Kaur T, Singh R, Singh AP. Effect of modulating the allosteric sites of N-methyl-D-aspartate receptors in ischemia-reperfusion induced acute kidney injury. *J Surg Res.* (2013) 183:668–77. doi: 10.1016/j.jss.2013.01.040
30. Wirthgen E, Hoeflich A, Rebl A, Günther J. Kynurenic Acid: the Janus-faced role of an immunomodulatory tryptophan metabolite and its link to pathological conditions. *Front Immunol.* (2018) 8:1957. doi: 10.3389/fimmu.2017.01957
31. Adelstein RS, Sellers JR. Effects of calcium on vascular smooth muscle contraction. *Am J Cardiol.* (1987) 59:4–10. doi: 10.1016/0002-9149(87)90076-2
32. Trzeciak S, Glaspey LJ, Dellinger RP, Durflinger P, Anderson K, Dezfulian C, et al. Randomized controlled trial of inhaled nitric oxide for the treatment of microcirculatory dysfunction in patients with sepsis*. *Crit Care Med.* (2014) 42:2482–92. doi: 10.1097/CCM.0000000000000549
33. Boerma EC, Koopmans M, Konijn A, Kaiferova K, Bakker AJ, van Roon EN, et al. Effects of nitroglycerin on sublingual microcirculatory blood flow in patients with severe sepsis/septic shock after a strict resuscitation protocol: a double-blind randomized placebo controlled trial. *Crit Care Med.* (2010) 38:93–100. doi: 10.1097/CCM.0b013e3181b02fc1
34. Wang J, Simonavicius N, Wu X, Swaminath G, Reagan J, Tian H, et al. Kynurenic acid as a ligand for orphan G protein-coupled receptor GPR35. *J Biol Chem.* (2006) 281:22021–8. doi: 10.1074/jbc.M603503200
35. Turski MP, Turska M, Paluszkiewicz P, Parada-Turska J, Oxenkrug GF. Kynurenic Acid in the digestive system-new facts, new challenges. *Int J Tryptophan Res.* (2013) 6:47–55. doi: 10.4137/IJTR.S12536
36. Bantel H, Schulze-Osthoff K. Cell death in sepsis: a matter of how, when, and where. *Crit Care.* (2009) 13:173. doi: 10.1186/cc7966
37. Harrington JS, Choi AMK, Nakahira K. Mitochondrial DNA in sepsis. *Curr Opin Crit Care.* (2017) 23:284–90. doi: 10.1097/MCC.0000000000000427
38. Nakahira K, Hisata S, Choi AMK. The roles of mitochondrial damage-associated molecular patterns in diseases. *Antioxidants Redox Signal.* (2015) 23:1329–50. doi: 10.1089/ars.2015.6407
39. Hart DW, Gore DC, Rinehart AJ, Asimakis GK, Chinkes DL. Sepsis-induced failure of hepatic energy metabolism. *J Surg Res.* (2003) 115:139–47. doi: 10.1016/S0022-4804(03)00284-1
40. Ferreira FS, Biasibetti-Brendler H, Pierozan P, Schmitz F, Bertó CG, Prezzi CA, et al. Kynurenic acid restores Nrf2 levels and prevents quinolinic acid-induced toxicity in rat striatal slices. *Mol Neurobiol.* (2018) 55:8538–49. doi: 10.1007/s12035-018-1003-2
41. Agudelo LZ, Ferreira DMS, Cervenka I, Bryzgalova G, Dadvar S, Jannig PR, et al. Kynurenic acid and Gpr35 regulate adipose tissue energy homeostasis and inflammation. *Cell Metab.* (2018) 27:378–92. doi: 10.1016/j.cmet.2018.01.004
42. Lukács M, Warfvinge K, Tajti J, Fülöp F, Toldi J, Vécsei L, et al. Topical dura mater application of CFA induces enhanced expression of c-fos and glutamate in rat trigeminal nucleus caudalis: attenuated by KYNA derivate (SZR72). *J Headache Pain.* (2017) 18:39. doi: 10.1186/s10194-017-0746-x
43. Fülöp F, Szatmári I, Toldi J, Vécsei L. Modifications on the carboxylic function of kynurenic acid. *J Neural Transm.* (2012) 119:109–14. doi: 10.1007/s00702-011-0721-7
44. Nesterov SV, Skorobogatova YA, Panteleeva AA, Pavlik LL, Mikheeva IB, Yaguzhinsky LS, et al. NMDA and GABA receptor presence in rat heart mitochondria. *Chem Biol Interact.* (2018) 291:40–6. doi: 10.1016/j.cbi.2018.06.004
45. Selin AA, Lobysheva NV, Nesterov SV, Skorobogatova YA, Byvshev IM, Pavlik LL, et al. On the regulative role of the glutamate receptor in mitochondria. *Biol Chem.* (2016) 397:445–58. doi: 10.1515/hsz-2015-0289
46. da Cunha AA, Pauli V, Saciura VC, Pires MG, Constantino LC, de Souza B, et al. N-methyl-D-aspartate glutamate receptor blockade attenuates lung injury associated with experimental sepsis. *Chest.* (2010) 137:297–302. doi: 10.1378/chest.09-1570
47. Zhe Z, Hongyuan B, Wenjuan Q, Peng W, Xiaowei L, Yan G. Blockade of glutamate receptor ameliorates lipopolysaccharide-induced sepsis through regulation of neuropeptides. *Biosci Rep.* (2018) 38:BSR20171629. doi: 10.1042/BSR20171629
48. Moullan N, Mouchiroud L, Wang X, Ryu D, Williams EG, Mottis A, et al. Tetracyclines disturb mitochondrial function across eukaryotic models: a call for caution in biomedical research. *Cell Rep.* (2015) 10:1681–91. doi: 10.1016/j.celrep.2015.02.034

Conflict of Interest: The authors declare that the research was conducted in the absence of any commercial or financial relationships that could be construed as a potential conflict of interest.

frontiers in Medicine

ORIGINAL RESEARCH
published: 21 December 2020
doi: 10.3389/fmed.2020.585462

A Pilot Study on the Association of Mitochondrial Oxygen Metabolism and Gas Exchange During Cardiopulmonary Exercise Testing: Is There a Mitochondrial Threshold?

Philipp Baumbach[1,2†], *Christiane Schmidt-Winter*[1,2†], *Jan Hoefer*[1,2], *Steffen Derlien*[3], *Norman Best*[3], *Marco Herbsleb*[4] *and Sina M. Coldewey*[1,2,5*]

[1] Department of Anesthesiology and Intensive Care Medicine, Jena University Hospital, Jena, Germany, [2] Septomics Research Center, Jena University Hospital, Jena, Germany, [3] Institute of Physiotherapy, Jena University Hospital, Jena, Germany, [4] Department of Sports Medicine and Health Promotion, Friedrich Schiller University, Jena, Germany, [5] Center for Sepsis Control and Care, Jena University Hospital, Jena, Germany

OPEN ACCESS

Edited by:
Inge Bauer,
University Hospital of Düsseldorf, Germany

Reviewed by:
Egbert Mik,
Erasmus Medical Center, Netherlands
Tobias Piegeler,
University Hospital Leipzig, Germany

***Correspondence:**
Sina M. Coldewey
sina.coldewey@med.uni-jena.de

[†] These authors have contributed equally to this work

Specialty section:
This article was submitted to Intensive Care Medicine and Anesthesiology, a section of the journal Frontiers in Medicine

Received: 20 July 2020
Accepted: 15 October 2020
Published: 21 December 2020

Citation:
Baumbach P, Schmidt-Winter C, Hoefer J, Derlien S, Best N, Herbsleb M and Coldewey SM (2020) A Pilot Study on the Association of Mitochondrial Oxygen Metabolism and Gas Exchange During Cardiopulmonary Exercise Testing: Is There a Mitochondrial Threshold? Front. Med. 7:585462. doi: 10.3389/fmed.2020.585462

Background: Mitochondria are the key players in aerobic energy generation via oxidative phosphorylation. Consequently, mitochondrial function has implications on physical performance in health and disease ranging from high performance sports to critical illness. The protoporphyrin IX-triplet state lifetime technique (PpIX-TSLT) allows *in vivo* measurements of mitochondrial oxygen tension (mitoPO$_2$). Hitherto, few data exist on the relation of mitochondrial oxygen metabolism and ergospirometry-derived variables during physical performance. This study investigates the association of mitochondrial oxygen metabolism with gas exchange and blood gas analysis variables assessed during cardiopulmonary exercise testing (CPET) in aerobic and anaerobic metabolic phases.

Methods: Seventeen volunteers underwent an exhaustive CPET (graded multistage protocol, 50 W/5 min increase), of which 14 were included in the analysis. At baseline and for every load level PpIX-TSLT-derived mitoPO$_2$ measurements were performed every 10 s with 1 intermediate dynamic measurement to obtain mitochondrial oxygen consumption and delivery (mito$\dot{V}O_2$, mito$\dot{D}O_2$). In addition, variables of gas exchange and capillary blood gas analyses were obtained to determine ventilatory and lactate thresholds (VT, LT). Metabolic phases were defined in relation to VT1 and VT2 (aerobic: <VT1, aerobic-anaerobic transition: ≥VT1 and <VT2 and anaerobic: ≥VT2). We used linear mixed models to compare variables of PpIX-TSLT between metabolic phases and to analyze their associations with variables of gas exchange and capillary blood gas analyses.

Results: MitoPO$_2$ increased from the aerobic to the aerobic-anaerobic phase followed by a subsequent decline. A mitoPO$_2$ peak, termed mitochondrial threshold (MT), was observed in most subjects close to LT2. Mito$\dot{D}O_2$ increased during CPET, while no changes in mito$\dot{V}O_2$ were observed. MitoPO$_2$ was negatively associated with partial pressure of end-tidal oxygen and capillary partial pressure of oxygen and positively associated with partial pressure

of end-tidal carbon dioxide and capillary partial pressure of carbon dioxide. Mito$\dot{D}O_2$ was associated with cardiovascular variables. We found no consistent association for mito$\dot{V}O_2$.

Conclusion: Our results indicate an association between pulmonary respiration and cutaneous mitoPO_2 during physical exercise. The observed mitochondrial threshold, coinciding with the metabolic transition from an aerobic to an anaerobic state, might be of importance in critical care as well as in sports medicine.

Keywords: COMET, mitochondrial oxygen tension (mitoPO_2), mitochondrial oxygen consumption (mito$\dot{V}O_2$), cardiopulmonary exercise testing (CPET), ergospirometry, protoporphyrin-IX triplet state lifetime technique, mitochondrial oxygen delivery (mito$\dot{D}O_2$)

INTRODUCTION

Mitochondria are the power houses of aerobic cells. Fueled by oxygen and energy-rich substrates of the glucose, fat, and protein metabolism, they generate ATP, the energy equivalents required for the work of muscles and function of organs. It is obvious that damage to these organelles leads to a reduced energy supply on a cellular level. Thus, mitochondria play a pivotal role in physiologic and pathophysiologic conditions. With a better understanding of the complex interactions in sepsis, microcirculation and mitochondrial dysfunction have become a major focus of research (1). Numerous sepsis-associated mitochondrial abnormalities have been described: disturbances of the electron transport chain and of oxidative phosphorylation, structural damage, oxidative and nitrosative stress, proton leak and uncoupling being only a small selection (2). In response to these findings, mitochondria targeted therapies are currently being developed (3).

However, a non-invasive diagnostic tool for the assessment of mitochondrial performance *in situ* that can be applied simultaneously with an event of interest, such as the onset of sepsis or other physiological or pathophysiological conditions, is as yet missing. Apart from few exceptions (2, 4), mitochondrial function has mostly been assessed by laboratory tests with vital cells following invasive measures on patients, such as blood withdrawal or muscle biopsy (4).

Since oxygen is crucial to achieve a sufficient energy supply by aerobic ATP generation, it seems logical to employ mitochondrial oxygen tension and its dynamics as a marker for mitochondrial performance. To enable direct and non-invasive measurements of mitochondrial oxygen metabolism, Mik et al. introduced the protoporphyrin IX-triplet state lifetime technique (PpIX-TSLT) (5). Recently, the measurement of mitochondrial oxygen tension (mitoPO_2) in skin became clinically available by the COMET system (Photonics Healthcare BV, Utrecht, Netherlands). Using the same system, oxygen consumption (mito$\dot{V}O_2$) (6) and oxygen delivery (mito$\dot{D}O_2$) (7) can be determined. A detailed description of the device is provided by Ubbink et al. (8). Up to now, just a few *in vivo* studies have been conducted and even less in patients or volunteers (7, 9–12).

The OXPHOS complex on the inner mitochondrial membrane is the final acceptor of oxygen, which is provided by respiration and transported to tissue by blood, where it is bound to hemoglobin of the erythrocytes (13). While resting and during light physical activity, aerobic energy generation from fatty acids and in second line carbon hydrates, is the dominant feature in generating ATP. Yet, with increasing work intensity, oxygen demand is no longer balanced by supply. The consequence is additional allocation of ATP by anaerobic glycolysis. The buffering of H^+ ions from the production of lactic acid yields extra CO_2 that must be eliminated via enhanced respiration. This is the physiologic equivalent of the first ventilatory threshold (VT1) detected in ergospirometry (also known as cardiopulmonary exercise testing, CPET) (14). CPET from light to maximal intensity displays three phases: aerobic metabolism, aerobic-anaerobic transition, and anaerobic metabolism (15, 16). Ventilatory thresholds VT1 and VT2 separate the phases, whereas VT2 denotes the respiratory compensation point (RCP) (17). At this point respiration is intensified once more in order to counterbalance metabolic acidosis caused by a disproportionate lactic acid increase. Lactate levels can be measured directly in arterial or capillary blood samples. Similar to VT1 and VT2, two metabolic thresholds of the lactate kinetics (LT1 and LT2) can be identified. The latter are related to but not equal to the ventilatory thresholds (17). Of note, not less than 25 different LT concepts have been described (18). CPET measurements reveal a complex but not comprehensive picture of metabolic and respiratory processes during exercise (see **Figure 1**). The integration of the chronological sequences in the mitochondrion during exercise into the macroscopic observations of the CPET might not only be a useful contribution to the current knowledge of the complex processes of physical activity but also provide insights into mitochondrial performance when reaching physiologic or pathologic limitations.

In critical illness, the aerobic-anaerobic and the anaerobic metabolism are of utmost importance, since the balance between oxygen supply and oxygen demand is frequently disturbed (1). Aim of our pilot study (PpIX-TSLT measurements during CPET) was to elucidate, if there is an association of cellular oxygen metabolism with gas exchange parameters in distinct metabolic phases. Hitherto, this question has not been addressed but is of great interest when exploring any perturbances of mitochondrial function as is assumed to be a major feature in, e.g., sepsis. In order to gain insights into the interactions of the different levels from organ to cell to cellular organelles, such mechanisms need to be explored in healthy humans

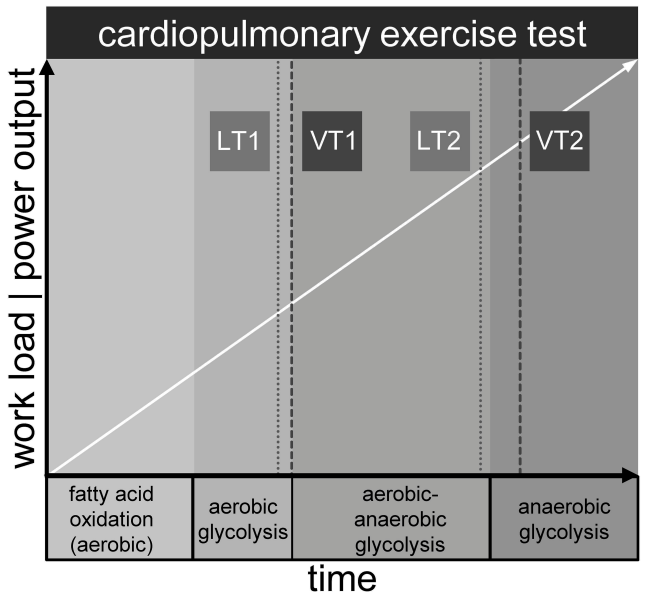

FIGURE 1 | Metabolic phases and exemplary location of lactate (LT1, LT2) and ventilatory thresholds (VT1, VT2) during maximum cardiopulmonary exercise testing.

first. Therefore, our study was designed to create all three phases of physical exertion: aerobic metabolism, aerobic-anaerobic transition and anaerobic metabolism by employing a graded multistage protocol. To approach our research question, parameters of mitochondrial oxygen metabolism (mitoPO_2, mito$\dot{V}O_2$, mito$\dot{D}O_2$) were measured in relation to respiratory gas exchange variables, lactate kinetics and other variables derived from capillary blood gas analyses during a maximal intensity CPET. We then analyzed the kinetics of mitoPO_2, mito$\dot{V}O_2$ and mito$\dot{D}O_2$ in relation to the metabolic phases and to the metabolic (LT1 and LT2) and ventilatory thresholds (VT1 and VT2) (17).

METHODS

Study Population

We recruited healthy male adults via the Jena University Hospital notice boards, notice boards in fitness-studios and social media. Participants had to be at least 18 years old, non-smoking, and should perform strength or fitness-oriented training at least three times a week. All candidates gave their written informed consent and according to the Physical Activity Readiness Questionnaire (19), showed readiness for physical activity, which the study team had to confirm. The following criteria lead to exclusion from participation: significant cardiac, pulmonary or musculoskeletal disease or condition, allergies to contents of the Alacare® plaster (Photonamic, Wedel, Germany), or to ingredients of Finalgon® CPD Wärmecreme (Sanofi Aventis, Germany), allergy to medical adhesive bandages, porphyria, skin conditions aggravated by sunlight or increased sensitivity to light, participation in another interventional study, or prior participation in this study. The study was approved by the ethics committee of the Friedrich Schiller University Jena (2019-1296-BO) and is registered at the German Clinical Trials Register (DRKS00016670).

Experimental Setup of the Study

The complete setup is summarized in **Figure 2**.

PpIX-TSLT Measurements

This optical method uses an endogenous organic compound, protoporphyrin IX (PpIX), as a fluorophore. After excitation with a pulse of green light, it will emit a red delayed fluorescence (20). In the presence of oxygen, the lifetime of the delayed fluorescence caused by the first excited triplet state of porphyrin is inversely related to PO_2 (20) as described by the Stern-Vollmer equation (21). The fact that oxygen is a quencher of fluorescence has been used to measure the oxygen content of mitochondria (5). Though PpIX, a natural precursor of heme in the heme biosynthetic pathway, is synthesized within the mitochondrion (22), its amounts are too small for the use as an oxygen-sensitive fluorophore. Because the conversion of PpIX to heme is a rate limiting step (23), its quantity can be enhanced by administering 5-aminolevulinic acid (5-ALA), a precursor of PpIX, to the measuring site (24). By pressure induced interruption of the local microcirculation oxygen consumption (mito$\dot{V}O_2$) can be calculated from the rate at which the oxygen tension declines, while replenishment is stopped (6). Mitochondrial oxygen delivery (mito$\dot{D}O_2$) however, is then calculated from the slope of the mitoPO_2 increase, when pressure is released (11).

Individuals were instructed to apply a 4 cm^2 adhesive patch containing 8 mg of 5-ALA (Alacare®, Photonamic, Wedel, Germany) to their left lumbar region at least 6 h prior to the measurement to ensure sufficient accumulation of PpIX. After application of Alacare®, the skin was protected from light with an adhesive plaster before and for 48 h after the test to prevent skin irritation. The lumbar region was chosen because of technical considerations: since the anterior chest wall, as proposed by Harms and colleagues (9), is not easily accessible and, in addition, is in constant movement while riding a bicycle, reliable measurements would not have been achieved. The measurements were performed with the COMET measurement system (Photonics Healthcare BV, Utrecht, Netherlands). After removal of the Alacare® plaster, the COMET Skin Sensor was fixed to the site with an adhesive tape to prevent shifting of the light source.

PpIX-TSLT measurements at baseline and during CPET always followed the same sequence (see **Figures 2A,B**). MitoPO_2 was measured every 10 s at the beginning and at the end of each stage (baseline, each load level of CPET). After the second minute of each stage (to achieve steady state conditions), dynamic measurements (one measurement per second) were done to obtain mito$\dot{V}O_2$ and mito$\dot{D}O_2$ (**Figure 2B**). In detail, after recording mitoPO_2 for about 20 s (one measurement per second), pressure was applied to the sensor to locally inhibit microcirculation. This resulted in a decrease of mitoPO_2, which posed the basis for the assessment of mito$\dot{V}O_2$. When mitoPO_2 dropped near to zero or showed no further decline, pressure was maintained for a further 10 s. Thereafter, the pressure was released to allow local reoxygenation, which was followed by an increase of mitoPO_2. This was used as the basis to obtain mito$\dot{D}O_2$. The dynamic measurements were analyzed by two independent raters (PB, JH) with a self-developed program under MATLAB (MATLAB and Statistics Toolbox Release 2017a,

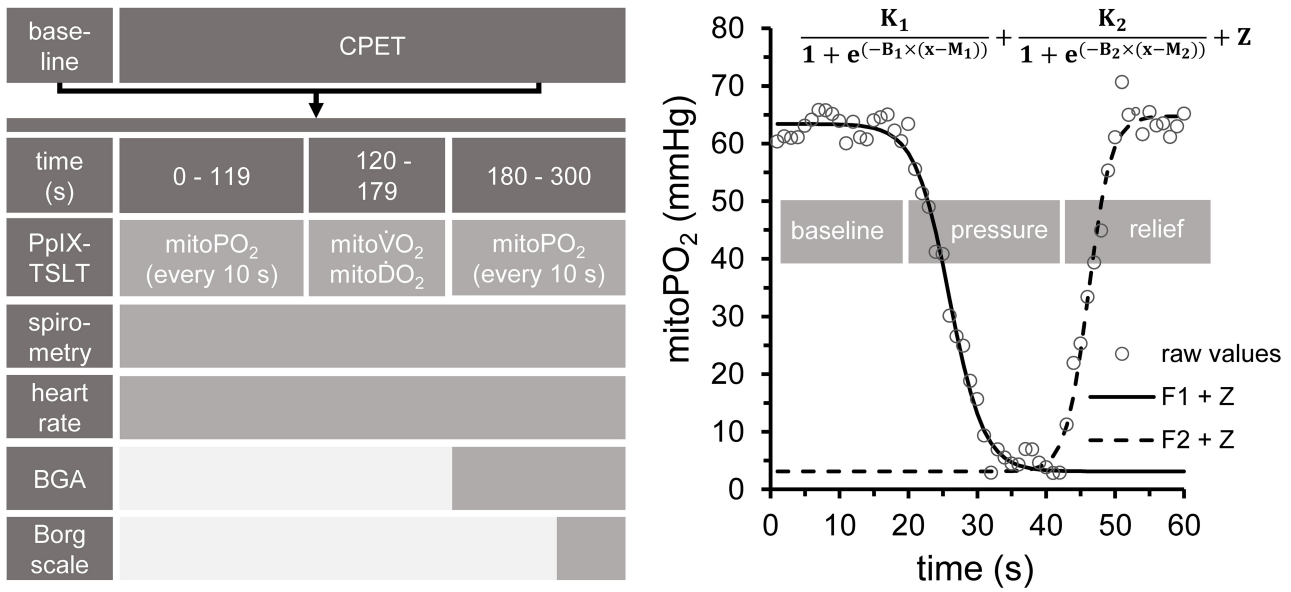

FIGURE 2 | Experimental setup. **(A)** All measurements at baseline, during cardiopulmonary exercise testing (CPET) and in the recovery phase followed the same sequence. PpIX-TSLT measurements were performed every 10 s during the first and last 2 min of each phase to obtain mitochondrial oxygen tension ($mitoPO_2$). Capillary blood samples for blood gas analysis (CBG) were taken after 180 s. Subjective ratings of exertion and dyspnea were assessed by the Borg Scale at the end of each phase. ECG and gas exchange parameters were monitored continuously. In addition, guideline-conform non-invasive blood pressure measurements were performed every 180 s. **(B)** After 2 min phase duration, dynamic PpIX-TSLT measurements were performed to assess mitochondrial oxygen consumption ($mito\dot{V}O_2$) and delivery ($mito\dot{D}O_2$). During the first 20 s, baseline $mitoPO_2$ measurements were obtained. Thereafter, pressure was applied to the sensor in order to locally inhibit microcirculation. When $mitoPO_2$ reached near to zero levels or showed no further decline, pressure was maintained for 10 s and then released. Based on the fitted parameters $mito\dot{V}O_2$ (F1: left part of the equation) and $mito\dot{D}O_2$ (F2: right part of the equation) were estimated [for details see (11)].

The MathWorks, Inc. Natick, Massachusetts, United States). In short, the algorithm fits two complementary sigmoid functions, which model average $mitoPO_2$ (without pressure), the decrease (during pressure) and the subsequent increase of $mitoPO_2$ (after pressure release, see **Figure 2B**). Based on the fitted function parameters, average $mito\dot{V}O_2$ and average $mito\dot{D}O_2$ are derived as previously described (7). Pressure to the skin sensor during dynamic measurements was applied by a handheld dynamometer (Hoggan MicroFET2 Dynamometer, Hoggan Scientific LLc, Salt Lake City, United States) in order to achieve equal pressure in each dynamic measurement. Skin temperature was recorded as the temperature of the skin sensor.

To analyze the individual kinetics of $mitoPO_2$ from single measurements (every 10 s) during baseline and CPET, thereby excluding dynamic measurements, the data points were smoothed using locally estimated scatterplot smoothing (LOESS, span = 0.75, degree = 2). The mitochondrial threshold (MT) was set as maximum and/or decline of the fitted curve during CPET. An example is given in **Figure 3** (**Supplementary Figure 1** displays the data for all subjects).

Cardiopulmonary Exercise Test (CPET)

A bicycle ergometer was used (Custo-Cardio Diagnostik, Custo-Med GmbH, Ottobrunn, Germany). After calibration of the gas analyzer and flow sensor, baseline measurements were obtained, and the exercise test (graded multistage protocol) was started at 50 W with a workload increase of 50 W every 5 min. Participants were instructed to maintain a pedal frequency of 60–80 rotations per minute receiving feedback when being out of this scope. Exhaustion was deemed to have occurred when the participant could no longer maintain the required power output or wished to stop. Objective exhaustion levels and causes for the premature termination of the test were determined by classical criteria stated in various guidelines (25–27). Furthermore, the Borg Rating of Perceived Exertion (RPE) scale was used for the self-assessment of subjective exertion [from 6 (= no exertion at all) to 20 (= maximum exertion)] and dyspnea [from 6 (= no breathing difficulty) to 20 (= maximum breathing difficulty)] (28–30) at baseline and at the end of each load level. During the test, ventilation and standard gas exchange variables were recorded continuously on a breath-by-breath basis by a Ganshorn LF8 PowerCube® pneumotachograph (Ganshorn Medizin Electronic GmbH, Niederlauer, Germany) and displayed in the form of a 9-panel diagram according to Wassermann (31). The recorded and calculated variables were: minute ventilation ($\dot{V}E$), oxygen consumption ($\dot{V}O_2$), carbon dioxide production ($\dot{V}CO_2$), ventilatory equivalents $\dot{V}E/\dot{V}O_2$ and $\dot{V}E/\dot{V}CO_2$, partial pressure of end-tidal oxygen ($PETO_2$) and carbon dioxide ($PETCO_2$) and respiratory exchange ratio (RER). For data analysis the breath-by-breath data were exported as 10 s time-averaged values. Ventilatory thresholds (VT1 and VT2) were determined *post-hoc* using the method described

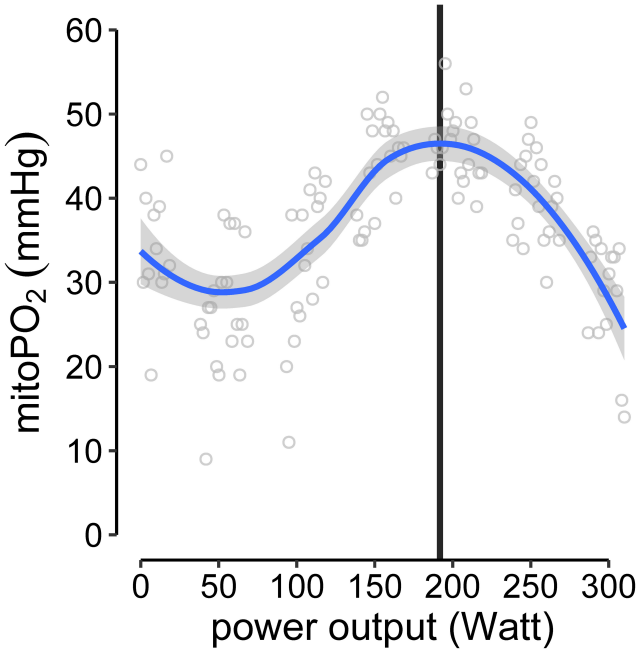

FIGURE 3 | Example of MT-identification (mitochondrial threshold, vertical black line). Raw mitoPO$_2$ values of single measurements were smoothed (locally estimated scatterplot smoothing, LOESS) and the maximum of the fitted curve was set as MT.

by Westhoff et al. (17). For monitoring reasons according to guidelines (25, 26), a 12-lead ECG was recorded continuously throughout the test, blood pressure was measured non-invasively every 2.5 min and oxygen saturation was monitored continuously by pulse oximetry (S_pO_2).

Capillary Blood Gases (CBG)

After pre-treatment of the right earlobe with Finalgon® CPD Wärmecreme, 2 capillary blood samples (80 and 70 µl) for blood gas analysis were taken at baseline and after 3 min into each load level. One blood sample was analyzed on site using a GEM Premier 5000 blood gas testing system (Instrumentation Laboratory, Bedford, United States), the second blood sample was taken to a Radiometer ABL90FLEX blood gas analyzer (Radiometer GmbH, Krefeld, Germany) within the same building but about 75 s away from the study room. A third sample was used for a lactate measurement with a portable lactate meter (Lactate Scout 4, EKF-diagnostic GmbH, Barleben, Germany). Single measurements were obtained for base excess (BE), total concentration of hemoglobin (ctHb) and S_cO_2 (capillary oxygen saturation) (ABL90FLEX), double measurements for capillary partial pressure of oxygen and carbon dioxide (P_cO_2, P_cCO_2), pH (ABL90FLEX and GEM Premier 5000). Triple measurements were acquired for lactate (plus Lactate Scout 4) when possible.

Lactate thresholds (LT1 and LT2) were calculated from the capillary blood samples (measurements of the different samples were averaged) taken at each workload level. The evaluation of the lactate thresholds was done independently by the examiner (MH) using software written for performance diagnostics (Ergonizer, Vers. 5.7.3 Build 81, Freiburg, Germany). The Ergonizer software uses the model of Dickhuth, where the individual anaerobic threshold (IAS = LT2) is determined as a 1.5 mmol lactate increase above the minimal lactate equivalent (LT1) (32, 33).

Statistical Analysis

In descriptive analysis, medians and first and third quartiles (Q_1/Q_3) are reported. For categorical variables we report absolute and relative frequencies.

To compare the variables of PpIX-TSLT, CPET (e.g., $PETO_2$, $PETCO_2$) and CBG between the different metabolic phases, we performed the following steps: The individual VT1 and VT2 were used to define the aerobic (all data points <VT1), the aerobic-anaerobic (all data points ≥VT1 and <VT2) and the anaerobic phase (all data points ≥VT2) for each subject. Due to the repeated measurements design and expected differences in baseline values, we used linear mixed models. In detail, the variables of PpIX-TSLT, CPET, and CBG served as dependent variables in the models. The phase was entered as categorical variable and served as independent variable (fixed effect). In addition, a random intercept for every subject was entered in the models. In the last step the estimated marginal means for the three phases were compared pairwise using the Tukey method.

To analyze the association between PpIX-TSLT variables and the variables of CPET and CBG we performed the following steps: All variables were standardized (mean ± SD: 0±1) before modeling (mixed models). In all models the PpIX-TSLT variables served as dependent variables. In the basic models the variables of CPET and CBG were entered as dependent variables (fixed effect). Here, the effect of the dependent variable was tested over all phases. In the next step, we obtained models estimating regression coefficients for every phase (phase specific models). Here the specific effect of the dependent variable was tested simultaneously for all phases. In the last step, the model fits of the basic models and the phase specific models were compared to test, if the phase specific models better explain the data. In addition, a random intercept for every subject was entered in all models. Because of the large number of tested regression coefficients, the *p*-values for mitoPO$_2$, mito$\dot{V}O_2$, and mito$\dot{D}O_2$ were adjusted using the Bonferroni-Holm method.

The statistical analysis was performed with R [Version 3.5.1, Vienna, Austria (34)].

RESULTS

Study Sample

Seventeen subjects participated in the study. Three subjects were excluded from the analysis for the following reasons: (a) wrong positioning of the ALA patch, which did not allow valid PpIX-TSLT measurements during CPET, (b) poor signal quality of PpIX-TSLT measurements for unknown reasons, (c) implausible CPET values during baseline measurements. The demographic characteristics of the 14 subjects in the final analysis sample are displayed in **Table 1**.

CPET-Derived Gas Exchange Measurements: Maximum Power Output Level, Ventilatory, and Metabolic Thresholds and Differences in $PETO_2$ and $PETCO_2$ Between the Different Metabolic Phases

Table 1 summarizes the maximum power output levels during CPET. Four subjects terminated CPET at 200 W and five subjects terminated CPET at 250 and 300 W, respectively. All subjects reached at least one of the objective termination criteria and the subjective termination criterion (Borg exertion, median: 18, $Q_{1|3}$: 17|19).

TABLE 1 | Demographic characteristics of the study sample (median, $Q_{1|3}$: first and third quartile) and frequencies of individual maximum power output levels during CPET.

Variable	Median	Q_1	Q_3	*n*
Age (years)	25.50	22.00	30.00	14
Weight (kg)	79.40	73.50	84.68	14
Height (m)	1.81	1.77	1.88	14

Level	Maximum phase		Cumulative	
	n	%	*n*	%
Baseline	0	0	14	100.0
50 (W)	0	0	14	100.0
100 (W)	0	0	14	100.0
150 (W)	0	0	14	100.0
200 (W)	4	28.6	14	100.0
250 (W)	5	35.7	10	71.4
300 (W)	5	35.7	5	35.7

Descriptive statistics on the obtained ventilatory and metabolic thresholds are displayed in **Table 2**. LT1 and VT1 were close to each other (median LT1: 116 W, median VT1: 111 W). LT2 was reached at a median of 156 W and VT2 was reached at a median of 238 W. The corresponding gas exchange variables at the thresholds are also depicted in **Table 2**. The individual VT1 and VT2 were used to define the individual aerobic (<VT1), aerobic-anaerobic (≥VT1 and <VT2), and anaerobic (≥VT2) phase.

Individual values and model predicted means of selected CPET variables for the different phases (aerobic, aerobic-anaerobic, anaerobic) are depicted in **Figures 4A–C**. There was a significant drop in mean $PETO_2$ (**Figure 4A**) in the aerobic-anaerobic phase compared to the aerobic phase. This was followed by a significant increase in the anaerobic phase. Compared to the aerobic phase, mean $PETO_2$ was significantly higher in the anaerobic phase.

Mean $PETCO_2$ significantly increased in the aerobic-anaerobic phase compared to the aerobic phase (**Figure 2B**). This was followed by a significant decrease in the anaerobic phase. Compared to the aerobic phase, mean $PETCO_2$ was significantly lower in the anaerobic phase.

With increasing power output, HR (**Figure 4C**) significantly increased from the aerobic via the aerobic-anaerobic to the anaerobic phase as physiologically expected. This was also true for $\dot{V}O_2$, $\dot{V}E$, $\dot{V}CO_2$, and RR. The detailed descriptive statistics of the main CPET variables are listed in **Supplementary Table 1**.

TABLE 2 | Descriptive statistics (median, $Q_{1|3}$: first and third quartile) on ventilatory, metabolic, and mitochondrial thresholds.

Variable	Statistic	Value	Power	Time		$\dot{V}O_2$	$\dot{V}CO_2$	RER	HR	RR	$PETO_2$	$PETCO_2$
			[W]	[s]	[%]	[l/min]	[l/min]		[/min]	[/min]	[mmHg]	[mmHg]
LT1	Median	**2.0**	**116**	**406**	**40**	**1.13**	**1.07**	**0.91**	**110**	**20**	**96.35**	**42.05**
	Q_1	1.2	95	274	35	0.87	0.78	0.88	94	17	95.00	41.09
	Q_3	3.4	134	463	43	1.26	1.16	0.93	123	22	98.88	43.54
VT1	Median		**111**	**365**	**37**	**1.09**	**1.00**	**0.89**	**104**	**17**	**96.46**	**42.94**
	Q_1		93	266	35	0.94	0.83	0.87	98	15	93.17	40.24
	Q_3		118	428	40	1.22	1.10	0.92	117	19	98.61	44.74
LT2	Median	**3.5**	**156**	**639**	**56**	**1.40**	**1.37**	**0.99**	**136**	**19**	**98.66**	**43.50**
	Q_1	2.7	140	538	52	1.25	1.27	0.95	120	17	97.04	42.06
	Q_3	4.9	196	877	61	1.87	1.91	1.02	140	22	100.49	46.09
VT2	Median		**238**	**1140**	**83**	**2.16**	**2.26**	**1.06**	**162**	**23**	**100.30**	**46.94**
	Q_1		214	999	82	2.05	2.17	1.02	154	22	97.09	44.08
	Q_3		266	1290	88	2.41	2.65	1.10	174	25	101.35	48.46
MT	Median	**78**	**173**	**752**	**60**	**1.71**	**1.64**	**0.99**	**143**	**24**	**99.79**	**44.43**
	Q_1	72	142	573	49	1.24	1.19	0.95	119	20	97.71	41.95
	Q_3	83	190	857	70	1.83	1.95	1.07	154	26	100.66	45.38

In addition, variables of gas exchange and physiological data at the corresponding threshold is shown.

LT1/2: first/second lactate threshold (value in mmol/l), VT1/2: first/second ventilatory threshold, MT: peak of mitochondrial oxygen tension ($mitoPO_2$, value in mmHg), $\dot{V}O_2$: oxygen uptake, $\dot{V}CO_2$: carbon dioxide output, RER: respiratory exchange ratio, HR: heart rate, RR: respiratory rate, $PETO_2$: end-tidal oxygen tension, $PETCO_2$: end-tidal carbon dioxide tension. Median values are printed in bold.

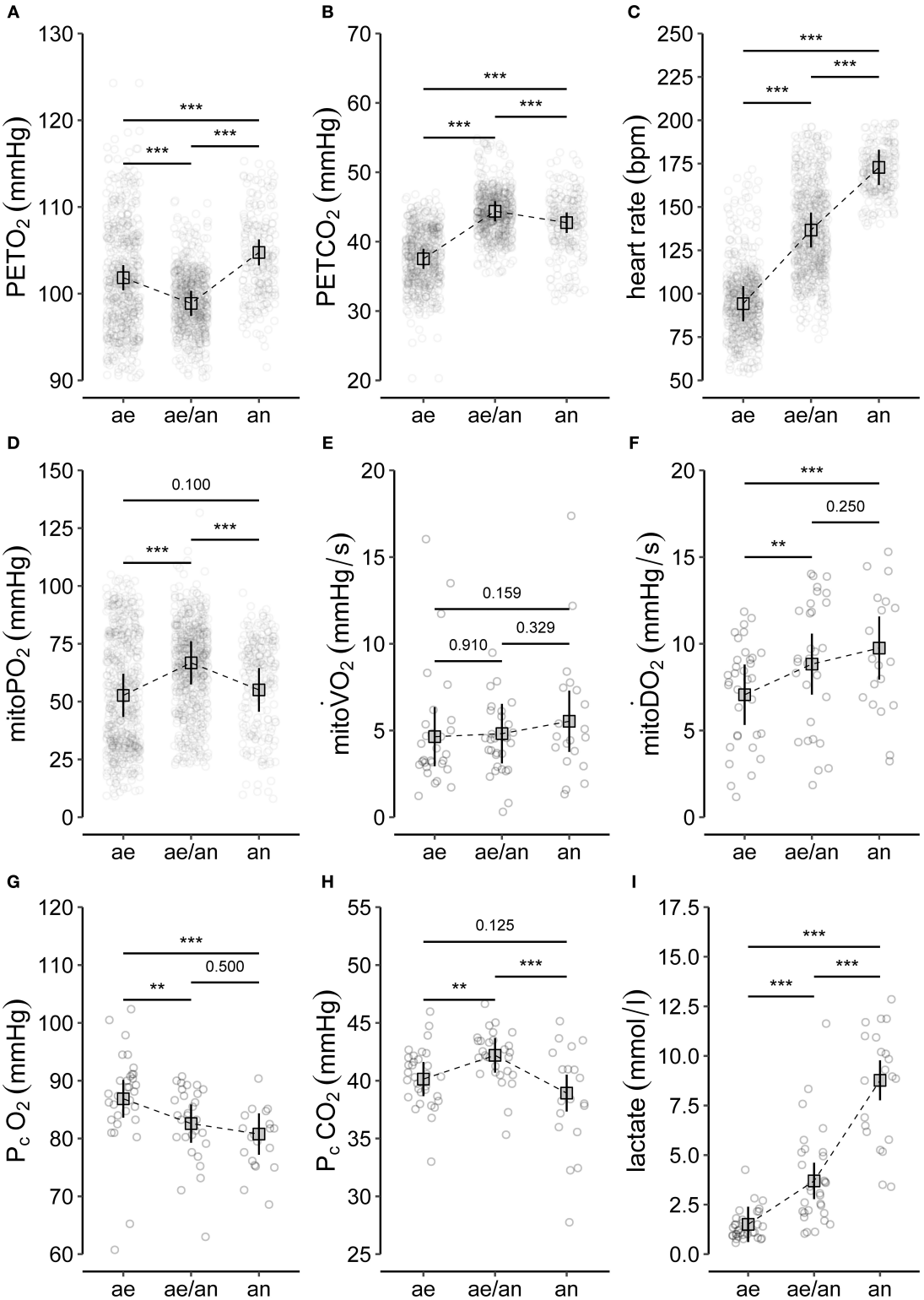

FIGURE 4 | Summary of **(A–C)** selected variables of CPET (end-tidal oxygen tension, $PETO_2$; end-tidal carbon dioxide tension, $PETCO_2$; heart rate), **(D–F)** main variables of PpIX-TSLT measurements (mitochondrial oxygen tension, $mitoPO_2$; mitochondrial oxygen consumption, $mito\dot{V}O_2$; mitochondrial oxygen delivery, $mito\dot{D}O_2$), and **(G–I)** variables of the capillary blood gas analysis (partial pressure of oxygen, P_cO_2; partial pressure of carbon dioxide, P_cCO_2; lactate). The dots refer to individual values of the variables during aerobic (ae, <VT1), aerobic-anaerobic (ae/an, ≥VT1 and <VT2), and anaerobic phase (an, ≥VT2). In addition, model predicted means (squares), corresponding 95% confidence intervals (lines) and adjusted *p*-values of comparisons between phases are displayed. $^*p < 0.05$, $^{**}p < 0.01$, $^{***}p < 0.001$.

PpIX-TSLT Measurements: Differences in MitoPO_2, Mito$\dot{V}O_2$, and Mito$\dot{D}O_2$ Between the Metabolic Phases and Description of the Mitochondrial Threshold

Individual values and model predicted means of the main PpIX-TSLT variables for the different phases are presented in **Figures 4D–F**.

Mean mitoPO_2 increased significantly from the aerobic to the aerobic-anaerobic phase (**Figure 4D**). This was followed by a significant decrease in the anaerobic phase, which resulted in non-significant mean differences between the aerobic and the anaerobic phase. Correspondingly, in 11 of 14 (78.6%) subjects, a peak followed by a final decrease or a decrease from a plateau (2/14, 14%) in mitoPO_2 was identified (see **Table 2** and **Supplementary Figure 1**). In analogy to ventilatory and metabolic thresholds, we termed this peak mitochondrial threshold (MT).

The relative location of MT compared to ventilatory and metabolic thresholds is displayed in **Figure 5**. In 13 of the 14 subjects, MT occurred later than LT1 and VT1. In one participant, MT was recorded after LT1 but slightly before VT1. Median MT was located in the vicinity of LT2 (median difference in time: −42 s, $Q_{1|3}$: −200 s | 53 s) and thus occurred slightly later but close to median LT2 at about 60% of maximum power output. In all subjects, MT occurred earlier than VT2. MitoPO_2 dynamics, selected variables of gas exchange, and corresponding ventilatory thresholds during baseline and throughout load levels are summarized in **Figure 6**.

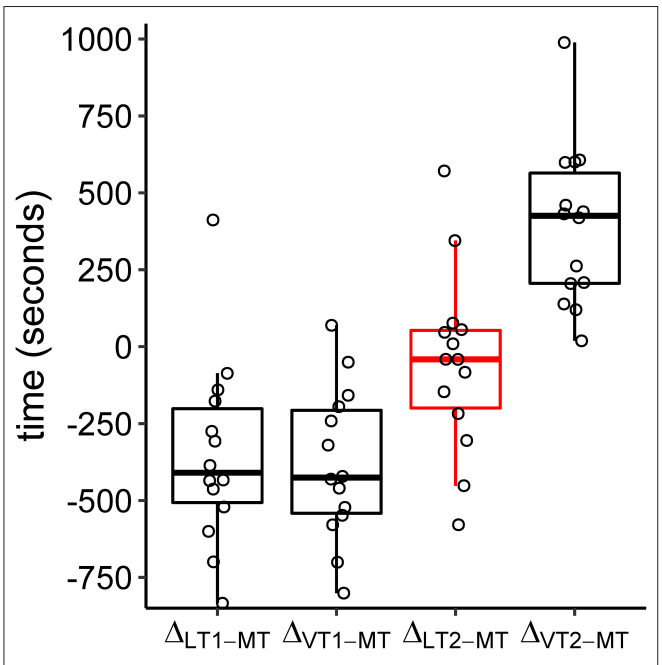

FIGURE 5 | Boxplots of time differences in lactate (LT1, LT2), ventilatory (VT1, VT2), and mitochondrial (MT) thresholds. The circles refer to the individual differences. Negative values indicate a later occurrence of MT compared to the other thresholds.

There were no significant differences in mean mito$\dot{V}O_2$ between the three metabolic phases (**Figure 4E**).

Mean mito$\dot{D}O_2$ increased significantly from the aerobic to the aerobic-anaerobic phase (**Figure 4F**). We found no significant differences in mean mito$\dot{D}O_2$ values between the aerobic-anaerobic and the anaerobic phase, but mean mito$\dot{D}O_2$ values were significantly higher in the anaerobic phase compared to the aerobic phase. The detailed descriptive statistics on the main variables of the PpIX-TSLT measurements are listed in **Supplementary Table 2**.

Differences in P_cO_2, P_cCO_2, and Lactate Between the Metabolic Phases

Individual values and model predicted means of selected CBG variables for the different metabolic phases are presented in **Figures 4G–I**.

Compared to the aerobic phase, mean P_cO_2 was significantly lower in the aerobic-anaerobic and in the anaerobic phase (**Figure 4G**). There were no significant differences between the aerobic-anaerobic and the anaerobic phase for mean P_cO_2.

Mean P_cCO_2 was significantly higher in the aerobic-anaerobic phase compared to the aerobic phase (**Figure 4H**). This initial increase was followed by a significant decrease in the anaerobic phase. Mean P_cCO_2 in the anaerobic phase did not differ significantly between the aerobic and the anaerobic phase.

Mean lactate values increased significantly between the phases (**Figure 4I**). The detailed descriptive statistics on the main CBG variables are listed in **Supplementary Table 3**.

Associations Between PpIX-TSLT-Derived Variables and Variables of CPET-Derived Gas Exchange and CBG

The results of the associative analyses are summarized in **Figure 7**.

MitoPO_2 and CPET variables showed different associations throughout the different phases (detailed information is listed in **Supplementary Table 4**). CPET variables which increased over the different phases ($\dot{V}E$, $\dot{V}O_2$, $\dot{V}CO_2$, RER, RR, and HR) mainly were positively associated with mitoPO_2 values within the aerobic and the aerobic-anaerobic phase. Most of these relations reversed within the anaerobic phase. $\dot{V}E/\dot{V}CO_2$ and $PETO_2$ were negatively associated with mitoPO_2. $PETCO_2$ was positively associated with mitoPO_2. Nonetheless, there were differences in the strength of the associations between the phases (better model fit for the models with phase specific regression coefficients). P_cCO_2 was positively and P_cO_2 was negatively associated with mitoPO_2. The models with specific effects for the phases did not show a better model fit. Lactate was positively associated with mitoPO_2 values in the aerobic phase.

Mito$\dot{V}O_2$ was negatively associated with $\dot{V}E/\dot{V}CO_2$ and positively associated with $PETCO_2$ in the anaerobic phase. We also found a positive association between mito$\dot{V}O_2$ and ctHb. However, only the *p*-value for ctHb in the anaerobic phase survived adjustment for multiple testing.

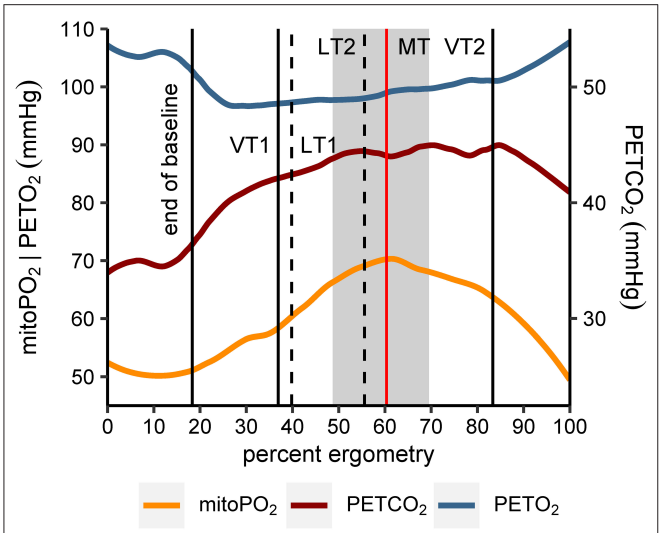

FIGURE 6 | Smoothed course (locally estimated scatterplot smoothing, LOESS) of mitochondrial oxygen tension (mitoPO$_2$), end-tidal oxygen tension (PETO$_2$), and end-tidal carbon dioxide tension (PETCO$_2$) for all subjects (n = 14). Values of the x-axis (percent ergometry) were scaled individually to the minimum (first measurement during baseline) and maximum power output level of the CPET (e.g., last measurement at 250 W). The vertical lines indicate end of baseline (median), first and second ventilatory and lactate threshold (medians of VT1|2, LT1|2) and mitochondrial threshold (median, MT). In addition, the gray area marks the interquartile range of MT.

MitoDO$_2$ was positively associated with variables showing an increase over the different phases ($\dot{V}$E, $\dot{V}O_2$, $\dot{V}CO_2$, RER, RR and HR, Borg scales). In addition, lactate showed a positive and pH showed a negative association with mitoDO$_2$ in the aerobic phase.

DISCUSSION

In this study we performed PpIX-TSLT measurements simultaneously with a cardiopulmonary exercise test to analyze mitochondrial oxygen metabolism and its association with variables of gas exchange and CBG. We found significant differences in mitoPO$_2$ and mitoDO$_2$ between the three different phases during CPET. In the majority of subjects, we observed a peak in mitoPO$_2$ which we termed mitochondrial threshold (MT). The peak occurred later than VT1 and LT1, but earlier than VT2. Its median appearance was timed around LT2. In the exploratory analysis we found significant associations between PpIX-TSLT variables and variables of CPET and CBG. Thus, our results clearly indicate an association between pulmonary respiration and cutaneous mitochondrial oxygen content during physical exercise.

Kinetics of MitoPO$_2$

In the group analysis, there was a significant increase of mitoPO$_2$ between the aerobic and the aerobic-anaerobic phase, which was followed by a significant drop in mitoPO$_2$ in the anaerobic phase. The increase of mitoPO$_2$ during bicycle ergometry has already been described in our previous study (7), but a subsequent decline was not seen. This is possibly due to the submaximal intensity protocol instead of maximal physical exertion. Cutaneous mean mitoPO$_2$ measurements at baseline (mean ± SD: 51.18 ± 21.93 mmHg) were slightly lower than previous values in humans acquired by the COMET system (7, 10). This might be due to differences in the study population [heterogeneous group pertaining to sex and age (7) and sepsis patients (10) vs. active young male participants] and the different measurement site (lumbar region vs. chest wall). The even lower values reported by Harms et al. (9) might be attributed to the use of a probe with a bigger measurement area in our study [COMET device (photonicshealthcare.com) vs. a clinical prototype device]. However, the variation of baseline mitoPO$_2$ was similar.

Mitochondrial (MT), Metabolic (LT1 and LT2), and Ventilatory (VT1 and VT2) Thresholds

In the majority of the participants, the mitochondrial oxygen tension increased during exercise until a peak (MT) was reached and then dropped again. In sports medicine, lactate thresholds are used to determine training intensities for endurance training assuming that LT2 denotes more or less accurately the maximum lactate steady state at which lactate production and elimination are still balanced. In the review of Faude et al. (18), it is speculated that working intensities near LT2 may induce a considerable increase in the oxidative metabolism of muscle cells, although anaerobic glycolysis is enhanced. Prolonged training at this power output intensity might stimulate aerobic metabolism in muscle cells and thus pose an appropriate level for endurance training. However, there is still debate on the correct determination of LT2 (18). A relatively new concept in training prescription is the identification and determination of training intensities near the critical power (CP), the highest power output which can be sustained for a longer period of time under predominantly aerobic conditions (35). In a most recent meta-analysis, the point in time of reaching CP was located between the maximal lactate steady state and RCP/VT2 (36), which would be in line with the temporal occurrence of MT in our study. The idea of using the moment of decline in mitochondrial performance might pose a new tool of validating LT2 or even the moment, when critical power is reached. To our knowledge, the concept of a mitochondrial threshold has not been proposed before. However, in the study of Römers et al. mitoPO$_2$ in hemodiluted pigs also behaved threshold-like (37). Further studies are needed to evaluate these findings.

MitoPO$_2$ and Its Relation to CPET-Derived Gas Exchange Variables

To our knowledge, data on associations of mitochondrial oxygen tension with CPET-derived gas exchange parameters hitherto do not exist. We were able to demonstrate a phase-dependent association of mitoPO$_2$ with $\dot{V}O_2$ and $\dot{V}CO_2$. During the aerobic phase, these parameters were positively associated, reflecting the balance between oxygen uptake and carbon dioxide elimination on the one side and the simultaneous increase of

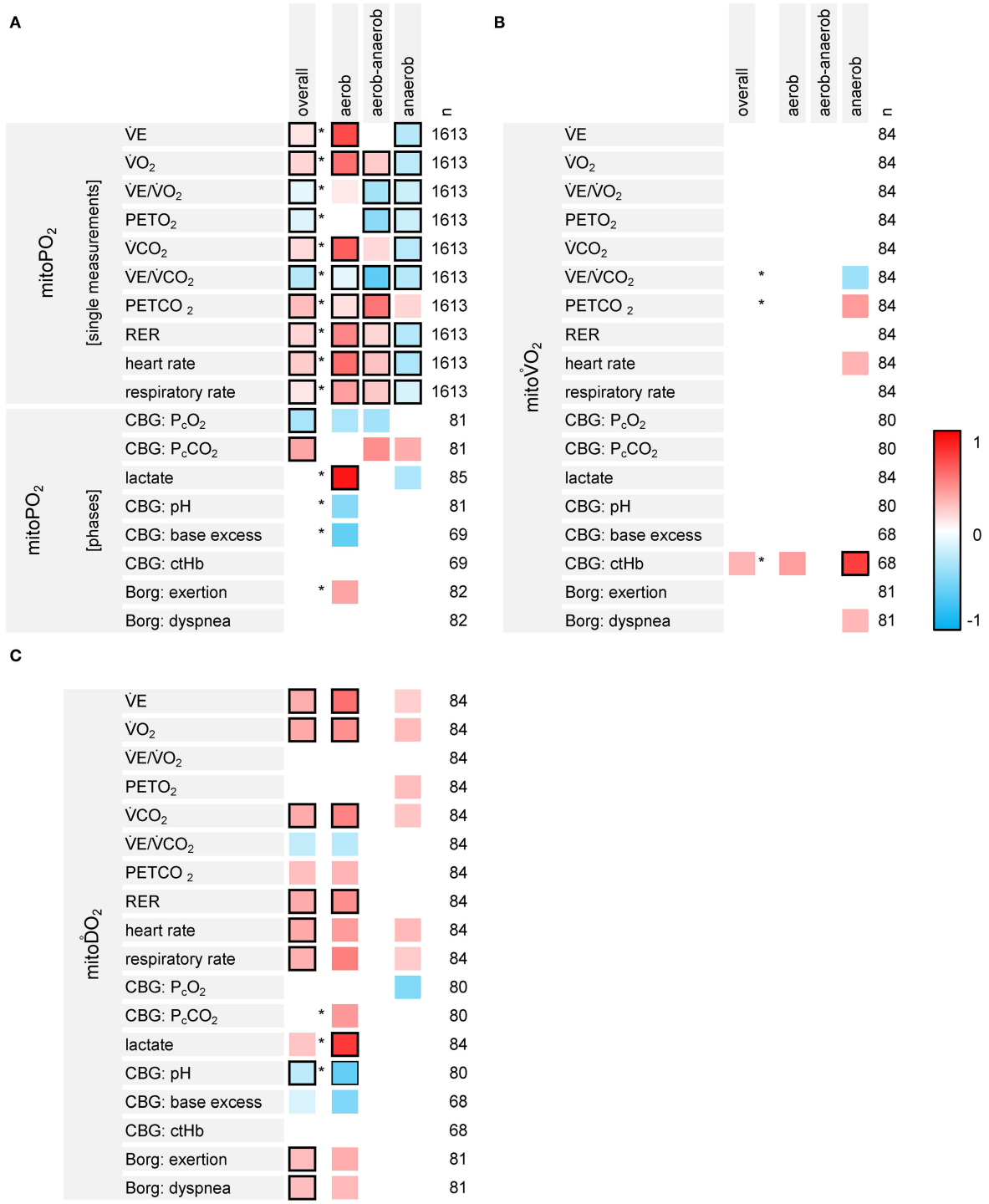

FIGURE 7 | Results of the exploratory analyses on the associations between the variables of PpIX-TSLT measurements (**A**: mitoPO$_2$, **B**: mitoV̊O$_2$, **C**: mitoḊO$_2$), CPET-derived gas exchange and capillary blood gases (CBG). The first column lists the dependent variables, the second column displays the independent variables. The overall column indicates the standardized regression coefficients for the independent variable (one coefficient for all three phases, basic models). Asterisks indicate, if the models estimating separate regression coefficients for the phases show a better model fit compared to the basic models. The columns aerobic, aerobic-anaerobic and anaerobic display the corresponding standardized regression coefficients for each phase. The column n refers to the number (*n*) of data points, which were entered into the model. Regression coefficients with raw *p*-values ≥0.05 were set to zero (white). Framed cells indicate regression coefficients with Bonferroni-Holm adjusted *p*-values <0.05.

mitochondrial oxygen content on the other side. During the aerobic-anaerobic transition phase, the positive correlation of $\dot{V}O_2$ with mitoPO_2 continued while a correlation with $\dot{V}CO_2$ was no longer statistically significant after *p*-value adjustment. This might indicate the increasing accumulation and expiration of additional CO_2 accruing from the beginning anaerobic glycolysis. During the anaerobic phase, both parameters were negatively associated with mitoPO_2. With rising levels of lactic acid, a huge amount of CO_2 is produced by the buffering of H^+ ions, so that the intensity of respiration is mainly driven by the need to eliminate the excess CO_2 (14). At the same time, mitoPO_2–derived from mitochondria in skin—declined despite a further increase in $\dot{V}O_2$. One reason could be that during anaerobic metabolism mitochondrial oxygen demand is no longer matched by supply. Another possible explanation might be that under the conditions of extreme physical exertion, mainly muscular mitochondria are in need of oxygen and therefore, a shift of the scarce substrate from skin to muscles is initiated. According to Boushel et al. muscular mitochondrial respiratory capacity exceeds maximal oxygen delivery in humans (38), thus resulting in a competitive situation between muscles and less active organs. Golub et al. proposed that oxygen demand increases oxygen supply by incremented diffusion gradients and a compensatory vascular response (39), which might support the above-mentioned hypothesis. The simultaneous mitoPO_2 measurement in muscular and cutaneous mitochondria might provide clarification. The closest positive association was seen between mitoPO_2 and $PETCO_2$ for all phases, the best negative association was between mitoPO_2 and $\dot{V}E/\dot{V}CO_2$ followed by mitoPO_2 and $PETO_2$. The latter could be accustomed for by the mitochondrial oxygen consumption, which consequently leads to a lower oxygen content in the exhaled air. Since $PETCO_2$ behaves contrary to $PETO_2$, this possibly explains the association without being causative.

MitoPO_2 and Its Relation to CBG Variables

MitoPO_2 was negatively associated with P_cO_2 in the aerobic and aerobic-anaerobic phases. Despite a decrease of the mean P_cO_2 over the three phases, mean mitoPO_2 at first increased from the aerobic to the aerobic-anaerobic phase and then decreased again in the anaerobic phase. In a hemodilution study in pigs, Römers et al. found a sudden drop in mitoPO_2 at a critical stage of hemodilution. Although Hb declined with each hemodilution step, a mitochondrial response was only seen at that critical point in time (37), hinting at a certain independence of mitochondrial oxygen tension from Hb levels and thus from arterial oxygen content before this moment. In contrast, P_cCO_2 was positively associated throughout all phases. Since P_aCO_2 is more or less consistent with P_ACO_2 (alveolar carbon dioxide partial pressure), which also is the same as $PETCO_2$ in healthy persons (14), this was expected. Only during the aerobic phase, lactate was positively associated with mitoPO_2. During aerobic-anaerobic transition, when anaerobic glycolysis starts and lactate levels rise, lactate was no longer associated with mitoPO_2. An even negative association was found during the anaerobic phase due to increasing lactate levels whilst mitoPO_2 decreased.

Mito$\dot{V}O_2$: Kinetics and Relation to Variables of CPET-Derived Gas Exchange and CBG

We observed no significant changes in mito$\dot{V}O_2$ during exercise. In the study of Baumbach et al. mito$\dot{V}O_2$ had significantly decreased in post-exercise measurements compared to baseline (7). However, no measurements were obtained during exercise. The study also differed insofar that only a submaximal power output was generated and that multiple measurements were done at each time point. Mito$\dot{V}O_2$ measurements at baseline (4.88 $\pm$ 3.00 mmHg) were in the range of previous measurements (7, 9–11). Of the CBG parameters only ctHb showed a positive association, indicating that mito$\dot{V}O_2$ might depend on the oxygen transport capacity of the blood and thus the overall availability of oxygen.

Mito$\dot{D}O_2$: Kinetics and Relation to Variables of CPET-Derived Gas Exchange and CBG

Mito$\dot{D}O_2$ increased from baseline to maximum exertion. In the study of Baumbach et al. mito$\dot{D}O_2$ tended to increase from baseline to post-exercise phases, but the increase was not significant (7). Again, the submaximal power output in that study and differences in the measurement protocol might explain the differences. Mito$\dot{D}O_2$ values at baseline were 6.78 $\pm$ 3.2 and comparable to results from Baumbach et al. (7) and Neu et al. (10). Since the cardiovascular system is responsible for the increase in oxygen delivery to the tissues (40), and since mito$\dot{D}O_2$ mainly reflects reperfusion and thus reoxygenation after temporary interruption of microcirculation, its positive association with HR was expected. A positive association with $\dot{V}E$, $\dot{V}O_2$ and $\dot{V}CO_2$ also was logical, because intensified ventilation is followed by increased O_2-uptake and also increased CO_2-elimination. However, the continuing increase of mito$\dot{D}O_2$, while mitoPO_2 decreased, might be indicative of a true limit of the system. Despite an accelerated oxygen delivery, the demand cannot be met. Mito$\dot{D}O_2$ increase might be attributed to a facilitated oxygen release when pH decreases and body temperature rises (41) as can be observed during high intensity exercise. In order to dispense of the extra heat generated by the physical exercise, skin perfusion is enhanced by vasodilation of cutaneous vessels and inhibition of the vasoconstrictor tone (40). This also might contribute to a rise in the slope of cutaneous mitoPO_2 increase after pressure release.

Limitations and Perspective

In the set-up of our trial, mitoPO_2 and its derivatives were analyzed in skin, not muscle. Research by Mellstrom et al. (42) and Venkatesh et al. (43) demonstrated that subcutaneous tissue PO_2 compares to that of intestinal mucosa and to ileal luminal PO_2, respectively. The rationale would be that oxygen tension in skin can be used as an indicator of the conditions in other organs. However, according to clinical and pre-clinical studies in oncologic dermatology, 5-ALA can only penetrate the epidermis and the upper layers of the dermis (44), making it difficult to translate the results of previous investigations to our findings. In addition, PpIX-TSLT measurements with the COMET device are restricted to a depth of about 0.1 mm in the epidermis (8). In

a recent study in rats, Wefers-Bettink et al. (45) found similar $mitoPO_2$ values measured with the probe placed directly on muscle compared to simultaneous measurements in abdominal skin at baseline. Yet, after 3 h, muscle $mitoPO_2$ was markedly higher than skin $mitoPO_2$. This was attributed to wound healing, nonetheless indicating that mitochondria in different organs can behave differently depending on local conditions. However, physical exercise is not limited to muscles but is a condition that affects the whole organism. Further studies will be needed to determine, if measurements of $mitoPO_2$ in epidermal cells represent an overall metabolic marker in the sense of a training relevant or disease severity indicating threshold.

Hitherto, only little evidence is available regarding intra- and interindividual variance in the absolute $mitoPO_2$ values (7, 9). The same is true for the magnitude of $mitoPO_2$ measured by PpIX-TSLT: earlier methodically different measurements and estimates ranged lower by one order of magnitude (46, 47). We found a large interindividual variance in COMET-derived $mitoPO_2$ measurements, which also was reported in previous studies (7, 10). The COMET system is a novel device for which influencing factors are studied only to some extent and in small groups of participants. The measurements deviate from previous measurements with a prototype device (9). Moreover, normal values do hitherto not exist. Therefore, further studies with larger cohorts of healthy people are required to define reference values and influencing variables. Overall, mean changes in $mitoPO_2$ and $mito\dot{D}O_2$ during the phases were highly significant, but compared to previously published data on stability of these variables ($mitoPO_2$ | $mito\dot{D}O_2$, standard error of measurement: 10 mmHg | 1.5 mmHg/s, minimum detectable difference: 30 mmHg | 4 mmHg/s) the differences were rather small. In accordance to the high interindividual variance, we also observed a high intraindividual variance regarding changes in $mitoPO_2$ over the metabolic phases (**Supplementary Figure 1**).

We found several statistically significant associations between variables of PpIX-TSLT, gas exchange and CBG. Nonetheless, only a small proportion of the variance (48) in $mitoPO_2$, $mito\dot{D}O_2$ and $mito\dot{V}O_2$ could be explained by the independent variables ($R^2_{marginal}$ for all models <0.15, median: 0.07, $Q_{1|3}$: 0.046 | 0.104). As described in the last paragraph, interindividual differences (modeled as random intercept) explained a much larger part of the variance ($R^2_{conditional-marginal}$, median: 0.56, $Q_{1|3}$: 0.46 | 0.61).

In our study we chose a graded exercise protocol with a relatively long duration of each load level in order to achieve a steady state. It is known that this type of protocol is favorable for blood lactate determination (49) but no so valuable for the identification of ventilatory thresholds (50). Nonetheless, it was shown in several studies that the determination of ventilatory thresholds is also feasible, when an incremental test design with steps of longer duration is used (32, 51).

Although a mitochondrial threshold was identified in the majority of subjects, its exact timing depended on the smoothing algorithm and might have been influenced by outlier values. Furthermore, $mitoPO_2$ single measurements might have been influenced to some degree by the intermediate dynamic measurements (e.g., rebound effect after reoxygenation). The measurements should be repeated using different protocols, e.g., ramp vs. stepwise protocol or shortened duration of workload levels, in order to create a more continuous rise in power output intensity. Furthermore, $mitoPO_2$ single measurements should not be interrupted by dynamic measurements. The simultaneous use of a second COMET system might be a reasonable alternative.

In our study population $\dot{V}O_{2max}$ on average was lower than mostly reported in the literature (see **Supplementary Table 5**). E.g., according to Heyward, a relative $\dot{V}O_{2max}$ of 42–45 ml/kg/min in 20 to 29-year-old men compares to a just moderate fitness level (52). In line with this, physically active students reached a $\dot{V}O_{2max}$ of about 49 ml/kg/min in a study of Boone et al. (53). In contrast, Zoll et al. reported a $\dot{V}O_{2max}$ of 36 ml/kg/min in physically active volunteers (54), which is more congruent with our findings. According to the recently in Germany executed population based Study of Health in Pomerania (SHIP) (55), which sought to implement reference values for CPET, the $\dot{V}O_{2max}$ values of the participants in our study were above the 5th quantile of age-, sex-, and weight-adjusted expected values. The following mechanisms and conditions might have affected $\dot{V}O_{2max}$: We did not ask the participants to refrain from exercise for 48 h prior to the test, nor did we give dietary instructions. The time of day varied among the tests. All three aspects are known to influence gas exchange parameters (14, 56). In addition, the relatively long duration of the test and also of the single load increments as well as the type of protocol (graded increments vs. ramp) might have contributed to our diverging results (53, 56, 57). Another mechanism that might have had an impact on $\dot{V}O_{2max}$ was the presence of light to moderate exercise induced arterial hypoxemia (EIAH) in 6 participants assessed by S_cO_2. This condition is found mainly in habitually active persons but also in athletes at a percentage of up to 50% and can negatively influence $\dot{V}O_{2max}$ (58). However, our study set-up was designed as a pilot study to test gas exchange and metabolic variables against a novel technique for measuring $mitoPO_2$. Thus, the absolute values of the mentioned variables were of minor importance.

Last but not least, the question remains how our findings can be put into the context of intensive care medicine and serious systemic disease such as sepsis. The mitochondrial threshold possibly indicates a breakpoint in mitochondrial performance. As such, the MT might well be a marker for the point of no return in the course of disease. It has already been shown that in planned procedures like, e.g., surgery, monitoring of $mitoPO_2$ is feasible and more sensitive than classical parameters (8). In the case of sepsis however, this would require the possibility of early and continuous monitoring. This would necessitate a faster uptake of 5-ALA in cutaneous cells and a prolonged availability after a one-time-application. Pharmacologic modifications to the 5-ALA patch could solve the problem. If it is possible to overcome these difficulties, the technique might develop into a useful instrument for the timing of interventions in critical illness.

CONCLUSION

In this pilot study we demonstrated that PpIX-TSLT measurements of $mitoPO_2$, $mito\dot{V}O_2$, and $mito\dot{D}O_2$ with

the COMET device are feasible simultaneously with CPET. Furthermore, we showed that mitoPO$_2$ and mitoDO$_2$ measured in skin are associated with gas exchange and CBG derived variables during exercise to exhaustion. Interestingly, we found a decline in mitoPO$_2$ after a peak or plateau (MT), which occurred between VT1 and VT2 around LT2. Because aerobic energy production originates from mitochondria, this phenomenon might well be indicative of a breakpoint in performance and could pose a valuable instrument in performance diagnostics as well as in serious disease. As our study population comprised of only 14 subjects, the results will have to be validated in larger cohorts and future studies should aim to relate mitochondrial oxygen kinetics not only to parameters of high-performance sports but also to such of critical illness.

DATA AVAILABILITY STATEMENT

The raw data supporting the conclusions of this article will be made available by the authors, without undue reservation.

ETHICS STATEMENT

The study involving human participants was reviewed and approved by the Ethics Committee of the Friedrich Schiller University Jena (2019-1296-BO). The participants provided their written informed consent to participate in this study.

AUTHOR CONTRIBUTIONS

CS-W, PB, MH, and SC: conception and design of the study. JH, PB, and SD: organization and performance of measurements. PB, CS-W, JH, and MH: data analysis. PB: statistical analysis. CS-W, PB, and SC: drafting the manuscript for important intellectual content. PB, CS-W, JH, SD, NB, MH, and SC: revising the manuscript prior to submission. All authors carefully reviewed and approved the manuscript.

FUNDING

This study was funded by the Federal Ministry of Education and Research within the Centre for Innovation Competence Septomics (Research Group Translational Septomics, Grant 03Z22JN12 to SC). The funding source had no involvement in the study design, the collection, analysis, and interpretation of data, in the writing of the report, or in the decision to submit the article for publication.

ACKNOWLEDGMENTS

We thank Anne Standke, Yalda Seyed Sadri, and Alina K. Plooij for their support during the measurements.

SUPPLEMENTARY MATERIAL

The Supplementary Material for this article can be found online at: https://www.frontiersin.org/articles/10.3389/fmed.2020.585462/full#supplementary-material

Supplementary Figure 1 | Smoothed course of mitochondrial oxygen partial pressure (mitoPO$_2$) during cardiopulmonary exercise testing for every study subject. The gray dots indicate raw mitoPO$_2$ values and the blue line indicates the fitted regression line using locally estimated scatterplot smoothing (LOESS, span = 0.75, degree = 2). The gray area depicts the 95% confidence interval. The individual mitochondrial threshold is marked with the black vertical line. It marks the maximum (ID 1, 2, 5, 6, 8, 9, 10, 11, 12, 15, 16) or local maximum (ID 3, 4, 13) of the fitted regression line.

Supplementary Tables 1–3 | Detailed descriptive statistics on all variables of CPET, PpIX-TSLT measurements and capillary blood gas analyses and estimated marginal means and contrasts for selected variables of CPET, PpIX-TSLT measurements and blood gas analyses.

Supplementary Table 4 | Coefficients of the regression models analyzing the association of variables of PpIX-TSLT measurement, CPET and capillary blood gas analyses.

Supplementary Table 5 | Detailed description of the $\dot{V}O_{2max}$ for all subjects.

REFERENCES

1. Singer M. The role of mitochondrial dysfunction in sepsis-induced multi-organ failure. *Virulence.* (2014) 5:66–72. doi: 10.4161/viru.26907
2. Stanzani G, Duchen MR, Singer M. The role of mitochondria in sepsis-induced cardiomyopathy. *Biochim Biophys Acta Mol Basis Dis.* (2019) 1865:759–73. doi: 10.1016/j.bbadis.2018.10.011
3. Zhang H, Feng YW, Yao YM. Potential therapy strategy: targeting mitochondrial dysfunction in sepsis. *Mil Med Res.* (2018) 5:41. doi: 10.1186/s40779-018-0187-0
4. Granata C, Jamnick NA, Bishop DJ. Training-induced changes in mitochondrial content and respiratory function in human skeletal muscle. *Sports Med.* (2018) 48:1809–28. doi: 10.1007/s40279-018-0936-y
5. Mik EG, Stap J, Sinaasappel M, Beek JF, Aten JA, van Leeuwen TG, et al. Mitochondrial PO$_2$ measured by delayed fluorescence of endogenous protoporphyrin IX. *Nat Methods.* (2006) 3:939–45. doi: 10.1038/nmeth940
6. Harms FA, Bodmer SI, Raat NJ, Mik EG. Non-invasive monitoring of mitochondrial oxygenation and respiration in critical illness using a novel technique. *Crit Care.* (2015) 19:343. doi: 10.1186/s13054-015-1056-9
7. Baumbach P, Neu C, Derlien S, Bauer M, Nisser M, Buder A, et al. A pilot study of exercise-induced changes in mitochondrial oxygen metabolism measured by a cellular oxygen metabolism monitor (PICOMET). *Biochim Biophys Acta Mol Basis Dis.* (2019) 1865:749–58. doi: 10.1016/j.bbadis.2018.12.003
8. Ubbink R, Bettink MAW, Janse R, Harms FA, Johannes T, Munker FM, et al. A monitor for Cellular Oxygen METabolism (COMET): monitoring tissue oxygenation at the mitochondrial level. *J Clin Monit Comput.* (2017) 31:1143–50. doi: 10.1007/s10877-016-9966-x
9. Harms FA, Stolker RJ, Mik EG. Cutaneous respirometry as novel technique to monitor mitochondrial function: a feasibility study in healthy volunteers. *PLoS ONE.* (2016) 11:e0159544. doi: 10.1371/journal.pone.0159544
10. Neu C, Baumbach P, Plooij AK, Skitek K, Götze J, von Loeffelholz C, et al. Non-invasive assessment of mitochondrial oxygen metabolism in the critically ill patient using the protoporphyrin IX-triplet state lifetime technique—a feasibility study. *Front Immunol.* (2020) 11:757. doi: 10.3389/fimmu.2020.00757
11. van Diemen MPJ, Berends CL, Akram N, Wezel J, Teeuwisse WM, Mik BG, et al. Validation of a pharmacological model for mitochondrial dysfunction in healthy subjects using simvastatin: A randomized placebo-controlled proof-of-pharmacology study. *Eur J Pharmacol.* (2017) 815:290–7. doi: 10.1016/j.ejphar.2017.09.031
12. van Dijk LJD, Ubbink R, Terlouw LG, van Noord D, Mik EG, Bruno MJ. Oxygen-dependent delayed fluorescence of protoporphyrin IX measured

in the stomach and duodenum during upper gastrointestinal endoscopy. *J Biophotonics*. (2019) 12:e201900025. doi: 10.1002/jbio.201900025
13. Alveolar gas equation. In: Huang C, Chambers D, Matthews G, (editors). *Basic Physiology for Anaesthetists*. 2nd ed. Cambridge: Cambridge University Press (2019). p. 77–9.
14. Kroidl RF, Schwarz S, Lehnigk BJF, (editors). *Kursbuch Spiroergometrie, Technik und Befundung verständlich gemacht* Stuttgart: Thieme Verlag (2015).
15. Antonutto G, Di Prampero PE. The concept of lactate threshold. A short review. *J Sports Med Phys Fitness*. (1995) 35:6–12.
16. Skinner JS, McLellan TH. The transition from aerobic to anaerobic metabolism. *Res Q Exerc Sport*. (1980) 51:234–48. doi: 10.1080/02701367.1980.10609285
17. Westhoff M, Ruhle KH, Greiwing A, Schomaker R, Eschenbacher H, Siepmann M, et al. Positional paper of the German working group "cardiopulmonary exercise testing" to ventilatory and metabolic (lactate) thresholds. *Dtsch Med Wochenschr*. (2013) 138:275–80. doi: 10.1055/s-0032-1332843
18. Faude O, Kindermann W, Meyer T. Lactate threshold concepts: how valid are they? *Sports Med*. (2009) 39:469–90. doi: 10.2165/00007256-200939060-00003
19. Thomas S, Reading J, Shephard RJ. Revision of the Physical Activity Readiness Questionnaire (PAR-Q). *Can J Sport Sci*. (1992) 17:338–45.
20. Mik EG. Special article: measuring mitochondrial oxygen tension: from basic principles to application in humans. *Anesth Analg*. (2013) 117:834–46. doi: 10.1213/ANE.0b013e31828f29da
21. Stern O, Volmer M. Über die Abklingungszeit der Fluoreszenz. *Phys Z*. (1919) 20:183–8.
22. Poulson R. The enzymic conversion of protoporphyrinogen IX to protoporphyrin IX in mammalian mitochondria. *J Biol Chem*. (1976) 251:3730–3.
23. Wachowska M, Muchowicz A, Firczuk M, Gabrysiak M, Winiarska M, Wanczyk M, et al. Aminolevulinic acid (ALA) as a prodrug in photodynamic therapy of cancer. *Molecules*. (2011) 16:4140–64. doi: 10.3390/molecules16054140
24. Donnelly RF, McCarron PA, Woolfson AD. Drug delivery of aminolevulinic acid from topical formulations intended for photodynamic therapy. *Photochem Photobiol*. (2005) 81:750–67. doi: 10.1562/2004-08-23-IR-283R1.1
25. American College of Sports Medicine. *Guidelines for Exercise Testing and Prescription*. Philadelphia, PA: Lea & Febiger (1986).
26. Fletcher GF, Ades PA, Kligfield P, Arena R, Balady GJ, Bittner VA, et al. Exercise standards for testing and training: a scientific statement from the American Heart Association. *Circulation*. (2013) 128:873–934. doi: 10.1161/CIR.0b013e31829b5b44
27. Klingenheben T, Löllgen H, Bosch R, Trappe HJ. Manual zum Stellenwert der Ergometrie. *Der Kardiol*. (2018) 12:342–55. doi: 10.1007/s12181-018-0265-2
28. Borg G. Anstrengungsempfinden und körperliche Aktivität. *Dtsch Arztebl Int*. (2004) 101:A-1016.
29. Borg GA. Psychophysical bases of perceived exertion. *Med Sci Sports Exerc*. (1982) 14:377–81. doi: 10.1249/00005768-198205000-00012
30. Löllgen H, Fahrenkrog I, Löllgen D. Bewertung ergometrischer Größen. In: Löllgen H, Erdmann E, Gitt AK, editors. *Ergometrie. 3*. Heidelberg: Springer Medizin Verlag (2010). p. 71. doi: 10.1007/978-3-540-92730-3
31. Binder RK, Wonisch M, Corra U, Cohen-Solal A, Vanhees L, Saner H, et al. Methodological approach to the first and second lactate threshold in incremental cardiopulmonary exercise testing. *Eur J Cardiovasc Prev Rehabil*. (2008) 15:726–34. doi: 10.1097/HJR.0b013e328304fed4
32. Dickhuth HH, Yin L, Niess A, Röcker K, Mayer F, Heitkamp HC, et al. Ventilatory, lactate-derived and catecholamine thresholds during incremental treadmill running: relationship and reproducibility. *Int J Sports Med*. (1999) 20:122–7. doi: 10.1055/s-2007-971105
33. Dickhuth H-H, Huonker M, Münzel T, Drexler H, Berg A, Keul J. Individual anaerobic threshold for evaluation of competitive athletes and patients with left ventricular dysfunction. In: Bachl N, Graham TE, Löllgen H, editors. *Advances in Ergometry*. Berlin; Heidelberg; New York, NY: Springer (1991). p. 173–9. doi: 10.1007/978-3-642-76442-4_26
34. R Development Core Team. *R: A Language and Environment for Statistical Computing*. Vienna: R Foundation for Statistical Computing (2013).
35. Poole DC, Burnley M, Vanhatalo A, Rossiter HB, Jones AM. Critical power: an important fatigue threshold in exercise physiology. *Med Sci Sports Exerc*. (2016) 48:2320–34. doi: 10.1249/MSS.0000000000000939
36. Galán-Rioja M, González-Mohíno F, Poole DC, González-Ravé JM. Relative proximity of critical power and metabolic/ventilatory thresholds: systematic review and meta-analysis. *Sports Med*. (2020) 50:1771–83. doi: 10.1007/s40279-020-01314-8
37. Romers LH, Bakker C, Dollee N, Hoeks SE, Lima A, Raat NJ, et al. Cutaneous mitochondrial PO_2, but not tissue oxygen saturation, is an early indicator of the physiologic limit of hemodilution in the pig. *Anesthesiology*. (2016) 125:124–32. doi: 10.1097/ALN.0000000000001156
38. Boushel R, Gnaiger E, Calbet JA, Gonzalez-Alonso J, Wright-Paradis C, Sondergaard H, et al. Muscle mitochondrial capacity exceeds maximal oxygen delivery in humans. *Mitochondrion*. (2011) 11:303–7. doi: 10.1016/j.mito.2010.12.006
39. Golub AS, Tevald MA, Pittman RN. Phosphorescence quenching microrespirometry of skeletal muscle *in situ*. *Am J Physiol Heart Circ Physiol*. (2011) 300:H135–43. doi: 10.1152/ajpheart.00626.2010
40. Burton DA, Stokes K, Hall GM. Physiological effects of exercise. *Contin Educ Anaesth Crit Care Pain*. (2004) 4:185–8. doi: 10.1093/bjaceaccp/mkh050
41. Forbes WH, Roughton FJ. The equilibrium between oxygen and haemoglobin: I. The oxygen dissociation curve of dilute blood solutions. *J Physiol*. (1931) 71:229–60. doi: 10.1113/jphysiol.1931.sp002729
42. Mellstrom A, Månsson P, Jonsson K, Hartmann M. Measurements of subcutaneous tissue PO_2 reflect oxygen metabolism of the small intestinal mucosa during hemorrhage and resuscitation. An experimental study in pigs. *Eur Surg Res*. (2009) 42:122–9. doi: 10.1159/000193295
43. Venkatesh B, Morgan TJ, Lipman J. Subcutaneous oxygen tensions provide similar information to ileal luminal CO_2 tensions in an animal model of haemorrhagic shock. *Intens Care Med*. (2000) 26:592–600. doi: 10.1007/s001340051209
44. de Bruijn HS, Meijers C, van der Ploeg-van den Heuvel A, Sterenborg HJ, Robinson DJ. Microscopic localisation of protoporphyrin IX in normal mouse skin after topical application of 5-aminolevulinic acid or methyl 5-aminolevulinate. *J Photochem Photobiol B*. (2008) 92:91–7. doi: 10.1016/j.jphotobiol.2008.05.005
45. Wefers Bettink MA, Harms FA, Dollee N, Specht PAC, Raat NJH, Schoonderwoerd GC, et al. Non-invasive versus *ex vivo* measurement of mitochondrial function in an endotoxemia model in rat: toward monitoring of mitochondrial therapy. *Mitochondrion*. (2020) 50:149–57. doi: 10.1016/j.mito.2019.11.003
46. Grote J. *Gewebeatmung in Physiologie des Menschen*. Berlin; Heidelberg; New York: Springer-Verlag (1997).
47. Ortiz-Prado E, Dunn JF, Vasconez J, Castillo D, Viscor G. Partial pressure of oxygen in the human body: a general review. *Am J Blood Res*. (2019) 9:1–14.
48. Nakagawa S, Johnson PCD, Schielzeth H. The coefficient of determination R(2) and intra-class correlation coefficient from generalized linear mixed-effects models revisited and expanded. *J R Soc Interface*. (2017) 14:134. doi: 10.1098/rsif.2017.0213
49. Bentley DJ, Newell J, Bishop D. Incremental exercise test design and analysis. *Sports Med*. (2007) 37:575–86. doi: 10.2165/00007256-200737070-00002
50. Meyer T, Lucía A, Earnest CP, Kindermann W. A conceptual framework for performance diagnosis and training prescription from submaximal gas exchange parameters–theory and application. *Int J Sports Med*. (2005) 26:S38–48. doi: 10.1055/s-2004-830514
51. Roecker K, Mayer F, Striegel H, Dickhuth HH. Increase characteristics of the cumulated excess-CO2 and the lactate concentration during exercise. *Int J Sports Med*. (2000) 21:419–23. doi: 10.1055/s-2000-3836
52. Heyward V. *Advanced Fitness Assessment and Exercise Prescription*. 5th ed. Champaign, IL: Human Kinetics (2006).
53. Boone J, Koppo K, Bouckaert J. The VO_2 response to submaximal ramp cycle exercise: Influence of ramp slope and training status. *Respir Physiol Neurobiol*. (2008) 161:291–7. doi: 10.1016/j.resp.2008.03.008

54. Zoll J, Sanchez H, N'Guessan B, Ribera F, Lampert E, Bigard X, et al. Physical activity changes the regulation of mitochondrial respiration in human skeletal muscle. *J Physiol.* (2002) 543:191–200. doi: 10.1113/jphysiol.2002.019661
55. Gläser S, Ittermann T, Schäper C, Obst A, Dörr M, Spielhagen T, et al. The Study of Health in Pomerania (SHIP) reference values for cardiopulmonary exercise testing. *Pneumologie.* (2013) 67:58–63. doi: 10.1055/s-0032-1325951
56. Boone J, Bourgois J. The oxygen uptake response to incremental ramp exercise: methodogical and physiological issues. *Sports Med.* (2012) 42:511–26. doi: 10.2165/11599690-000000000-00000
57. Hansen JE, Casaburi R, Cooper DM, Wasserman K. Oxygen uptake as related to work rate increment during cycle ergometer exercise. *Eur J Appl Physiol Occupat Physiol.* (1988) 57:140–5. doi: 10.1007/BF00640653
58. Dempsey JA, Wagner PD. Exercise-induced arterial hypoxemia. *J Appl Physiol (1985).* (1999) 87:1997–2006. doi: 10.1152/jappl.1999.87.6.1997

Conflict of Interest: The authors declare that the research was conducted in the absence of any commercial or financial relationships that could be construed as a potential conflict of interest.

Advantages of publishing in Frontiers

OPEN ACCESS
Articles are free to read for greatest visibility and readership

FAST PUBLICATION
Around 90 days from submission to decision

HIGH QUALITY PEER-REVIEW
Rigorous, collaborative, and constructive peer-review

TRANSPARENT PEER-REVIEW
Editors and reviewers acknowledged by name on published articles

Frontiers
Avenue du Tribunal-Fédéral 34
1005 Lausanne | Switzerland

Visit us: www.frontiersin.org
Contact us: frontiersin.org/about/contact

REPRODUCIBILITY OF RESEARCH
Support open data and methods to enhance research reproducibility

DIGITAL PUBLISHING
Articles designed for optimal readership across devices

FOLLOW US
@frontiersin

IMPACT METRICS
Advanced article metrics track visibility across digital media

EXTENSIVE PROMOTION
Marketing and promotion of impactful research

LOOP RESEARCH NETWORK
Our network increases your article's readership